

Dissertation zur Erlangung des Doktorgrades  
der Fakultät für Chemie und Pharmazie  
der Ludwig-Maximilians-Universität München

# Calcium Iron Palladium Arsenides and related compounds

Christine Stürzer, geb. Hieke

aus

Gunzenhausen, Deutschland

2015



## **Erklärung**

Diese Dissertation wurde im Sinne von § 7 der Promotionsordnung vom 28. November 2011 von Herrn Prof. Dr. Dirk Johrendt betreut.

## **Eidesstattliche Versicherung**

Diese Dissertation wurde eigenständig und ohne unerlaubte Hilfe erarbeitet.

München,

---

Christine Stürzer

Dissertation eingereicht: 23.07.2015

1. Gutachter: Prof. Dr. Dirk Johrendt

2. Gutachter: Prof. Dr. Konstantin Karaghiosoff

Mündliche Prüfung: 07.09.2015



*Dem großen Herrn Fritz Gismann,*

*meinem Opa*



## **Danksagung**

Mein großer Dank gilt Herrn Prof. Dr. Dirk Johrendt für die herzliche Aufnahme in seinen Arbeitskreis und die Möglichkeit, meine Doktorarbeit in seiner Gruppe anzufertigen. Durch die eigenen Freiheiten bei der Bearbeitung dieses komplexen und vielfältigen Themas, konstruktiven Diskussionen und stets offenen Türen war ein Gelingen dieser Arbeit erst möglich. Dankeschön.

Herrn Prof. Dr. Konstantin Karaghiosoff danke ich herzlich für die Teilnahme an meiner Promotionsprüfung sowie die bereitwillige Übernahme des Koreferats.

Darüberhinaus danke ich Herrn Prof. Dr. Wolfgang Schnick, Herrn Prof. Dr. Peter Gille, Herrn Prof. Dr. Hubert Huppertz und Herrn Prof. Dr. Hans-Christian Böttcher für die weitere Bildung meiner Prüfungskommission. Vielen Dank, dass Sie sich die Zeit nehmen, am Tag meines Rigosums als Prüfer zu fungieren.

Ich danke den aktuellen und ehemaligen Arbeitskreismitgliedern, die mich in meiner Zeit im AK Johrendt begleitet haben, Herrn Rainer Frankovsky, Frau Gina Friederichs, Frau Franziska Hummel, Frau Catrin Löhnert, Herrn Fabian Nitsche, Frau Ursula Pachmayr, Herrn Simon Peschke, Herrn Roman Pobel, Frau Juliane Stahl, Herrn Tobias Stürzer, Herrn Marcus Tegel, Herrn Erwin Wiesenmayer und Frau Veronika Zinth. Es war angenehm und konstruktiv mit Euch zu arbeiten. Vielen Dank für die zahlreichen Messungen, Diskussionen und Antworten.

Besonders meinen Laborkollegen Herrn Tobias Stürzer und Herrn Erwin Wiesenmayer aus unserem halben D 2.049 danke ich für das tolle Arbeitsklima im Labor. Ich gehe immer gern durch diese Tür.

Herzlichen Dank an Frau Catrin Löhnert für die nette Aufnahme, die immerwährende Freundlichkeit und Hilfsbereitschaft. Deine nützlichen Arbeitsalltagstipps und gute Laune haben sehr zu meinem Wohlfühlen beigetragen. Danke, dass ich auch Dir immer mal wieder helfen durfte.

Vielen Dank allen Kollegen der Arbeitskreise Schnick, Lotsch, Oeckler, Hoch und Schmedt auf der Günte für die angenehme und hilfsbereite Atmosphäre im 2. Stock, die unvergessliche Zeit und gemeinsamen Erlebnisse.

Meinen Praktikantinnen Frau Linda Wehner, Frau Judith Lippmann, Frau Anne Schulz, Frau Dimitra Pournara und Frau Stefanie Beck danke ich sehr für die fleißige Unterstützung. Danke für euren Eifer, all eure Ideen und Fragen.

Für die geduldige Messung und Aufbereitung unzähliger Kristalldaten danke ich herzlich Herrn Tobias Stürzer sowie Herrn Fabian Nitsche.

Vielen Dank an Herrn Christian Minke für die Durchführung einer großen Zahl an EDX-Messungen in der Vor-Zeiss-Zeit. Gerne gleiche ich das nun bei Bedarf aus.

Für ihren Einsatz, Rat und Tat in Organisations-, Sicherheits- und Computerfragen danke ich Frau Catrin Löhnert, Frau Olga Lorenz, Herrn Thomas Miller und Herrn Wolfgang Wünschheim, denn nur in einem reibungslosen und funktionstüchtigen Umfeld ist die erfolgreiche Konzentration auf die eigene Forschung möglich.

Herrn Florian Winter und Herrn Prof. Dr. Rainer Pöttgen der Universität Münster danke ich vielmals für die Durchführung von Mößbauer-Messungen.

Für das effektive Korrekturlesen dieser Arbeit möchte ich mich ganz herzlich bei Herrn Tobias Stürzer bedanken.

Ein unermesslicher Dank gilt meinen Eltern Frau Karin und Herrn Bernhard Hieke, für ihr bedingungsloses Engagement in allen Lebenslagen, die Ermöglichung meines Studiums und ihre stets wirkungsvollen Worte und Taten, wohin auch immer es mich verschlägt. Danke, dass ich mir eurer Unterstützung und Liebe so sicher sein kann. Ihr habt eine großartige Familie geschaffen.

Vielen lieben Dank meiner wunderbaren Schwester Anja („Wir beide“). Ich bin so stolz auf Dich. Tausend Dank liebe Anja, lieber Jürgen, liebe Janina und liebe Lena für eure Begeisterung, Zuneigung und die unbeschreiblich tolle Zeit, die ich mit der ganzen Familie Bauer erleben darf. Schön, dass ich eure Bangn bin.

Ich bin dankbar für meinen Opa Herrn Fritz Gismann, für deine uneingeschränkte Unterstützung und reges Interesse, für all deine Geschichten, Ideen und Erklärungen, die nicht nur mein Interesse an der Wissenschaft immer vorangetrieben haben.

Meiner Oma Frau Maria Gismann, vielen lieben Dank, für Alles, was Du mir gabst und was ich von Dir lernen durfte.

Der größte Dank gilt meinem Mann Herrn Tobias Stürzer, für all die gemeinsamen Wege während unseres Studiums und in die Welt hinaus. Danke, lieber Tobi, für deinen Zuspruch, deine immerwährende Unterstützung, und dass ich Dich stets an meiner Seite weiß. Alles ist so viel besser, wenn wir beide zusammen sind.



*„Umwege erweitern die Ortskenntnis“*

*(Kurt Tucholsky)*



## Table of Contents

|          |   |           |
|----------|---|-----------|
| <b>1</b> | <b>Introduction.....</b>  | <b>1</b>  |
| <b>2</b> | <b>New Palladium Iron Arsenides (CaFeAs)<sub>10</sub>Pd<sub>3</sub>As<sub>8</sub> .....</b>   | <b>16</b> |
| 2.1      | Superconductivity and Crystal Structure of the Palladium Iron Arsenides<br>(CaFe <sub>1-x</sub> Pd <sub>x</sub> As) <sub>10</sub> Pd <sub>3</sub> As <sub>8</sub> ..... | 16        |
| 2.1.1    | Introduction .....  | 17        |
| 2.1.2    | Results and Discussion.....   | 18        |
| 2.1.3    | Conclusion.....   | 25        |
| 2.1.4    | References .....  | 26        |
| 2.2      | (CaFe <sub>1-x</sub> Pd <sub>x</sub> As) <sub>10</sub> Pd <sub>3</sub> As <sub>8</sub> with Parent-like Properties .....  | 29        |
| 2.2.1    | Introduction .....  | 29        |
| 2.2.2    | Results and Discussion.....   | 31        |
| 2.2.3    | Experimental Section .....  | 34        |
| 2.2.4    | Conclusion.....   | 34        |
| 2.2.5    | References .....  | 35        |
| 2.3      | Site Preference of Rare Earth Doping in Palladium Iron Arsenide<br>Superconductors .....  | 37        |
| 2.3.1    | Introduction .....  | 38        |
| 2.3.2    | Results and Discussion.....   | 39        |
| 2.3.3    | Experimental Section .....  | 45        |
| 2.3.4    | Conclusion.....   | 46        |
| 2.3.5    | References .....  | 46        |
| 2.4      | (Ca <sub>1-y</sub> RE <sub>y</sub> FeAs) <sub>10</sub> Pd <sub>3</sub> As <sub>8</sub> series with RE = La – Nd, Sm – Lu and y = 0.05, 0.10 ...                         | 49        |
| 2.4.1    | Introduction .....  | 49        |
| 2.4.2    | Results and Discussion.....   | 51        |
| 2.4.3    | Experimental Section .....  | 56        |
| 2.4.4    | Conclusion.....   | 56        |
| 2.4.5    | References .....  | 57        |

|          |  |           |
|----------|--|-----------|
| <b>3</b> | <b>Combination of Palladium and Platinum 1038 Phases in <math>(\text{CaFe}_{1-x}\text{Pd}_x\text{As})_{10}\text{Pt}_3\text{As}_8</math> ..</b> | <b>59</b> |
| 3.1      | Introduction.....  | 60        |
| 3.2      | Results and Discussion.....  | 61        |
| 3.3      | Experimental Section .....   | 66        |
| 3.4      | Conclusion .....   | 67        |
| 3.5      | References.....  | 67        |
| <b>4</b> | <b>Structure and Properties of <math>(\text{CaFe}_{1-x}\text{Pd}_x\text{As})_{10}\text{Pd}_4\text{As}_8</math>.....</b>                        | <b>69</b> |
| 4.1      | Introduction.....  | 69        |
| 4.2      | Results and Discussion.....  | 70        |
| 4.3      | Experimental Section .....   | 77        |
| 4.4      | Conclusion .....   | 78        |
| 4.5      | References.....  | 79        |
| <b>5</b> | <b>New Structure with substituted Iron Arsenides Layers <math>\text{CaFe}_{1-x}\text{Pd}_x\text{As}_2</math>.....</b>                          | <b>81</b> |
| 5.1      | Introduction.....  | 81        |
| 5.2      | Results and Discussion.....  | 82        |
| 5.3      | Conclusion .....   | 90        |
| 5.4      | References.....  | 90        |
| <b>6</b> | <b>Properties of <math>\text{Ca}_{1-x}\text{Pr}_x\text{FeAs}_2</math> with <math>x = 0.15 - 0.25</math> .....</b>                              | <b>93</b> |
| 6.1      | Introduction.....  | 93        |
| 6.2      | Results and Discussion.....  | 94        |
| 6.3      | Experimental Section .....   | 100       |
| 6.4      | Conclusion .....   | 100       |
| 6.5      | References.....  | 101       |

|           |  |            |
|-----------|--|------------|
| <b>7</b>  | <b>Framework Structures of interconnected Layers in Calcium Iron Arsenides.....</b>    | <b>103</b> |
| 7.1       | Introduction .....   | 103        |
| 7.2       | Experimental Details .....   | 104        |
| 7.3       | Results and Discussion .....   | 106        |
| 7.4       | Conclusion.....  | 113        |
| 7.5       | References .....   | 113        |
| <b>8</b>  | <b>Summary.....</b>  | <b>115</b> |
| <b>9</b>  | <b>Conclusion .....</b>  | <b>123</b> |
| <b>10</b> | <b>Appendix.....</b>   | <b>124</b> |
| 10.1      | Crystallographic Data of $(\text{CaFeAs})_{10}\text{Pd}_3\text{As}_8$ .....            | 124        |
| 10.2      | Crystallographic Data of $\alpha$ - $(\text{CaFeAs})_{10}\text{Pd}_4\text{As}_8$ ..... | 126        |
| 10.3      | Crystallographic data of $\text{Ca}(\text{Fe}_{1-x}\text{Pd}_x)\text{As}_{2-z}$ .....  | 127        |
| 10.4      | Crystallographic Data of Framework Structures .....                                    | 128        |
| 10.4.1    | $\beta$ - $\text{Ca}_3\text{Fe}_8\text{PdAs}_6$ .....                                  | 128        |
| 10.4.2    | $\gamma$ - $\text{Ca}_3\text{Fe}_8\text{PdAs}_6$ .....                                 | 129        |
| 10.4.3    | $\alpha$ - $\text{Ca}_6\text{Fe}_{11}\text{Pd}_3\text{As}_{10}$ .....                  | 130        |
| 10.5      | CSD Numbers.....   | 132        |
| <b>11</b> | <b>Abbreviations and Quantities .....</b>  | <b>133</b> |
| 11.1      | Abbreviations .....  | 133        |
| 11.2      | Magnetic Quantities.....   | 134        |
| 11.3      | Crystallographic Quantities .....  | 135        |
| 11.4      | Other Quantities.....  | 135        |

|  |            |
|--|------------|
| <b>12 Publications .....</b>               | <b>137</b> |
| 12.1 Publications within this Thesis ..... | 137        |
| 12.2 Publications beyond this Thesis ..... | 139        |
| 12.3 Conference Contributions .....        | 140        |
| <b>13 Curriculum Vitae.....</b>            | <b>141</b> |

# 1 Introduction

For a long time *Aristotle's* theorem *corpora non agunt nisi fluida* (About: Solids do not react, unless they are fluid) was guiding material science research. With the beginning of the 20<sup>th</sup> century new achievements founded the field of modern solid state chemistry. Ever since the application of computer-based crystal structure determination was established, the plethora of natural and synthesized solids was started to be discovered. From this family the huge class of transition-metal pnictides comes up with a particularly versatile structural chemistry and therewith associated outstanding physical properties. Due to the moderate electronegativity of pnictides these materials often range between metallic and ionic solids,<sup>[1]</sup> which is why their interesting features are always good to turn over a new leaf in research and application. One of the latest breakthroughs was the dawn of the iron age of superconductivity<sup>[2]</sup> starting with experiments of *Hosono* et al. in 2008.<sup>[3]</sup>

The effect of the crystal structure on the physical properties often plays a decisive role. Given the variety of different crystal structures adopted by transition-metal pnictides these compounds are predestinated also to adjust their exceptional features. Focusing on layered structures even in the group of simple ternary  $AMPn$ ,  $AMPn_2$ , and  $AM_2Pn_2$  phases ( $A = A, AE, RE$ ;  $M =$  transition-metal;  $Pn = P, As, Sb$ ) several structure types are present. Next to trigonal and square planar coordination the most prominent motif is tetrahedral coordination of transition-metals by pnictides. Equiatomic  $AMPn$  compounds form layers of edge-sharing tetrahedra in the *anti*-PbFCl type<sup>[4]</sup> (ternary  $Cu_2Sb$ ) like the iron arsenides  $AFeAs$  ( $A = Li, Na$ ).<sup>[5,6]</sup> Networks of corner- and edge-sharing tetrahedra are present for example in  $REPdAs$ <sup>[7]</sup> with TiNiSi-type<sup>[8]</sup> (ternary *anti*-PbCl<sub>2</sub>) or ZrNiAl-type<sup>[9]</sup> (ternary  $Fe_2P$ ) structure. Trigonal coordinated palladium is present in  $APdAs$  ( $A = AE, RE$ )<sup>[7,10]</sup> featuring a planar honeycomb motif in the hexagonal ZrBeSi-type<sup>[11]</sup> (ternary  $Ni_2In$ ) structure. Moreover several palladium and platinum pnictides show networks with noble-metals in threefold coordinated positions.<sup>[12-14]</sup> In  $AMPn_2$  two different pnictide positions result in coplanar alternate stacking of tetrahedra and pnictide layers each separated by cations. According to the array of pnictide atoms *zigzag* chains ( $SrZnSb_2$  type)<sup>[15]</sup> or square nets ( $HfCuSi_2$  type)<sup>[16]</sup> as well as a distorted variant with *cis-trans* chains<sup>[17]</sup> are known. By arranging the *zigzag* chains perpendicular to the tetrahedra layers the distances between both allow for the formation of bonds, like in orthorhombic  $BaPdAs_2$ <sup>[18]</sup> ( $CeNiSi_2$  type)<sup>[19]</sup> with pnictide-centered tetrahedra. As tetrel containing variants iron silicides with  $FeSi_{4/4}$  tetrahedra ( $LaMnSi_2$  type)<sup>[20]</sup> as well as  $SiFe_{4/4}$ <sup>[21]</sup> motif in monoclinic  $NdRuSi_2$ -type<sup>[22]</sup> phases can be distinguished. Finally  $AM_2Pn_2$  compounds comprise

$MPn_{4/4}$  tetrahedra in the common  $\text{ThCr}_2\text{Si}_2$ -type (ternary  $\text{BaAl}_4$ ) structure<sup>[23]</sup> or the enlarged  $\text{BaZn}_2\text{P}_2$ -type variant,<sup>[24]</sup> respectively. Interchanging the positions in every second tetrahedra layer leads to the  $\text{CaBe}_2\text{Ge}_2$ -type structure,<sup>[25]</sup> while trigonal  $\text{CaAl}_2\text{Si}_2$ -type compounds<sup>[26]</sup> feature only three shared tetrahedra edges. Extraordinary  $\text{BaPd}_2\text{As}_2$ <sup>[27]</sup> crystallizes in the  $\text{ThCr}_2\text{Si}_2$ -type structure as well as a stacking variant of combined  $\text{CeMg}_2\text{Si}_2$  and  $\text{CaBe}_2\text{Ge}_2$  blocks with interchanged tetrahedra layers. Moreover a third modification forms planar four-fold coordinated metal positions with  $\text{CeMg}_2\text{Si}_2$ -type structure.<sup>[28]</sup> This polymorphism<sup>[29]</sup> emphasizes the structural flexibility of palladium arsenides.

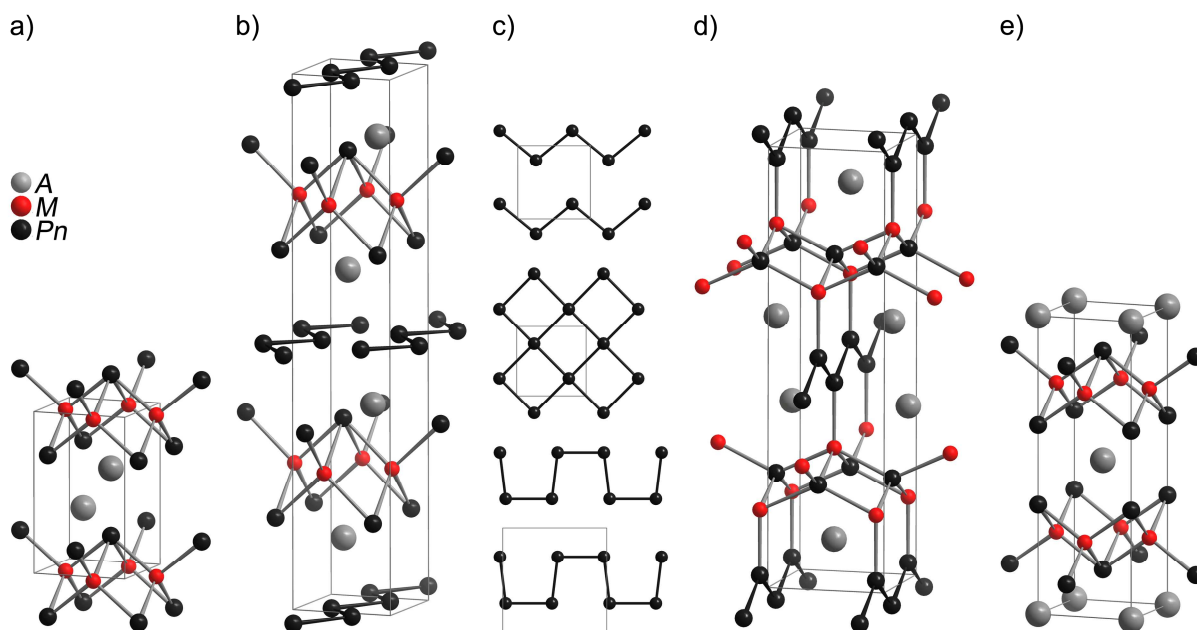


**Figure 1:** Common crystal structures of ternary transition-metal pnictides with 111, 112, and 122 compositions. a)  $AMPn$  (*anti*-PbFCI type), b)  $AMPn_2$  ( $\text{SrZnSb}_2$  type), c) *zigzag*, *netlike*, and *cis-trans* motifs as variants of pnictide layers coplanar to the tetrahedra layers, d)  $AMPn_2$  ( $\text{CeNiSi}_2$  type), and e)  $AM_2Pn_2$  ( $\text{ThCr}_2\text{Si}_2$  type).

The variety of magnetic phenomena among these compounds is hardly without equal. Whereas often *Pauli* paramagnetism is present,  $3d$  and  $4f$  elements can contribute to more apparent physical properties.<sup>[1]</sup> Next to special magnetic states including temperature-dependent behavior, anisotropic properties, and complex phase transitions the outstanding effect of superconductivity occurs in transition-metal pnictides. This extraordinary phenomenon was discovered 1911 by *Kamerlingh Onnes* in his cryogenics laboratory in Leiden<sup>[30]</sup> three years after he managed to liquefy helium.<sup>[31]</sup> In 1913 he was already honored with the *Nobel Prize*, due to the enormous importance his discovery was attributed to.<sup>[32]</sup> By cooling mercury he observed the spontaneous loss of electrical resistivity within a small range of temperature below the critical temperature ( $T_c$ ) of 4.2 K. Therefore he named this new state with *extraordinary electrical properties* the *superconductive state*.<sup>[30]</sup> The second important feature of superconductors was

discovered 1933 by *Meißner* and *Ochsenfeld*.<sup>[33]</sup> Below  $T_c$  the almost complete expulsion of external magnetic fields characterizes superconductors as perfect diamagnets. In contrast to the idea of a perfect conductor the superconducting state is reversible with regard to the chronological order of changing external conditions and was therefore classified as a real thermodynamic state.<sup>[32]</sup> The equations of *London* and *London* combine both basic properties of superconductivity in terms of electrodynamics. As a consequence of the *London* penetration depth the *London* equations confirm the state of perfect diamagnetism within a superconductor, since the magnetic flux density as well as the superconducting current density perpendicular to the magnetic field decrease exponentially from the surface.<sup>[34]</sup> Later *London* expanded the work by considering superconductivity as a macroscopic quantum phenomenon.<sup>[35]</sup> The introduction of a coherence length by *Pippard* led to a non-local generalization of the *London* equations.<sup>[36]</sup> Further progress on the theoretical description of superconductivity were made by *Ginzburg* and *Landau*,<sup>[37]</sup> whose work was later on substantiated by the results of *Gor'kov*.<sup>[38]</sup> Based on that theory *Abrikosov* manifested the differentiation between two types of superconductors and succeeded in the prediction of flux lines within type II superconductors.<sup>[39]</sup> Depending on the behavior in external magnetic fields two types of superconductors have to be discussed. As long as the external field does not exceed the critical field, type I superconductors act as perfect diamagnets (*Meißner* state). Thereover a complete penetration of the magnetic field into the interior of the material occurs. Type II superconductors behave analogue below the first critical field. However, further exposure to higher external fields yield the penetration of magnetic flux vortices each comprising one fluxon (*Shubnikov* state). Meanwhile the remaining material stays superconducting until approaching the upper critical field induces the entire loss of superconductivity.<sup>[40]</sup> As another consequence of the macroscopic quantum state *Josephson* postulated the effect of tunneling *Cooper* pairs between weakly coupled superconductors later implemented in several applications.<sup>[41]</sup> Shortly afterwards his theory was confirmed by *Anderson* and *Rowell*.<sup>[42]</sup>

With their microscopic theory *Bardeen*, *Cooper*, and *Schrieffer* (BCS) developed the first generally accepted model of superconductivity.<sup>[43]</sup> The essence of their work describes phonon mediated attractive interactions between the free conduction electrons to induce the formation of *Cooper* pairs, which was confirmed by the simultaneous experimental evidence of the flux quantization by *Doll* and *Näbauer*<sup>[44]</sup> as well as *Deaver* and *Fairbank*.<sup>[45]</sup> Below the critical temperature these electron pairs are present in a coherent many-body ground state. As a consequence the BCS theory predicted further an energy gap at the *Fermi* level caused by the *Cooper* pair bonding. The importance of quantized lattice vibrations in the scope of

pairing mediation was later demonstrated by the dependency of the critical temperature from the atomic isotope mass.<sup>[46,47]</sup>

Since the discovery of this extraordinary phenomenon not only the theoretical advancement, but also the experimental progress to find appropriate materials was running at all times. For a large number of the pure elements analyses reveal either superconducting properties with the maximum at niobium ( $T_c = 9.25$  K)<sup>[48]</sup> or magnetic ordering at low temperatures for several  $3d$  transition-metals or  $4f$  rare earths.<sup>[32]</sup> Higher critical temperatures were reached with metallic alloys. Especially  $A15$ -type compounds<sup>[49]</sup> feature high critical fields like  $V_3Si$  ( $T_c = 17$  K),<sup>[50]</sup>  $Nb_3Sn$  ( $T_c = 18$  K),<sup>[51]</sup> or  $Nb_3Ge$  ( $T_c = 23$  K)<sup>[52]</sup> being the record holder for many years. In other materials like *Chevrel* phases<sup>[53]</sup> with the prominent representative  $PbMo_6S_8$  ( $T_c = 14$  K)<sup>[54]</sup> and boron carbides like  $YPd_2B_2C$ <sup>[55]</sup> superconductivity occurs, furthermore in potential coexistence with antiferromagnetic ordering. Based on electron phonon interactions highest critical temperatures were measured so far for fullerides ( $T_c = 40$  K)<sup>[56]</sup> and  $MgB_2$  ( $T_c = 39$  K).<sup>[57]</sup> Whereas these conventional superconductors can be described in the scope of the BSC theory, the discovery of high-temperature superconductivity in copper oxides 1986 faced the scientific community with new unforeseen challenges. In the first place *Bednorz* and *Müller* surprisingly measured superconducting properties in oxidic lanthanum barium cuprates with  $T_c = 25$  K.<sup>[58]</sup> Subsequently, further investigations on  $YBa_2Cu_3O_{7-x}$  ( $T_c = 93$  K)<sup>[59]</sup> took its course for liquid nitrogen-compatible critical temperatures. So far highest values were achieved with  $T_c = 138$  K<sup>[60]</sup> under ambient pressure in fluorine doped mercury barium cuprates and  $T_c = 164$  K under quasihydrostatic pressure<sup>[61]</sup> in  $HgBa_2Ca_2Cu_3O_{8+x}$ . While undoped copper oxides are strong magnets and *Mott* insulators with one localized valence electron per copper atom, doping induces superconductivity with a dome-like dependency of the critical temperature from the concentration of substituted charge carriers.<sup>[62]</sup> The formation of *Cooper* pairs in these high-temperature superconductors is under discussion to be affected by magnetic spin fluctuations<sup>[63]</sup> additionally to electron phonon interactions.<sup>[64]</sup> In contrast to the phonon-mediated pairing mechanism of conventional superconductors with  $s$ -wave symmetry, the superconducting order parameter in cuprates shows anisotropic  $d$ -wave symmetry.<sup>[65,66]</sup> The majority of cuprates feature a closely related structural chemistry with only weakly coupled two-dimensional  $CuO_2$  layers responsible for superconductivity.<sup>[67]</sup> In the often perovskite-like or rock-salt-type stacking the geometry of the copper oxide sheets as well as the structural and electronic situation of the interlayers affect the overall magnetic properties. Despite their economically convenient critical temperatures, technical applicability of these ceramics is exceptional challenging due to their intrinsic brittleness. Moreover the

anisotropy of their superconducting properties is the main impediment of cuprates in terms of technical application as wires or coils. Additionally the critical magnetic field ( $H_c$ ) and current density ( $J_c$ ) have to be considered as significant values below which superconductivity occurs. Therefore nowadays especially *A15*-type compounds and niobium titanium alloys are used for applications.

Superconductors are indispensable to generate strong and constant magnetic fields. As the major field of application coils of stabilized superconductors are used for MRI scanners. Moreover particle accelerators and nuclear fusion reactors need appropriate magnetic coils. Cavity resonators, sensitive analytics like SQUID magnetometers based on *Josephson* contacts and NMR instruments as well as various detectors, sensors, or generators are possible fields of utilization. Despite the expensive cooling with liquid helium several industries require the irreplaceable application of superconductors. One day the combination of metallic behavior for technical workability and sufficient critical values for economical purpose could mean a giant stride in development and progress. Therefore even a hundred years after the first discovery of superconductivity scientists around the world still stay with further investigations of potential new materials and the theoretical comprehension of the same. With the *iron boost*<sup>[62]</sup> starting in 2008 this important and intriguing field experienced a renaissance in the research on high-temperature superconductivity. While the class of iron-based superconductors still hesitates by reaching the magic value of 77 K for critical temperatures, other terms for material properties are promising. Next to the indispensable metallic behavior iron pnictides and chalcogenides feature low anisotropy as well as convenient critical field and current density values for technical applications. First pioneering projects are already on its way.<sup>[68]</sup>

All iron-based superconductors share the common structural element of edge-sharing iron-centered  $\text{FeX}_{4/4}$  tetrahedra. The compounds are build up from a coplanar stacking of these tetrahedra layers and optional various implemented interlayers, often derived from long known structure types. As the simplest representative tetragonal iron chalcogenides  $\text{FeSe}_{1-x}\text{Te}_x$ <sup>[69-71]</sup> (*anti*-PbO type) with a maximal critical temperature of  $T_c = 15.2$  K feature exclusively tetrahedra layers. In the class of ternary iron pnictides  $A\text{FeAs}$  with  $A = \text{Li}, \text{Na}$  (*anti*-PbFCl type),<sup>[6,72]</sup>  $\text{Ca}_{1-x}\text{RE}_x\text{FeAs}_2$  with  $\text{RE} = \text{La} - \text{Nd}, \text{Sm} - \text{Gd}$  (modified  $\text{SrZnSb}_2$  type),<sup>[73-75]</sup> and  $A\text{Fe}_2\text{As}_2$  with  $A = \text{Na}, \text{K}, \text{Rb}, \text{Cs}, \text{Ca}, \text{Sr}, \text{Ba}, \text{Eu}$  ( $\text{ThCr}_2\text{Si}_2$  type)<sup>[76-83]</sup> reach critical temperatures of  $T_c = 18$  K in 111-type superconductors,<sup>[72]</sup>  $T_c = 47$  K in multiple doped 112 type compounds,<sup>[84]</sup> and up to  $T_c = 38$  K in hole doped  $\text{Ba}_{1-x}\text{K}_x\text{Fe}_2\text{As}_2$  (122

type).<sup>[85]</sup> High- $T_c$  properties were also obtained in the oxygen containing materials  $REOFeAs$  with  $RE = La - Nd, Sm, Gd$  (ZrCuSiAs type)<sup>[3,86-91]</sup> with record  $T_c = 56\text{ K}$ <sup>[92]</sup> as well as  $AE_2MO_3FeAs$  ( $AE = Sr, Ba; M = Sc, V, Cr$ ) with perovskite-adapted  $Sr_2GaO_3CuS$ -type structure<sup>[93-95]</sup> and  $T_c = 37\text{ K}$ .<sup>[95]</sup> As the most remarkable member  $(CaFeAs)_{10}Pt_3As_8$ <sup>[96,97]</sup> was added in 2011 to this class of high-temperature superconductors with  $T_c = 38\text{ K}$ .<sup>[98]</sup> Due to its two negatively charged metal pnictide layers and unprecedented low crystal symmetry the investigation of  $(CaFeAs)_{10}Pt_3As_8$  contributes to the understanding of the specific characteristics of iron-based superconductors.

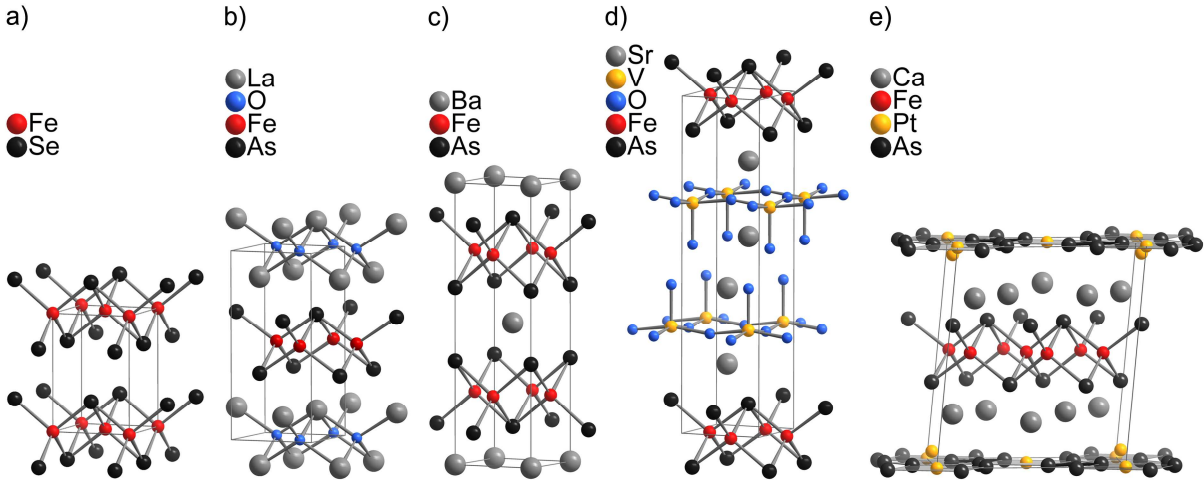


**Figure 2:** Crystal structures of the prominent iron-based superconductors a) FeSe, b) LaOFeAs, c) BaFe<sub>2</sub>As<sub>2</sub>, d) Sr<sub>2</sub>VO<sub>3</sub>FeAs, and e) (CaFeAs)<sub>10</sub>Pt<sub>3</sub>As<sub>8</sub>.

Almost all undoped parent compounds are not superconducting, but poor metals. Upon cooling they pass a correlated structural and magnetic phase transition. The structural distortion leads to a symmetry reduction in the square iron arsenide lattice in a maximal group-subgroup transition. While compounds with tetragonal space groups like LaOFeAs ( $P4/nmm \rightarrow Cmme$ )<sup>[99]</sup> or BaFe<sub>2</sub>As<sub>2</sub> ( $I4/mmm \rightarrow Fmmm$ )<sup>[83]</sup> feature a change of the crystal system, an analogue distortion of the local tetragonal symmetry within the tetrahedral layer takes place in triclinic  $(CaFeAs)_{10}Pt_3As_8$  ( $P\bar{1} \rightarrow P\bar{1}$ ).<sup>[100]</sup> This finding confirmed the distortion of the crucial iron arsenide layer as the decisive point. Therewith accompanied the iron spins arrange in a stripe-type antiferromagnetic order aligned parallel to the longer orthorhombic base axis. Electronic band calculations reveal the stoichiometric materials as magnetic semimetals.<sup>[101]</sup> The two-dimensional character of the *Fermi* surfaces features electron and hole pockets arranged in cylinder-like sheets (Figure 3).<sup>[102]</sup> Instabilities caused by *Fermi* surface nesting are discussed as origin of spin density wave (SDW) ordering<sup>[103]</sup> similar to the cuprates.

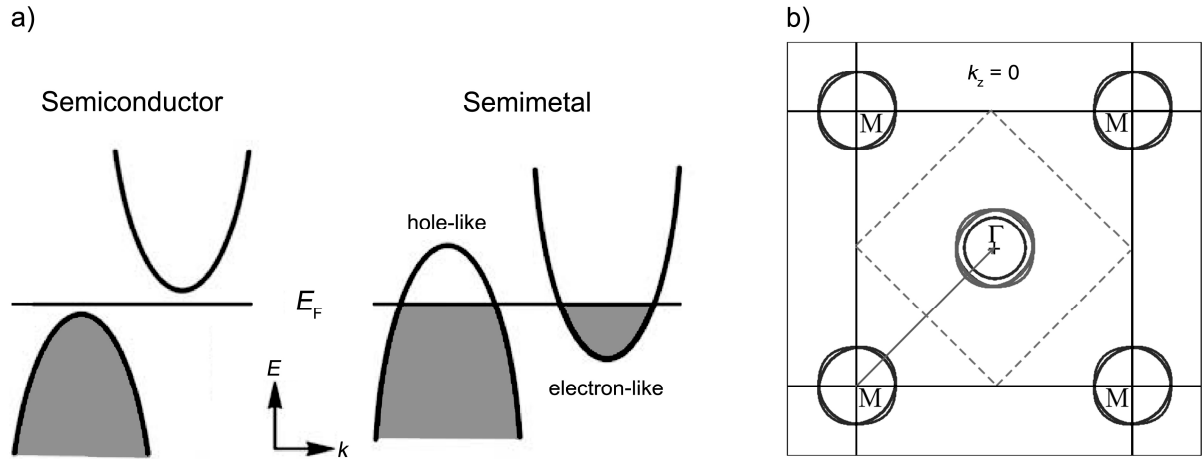


**Figure 3:** a) Schematic electronic structure of a semimetal in one-dimensional  $k$ -space developed from a semiconductor and b)  $Fermi$  surface section of a typical iron-based superconductor at  $k_z = 0$  with cylinder-like shapes around M (electron-like) and  $\Gamma$  (hole-like) points.<sup>[102,103]</sup>

In the last years several scenarios to induce superconductivity in paramagnetic parent compounds were conceived and repeatedly confirmed by experiments. Direct substitution by introducing impurities in the iron layer yields superconductivity with maximal critical temperatures of  $T_c = 24$  K in  $Ba(Fe_{1-x}Co_x)_2As_2$ .<sup>[104]</sup> Charge doping within the interlayers reveals higher values like in hole doped  $Ba_{1-x}K_xFe_2As_2$  ( $T_c = 38$  K)<sup>[85]</sup> or electron doped  $SmFeAsO_{1-x}F_x$  ( $T_c = 56$  K).<sup>[92]</sup> The origin of induced charge carriers was found to be irrelevant comparing two possible variants of electron doping in  $(Ca_{1-y}La_yFeAs)_{10}Pt_3As_8$  and  $(CaFeAs)_{10}Pt_4As_8$ , respectively.<sup>[105,106]</sup> Investigations on co-doped compounds characterized the effects of additional charge carriers as reversible since a retraction of superconducting properties was enabled in  $Ba_{1-y}K_y(Fe_{1-x}Co_x)_2As_2$ <sup>[106]</sup> and  $(Ca_{1-y}Na_yFeAs)_{10}Pt_4As_8$ <sup>[108]</sup> resulting in a return to a parent-like state. Moreover the effect of chemical pressure by the substitution of homologous dopants in  $BaFe_2(As_{1-x}P_x)_2$  ( $T_c = 30$  K)<sup>[109]</sup> or physical pressure like in  $SrFe_2As_2$  ( $T_c = 27$  K) and  $BaFe_2As_2$  ( $T_c = 29$  K)<sup>[110]</sup> are established methods for the manipulation of magnetic properties.

In the words of *Mazin* within the scope of modern superconductor research *materials of interest are likely to be complex chemical compounds* and therefore the work of solid state chemists might be essential for a continuing successful progress.<sup>[62]</sup> The intensive years of research concerning the second age of high-temperature superconductors with so far about 2500 reported articles substantiated iron-centered tetrahedra layers as the key component. Moreover the most versatile structures and properties were obtained by the interaction with calcium indicating the element as the perfect candidate for further investigations. As an unique characteristic the parent compound  $CaFe_2As_2$  features a second, so-called collapsed variant of the

tetragonal structure<sup>[111]</sup> and several possibilities of substitution. High critical temperatures occur in the fascinating class of calcium iron platinum arsenides (1038/ 1048) as well as the recently reported 112-type phases lacking the stoichiometric compound  $\text{CaFeAs}_2$ . Moreover the discovery of  $\text{CaFe}_4\text{As}_3$ <sup>[112]</sup> intrigued the community. In  $\text{CaFe}_4\text{As}_3$  firstly the tetrahedral layers are not arranged in a coplanar stacking structure, but in an interconnected three-dimensional network filled with calcium ions. The field of transition-metal arsenides can draw from an almost unlimited resource of crystal structure types, wherefore the variety of iron arsenide compounds was constantly expanded since the beginning in 2008.

Within this dissertation different calcium iron arsenides were investigated in the context of structural chemistry and superconductivity. The main part focuses on the synthesis and characterization of the palladium compound  $(\text{CaFeAs})_{10}\text{Pd}_3\text{As}_8$  (abbreviated as Pd1038) by analogy with the reported platinum phase. Novel Pd1038 was confirmed by single crystal and powder diffraction as well as various magnetic and electric measurements, interestingly not repeating the expected features of the platinum homolog. The results were supplemented by temperature-dependent analyses of parent-like properties. Series of rare earth doped  $(\text{Ca}_{1-y}\text{RE}_y\text{FeAs})_{10}\text{Pd}_3\text{As}_8$  were studied with varying substituents and concentrations to finesse the specific peculiarities and induce superconductivity (Chapter 2). With regard to the dominant substitution of iron by palladium this scenario was additionally analyzed in Chapter 3 by the targeted doping series of Pt1038 with palladium. Moreover the new compound  $(\text{CaFeAs})_{10}\text{Pd}_4\text{As}_8$  was investigated in terms of polymorphism, crystal structures, and properties (Chapter 4). Chapter 5 is dedicated to  $\text{CaFe}_{1-x}\text{Pd}_x\text{As}_2$ , a newly discovered compound with iron arsenide tetrahedra layers. The crystal structure is discussed with respect to known related structure types and electrical and magnetic analyses are presented. Critical investigations on the properties of recently published  $\text{Ca}_{1-x}\text{Pr}_x\text{FeAs}_2$  are outlined in Chapter 6. A family of newly discovered compounds with interconnected iron arsenide framework structures is introduced in Chapter 7. A systematic structural characterization of this new class and their relation to  $\text{CaFe}_4\text{As}_3$  is given. These results on new iron arsenides impressively extend the structural chemistry of this class emphasizing their structural potential beyond simple layered compounds.

## References

- [1] D. Johrendt, C. Hieke, T. Stürzer, *Comprehensive Inorganic Chemistry II*, Elsevier Ltd., **2013**.
- [2] P. M. Grant, *Nature*, **2008**, *453*, 1000.
- [3] Y. Kamihara, T. Watanabe, M. Hirano, H. Hosono, *J. Am. Chem. Soc.* **2008**, *130*, 3296.
- [4] F. A. Bannister, M. H. Hey, *Mineral. Mag. J. M. Soc.* **1934**, *23*, 587.
- [5] R. Juza, K. Langer, *Z. Anorg. Allg. Chem.* **1968**, *361*, 58.
- [6] D. R. Parker, M. J. Pitcher, P. J. Baker, I. Franke, T. Lancaster, S. J. Blundell, S. J. Clarke, *Chem. Commun.* **2009**, *16*, 2189.
- [7] D. Johrendt, A. Mewis, *J. Alloys Compd.* **1992**, *183*, 210.
- [8] C. B. Shoemaker, D. P. Shoemaker, *Acta Crystallogr.* **1965**, *18*, 900.
- [9] V. Y. Markiv, N. F. Matushevskaya, S. N. Rozum, Y. B. Kuz'ma, *Inorg. Mater.* **1966**, *2*, 1356.
- [10] D. Johrendt, A. Mewis, *Z. Anorg. Allg. Chem.* **1992**, *618*, 30.
- [11] J. W. Nielsen, N. C. Baenziger, *Acta Crystallogr.* **1954**, *7*, 132.
- [12] G. Wenski, A. Mewis, *Z. Anorg. Allg. Chem.* **1986**, *535*, 110.
- [13] G. Wenski, A. Mewis, *Z. Anorg. Allg. Chem.* **1986**, *543*, 49.
- [14] D. Johrendt, A. Mewis, *J. Alloys Compd.* **1994**, *205*, 183.
- [15] E. Brechtel, G. Cordier, H. Schäfer, *Z. Naturforsch. B* **1979**, *34*, 251.
- [16] H. Sprenger, *J. Less-Common Met.* **1974**, *34*, 39.
- [17] R. Demchyna, J. P. Jemetio Feudjio, Y. M. Prots', T. Doert, L. G. Aksel'rud, W. Schnelle, Y. B. Kuz'ma, Y. Grin, *Z. Anorg. Allg. Chem.* **2004**, *630*, 635.
- [18] D. Johrendt, C. Lux, A. Mewis, *Z. Naturforsch. B* **1996**, *51*, 1213.
- [19] O. I. Bodak, E. I. Gladyshevskii, *Inorg. Mater.* **1969**, *5*, 1754.

- [20] G. Venturini, B. Malaman, M. Meot Meyer, D. Fruchart, G. le Caer, D. Malterre, B. Roques, *Rev. Chim. Miner.* **1986**, 23, 162.
- [21] I. Ijjaali, G. Venturini, B. Malaman, *J. Alloys Compd.* **1999**, 282, 153.
- [22] K. Cenzual, R. E. Gladyshevskii, E. Parthe, *Acta Crystallogr. C* **1992**, 48, 225.
- [23] Z. Ban, M. Sikirica, *Acta Crystallogr.* **1965**, 18, 594.
- [24] P. Klüfers, A. Mewis, *Z. Naturforsch. B* **1978**, 33, 151.
- [25] B. Eisenmann, N. May, W. Müller, H. Schäfer, *Z. Naturforsch. B* **1972**, 27, 1155.
- [26] E. I. Gladyshevskii, P. I. Kripyakevich, O. I. Bodak, *Ukr. Phys. J.* **1967**, 12, 447.
- [27] A. Mewis, *Z. Naturforsch. B* **1984**, 39, 713.
- [28] O. F. Zmii, E. I. Gladyshevskii, *Kristallografiya* **1970**, 15, 939.
- [29] A. Mewis, *Z. Anorg. Allg. Chem.* **1986**, 536, 7.
- [30] H. Kamerlingh Onnes, *Commun. Phys. Lab. Univ. Leiden* **1911**, 120b.
- [31] H. Kamerlingh Onnes, *Proc. Roy. Acad. Amsterdam* **1908**, 11, 168.
- [32] R. Gross, A. Marx, *Festkörperphysik*, Oldenbourg, München, **2012**.
- [33] W. Meißner, R. Ochsenfeld, *Naturwissenschaften* **1933**, 21, 787.
- [34] F. London, H. London, *Proc. Roy. Soc. Lond. A* **1935**, 149, 71.
- [35] F. London, *Superfluids*, Wiley, New York, **1950**.
- [36] A. B. Pippard, *Proc. Roy. Soc. London A* **1953**, 216, 547.
- [37] V. L. Ginzburg, L. D. Landau, *Zh. Eksperim. Teor. Fiz.* **1950**, 20, 1064.
- [38] L. P. Gor'kov, *Zh. Eksperim. Teor. Fiz.* **1959**, 36, 1918.
- [39] A. A. Abrikosov, *Zh. Eksperim. Teor. Fiz.* **1957**, 32, 1141.
- [40] J. N. Rjabinin, L. W. Shubnikov, *Phys. Z. Sowjetunion* **1935**, 7, 122.
- [41] B. D. Josephson, *Phys. Lett.* **1962**, 1, 251.
- [42] P. W. Anderson, J. M. Roswell, *Phys. Rev. Lett.* **1963**, 10, 230.

- [43] J. Bardeen, L. N. Cooper, J. R. Schrieffer, *Phys. Rev.* **1957**, *106*, 162.
- [44] R. Doll, M. Näbauer, *Phys. Rev. Lett.* **1961**, *7*, 51.
- [45] B. S. Deaver Jr., W. M. Fairbank, *Phys. Rev. Lett.* **1961**, *7*, 43.
- [46] C. A. Reynolds, B. Serin, W. H. Wright, L. B. Nesbitt, *Phys. Rev.* **1950**, *78*, 487.
- [47] E. Maxwell, *Phys. Rev.* **1950**, *78*, 477.
- [48] D. K. Finnemore, T. F. Stromberg, C. A. Swenson, *Phys. Rev.* **1966**, *149*, 231.
- [49] H. Hartmann, F. Ebert, O. Bretschneider, *Z. Allg. Anorg. Chem.* **1931**, *198*, 116.
- [50] G. F. Hardy, J. K. Hulm, *Phys. Rev.* **1954**, *93*, 1004.
- [51] B. T. Matthias, T. H. Geballe, S. Geller, E. Corenzwit, *Phys. Rev.* **1954**, *95*, 1435.
- [52] J. R. Gavaler, *Appl. Phys. Lett.* **1973**, *23*, 480.
- [53] R. Chevrel, M. Sergent, J. Prigent, *J. Solid State Chem.* **1971**, *3*, 515.
- [54] J. A. Woollam, S. A. Alterovitz, *Phys. Rev. B* **1979**, *19*, 749.
- [55] R. J. Cava, H. Takagi, B. Batlogg, H. W. Zandbergen, J. J. Krajewski, W. F. Peck, R. B. van Dover, R. J. Felder, T. Siegrist, K. Mizuhashi, J. O. Lee, H. Eisaki, S. A. Carter, S. Uchida, *Nature* **1994**, *367*, 146.
- [56] C. H. Pennington, V. A. Stenger, *Rev. Mod. Phys.* **1996**, *68*, 855.
- [57] J. Nagamatsu, N. Nakagawa, T. Muranaka, Y. Zenitani, J. Akimitsu, *Nature* **2001**, *410*, 63.
- [58] J. G. Bednorz, K. A. Müller, *Z. Phys. B* **1986**, *64*, 189.
- [59] M. K. Wu, J. R. Ashburn, C. T. Torng, P. H. Hor, R. L. Meng, L. Gao, Z. J. Huang, Y. Q. Wang, C. W. Chu, *Phys. Rev. Lett.* **1987**, *58*, 908.
- [60] S. N. Putilin, E. V. Antipov, A. M. Abakumov, M. G. Rozova, K. A. Lokshin, D. A. Pavlov, A. M. Balagurov, D. V. Sheptyakov, M. Marezio, *Physica C* **2001**, *338*, 52.
- [61] L. Gao, Y. Y. Xue, F. Chen, Q. Xiong, R. L. Meng, D. Ramirez, C. W. Chu, J. H. Eggert, H. K. Mao, *Phys. Rev. B* **1994**, *50*, 4260(R).

- [62] I. I. Mazin, *Nature* **2010**, *464*, 183.
- [63] P. Monthoux, A. V. Balatsky, D. Pines, *Phys. Rev. Lett.* **1991**, *67*, 3448.
- [64] R. H. Liu, T. Wu, G. Wu, H. Chen, X. F. Wang, Y. L. Xie, J. J. Ying, Y. J. Yan, Q. J. Li, B. C. Shi, W. S. Chu, Z. Y. Wu, X. H. Chen, *Nature* **2009**, *459*, 64.
- [65] P. Monthoux, A. V. Balatsky, D. Pines, *Phys. Rev. B* **1992**, *46*, 14803.
- [66] C. C. Tsuei, J. R. Kirtley, *Rev. Mod. Phys.* **2000**, *72*, 969.
- [67] C. Park, R. L. Snyder, *Appl. Supercond.* **1995**, *3*, 73.
- [68] K. Tanabe, H. Hosono, *Jpn. J. Appl. Phys.* **2012**, *51*, 010005.
- [69] G. Hägg, A. L. Kindström, *Z. Phys. Chem. (Abt. B)* **1933**, *22*, 453.
- [70] F.-C. Hsu, J.-Y. Luo, K.-W. Yeh, T.-K. Chen, T.-W. Huang, P. M. Wu, Y.-C. Lee, Y.-L. Huang, Y.-Y. Chu, D.-C. Yan, M.-K. Wu, *Proc. Natl. Acad. Sci.* **2008**, *105*, 14262.
- [71] K.-W. Yeh, T.-W. Huang, Y.-I. Huang, T.-K. Chen, F.-C. Hsu, P. M. Wu, Y.-C. Lee, Y.-Y. Chu, C.-L. Chen, J.-Y. Luo, D.-C. Yan, M.-K. Wu, *Europhys. Lett.* **2008**, *84*, 37002.
- [72] J. H. Tapp, Z. Tang, B. Lv, K. Sasmal, B. Lorenz, P. C. W. Chu, A. M. Guloy, *Phys. Rev. B* **2008**, *78*, 060505(R).
- [73] N. Katayama, K. Kudo, S. Onari, T. Mizukami, K. Sugawara, Y. Kitahama, K. Iba, K. Fujimura, N. Nishimoto, M. Nohara, H. Sawa, *J. Phys. Soc. Jpn.* **2013**, *82*, 123702.
- [74] H. Yakita, H. Ogino, T. Okada, A. Yamamoto, K. Kishio, T. Tohei, Y. Ikuhara, Y. Gotoh, H. Fujihisa, K. Kataoka, H. Eisaki, J. Shimoyama, *J. Am. Chem. Soc.* **2014**, *136*, 846.
- [75] A. Sala, H. Yakita, H. Ogino, T. Okada, A. Yamamoto, K. Kishio, S. Ishida, A. Iyo, H. Eisaki, M. Fujioka, Y. Takano, M. Putti, J. Shimoyama, *Appl. Phys. Express* **2014**, *7*, 073102.
- [76] R. Marchand, W. Jeitschko, *J. Solid State Chem.* **1978**, *24*, 351.
- [77] M. Pfisterer, G. Nagorsen, *Z. Naturforsch.* **1980**, *35*, 703.

- [78] G. M. Friederichs, I. Schellenberg, R. Pöttgen, V. Duppel, L. Kienle, J. Schmedt auf der Günne, D. Johrendt, *Inorg. Chem.* **2012**, *51*, 8161.
- [79] K. Sasmal, B. Lv, B. Lorenz, A. Guloy, F. Chen, Y. Xue, C. W. Chu, *Phys. Rev. Lett.* **2008**, *101*, 107007.
- [80] M. Aftabuzzaman, A. K. M. A. Islam, *Physica C* **2010**, *470*, 202.
- [81] F. Ronning, T. Klimczuk, E. D. Bauer, H. Volz, J. D. Thompson, *J. Phys.: Condens. Matter* **2008**, *20*, 322201.
- [82] M. Tegel, M. Rotter, V. Weiss, F. M. Schappacher, R. Pöttgen, D. Johrendt, *J. Phys.: Condens. Matter* **2008**, *20*, 452201.
- [83] M. Rotter, M. Tegel, I. Schellenberg, W. Hermes, R. Pöttgen, D. Johrendt, *Phys. Rev. B* **2008**, *78*, 020503(R).
- [84] K. Kudo, Y. Kitahama, K. Fujimura, T. Mizukami, H. Ota, M. Nohara, *J. Phys. Soc. Jpn.* **2014**, *83*, 093705.
- [85] M. Rotter, M. Tegel, D. Johrendt, *Phys. Rev. Lett.* **2008**, *101*, 107006.
- [86] P. Quebe, L. J. Terbüchte, W. Jeitschko, *J. Alloys Compd.* **2000**, *302*, 70.
- [87] G. F. Chen, Z. Li, D. Wu, G. Li, W. Z. Hu, J. Dong, P. Zheng, J. L. Luo, N. L. Wang, *Phys. Rev. Lett.* **2008**, *100*, 247002.
- [88] Z.-A. Ren, J. Yang, W. Lu, W. Yi, G.-C. Che, X.-L. Dong, L.-L. Sun, Z.-X. Zhao, *Mater. Res. Innov.* **2008**, *12*, 105.
- [89] Z.-A. Ren, J. Yang, W. Lu, W. Yi, X.-L. Shen, Z.-C. Li, G.-C. Che, X.-L. Dong, L.-L. Sun, F. Zhou, Z.-X. Zhao, *Europhys. Lett.* **2008**, *82*, 57002.
- [90] Z.-A. Ren, W. Lu, J. Yang, W. Yi, X.-L. Shen, Z.-C. Li, G.-C. Che, X.-L. Dong, L.-L. Sun, F. Zhou, Z.-X. Zhao, *Chin. Phys. Lett.* **2008**, *25*, 2215.
- [91] G. F. Chen, Z. Li, D. Wu, J. Dong, G. Li, W. Z. Hu, P. Zheng, J. L. Luo, N. L. Wang, *Chin. Phys. Lett.* **2008**, *25*, 2235.
- [92] G. Wu, Y. L. Xie, H. Chen, M. Zhong, R. H. Liu, B. C. Shi, Q. J. Li, X. F. Wang, T. Wu, Y. J. Yan, J. J. Ying, X. H. Chen, *J. Phys.: Condens. Matter* **2009**, *21*, 142203.

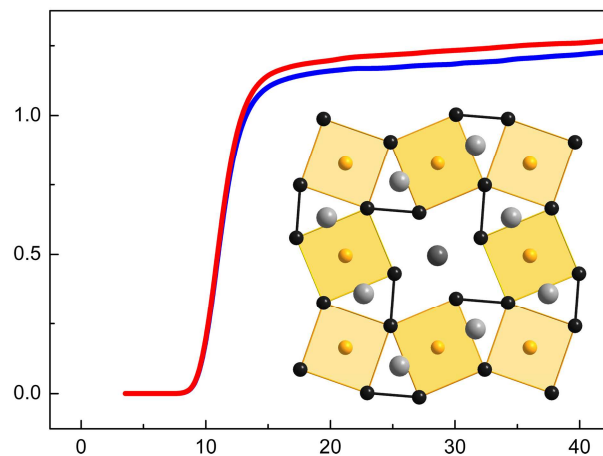
- [93] H. Ogino, Y. Katsura, S. Horii, K. Kishio, J. Shimoyama, *Supercond. Sci. Technol.* **2009**, *22*, 085001.
- [94] M. Tegel, F. Hummel, S. Lackner, I. Schellenberg, R. Pöttgen, D. Johrendt, *Z. Anorg. Allg. Chem.* **2009**, *635*, 2242.
- [95] X. Zhu, F. Han, G. Mu, P. Cheng, B. Shen, B. Zeng, H.-H. Wen, *Phys. Rev. B* **2008**, *79*, 220512(R).
- [96] C. Löhnert, T. Stürzer, M. Tegel, R. Frankovsky, G. Friederichs, D. Johrendt, *Angew. Chem. Int. Ed.* **2011**, *50*, 9195.
- [97] N. Ni, J. M. Allred, B. C. Chan, R. J. Cava, *Proc. Natl. Acad. Sci* **2011**, *108*, E1019.
- [98] S. Kakiya, K. Kudo, Y. Nishikubo, K. Oku, E. Nishibori, H. Sawa, T. Yamamoto, T. Nozaka, M. Nohara, *J. Phys. Soc. Jpn.* **2011**, *80*, 093704.
- [99] T. Nomura, S. W. Kim, Y. Kamihara, M. Hirano, P. V. Sushko, K. Kato, M. Takata, A. L. Shluger, H. Hosono, *Supercond. Sci. Technol.* **2008**, *21*, 125028.
- [100] T. Stürzer, G. M. Friederichs, H. Luetkens, A. Amato, H.-H. Klauss, D. Johrendt, *J. Phys.: Condens. Matter* **2013**, *25*, 122203.
- [101] F. Ma, Z.-Y. Lu, *Phys. Rev. B* **2008**, *78*, 033111.
- [102] D. Johrendt, *J. Mater. Chem.* **2011**, *21*, 13726.
- [103] J. Dong, H. J. Zhang, G. Xu, Z. Li, G. Li, W. Z. Hu, D. Wu, G. F. Chen, X. Dai, J. L. Luo, Z. Fang, N. L. Wang, *Europhys. Lett.* **2008**, *83*, 27006.
- [104] J.-H. Chu, J. G. Analytis, C. Kucharczyk, I. R. Fisher, *Phys. Rev. B* **2009**, *79*, 014506.
- [105] T. Stürzer, G. Derondeau, D. Johrendt, *Phys. Rev. B* **2012**, *86*, 060516(R).
- [106] T. Stürzer, G. Derondeau, D. Johrendt, *Solid State Commun.* **2015**, *201*, 36.
- [107] V. Zinth, T. Dellmann, H.-H. Klauss, D. Johrendt, *Angew. Chem. Int. Ed.* **2011**, *50*, 7919.
- [108] T. Stürzer, *Dissertation*, LMU München, **2015**.
- [109] M. Rotter, C. Hieke, D. Johrendt, *Phys. Rev. B* **2010**, *82*, 014513.

- [110] P. L. Alireza, Y. T. C. Ko, J. Gillett, C. M. Petrone, J. M. Cole, S. E. Sebastian, G. G. Lonzarich, *J. Phys.: Condens. Matter* **2008**, *21*, 012208.
- [111] A. Kreyssig, M. A. Green, Y. Lee, G. D. Samolyuk, P. Zajdel, J. W. Lynn, S. L. Bud'ko, M. S. Torikachvili, N. Ni, S. Nandi, J. Leao, S. J. Poulton, D. N. Argyriou, B. N. Harmon, P. C. Canfield, R. J. McQueeney, A. I. Goldman, *Phys. Rev. B* **2008**, *78*, 184517.
- [112] I. Todorov, D. Y. Chung, C. D. Malliakas, Q. A. Li, T. Bakas, A. Douvalis, G. Trimarchi, K. Gray, J. F. Mitchell, A. J. Freeman, M. G. Kanatzidis, *J. Am. Chem. Soc.* **2009**, *131*, 5405.

## 2 New Palladium Iron Arsenides $(\text{CaFeAs})_{10}\text{Pd}_3\text{As}_8$

### 2.1 Superconductivity and Crystal Structure of the Palladium Iron Arsenides $(\text{CaFe}_{1-x}\text{Pd}_x\text{As})_{10}\text{Pd}_3\text{As}_8$

C. Hieke, J. Lippmann, T. Stürzer, G. Friederichs, F. Nitsche, F. Winter, R. Pöttgen, D. Johrendt



**published in:** *Philos. Mag.* **2013**, *93*, 3680 – 3689.

Copyright 2013, Taylor & Francis.

#### Abstract

The palladium iron arsenides  $(\text{CaFe}_{1-x}\text{Pd}_x\text{As})_{10}\text{Pd}_3\text{As}_8$  were synthesized by solid state methods and characterized by X-ray powder and single crystal diffraction. The triclinic crystal structure (space group  $P\bar{1}$ ) is isotypic to the homologous platinum 1038-type superconductors with alternating  $\text{FeAs}_{4/4}$  and  $\text{Pd}_3\text{As}_8$  layers, each separated by layers of calcium atoms. Iron is tetrahedral and palladium is planar coordinated by four arsenic atoms.  $\text{As}_2$  dimers ( $d_{\text{As-As}} \approx 250$  pm) are present in the  $\text{Pd}_3\text{As}_8$  layer. Even though each layer itself has a fourfold rotational symmetry, the shifted layer stacking causes the triclinic space group. Resistivity measurements of La doped samples show the onset of superconductivity at 17 K and zero resistivity below 10 K. The magnetic shielding fraction is about 20 % at 3.5 K.  $^{57}\text{Fe}$ -Mössbauer spectra exhibit one absorption line and show no hint to magnetic ordering. The electronic structure is very similar to the known iron arsenides with cylinder-like FS and partial nesting between hole- and electron-like sheets. Our results show that superconductivity in the palla-

dium iron compounds is present but complicated by too high substitution of iron by palladium in the active FeAs layers. Since the electronic preconditions are satisfied, we expect higher critical temperatures of Pd1038 materials with low or even without Pd doping in the FeAs layer.

### 2.1.1 Introduction

Iron arsenide and iron selenide materials represent a new class of high- $T_c$  superconductors beyond the copper oxides.<sup>[1,2]</sup> Both materials have layer-like crystal structures, where the active layers are  $\text{CuO}_2$  or  $\text{FeX}$  ( $X = \text{As}, \text{Se}$ ), respectively. Superconductivity emerges in these active layers in the proximity of antiferromagnetic ordering that becomes suppressed by doping. It is widely accepted that the pairing in copper oxides and iron arsenides is unconventional, and many recent results indicate that magnetic fluctuations play a fundamental role.<sup>[3]</sup>

Considering the fact that superconductivity develops in  $\text{CuO}_2$  or  $\text{FeX}$  layers, the large variations of the critical temperatures in compounds with different crystal structures yet the same active layers are as remarkable as poorly understood. It is obvious that the surrounding part of the crystal structure plays a crucial role beyond the function as charge reservoir. However, a more detailed understanding has yet to be achieved.

Until 2011 the family of iron arsenide superconductors consisted of compounds with relatively simple and well known types of crystal structures, mostly variants of the  $\text{PbFCI}$  and  $\text{ThCr}_2\text{Si}_2$  types. Therein, the negatively charged FeAs layers are separated and charge balanced by layers of alkaline or alkaline earth ions like in  $\text{BaFe}_2\text{As}_2$  or  $\text{NaFeAs}$ , or by positively charged layers of rare earth oxide like in  $\text{LaOFeAs}$ . A certain expansion provided the compounds where the FeAs layers are separated by thicker perovskite-like oxide blocks as in  $\text{Sr}_2\text{VO}_3\text{FeAs}$ ,<sup>[4]</sup> which is isostructural to the copper sulphide  $\text{Sr}_2\text{GaO}_3\text{CuS}$ . All these separating layers are itself insulating or semiconducting. By combination with the metallic FeAs layer the *Fermi* surface remains unaffected, as soon as the *Fermi* level remains in the gap of electronic states of the separating layers. This is always the case if the gap is large enough (as it usually is in oxides), and naturally if the separating layers consist only of very electropositive alkaline or alkaline earth atoms.

Recently new iron-based superconductors were found where the FeAs layers are separated by calcium atoms and semiconducting negatively charged platinum arsenide layers.<sup>[5-7]</sup> The compounds  $(\text{CaFeAs})_{10}\text{Pt}_3\text{As}_8$  (referred to as 1038) and  $(\text{CaFeAs})_{10}\text{Pt}_4\text{As}_8$  (referred to as 1048)

exhibit superconductivity up to 38 K and have raised the chemical and structural complexity of the iron arsenide family. Recently we have shown that triclinic  $(\text{CaFeAs})_{10}\text{Pt}_3\text{As}_8$  is the non-superconducting and magnetically ordered parent compound of these materials.<sup>[8]</sup> Superconductivity can be induced by Pt doping of the FeAs layers ( $(\text{CaFe}_{1-x}\text{Pt}_x\text{As})_{10}\text{Pt}_3\text{As}_8$ ,  $T_c \leq 15$  K) or by electron doping either via La substitution ( $(\text{Ca}_{1-y}\text{La}_y\text{FeAs})_{10}\text{Pt}_3\text{As}_8$ ,  $T_c \approx 35$  K) or by charge transfer from the platinum arsenide layer ( $(\text{CaFeAs})_{10}\text{Pt}_4\text{As}_8$ ,  $T_c \approx 38$  K).<sup>[9]</sup> Already from the relatively high critical temperatures one may assume that the *Fermi* surface (FS) originates from the FeAs layers and is scarcely affected by states from the platinum arsenide layers. This is supported by band structure calculations,<sup>[5]</sup> photoemission experiments,<sup>[10]</sup> and specific heat data.<sup>[11]</sup> In other words, the *Fermi* energy of the metallic FeAs layer lies just in the small gap of the semiconducting  $\text{Pt}_3\text{As}_8$  layer. This is inherently remarkable, and moreover on precondition for the high critical temperatures which are believed to be tied to a special FS topology generated by the FeAs layer alone.

In face of this special situation, one might assume that the  $(\text{CaFeAs})_{10}\text{Pt}_3\text{As}_8$ -type superconductors (Pt1038) are rather unique and possibly intolerant against substitution of the  $\text{Pt}_z\text{As}_8$  layers. In this letter we show that this is not the case, and report the synthesis, crystal structure, superconducting properties, and electronic structure of the palladium iron arsenides  $(\text{CaFe}_{1-x}\text{Pd}_x\text{As})_{10}\text{Pd}_3\text{As}_8$  referred to as Pd1038 compounds.

## 2.1.2 Results and Discussion

### 2.1.2.1 Synthesis and Crystal Structure

Polycrystalline samples of the palladium iron arsenides were synthesized by solid state methods. Stoichiometric mixtures of pure elements ( $> 99.5$  %) were heated at 1000 °C in alumina crucibles sealed in silica tubes under purified argon. X-ray powder patterns were similar to the Pt1038 compounds suggesting an isotopic crystal structure. In order to confirm this, a small single crystal ( $12 \times 5 \times 1 \mu\text{m}^3$ ) was selected for X-ray single crystal structure determination. Reflection data processing and structure refinement turned out difficult due to diffuse scattering along the stacking direction, and additionally to partial merohedral twinning. Structure refinement was successful in space group  $P\bar{1}$  by using four twin domains with the JANA program package.<sup>[12]</sup> The tetragonal layer symmetry of the FeAs and  $\text{Ca}_{10}\text{Pd}_3\text{As}_8$  substructures is reduced to inversion in the 3D arrangement due to mismatched stacking. The square basal plane of the triclinic cell ( $a = b$ ,  $\gamma = 90^\circ$ ) still reflects the tetragonal motifs of the

layers. As a consequence, partial merohedral twinning occurs where reflections of all domains with  $2h + k = 5n$  coincide. Results of the crystal structure refinement are compiled in Table 1 together with selected interatomic distances and angles within the Fe<sub>1-x</sub>Pd<sub>x</sub>As and Pd<sub>3</sub>As<sub>8</sub> layers.

The crystal structure of (CaFe<sub>0.84</sub>Pd<sub>0.16</sub>As)<sub>10</sub>Pd<sub>2.8</sub>As<sub>8</sub> is depicted in Figure 1. The bond lengths within the tetrahedral Fe<sub>1-x</sub>Pd<sub>x</sub>As layers (red tetrahedra) match with typical values around 240 pm known from other iron arsenide superconductors.<sup>[13,14]</sup> However, we observe slightly longer distances up to 247 pm if the palladium doping level at the iron sites increases. The bond angles within the tetrahedra are all close to the ideal value of 109.4 ° which is believed favorable for high critical temperatures.<sup>[15]</sup> The Pd<sub>3</sub>As<sub>8</sub> layer consists of corner-sharing PdAs<sub>4/4</sub> squares where the arsenic atoms form As<sub>2</sub> dimers with As–As bond lengths of 248 and 250 pm, which is slightly longer than twice the covalent radius of arsenic that is 242 pm.<sup>[16]</sup>

**Table 1:** Crystal data and structure refinement for Pd1038, space group  $P\bar{1}$ ,  $Z = 1$ .

|   |  |
|---|--|
| Empirical formula                                   | (CaFe <sub>0.84</sub> Pd <sub>0.16</sub> As) <sub>10</sub> Pd <sub>2.8</sub> As <sub>8</sub>   |
| Molar mass  | 2685.5 g mol <sup>-1</sup>   |
| Unit cell dimensions<br>(single crystal)            | $a = 880.0(1)$ pm<br>$b = 880.0(1)$ pm<br>$c = 1060.3(2)$ pm<br>$\alpha = 85.271(2)$ °<br>$\beta = 75.561(2)$ °<br>$\gamma = 90.003(6)$ °<br>$V = 0.7922(1)$ nm <sup>3</sup> |
| Calculated density                                  | 5.63 g cm <sup>-3</sup>  |
| Crystal size  | 12 × 5 × 1 μm <sup>3</sup>   |
| Wave length   | 71.073 pm (Mo-K $\alpha$ )   |
| Transmission ratio (max / min)                      | 0.1341 / 0.0229  |
| Absorption coefficient                              | 26.45 mm <sup>-1</sup>   |
| Θ range   | 1.99 - 30.31 °   |
| Range in $hkl$                                      | ± 12, ± 12, ± 15   |
| Total number reflections                            | 121430   |
| Independent reflections / $R_{\text{int}}$          | 27887 / 0.1369   |
| Reflections with $I \geq 3\sigma(I)$ / $R_{\sigma}$ | 7090 / 0.1239  |
| Data / parameters                                   | 7090 / 147   |
| Goodness-of-fit on $F$                              | 4.29   |
| $R1$ / $wR2$ for $I \geq 3\sigma(I)$                | 0.0883 / 0.986   |
| $R1$ / $wR2$ for all data                           | 0.0883 / 0.986   |
| Largest diff. peak / hole                           | 8.82 / -3.43 e Å <sup>-3</sup>   |

## Interatomic distances and angles

 Fe<sub>1-x</sub>Pd<sub>x</sub>As layer

$$d_{(\text{Fe/Pd-As})} = 237.3(4) - 247.5(4) \text{ pm}$$

$$\angle_{(\text{As-Fe/Pd-As})} = 107.9(4) - 110.1(4)^\circ$$

 Pd<sub>3</sub>As<sub>8</sub> layer

$$d_{(\text{Pd-As})} = 235.0(2) - 258.6(2) \text{ pm}$$

$$d_{(\text{As-As})} = 248.5(2), 250.6(2) \text{ pm}$$

$$\angle_{(\text{As-Pd-As})} = 85.2(5) - 94.8(5)^\circ$$

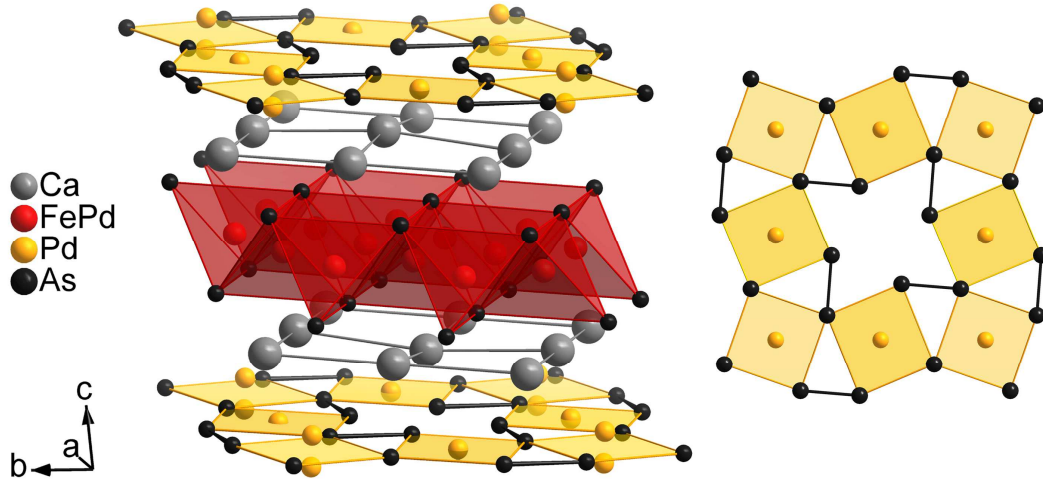


**Figure 1:** Crystal structure of (CaFe<sub>0.84</sub>Pd<sub>0.16</sub>As)<sub>10</sub>Pd<sub>2.8</sub>As<sub>8</sub>. Left: Stacking of the active Fe<sub>1-x</sub>Pd<sub>x</sub>As with the Pd<sub>3</sub>As<sub>8</sub> layers, each separated by calcium atoms. Right: View of the Pd<sub>3</sub>As<sub>8</sub> layer emphasizing the square coordination of palladium and the As<sub>2</sub> dimers.

By assuming an idealized composition (CaFeAs)<sub>10</sub>Pd<sub>3</sub>As<sub>8</sub> and typical oxidation states, we arrive at the charge balanced formula Ca<sub>10</sub><sup>2+</sup>(Fe<sup>2+</sup>As<sup>3-</sup>)<sub>10</sub>(Pd<sub>3</sub><sup>2+</sup>As<sub>8</sub><sup>2-</sup>). The charge of the arsenic atoms in the Pd<sub>3</sub>As<sub>8</sub> layer is 2- due to the homonuclear bonds of the As<sub>2</sub> dimers, thus the parent Pd1038 phase ranks among the *Zintl* phases. Note that the iron arsenide layer in (CaFeAs)<sub>10</sub>Pd<sub>3</sub>As<sub>8</sub> carries one negative charge exactly as the known parent compounds LaOFeAs, BaFe<sub>2</sub>As<sub>2</sub>, or NaFeAs. So far we were not able to synthesize the pure parent compound without Pd substitution at the iron site. Furthermore the single crystal structure refinement indicated a small Pd deficiency in the Pd<sub>3</sub>As<sub>8</sub> layer according to Pd<sub>2.8</sub>As<sub>8</sub>. Initially the homogeneity of polycrystalline samples was rather poor, but could be improved by additional La doping at the Ca position. This effect was known from the Pt1038 compounds and is probably caused by the increased lattice energy if La<sup>3+</sup> ions replace the lower charged Ca<sup>2+</sup> ions at certain positions.<sup>[9]</sup> Figure 2 shows the X-ray powder pattern and Rietveld refinement (program TOPAS<sup>[17]</sup>) of a La doped sample with composition (Ca<sub>0.92</sub>La<sub>0.08</sub>Fe<sub>0.86</sub>Pd<sub>0.14</sub>As)<sub>10</sub>Pd<sub>2.8</sub>As<sub>8</sub>. This profile fit bases on the structural data obtained from the single crystal experiment, and attests a polycrystalline sample of the La doped Pd1038 phase with a minor impurity of FeAs ( $\approx 10\%$ ).

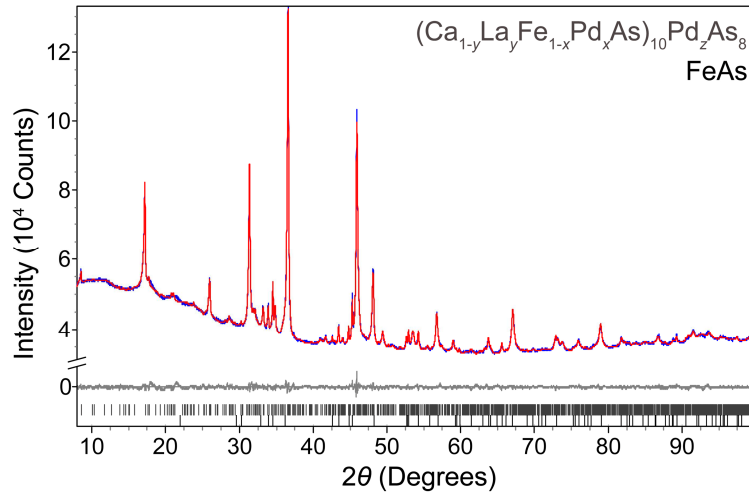


**Figure 2:** X-ray diffraction pattern (blue) and Rietveld fit (red) of  $(\text{Ca}_{0.92}\text{La}_{0.08}\text{Fe}_{0.86}\text{Pd}_{0.14}\text{As})_{10}\text{Pd}_{2.8}\text{As}_8$  ( $P\bar{1}$ ,  $a = 880.57(3)$  pm,  $b = 881.34(2)$  pm,  $c = 1063.9(3)$  pm,  $\alpha = 85.239(1)^\circ$ ,  $\beta = 75.653(2)^\circ$ ,  $\gamma = 89.879(2)^\circ$ ,  $R_{\text{wp}} = 0.0086$ ).

### 2.1.2.2 Resistivity and Magnetic Susceptibility

Figure 3 shows the dc-resistivity of the La doped Pd1038 sample. The cold pressed pellet reveals the onset of a superconducting transition at 17 K while zero resistivity is achieved below 10 K. This is in agreement with the ac-susceptibility measurement shown in the inset. The shielding fraction is about 20 % at 3.5 K and not fully developed at this temperature. Thus we expect larger shielding fractions at lower temperatures according to bulk superconductivity. The rather broad superconducting transition together with the weak shielding is very probable a consequence of inhomogeneous distribution of the different dopants. This is not surprising because a homogeneous distribution of Ca/La and Fe/Pd substitution together with Pd deficiency in the  $\text{Pd}_3\text{As}_8$  layer is certainly hard to achieve. Nevertheless our results prove that superconductivity emerges in the Pd1038 compound even though the critical temperature is still lower when compared with the Pt1038 materials. We actually would not expect superconductivity if the composition is  $(\text{Ca}_{0.92}\text{La}_{0.08}\text{Fe}_{0.86}\text{Pd}_{0.14}\text{As})_{10}\text{Pd}_{2.8}\text{As}_8$  throughout the sample. From the phase diagrams of  $\text{Ba}(\text{Fe}_{1-x}\text{Pd}_x)_2\text{As}_2$ <sup>[18]</sup> and the Pt1038 compounds  $(\text{CaFe}_{1-x}\text{Pt}_x\text{As})_{10}\text{Pt}_3\text{As}_8$ <sup>[9,19]</sup> we know that superconductivity is induced by Pd or Pt doping, but only at low doping levels up to about 8 %. On the other hand, we have shown that superconductivity in the Pt1038 phase can be induced by La doping if Pt doping at the Fe site is absent.<sup>[9]</sup> Thus our results suggest that the sample contains fractions where the Pd substitution is low enough to allow superconductivity, which also explains the reduced shielding fraction.

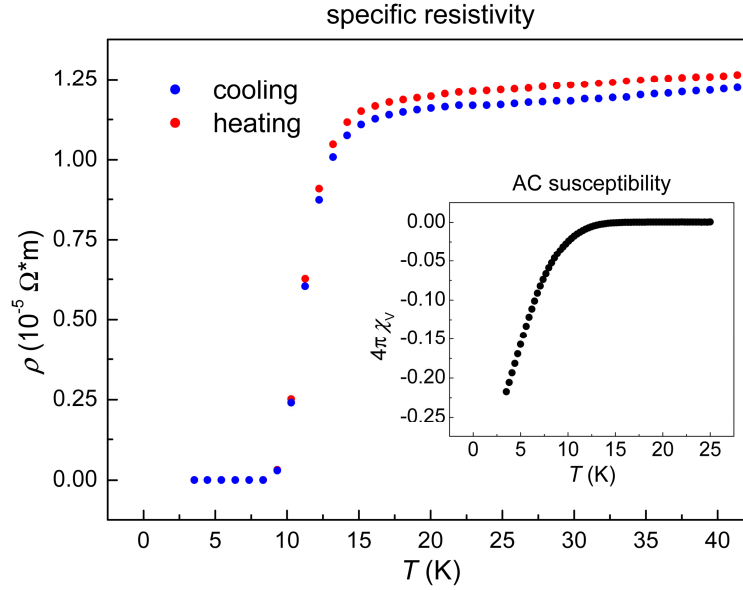


**Figure 3:** Dc-resistivity of polycrystalline  $(\text{Ca}_{0.92}\text{La}_{0.08}\text{Fe}_{0.86}\text{Pd}_{0.14}\text{As})_{10}\text{Pd}_{2.8}\text{As}_8$ . Insert: Ac-susceptibility measured at 3 Oe and 1333 Hz.

### 2.1.2.3 $^{57}\text{Fe}$ -Mössbauer Spectroscopy

The  $^{57}\text{Fe}$ -Mössbauer spectra for the  $(\text{Ca}_{0.87}\text{La}_{0.13}\text{Fe}_{0.86}\text{Pd}_{0.14}\text{As})_{10}\text{Pd}_{2.8}\text{As}_8$  sample collected at various temperatures are shown in Figure 4 together with transmission integral fits.<sup>[20]</sup> The corresponding fitting parameters are listed in Table 2. The three spectra are well reproduced with single signals, however, with slightly enhanced line widths, especially towards lower temperature. The iron atoms are distributed over five crystallographically independent sites. Thus we observe a distribution of five subspectra and the experimental one is the superposition. Since the parameters of the subspectra are very close, we only observe the envelope curve. The line width enhancement in the 5 K spectrum can be explained by a distribution of different distortions of the  $\text{Fe}_{1-x}\text{Pd}_x\text{As}_4$  tetrahedra. This is also expressed by the slightly enhanced quadrupole splitting parameter (Table 2). The isomer shift (due to the superposition we get an average value) increases from 0.31 mm/s at 293 K to 0.45 mm/s at 5 K, a consequence of a second order Doppler shift (SODS). The absolute  $\delta$  values compare well with other iron arsenides, e.g. the solid solution  $\text{Ba}_{1-x}\text{K}_x\text{Fe}_2\text{As}_2$ <sup>[21,22]</sup> or  $\text{Sr}_3\text{Sc}_2\text{O}_5\text{Fe}_2\text{As}_2$ .<sup>[23]</sup> The 78 K and 5 K spectra give no hint for a hyperfine field contribution thus no magnetic ordering is present.

**Table 2:** Fitting parameters of  $^{57}\text{Fe}$ -Mössbauer spectra of  $(\text{Ca}_{0.87}\text{La}_{0.13}\text{Fe}_{0.86}\text{Pd}_{0.14}\text{As})_{10}\text{Pd}_{2.8}\text{As}_8$  at different temperatures.  $\Gamma$ : Experimental line width,  $\delta$ : Isomer shift,  $\Delta E_Q$ : Electric quadrupole splitting parameter (For details see text).

| $T$ (K) | $\delta$ ( $\text{mm s}^{-1}$ ) | $\Delta E_Q$ ( $\text{mm s}^{-1}$ ) | $\Gamma$ ( $\text{mm s}^{-1}$ ) |
|---------|---------------------------------|-------------------------------------|---------------------------------|
| 293     | 0.31(1)                         | 0.21(3)                             | 0.45(4)                         |
| 78      | 0.43(1)                         | 0.34(6)                             | 0.91(6)                         |
| 5       | 0.45(2)                         | 0.54(6)                             | 1.23(8)                         |

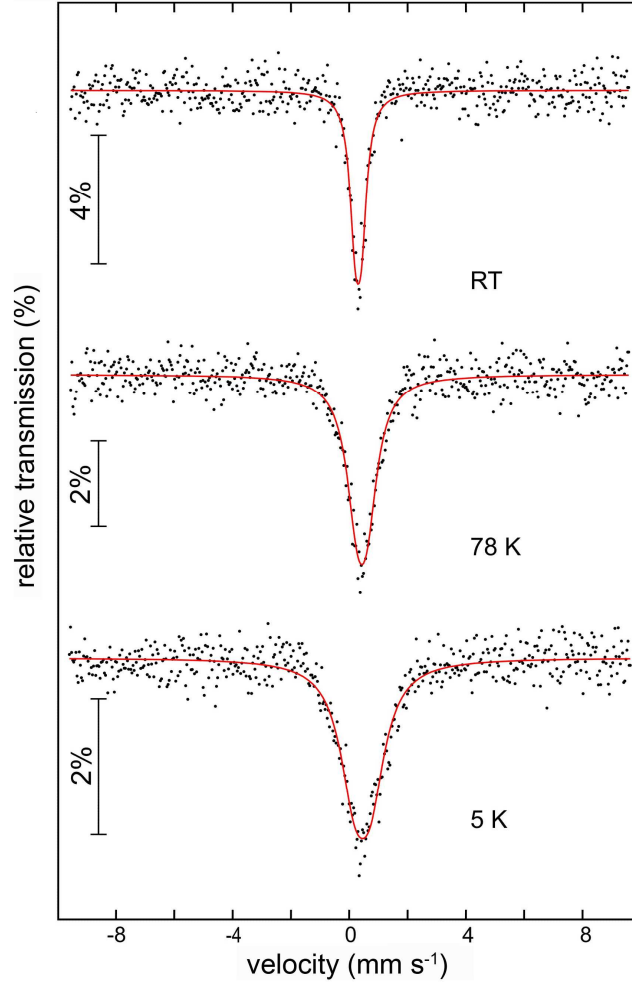


**Figure 4:** Experimental and simulated  $^{57}\text{Fe}$ -Mössbauer spectra ( $^{57}\text{Co}/\text{Rh}$  source) of  $(\text{Ca}_{0.87}\text{La}_{0.13}\text{Fe}_{0.86}\text{Pd}_{0.14}\text{As})_{10}\text{Pd}_{2.8}\text{As}_8$  at various temperatures.

#### 2.1.2.4 Electronic Structure Calculation

The electronic structure of  $(\text{CaFeAs})_{10}\text{Pd}_3\text{As}_8$  was calculated by the full-potential LAPW-lo method<sup>[24]</sup> using the WIEN2k package.<sup>[25,26]</sup> Figure 5a shows the total electronic density of states (DOS) together with partial DOS projections (pDOS) of the FeAs and  $\text{Pd}_3\text{As}_8$  layers. The FeAs pDOS (red curve) is very similar to other iron arsenide materials, which suggests almost independent electronic systems, i.e. very weak coupling between iron arsenide and

palladium arsenide layers in  $(\text{CaFeAs})_{10}\text{Pd}_3\text{As}_8$ . The states at the *Fermi* energy ( $E_F$ ) are dominated by FeAs, even though a certain contribution of orbitals from the  $\text{Pd}_3\text{As}_8$  layer (blue line) is discernible. From the pDOS values at  $E_F$  we estimate 86 % FeAs and 14 %  $\text{Pd}_3\text{As}_8$  states, respectively, while calcium orbitals are negligible at  $E_F$ .

The calculated *Fermi* surface (FS) topology of triclinic  $(\text{CaFeAs})_{10}\text{Pd}_3\text{As}_8$  is depicted in the Figures 5b-f. For clarity we show the different sheets (Figures b-e) and the complete FS (Figure 5f) separately. Cylinders along  $c^*$  around the  $\Gamma$  point (Figure 5b+c) and the zone corners (Figure 5c) show the two-dimensionality of the electronic structure, and strongly resembles the FS topology of other iron arsenide superconductors like  $\text{CaFe}_2\text{As}_2$  shown in Figure 5g for comparison. Nesting between hole-like and electron-like FS sheets with a momentum vector  $q = (\frac{1}{2} \frac{1}{2} 0)$  is intensively discussed as being essential for high- $T_c$  in iron arsenides.<sup>[27-30]</sup> Spin fluctuations with this momentum vector were found experimentally,<sup>[31,32]</sup> and they are now thought to play a key role for the pairing mechanism.<sup>[3]</sup> Indeed significant parts of the FS in Figure 5f nearly coincide when shifted by  $(\frac{1}{2} \frac{1}{2} 0)$ , and qualifies  $(\text{CaFeAs})_{10}\text{Pd}_3\text{As}_8$  as typical iron arsenide material from the view of the electronic structure. However, we also observe some deviations of the FS as seen in Figure 5e, where the cylinders become a torus-like shape that is not present in the other FeAs compounds. However, these perturbations are much weaker than those calculated for  $\text{Sr}_2\text{VO}_3\text{FeAs}$  by assuming non-magnetic vanadium.<sup>[33,34]</sup>

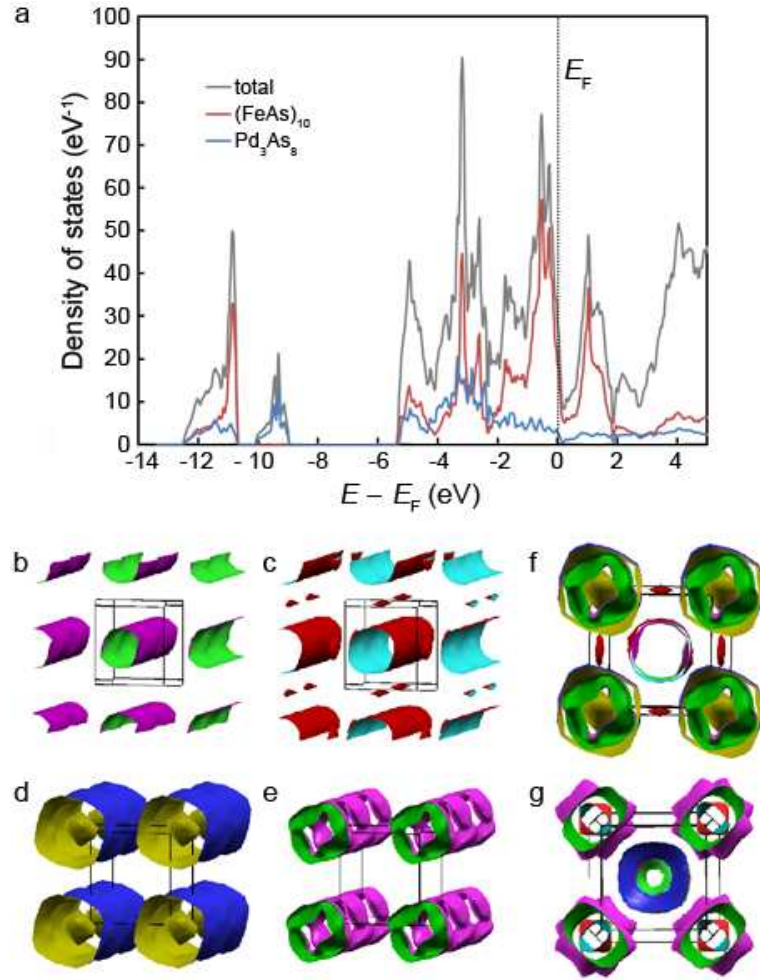


**Figure 5:** a) Electronic density of states (DOS) of  $(\text{CaFeAs})_{10}\text{Pd}_3\text{As}_8$ . Total DOS (gray), contributions of the FeAs (red), and  $\text{Pd}_3\text{As}_8$  layers (blue). b-e) *Fermi* surface sheets, f) Sheets b-e merged, g) *Fermi* surface of  $\text{CaFe}_2\text{As}_2$ .

### 2.1.3 Conclusion

We have shown that 1038-type superconductors exist with palladium arsenide layers. The single crystal X-ray structure determination confirmed the triclinic crystal structure of  $(\text{CaFe}_{1-x}\text{Pd}_x\text{As})_{10}\text{Pd}_3\text{As}_8$  isotypic to Pt1038, even though the data accuracy is slightly lowered due to partial merohedral twinning and diffuse scattering. Polycrystalline samples of  $(\text{Ca}_{0.92}\text{La}_{0.08}\text{Fe}_{0.86}\text{Pd}_{0.14}\text{As})_{10}\text{Pd}_{2.8}\text{As}_8$  reveal the onset of a superconducting transition at 17 K and still incomplete magnetic shielding of about 20 %. The relative low  $T_c$  when compared with the Pt compounds and the relatively weak shielding are ascribed to sample issues, where Pd over-doping at the Fe site is detrimental to superconductivity. We suggest that the inhomogeneous distribution of the Pd atoms in the Fe layer produces certain fractions that have Pd concentrations low enough to allow superconductivity.  $^{57}\text{Fe}$ -Mössbauer data agree well with other FeAs superconductors and show no hints of magnetic ordering. Electronic structure

calculations of the idealized parent compound (CaFeAs)<sub>10</sub>Pd<sub>3</sub>As<sub>8</sub> reveal weak coupling between the FeAs and Pd<sub>3</sub>As<sub>8</sub> layers, and a FS topology very similar to the known FeAs superconductors. Typical FS features like cylinders at  $\Gamma$  and X as well as partial FS nesting qualifies the new compounds as typical iron arsenide superconductors. From this we conclude that the Pd1038 compounds will exhibit higher critical temperatures in samples with lower or ideally without Pd doping in the FeAs layer.

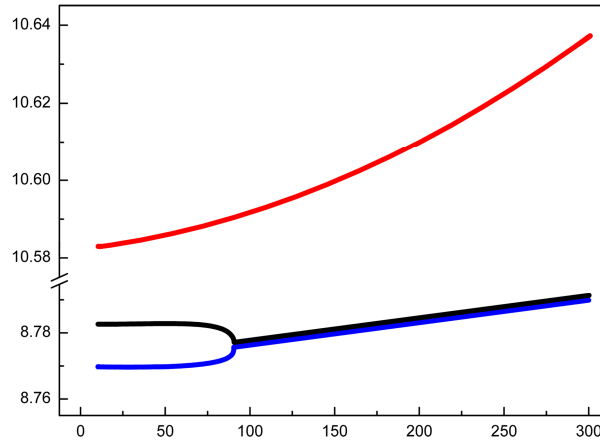
#### 2.1.4 References

- [1] G. R. Stewart, *Rev. Mod. Phys.* **2011**, *83*, 1589.
- [2] D. Johrendt, R. Pöttgen, *Angew. Chem. Int. Ed.* **2008**, *47*, 4782.
- [3] D. J. Scalapino, *Rev. Mod. Phys.* **2012**, *84*, 1383.
- [4] X. Zhu, F. Han, G. Mu, P. Cheng, B. Shen, B. Zeng, H.-H. Wen, *Phys. Rev. B* **2009**, *79*, 220512.
- [5] C. Löhnert, T. Stürzer, M. Tegel, R. Frankovsky, G. Friederichs, D. Johrendt, *Angew. Chem. Int. Ed.* **2011**, *50*, 9195.
- [6] N. Ni, J. M. Allred, B. C. Chan, R. J. Cava, *Proc. Natl. Acad. Sci. U. S. A.* **2011**, *108*, E1019.
- [7] S. Kakiya, K. Kudo, Y. Nishikubo, K. Oku, E. Nishibori, H. Sawa, T. Yamamoto, T. Nozaka, M. Nohara, *J. Phys. Soc. Jpn.* **2011**, *80*, 093704.
- [8] T. Stürzer, G. M. Friederichs, H. Luetkens, A. Amato, H.-H. Klauss, D. Johrendt, *J. Phys.: Condens. Matter* **2013**, *25*, 122203.
- [9] T. Stürzer, G. Derondeau, D. Johrendt, *Phys. Rev. B* **2012**, *86*, 060516(R).
- [10] M. Neupane, C. Liu, S.-Y. Xu, Y. J. Wang, N. Ni, J. M. Allred, L. A. Wray, H. Lin, R. S. Markiewicz, A. Bansil, R. J. Cava, M. Z. Hasan, *Phys. Rev. B* **2012**, *85*, 094510.
- [11] J. S. Kim, T. Stürzer, D. Johrendt, G. R. Stewart, *J. Phys.: Condens. Matter* **2013**, *25*, 135701.
- [12] V. Petricek, M. Dusek, L. Palatinus, JANA2006: Structure Determination Software Programs, Institute of Physics, Praha, **2009**.

- [13] M. Rotter, M. Tegel, I. Schellenberg, W. Hermes, R. Pöttgen, D. Johrendt, *Phys. Rev. B* **2008**, 78, 020503(R).
- [14] M. Tegel, S. Johansson, V. Weiß, I. Schellenberg, W. Hermes, R. Pöttgen, D. Johrendt, *Europhys. Lett.* **2008**, 84, 67007.
- [15] C. H. Lee, A. Iyo, H. Eisaki, H. Kito, M. T. Fernandez-Diaz, T. Ito, K. Kihou, H. Matsuhata, M. Braden, K. Yamada, *J. Phys. Soc. Jpn.* **2008**, 77, 083704.
- [16] L. Pauling, *The Nature of the Chemical Bond and the Structure of Molecules and Crystals: An Introduction to Modern Structural Chemistry*, Cornell University Press, Ithaca, New York, **1960**.
- [17] A. Coelho, TOPAS-Academic, Version 4.1, Coelho Software, Brisbane, **2007**.
- [18] N. Ni, A. Thaler, A. Kracher, J. Q. Yan, S. L. Bud'ko, P. C. Canfield, *Phys. Rev. B* **2009**, 80, 024511.
- [19] K. Cho, M. A. Tanatar, H. Kim, W. E. Straszheim, N. Ni, R. J. Cava, R. Prozorov, *Phys. Rev. B* **2012**, 85, 020504.
- [20] R. A. Brand, Normos Mössbauer fitting Program, Universität Dortmund, **2002**.
- [21] M. Rotter, M. Tegel, I. Schellenberg, F. M. Schappacher, R. Pöttgen, J. Deisenhofer, A. Gunther, F. Schrettle, A. Loidl, D. Johrendt, *New J. Phys.* **2009**, 11, 025014.
- [22] D. Johrendt, R. Pöttgen, *Physica C* **2009**, 469, 332.
- [23] M. Tegel, I. Schellenberg, F. Hummel, R. Pöttgen, D. Johrendt, *Z. Naturforsch. B* **2009**, 64, 815.
- [24] G. K. H. Madsen, P. Blaha, K. Schwarz, E. Sjöstedt, L. Nordstrom, *Phys. Rev. B* **2001**, 64, 195134/1.
- [25] P. Blaha, K. Schwarz, G. K. H. Madsen, D. Kvasnicka, J. Luitz, WIEN2k – An Augmented Plane Wave + Local Orbitals Program for Calculating Crystal Properties, Technische Universität Wien, **2001**.
- [26] K. Schwarz, P. Blaha, *Comput. Mat. Sci.* **2003**, 28, 259.
- [27] I. I. Mazin, D. J. Singh, M. D. Johannes, M. H. Du, *Phys. Rev. Lett.* **2008**, 101, 057003.

- [28] K. Terashima, Y. Sekiba, J. H. Bowen, K. Nakayama, T. Kawahara, T. Sato, P. Richard, Y.-M. Xu, L. J. Li, G. H. Cao, Z.-A. Xu, H. Ding, T. Takahashi, *Proc. Natl. Acad. Sci. U. S. A.* **2009**, *106*, 7330.
- [29] I. I. Mazin, *Nature* **2010**, *464*, 183.
- [30] P. Richard, T. Sato, K. Nakayama, T. Takahashi, H. Ding, *Rep. Prog. Phys.* **2011**, *74*, 124512.
- [31] A. D. Christianson, E. A. Goremychkin, R. Osborn, S. Rosenkranz, M. D. Lumsden, C. D. Malliakas, I. S. Todorov, H. Claus, D. Y. Chung, M. G. Kanatzidis, R. I. Bewley, T. Guidi, *Nature* **2008**, *456*, 930.
- [32] P. Dai, J. Hu, E. Dagotto, *Nature Phys.* **2012**, *8*, 709.
- [33] K. W. Lee, W. E. Pickett, *Europhys. Lett.* **2010**, *89*, 57008.
- [34] M. Tegel, T. Schmid, T. Stürzer, M. Egawa, Y. X. Su, A. Senyshyn, D. Johrendt, *Phys. Rev. B* **2010**, *82*, 140507.

## 2.2 (CaFe<sub>1-x</sub>Pd<sub>x</sub>As)<sub>10</sub>Pd<sub>3</sub>As<sub>8</sub> with Parent-like Properties



### 2.2.1 Introduction

In the field of iron arsenide superconductors particular attention lays on the magneto-structural transitions of their undoped parent compounds.<sup>[1]</sup> At specific transition temperatures the tetragonal structures of the stoichiometric phases like LaOFeAs (130 K),<sup>[2]</sup> BaFe<sub>2</sub>As<sub>2</sub> (140 K),<sup>[3]</sup> or NaFeAs (50 K)<sup>[4]</sup> distort to an orthorhombic crystal system. Additionally the parent compounds feature spin density wave anomalies with stripe-type antiferromagnetic ordering in the vicinity of the structural phase transition. Doping or pressure can suppress these transitions giving rise to superconductivity with high critical temperatures up to 56 K.<sup>[5]</sup> Soon after 2011 the new member (CaFe<sub>1-x</sub>Pt<sub>x</sub>As)<sub>10</sub>Pt<sub>3</sub>As<sub>8</sub> (Pt1038)<sup>[6,7]</sup> within layered iron arsenides was discovered, undoped Pt1038 ( $x = 0$ ) was proven as the corresponding parent.<sup>[8]</sup> Although fourfold rotational symmetry is persevered within each layer the skew stacking results in a triclinic crystal structure (space group  $P\bar{1}$ ). As illustrated in Figure 1 a  $\sqrt{5} \times \sqrt{5}$  superstructure of the CaFe<sub>2</sub>As<sub>2</sub><sup>[9]</sup> motif (ThCr<sub>2</sub>Si<sub>2</sub> type) is formed at that. Although the triclinic crystal system precludes another symmetry reduction in this case, a phase transition at 120 K<sup>[8]</sup> was found to break local tetragonal symmetry by an orthorhombic distortion of the square  $ab$  basal plane. This finding emphasized the importance of local symmetry in this class and the close relation of the 1038 system to simpler iron arsenides. Simultaneously stripe-type static magnetism develops.<sup>[10,11]</sup> Pt1038 proved as typical iron arsenide compound,<sup>[12]</sup> since the phase transitions can be suppressed and superconductivity is induced by direct doping in (CaFe<sub>1-x</sub>M<sub>x</sub>As)<sub>10</sub>Pt<sub>3</sub>As<sub>8</sub> with  $M = \text{Co, Ni, Pd, Pt}$ <sup>[13-15]</sup> or charge doping in (CaFe<sub>1-x</sub>Pt<sub>x</sub>As)<sub>10</sub>Pt<sub>4</sub>As<sub>8</sub><sup>[15]</sup> and (Ca<sub>1-y</sub>RE<sub>y</sub>FeAs)<sub>10</sub>Pt<sub>3</sub>As<sub>8</sub> with  $RE = \text{Y, La - Nd, Sm, Gd - Lu}$ .<sup>[16]</sup>

Furthermore first experiments on the homologous palladium compound  $(\text{CaFe}_{1-x}\text{Pd}_x\text{As})_{10}\text{Pd}_3\text{As}_8$  (Pd1038) were already performed.<sup>[17]</sup> Pd1038 was identified by single crystal structure determination with a palladium substitution of  $x = 0.16$  and a reduced palladium content of  $z = 2.8$ . Despite  $(\text{CaFe}_{1-x}\text{Pd}_x\text{As})_{10}\text{Pd}_3\text{As}_8$  features an analogue crystal structure as the related platinum compound, surprisingly no superconductivity was induced in directly palladium doped  $(\text{CaFe}_{1-x}\text{Pd}_x\text{As})_{10}\text{Pd}_3\text{As}_8$  (Figure 1). Early explanations rationalized this absence of superconductivity with too high palladium substitution on the iron sites being omnipresent in these compounds. Although restricting palladium substitution on the tetrahedral coordinated iron position to a minimum turned out challenging, investigations on the effects of palladium mixing in the 1038 system, however, revealed superconductivity in  $(\text{CaFe}_{1-x}\text{Pd}_x\text{As})_{10}\text{Pt}_3\text{As}_8$  up to  $x = 0.16$ .<sup>[14]</sup>

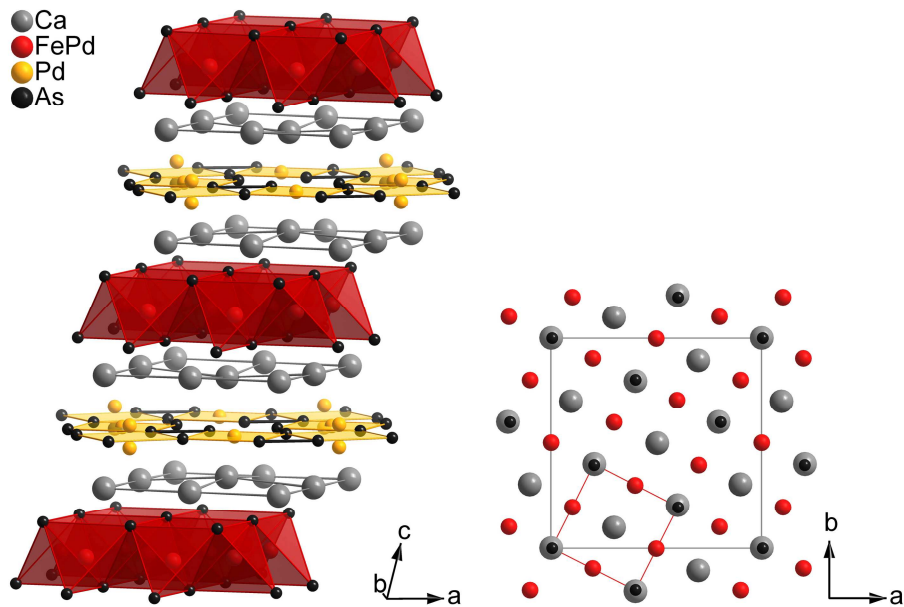


**Figure 1:** Stacking within the crystal structure of  $(\text{CaFe}_{1-x}\text{Pd}_x\text{As})_{10}\text{Pd}_3\text{As}_8$  (left) and top-view of calcium iron arsenide motif (right). The relation of the unit cell of Pd1038 (gray square) and the basis cell of the  $\text{CaFe}_2\text{As}_2$  substructure (red square) is emphasized.

In studies on charged doped  $(\text{CaFe}_{1-x}\text{M}_x\text{As})_{10}\text{M}_4\text{As}_8$  (1048)<sup>[7,15]</sup> with  $M = \text{Pd}, \text{Pt}$  different magnetic properties occurred with no superconductivity in the palladium compound so far (Chapter 4). Nevertheless, electron doping by rare earth substitution<sup>[18]</sup> (Chapter 2.4) yields superconducting properties in  $(\text{Ca}_{1-y}\text{RE}_y\text{FeAs})_{10}\text{Pd}_3\text{As}_8$ . High quality powder samples to analyze the polycrystalline properties of Pd1038 without additional charge carriers were not available so far. Moreover the presence of a parent-like state with an absence or low content of palladium on the iron positions could only be theoretically assumed. In this chapter successful synthesis optimization gave rise to polycrystalline  $(\text{CaFe}_{1-x}\text{Pd}_x\text{As})_{10}\text{Pd}_3\text{As}_8$  with a low palladium mixing level on the iron sites. Temperature-depending powder diffraction,

resistivity, and susceptibility measurements substantiated the idea of a parent-type state in  $(\text{CaFeAs})_{10}\text{Pd}_3\text{As}_8$  similar to Pt1038.

## 2.2.2 Results and Discussion

### 2.2.2.1 X-Ray Powder Diffraction

High quality powder sample of  $(\text{CaFe}_{1-x}\text{Pd}_x\text{As})_{10}\text{Pd}_3\text{As}_8$  was obtained by a three-step solid state reaction starting from the elements. The sample was characterized by X-ray powder diffraction and Rietveld refinement (Figure 2). To minimize the formation of  $(\text{CaFe}_{1-x}\text{Pd}_x\text{As})_{10}\text{Pd}_4\text{As}_8$  (Pd1048) as well as the mixing of iron and palladium in the tetrahedral layers the nominal palladium amount was reduced to  $z = 2.5$ . Therefore the palladium-free impurity phases FeAs and  $\text{CaFe}_2\text{As}_2$  were identified. Additionally the diffractogram showed hints of minor amounts of Pd1048, however, an adequate refinement was not reasonable.

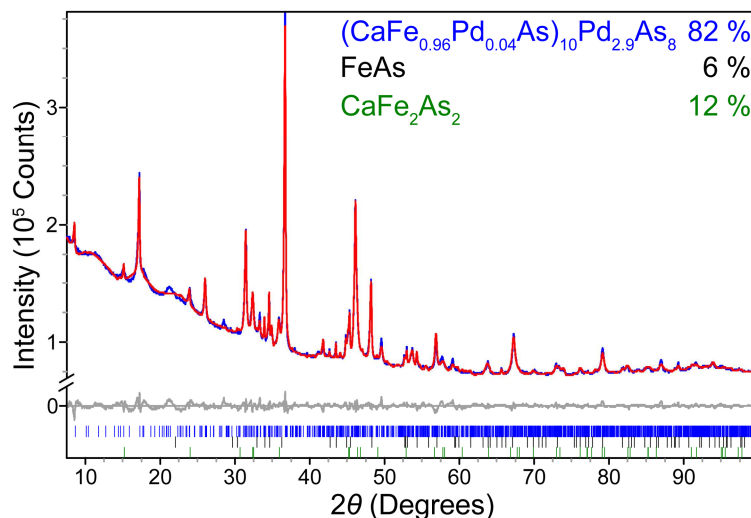


**Figure 2:** X-ray powder data at room temperature (blue) with Rietveld fit (red) of  $(\text{CaFe}_{1-x}\text{Pd}_x\text{As})_{10}\text{Pd}_z\text{As}_8$ .

The refinement revealed small palladium occupancy on the iron position of  $x = 0.04(1)$  and a slightly reduced palladium content in the  $\text{Pd}_3\text{As}_8$  layer of  $z = 2.9(1)$ . This reduction is also known from single crystal data of  $(\text{CaFe}_{1-x}\text{Pd}_x\text{As})_{10}\text{Pd}_z\text{As}_8$ <sup>[17]</sup> as well as several substituted phases. Furthermore the composition was confirmed by X-ray spectroscopy (EDX) yielding a total iron/ palladium content of  $\text{Fe}_{9.8(3)}\text{Pd}_{2.8(2)}$  averaged from various independent data points in good agreement with the composition obtained from powder diffraction. This minor palladium substitution of the iron layer renders the compound suitable for investigations regarding a possible parent-state in Pd1038.

Temperature-dependent XRD measurements in the range of 10 – 300 K revealed a sudden splitting of the lattice parameters  $a$  and  $b$  below 90 K. The almost square basal plane distorts to  $a > b$ , while simultaneously the in-plane  $\gamma$  angle changes (Figure 3). The  $c$  axis shows the expected decrease with decreasing temperature. A comparable distortion from tetragonal to orthorhombic symmetry is known from other iron arsenide parent compounds like  $\text{LaOFeAs}$  ( $P4/nmm \rightarrow Cmme$ )<sup>[19]</sup> or  $\text{BaFe}_2\text{As}_2$  ( $I4/mmm \rightarrow Fmmm$ ).<sup>[3]</sup> Like in triclinic  $\text{Pt1038}$ <sup>[8]</sup> precluding further symmetry reduction the structural phase transition in  $(\text{CaFe}_{1-x}\text{Pd}_x\text{As})_{10}\text{Pd}_3\text{As}_8$  breaks the tetragonal symmetry of the iron arsenide sheets according to  $p4mm \rightarrow p2mm$  in terms of layer symmetry. Although the structural order parameter is quite small, the orthorhombic distortion of the square basal plane is significant. Most likely a minor substitution of iron by palladium prevents a more distinct splitting as observed for pure  $(\text{CaFeAs})_{10}\text{Pt}_3\text{As}_8$ .<sup>[8]</sup> Analogue palladium substituted  $\text{Pt1038}$  with  $x = 0.035$  features a reduced distortion compared to the parent compound.<sup>[14]</sup> Therefore with clean iron arsenide layers in theoretical stoichiometric  $\text{Pd1038}$  a higher structural order parameter is expected.

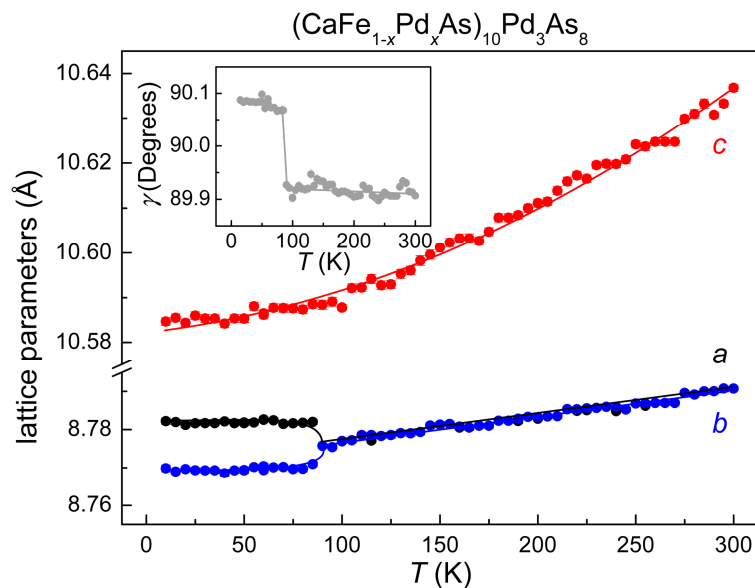


**Figure 3:** Lattice parameters of  $(\text{CaFe}_{0.96}\text{Pd}_{0.04}\text{As})_{10}\text{Pd}_3\text{As}_8$  from temperature-dependent XRD measurements. Inset: Change of  $\gamma$  angle in  $ab$  basal plane.

### 2.2.2.2 Electric and Magnetic Properties

The electrical resistivity illustrated in Figure 4 showed metallic behavior until a sharp drop at 6 K. Zero resistivity is achieved at 3.5 K indicating superconductivity. At about 85 K the onset of an anomaly points out a phase transition. At the same temperature a structural distortion was already observed by temperature-depending XRD analysis. Resistivity of a nominal

$(\text{CaFeAs})_{10}\text{Pd}_4\text{As}_8$  powder sample revealed similar behavior in a lower magnitude (Chapter 4), while lanthanum doped Pd1038 showed no anomaly in the range of 3.5 – 300 K.<sup>[17]</sup>

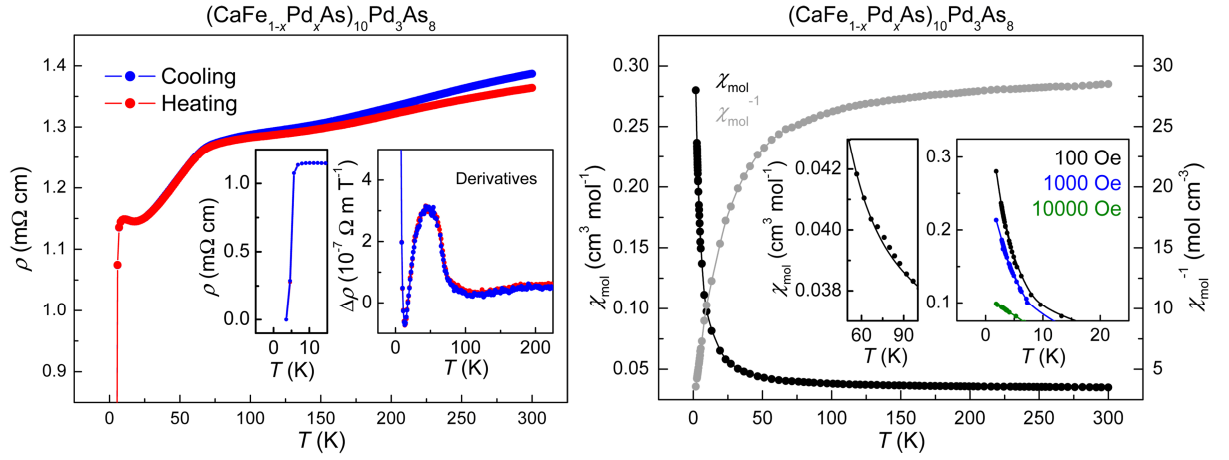


**Figure 4:** Electrical resistivity of  $(\text{CaFe}_{0.96}\text{Pd}_{0.04}\text{As})_{10}\text{Pd}_3\text{As}_8$  (left). Completed low-temperature range and derivatives are shown in the insets. Molar susceptibility and inverse data at 100 Oe (right). The temperature range of the phase transition and low-temperature range significant for superconductivity at different external fields are illustrated in the insets.

Magnetic susceptibility measurements at different external fields revealed weak paramagnetic behavior of  $(\text{CaFe}_{1-x}\text{Pd}_x\text{As})_{10}\text{Pd}_3\text{As}_8$  (Figure 4). By having a close look the curve of molar susceptibility also indicates a magnetic transition in the range of 70 – 90 K associated with the structural distortion at 85 K. Inverse susceptibilities were not suited for *Curie Weiss* fits. The absence of any hysteresis in magnetization from -50 kOe to 50 kOe at 1.8 K and 300 K revealed no ferromagnetic impurities. Also the measurement in *zero-field-cooled* and *field-cooled* mode confirmed the paramagnetic behavior and revealed only a minimal splitting of the two branches below 8 K. Dc-susceptibility with  $H = 100, 1000, 10000$  Oe did not reveal any superconducting properties. Therefore the hint of superconductivity in electrical resistivity is most likely not a property of  $(\text{CaFe}_{1-x}\text{Pd}_x\text{As})_{10}\text{Pd}_3\text{As}_8$ , but has to be assigned to some minor impurity phase. In contrast to related  $(\text{CaFe}_{1-x}\text{Pt}_x\text{As})_{10}\text{Pt}_3\text{As}_8$  with superconductivity for about  $0.03 < x < 0.08$  and  $T_c = 15$  K,<sup>[20]</sup> even with a low refined substitution level of  $x = 0.04(1)$  analogue Pd1038 did not show bulk superconducting properties. Although higher palladium doping up to 16 % in Pt1038 was proven not to be an exclusion criterion for the induction of superconductivity in 1038 compounds.<sup>[14]</sup> In addition to the structural distortion at 85 K indications of a magnetic phase transition in  $(\text{CaFe}_{1-x}\text{Pd}_x\text{As})_{10}\text{Pd}_3\text{As}_8$  at the same temperature, visible in electrical as well as magnetic measurements are present. The weakness of these anomalies is ascribed to the remaining minor iron/ palladium substitution and varying dopant distribution. Superconductivity observed in resistivity measurement is attributed to the presence of impurity phases or inhomogeneous substitution.

### 2.2.3 Experimental Section

The polycrystalline sample was synthesized by solid state reaction. A mixture of the pure elements ( $> 99.9\%$ ) with a reduced palladium content of  $z = 2.5$  and an excess of calcium of  $5\%$  was filled in an alumina crucible and sealed in silica under purified argon. After heating for 10 h each at  $600\text{ }^\circ\text{C}$  followed by  $1000\text{ }^\circ\text{C}$ , the product was grounded and annealed twice at  $900\text{ }^\circ\text{C}$  for 25 h pelletized in the last step. The obtained powder sample was characterized by X-ray powder diffraction at room temperature using a Huber Imaging Plate Guinier diffractometer with primary monochromator and copper radiation. Temperature-dependent powder data were measured on a Huber Imaging Plate Guinier diffractometer with primary monochromator and cobalt radiation equipped with a close-cycle Helium cryostat. All Rietveld refinements were performed using the TOPAS program package.<sup>[21]</sup> Sample composition was confirmed by X-ray spectroscopy on a Carl Zeiss EVO-MA 10 equipped with a Bruker Nano EDX detector. Dc-resistivity was measured using a standard four-probe method on a cold pressed pellet, which was annealed at  $900\text{ }^\circ\text{C}$  for 25 h. Dc-susceptibility, magnetization, and *zero-field-cooled/ field-cooled* data in the range of  $1.8 - 300\text{ K}$  were measured using a Quantum Design MPMS-XL5 SQUID magnetometer at varying external fields of  $-50 - 50\text{ kOe}$ .

### 2.2.4 Conclusion

Polycrystalline  $(\text{CaFe}_{1-x}\text{Pd}_x\text{As})_{10}\text{Pd}_3\text{As}_8$  was synthesized and characterized to investigate the presence of a parent state in resemblance to related Pt1038. The optimized synthesis gave high quality Pd1038 with a phase amount over  $80\%$ . Refined X-ray powder diffraction revealed very small palladium substitution on the iron sites of  $x = 0.04$  and a characteristic palladium deficiency of  $z = 2.9$ . The composition was confirmed by EDX measurements. A structural phase transition at  $85\text{ K}$  was evident from temperature-dependent X-ray powder diffraction with an orthorhombic distortion of the square basal plane. The corresponding iron arsenide layer features a symmetry reduction according to  $p4mm \rightarrow p2mm$  in terms of layer symmetry. Furthermore an associated magnetic transition in the same temperature range is indicated in resistivity as well as magnetic measurements. Both phase transitions are moderately distinct, probably due to remaining palladium substitution. Hints of superconducting properties at very low temperatures from resistivity analysis were not confirmed by susceptibility data, but have to be assigned to sample inhomogeneity or side phases. Therefore the previously assumed presence of a parent-like state analogue to Pt1038 and other iron arsenide

compounds is also experimentally substantiated for (CaFe<sub>1-x</sub>Pd<sub>x</sub>As)<sub>10</sub>Pd<sub>3</sub>As<sub>8</sub>. More distinct phase transitions at an increased temperature are expected in fully stoichiometric Pd1038.

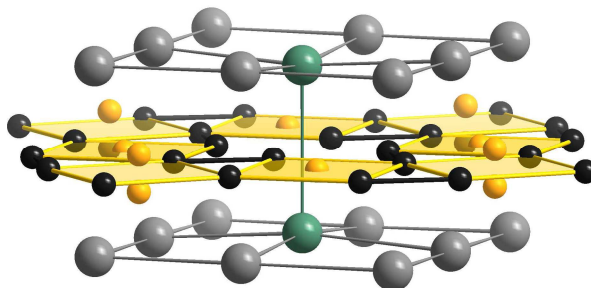
### 2.2.5 References

- [1] D. Johrendt, *J. Mater. Chem.* **2011**, *21*, 13726.
- [2] Y. Kamihara, T. Watanabe, M. Hirano, H. Hosono, *J. Am. Chem. Soc.* **2008**, *130*, 3296.
- [3] M. Rotter, M. Tegel, I. Schellenberg, W. Hermes, R. Pöttgen, D. Johrendt, *Phys. Rev. B* **2008**, *78*, 020503(R).
- [4] D. R. Parker, M. J. Pitcher, P. J. Baker, I. Franke, T. Lancaster, S. J. Blundell, S. J. Clarke, *Chem. Commun.* **2009**, *16*, 2189.
- [5] G. Wu, Y. L. Xie, H. Chen, M. Zhong, R. H. Liu, B. C. Shi, Q. J. Li, X. F. Wang, T. Wu, Y. J. Yan, J. J. Ying, X. H. Chen, *J. Phys.: Condens. Matter* **2009**, *21*, 142203.
- [6] N. Ni, J. M. Allred, B. C. Chan, R. J. Cava, *Proc. Natl. Acad. Sci* **2011**, *108*, E1019.
- [7] C. Löhnert, T. Stürzer, M. Tegel, R. Frankovsky, G. Friederichs, D. Johrendt, *Angew. Chem. Int. Ed.* **2011**, *50*, 9195.
- [8] T. Stürzer, G. M. Friederichs, H. Luetkens, A. Amato, H.-H. Klauss, F. Winter, R. Pöttgen, D. Johrendt, *J. Phys.: Condens. Matter* **2013**, *25*, 122203.
- [9] F. Ronning, T. Klimczuk, E. D. Bauer, H. Volz, J. D. Thompson, *J. Phys.: Condens. Matter* **2008**, *20*, 322201.
- [10] T. Zhou, G. Koutroulakis, J. Lodico, N. Ni, J. D. Thompson, R. J. Cava, S. E. Brown, *J. Phys.: Condens. Matter* **2013**, *25*, 122201.
- [11] A. Sapkota, G. S. Tucker, M. Ramazanoglu, W. Tian, N. Ni, R. J. Cava, R. J. McQueeney, A. I. Goldman, A. Kreyssig, *Phys. Rev. B* **2014**, *90*, 100504(R).
- [12] T. Stürzer, *Dissertation*, LMU München, **2015**.
- [13] T. Stürzer, F. Kessler, D. Johrendt, *Philos. Mag.* **2014**, *94*, 3632.
- [14] C. Stürzer, D. Johrendt, **2015**, *in preperation*. (see Chapter 3)

- [15] T. Stürzer, G. Derondeau, D. Johrendt, *Phys. Rev. B* **2012**, *86*, 060516(R).
- [16] T. Stürzer, G. Derondeau, D. Johrendt, *Solid State Commun.* **2015**, *201*, 36.
- [17] C. Hieke, J. Lippmann, T. Stürzer, G. M. Friederichs, F. Nitsche, F. Winter, R. Pöttgen, D. Johrendt, *Philos. Mag.* **2013**, *93*, 3680.
- [18] C. Stürzer, A. Schulz, D. Johrendt, *Z. Anorg. Allg. Chem.* **2014**, *640*, 3143.
- [19] T. Nomura, S. W. Kim, Y. Kamihara, M. Hirano, P. V. Sushko, K. Kato, M. Takata, A. L. Shluger, H. Hosono, *Supercond. Sci. Technol.* **2008**, *21*, 125028.
- [20] T. Stürzer, G. Derondeau, D. Johrendt, *Phys. Rev. B* **2012**, *86*, 060516(R).
- [21] A. Coelho, TOPAS-Academic, Version 4.1, Coelho Software, Brisbane, **2007**.

## 2.3 Site Preference of Rare Earth Doping in Palladium Iron Arsenide Superconductors

Christine Stürzer, Anne Schulz, Dirk Johrendt



**published in:** *Z. Anorg. Allg. Chem.* **2014**, *640*, 3143 – 3147.

Copyright 2014, Wiley-VCH Verlag GmbH & Co. KGaA, Weinheim.

### Abstract

The solid solutions (Ca<sub>1-y</sub>RE<sub>y</sub>Fe<sub>1-x</sub>Pd<sub>x</sub>As)<sub>10</sub>Pd<sub>z</sub>As<sub>8</sub> with RE = La, Ce, and Pr were synthesized by solid state methods and characterized by X-ray powder diffraction with subsequent Rietveld refinements ((CaFeAs)<sub>10</sub>Pt<sub>3</sub>As<sub>8</sub>-type structure (“1038 type”),  $P\bar{1}$ ,  $Z = 1$ ). Substitution levels (Ca/RE, Fe/Pd, and Pd/□) obtained from Rietveld refinements coincide well with the nominal values according to EDS and the linear courses of the lattice parameters as expected from the ionic radii. The RE atoms favor the one out of five calcium sites, which is eightfold coordinated by arsenic. This leads to significant stabilization of the structure, and especially prevents palladium over-doping in the iron arsenide layers as observed in the pristine compound (CaFe<sub>1-x</sub>Pd<sub>x</sub>As)<sub>10</sub>Pd<sub>z</sub>As<sub>8</sub>. While the stabilization energy is estimated to about 40 kJ/mol by electronic structure calculations, the reason for the diminished Fe/Pd substitution through RE doping is still not yet understood. We suggest that the electrons transferred from RE<sup>3+</sup> to the (Fe<sub>1-x</sub>Pd<sub>x</sub>)As layer makes higher palladium concentrations unfavorable. Anyway the reduced palladium doping enables superconductivity with critical temperatures up to 20 K (onset) in the RE doped Pd1038 samples, which could not be obtained earlier due to palladium over-doping in the active iron arsenide layers.

### 2.3.1 Introduction

Recently the family of iron-based superconductors<sup>[1-3]</sup> was enriched by a new class of compounds which raised their structural complexity. In the triclinic crystal structure of  $(\text{CaFeAs})_{10}\text{Pt}_3\text{As}_8$ , referred to as Pt1038,<sup>[4-6]</sup> the iron arsenide layers are stacked with platinum arsenide slabs, which is the first case of an iron arsenide superconductor with two different negatively charged layers.<sup>[7]</sup> We have shown that stoichiometric  $(\text{CaFeAs})_{10}\text{Pt}_3\text{As}_8$  is not superconducting,<sup>[8]</sup> but exhibits a magnetic and structural phase transition at 120 K similar to known parent compounds like  $\text{LaFeAsO}$ <sup>[9]</sup> or  $\text{BaFe}_2\text{As}_2$ .<sup>[10]</sup> Evoked by doping this transition can be suppressed and superconductivity up to 38 K emerges in Pt1038, whereby also this structurally more complex compounds perfectly fit to the scenario drawn for typical iron arsenide superconductors.<sup>[3]</sup>

Since the crystal chemistry of platinum and palladium arsenides is often similar,<sup>[11]</sup> we expected also the analogous palladium compound  $(\text{CaFeAs})_{10}\text{Pd}_3\text{As}_8$  (Pd1038) to exist. Recently we were able to synthesize polycrystalline samples of Pd1038.<sup>[12]</sup> The crystal structure as shown in Figure 1 is isotypic to the platinum compound. Iron arsenide and palladium arsenide layers each separated by calcium are alternately stacked along the  $c$  axis. The top view of the palladium arsenide layer (Fig. 1, right hand side) shows the planar fourfold coordination of palladium by arsenic. The corner-sharing squares connected by  $\text{As}_2$  dimers ( $d_{\text{As-As}} \approx 2.5 \text{ \AA}$ )<sup>[12]</sup> leave one palladium position vacant, concomitant with a slight shift of calcium ions above and below the vacant palladium site from the calcium layers.

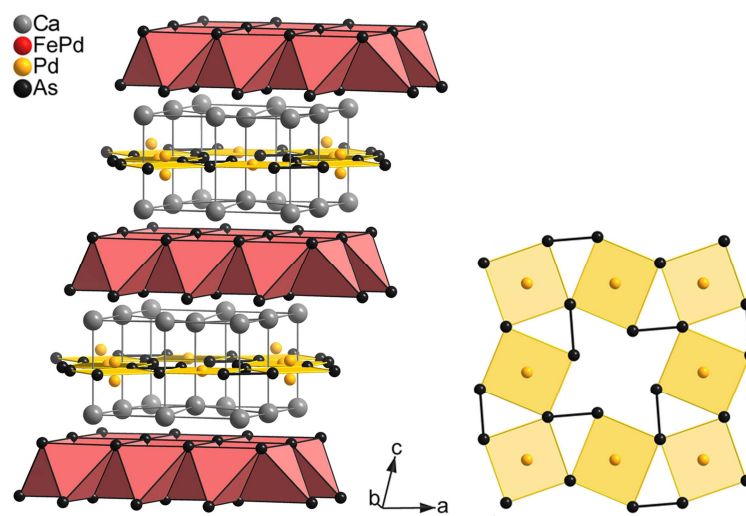


**Figure 1:** Crystal structure of  $(\text{CaFe}_{1-x}\text{Pd}_x\text{As})_{10}\text{Pd}_z\text{As}_8$  (left) and top view of the palladium arsenide layer (right).

While the platinum compound Pt1038 shows superconductivity by platinum doping at the iron sites in  $(\text{CaFe}_{1-x}\text{Pt}_x\text{As})_{10}\text{Pt}_3\text{As}_8$  with  $x = 0.03 - 0.07$ <sup>[7,13]</sup> and by rare earth doping in  $(\text{Ca}_{1-y}\text{RE}_y\text{FeAs})_{10}\text{Pt}_3\text{As}_8$  with  $\text{RE} = \text{Y}, \text{La}, \text{Ce}, \text{Pr}, \text{Nd}, \text{Sm}, \text{and Gd} - \text{Lu}$ <sup>[7,14,15]</sup> the palladium compound turned out to be more complicated. X-ray single crystal and powder diffraction experiments revealed ever-present high palladium substitution at the iron positions. It is known from 122-type iron arsenides that superconductivity is confined to small palladium doping levels, and absent above 8 %.<sup>[16]</sup> This value is by far exceeded in our Pd1038 samples which contained up to 20 % palladium at the iron sites. Consequently, these intrinsically over-doped samples of Pd1038 are not superconducting.

In this paper a systematic study of the solid solution  $(\text{Ca}_{1-y}\text{RE}_y\text{Fe}_{1-x}\text{Pd}_x\text{As})_{10}\text{Pd}_z\text{As}_8$  with  $\text{RE} = \text{La}, \text{Ce}, \text{and Pr}$ , respectively, is presented. Surprisingly, this complicated doping scenario leads to improved phase formation as well as to superconductivity in  $(\text{Ca}_{1-y}\text{RE}_y\text{Fe}_{1-x}\text{Pd}_x\text{As})_{10}\text{Pd}_z\text{As}_8$ . The triclinic crystal structures exhibit up to three different sites with statistically distributed atoms, namely  $\text{Ca}/\text{RE}$ ,  $\text{Fe}/\text{Pd}$ , and  $\text{Pd}/\square$ . Together with possible stacking faults intrinsic for this class of compounds, their detailed analysis by X-ray powder diffraction is challenging and represents an example of the capability of today' powder diffraction and Rietveld refinement methods.

### 2.3.2 Results and Discussion

Polycrystalline samples of  $(\text{Ca}_{1-y}\text{RE}_y\text{Fe}_{1-x}\text{Pd}_x\text{As})_{10}\text{Pd}_z\text{As}_8$  with  $\text{RE} = \text{La}, \text{Ce}, \text{Pr}$  and  $y = 0.025 - 0.20$  were synthesized by solid state reactions. With lower rare earth content nearly pure samples could be obtained. Figure 2 shows powder diffraction patterns with Rietveld refinements of each one lanthanum, cerium, and praseodymium doped palladium iron arsenide. Most of the samples contain FeAs as impurity phase almost entirely around 5 weight% of the binary.

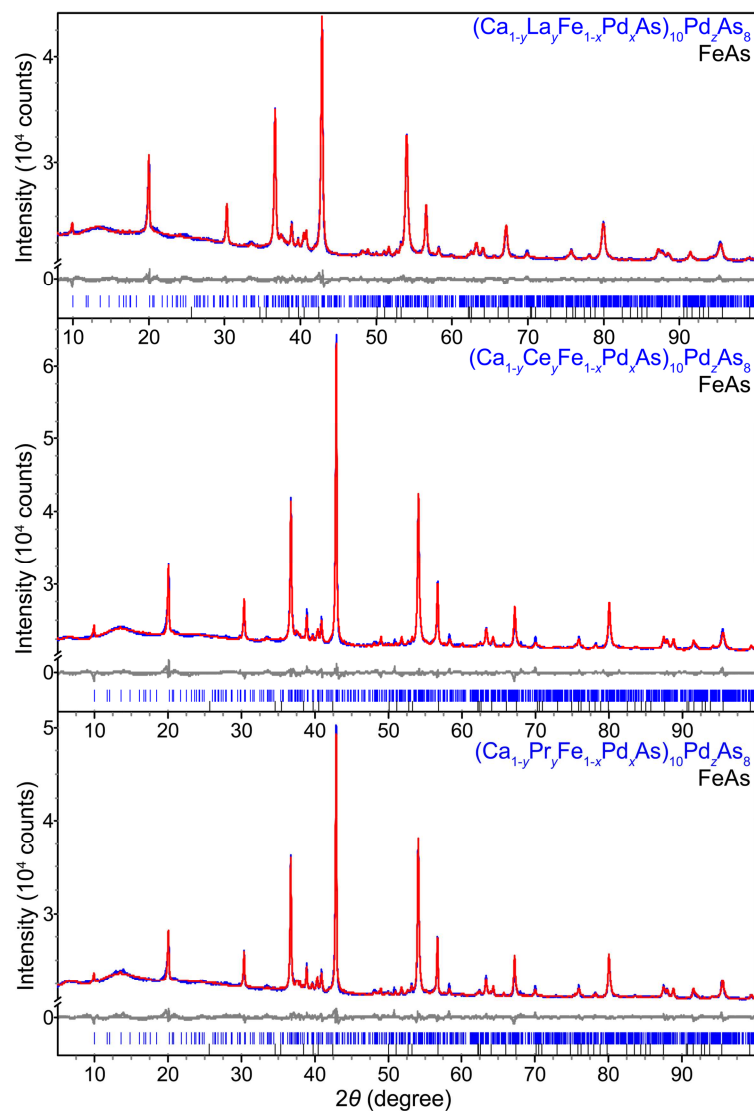


**Figure 2:** X-ray powder patterns (blue) with Rietveld fits (red) of La, Ce, and Pr doped palladium iron arsenides.

Although the compounds have variable compositions at three different sites with rare earth substitution at the calcium position, palladium mixing on the iron sites, and potential palladium vacancies in the  $\text{Pd}_3\text{As}_8$  layer, we were able to refine the total compositions from X-ray powder data. Figure 3 plots the refined compositions against the nominal rare earth contents.

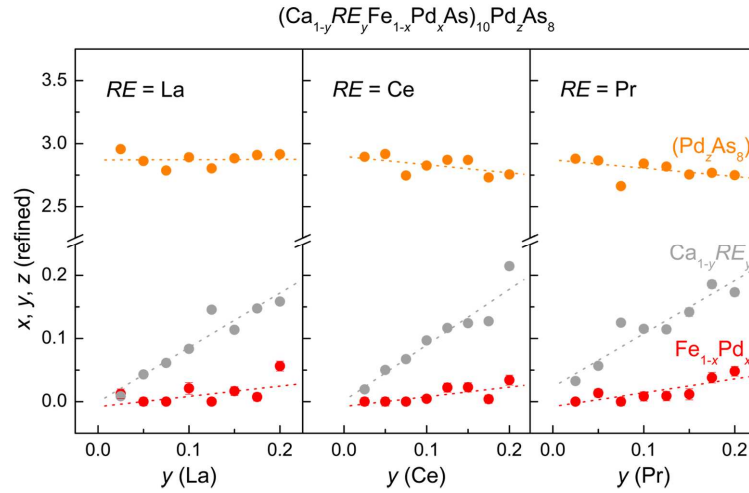


**Figure 3:** Compositions of  $(\text{Ca}_{1-y}\text{RE}_y\text{Fe}_{1-x}\text{Pd}_x\text{As})_{10}\text{Pd}_z\text{As}_8$  from Rietveld refinements for  $\text{RE} = \text{La}, \text{Ce}, \text{Pr}$  and  $y = 0.025 - 0.20$ . Gray circles:  $\text{RE}$  at the Ca positions, red circles: Pd at the Fe positions in the FeAs layer, yellow circles: Pd in the  $\text{Pd}_3\text{As}_8$  layer.

The refined rare earth contents (gray circles in Fig. 3) increase linear with the nominal composition, while palladium occupancies at the iron sites remain well below 5 % especially for lower  $\text{RE}$  concentrations (red circles). Obviously rare earth substitution provides for significantly “cleaner” iron arsenide layers compared to the pristine compound, where too high palladium substitution in the FeAs layers suppresses superconductivity. The palladium content in the palladium arsenide layer decreases slightly with increasing rare earth substitution to  $z = 2.7 - 3.0$  in agreement with our single crystal analysis.<sup>[12]</sup> This was correspondingly regarded in the syntheses.

Given five crystallographic different calcium sites in the 1038-type structure, a homogenous distribution of the rare earth substitution may be expected. However, four positions are sevenfold coordinated by arsenic from the two adjacent metal arsenide layers, while just one position is located in a square *anti*-prism of arsenic and is eightfold coordinated. This position is placed right above the vacant palladium position in the palladium arsenide layer, as depicted in Figure 4. Our structure refinements clearly reveal strong site preferences of the  $\text{RE}$  atoms to this position, which is probably driven through a gain of lattice energy when the  $\text{RE}^{3+}$  cation occupies this favorable position with higher arsenic coordination. This is supported by DFT electronic structure calculations. By comparing the total energies of the five possible configurations in  $(\text{Ca}_{0.8}\text{La}_{0.2}\text{FeAs})_{10}\text{Pd}_3\text{As}_8$  we found that lanthanum at the eightfold coordinated site stabilizes the structure by 40 kJ/mol (Fig. 4, right hand side). Relaxation of the atomic coordinates based on force minimization reveals that the lanthanum atom at the eightfold site shifts 0.24 Å out of the plane of the calcium atoms towards the  $\text{Pd}_3\text{As}_8$  layer in agreement with the single crystal data. The significant electronic stabilization of the structure also explains the

increased sample quality and reduced stacking disorder of the rare earth substituted samples when compared with the undoped ones.

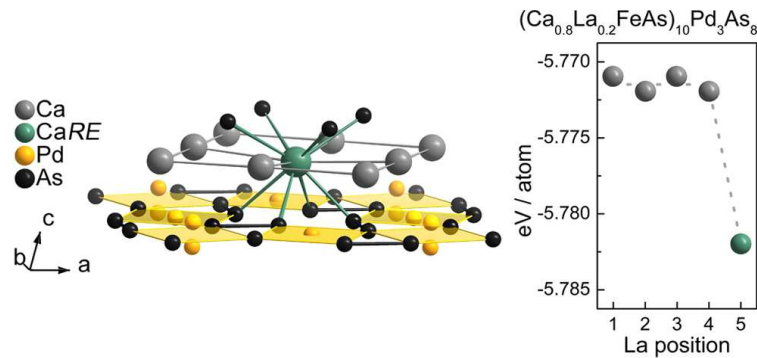


**Figure 4:** Favorable eightfold coordinated position (green) for rare earth substitution at the calcium sites (left) and energy per atom from DFT calculations using the five possible positions for lanthanum (right).

The lattice parameters show basically linear trends with increasing *RE* doping level (Figure 5). For lanthanum with slightly bigger radius ( $1.30 \text{ \AA}$ ) than calcium ( $1.26 \text{ \AA}$ ) the lattice parameters *a* and *c* increase with growing rare earth concentration. For cerium ( $1.28 \text{ \AA}$ ) and praseodymium the *a* parameters are approximately constant while the *c* axes slightly decreases. This can be understood by the higher charge of the  $\text{RE}^{3+}$  ions compared with  $\text{Ca}^{2+}$  ion which increases the coulomb attraction between the layers. No significant changes in the unit cell angles were detected, therefore the cell volume of the lanthanum samples linearly increase, and the cell volumes of the cerium and praseodymium compounds slightly decrease (not shown).

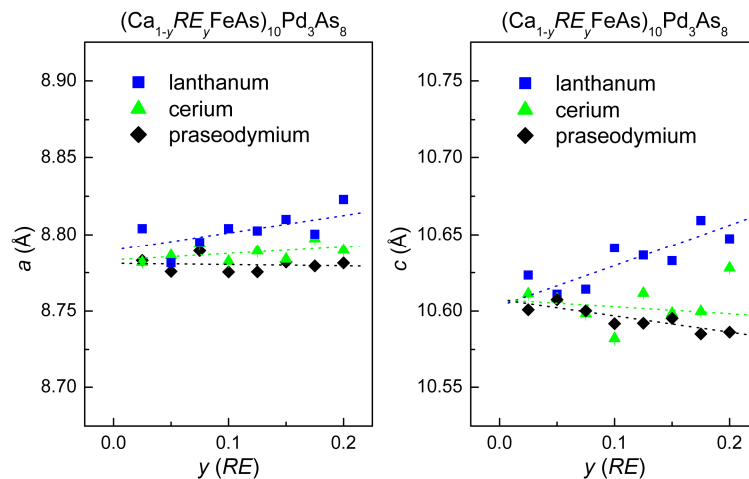


**Figure 5:** Refined lattice parameters for La, Ce, and Pr substitution with different doping ratios.

The compositions obtained from the Rietveld refinements were checked by EDS measurements. Figure 6 summarizes the results by plotting the EDS and Rietveld data against the nominal *RE* concentrations. Both experimental series keep very close to the theoretical value,

confirming the successful synthesis of the three  $(\text{Ca}_{1-y}\text{RE}_y\text{Fe}_{1-x}\text{Pd}_x\text{As})_{10}\text{Pd}_z\text{As}_8$  series. However, the X-ray diffraction powder data are slightly below the nominal line, while the quantification data obtained from EDS are slightly above the nominal values.

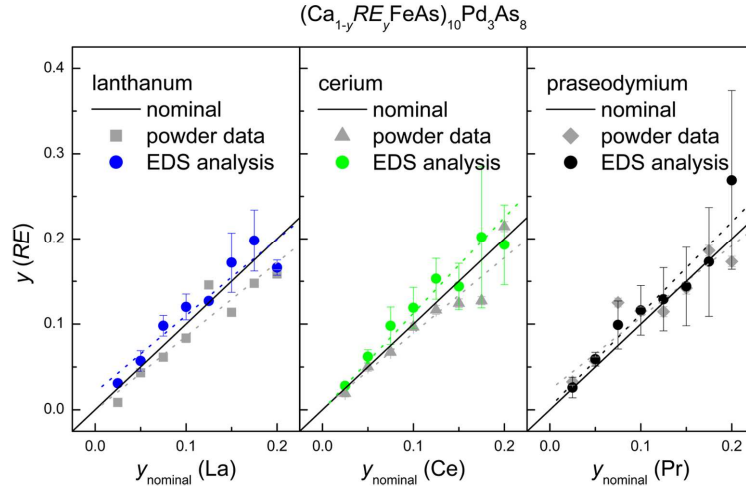


**Figure 6:** Comparison of rare earth substitution levels from refined X-ray powder data (gray) and EDS measurements (blue, green, black) with nominal values (solid black lines are guides to the eye).

Electronic band structure calculations of the idealized parent compound  $(\text{CaFeAs})_{10}\text{Pd}_3\text{As}_8$  have shown that the *Fermi* energy is dominated by orbital contributions from the iron arsenide layers.<sup>[12]</sup> Additional electrons through  $\text{RE}^{3+}$  doping will be transferred to these layers and can induce superconductivity as known from other iron arsenide superconductors.<sup>[3]</sup> As mentioned above, superconductivity is absent in  $(\text{CaFe}_{1-x}\text{Pd}_x\text{As})_{10}\text{Pd}_z\text{As}_8$  probably due to Pd over-doping with  $x > 0.08$ . The latter is strongly reduced in our *RE* doped compound samples and consequently we observe superconductivity. Figure 7 shows the ac-susceptibility data for the three series with La, Ce, and Pr which show superconductivity in the range of  $0.025 \leq y \leq 0.175$ , respectively.

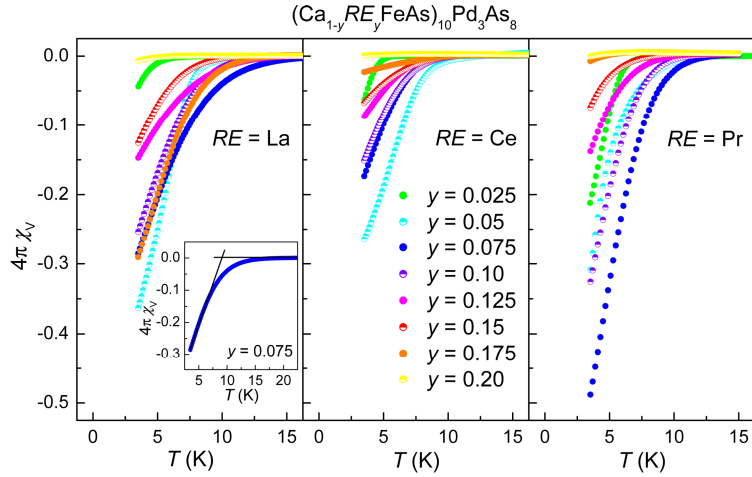


**Figure 7:** Magnetic susceptibility of  $(\text{Ca}_{1-y}\text{RE}_y\text{FeAs})_{10}\text{Pd}_3\text{As}_8$  with  $\text{RE} = \text{La}, \text{Ce}, \text{Pr}$  at different doping levels measured at 1333 Hz.

The highest critical temperatures occur at  $\text{RE}$  doping levels near 0.05 – 0.075 unlike other electron doped iron arsenide superconductors, where typically the highest  $T_c$  are close to 0.15 excess electrons per iron. The highest critical temperatures were obtained for lanthanum doped Pd1038 with an onset of superconductivity at 20 K and a main transition at about 9.5 K.  $(\text{Ca}_{0.95}\text{Ce}_{0.05}\text{FeAs})_{10}\text{Pd}_3\text{As}_8$  shows onset critical temperatures up to 18 K and  $(\text{Ca}_{0.925}\text{Pr}_{0.075}\text{FeAs})_{10}\text{Pd}_3\text{As}_8$  of about 14 K. The main transitions range from 5 K to 9 K for all samples.

*Zero-field-cooled* and *field-cooled* dc-magnetic susceptibility measurements at 15 Oe of each one lanthanum and cerium compound on a SQUID magnetometer show similar results with onsets of superconductivity at 19 K and 16 K, respectively, while the main transitions occur also around 8 K (Figure 8).

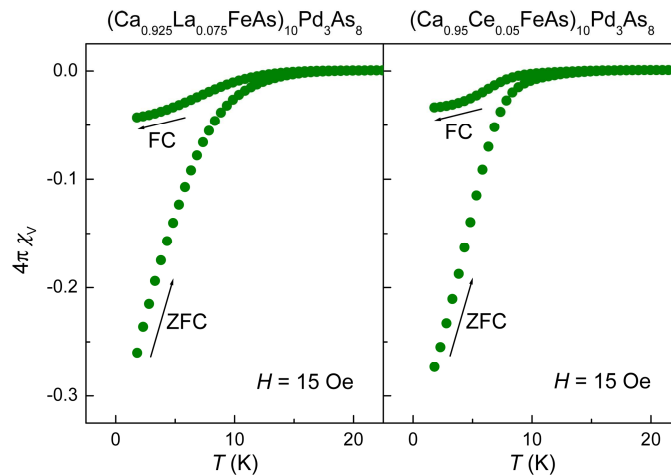


**Figure 8:** *Zero-field-cooled* and *field-cooled* measurements of La and Ce doped samples measured at 15 Oe.

The critical temperatures of the *RE* doped Pd1038 compounds are well below those of the isotypic Pt1038 phases which reach up to 35 K.<sup>[7]</sup> Furthermore the phase transitions are broad, and the superconducting volume fractions approximated from shielding data are 50 % at most. We attribute the lower  $T_c$  to the still present unfavorable palladium doping in the iron arsenide layer. The highest  $T_c$  in Pd doped  $\text{BaFe}_2\text{As}_2$  is about 20 K and occurs at  $x = 0.05$ .<sup>[16,17]</sup> Our Pd1038 samples still contain up to 5 % palladium in the iron arsenide layers, and together with the electrons from the  $RE^{3+}$  doping we are still at the border to over-doping and therefore  $T_c$  decreases. This intrinsically present Pd doping also explains why we observe the highest critical temperatures already at 7.5 % *RE* and not at 15 – 20 % as in Pt1038 and other iron arsenides. Broad transitions and relatively low superconducting phase fractions indicate inhomogeneous doping distribution. Parts of the sample may still have too high palladium concentrations in the iron arsenide layer which prevents superconductivity. To further clarify the situation one would need the parent compound “ $(\text{CaFeAs})\text{Pd}_3\text{As}_8$ ” which should be non-superconducting but magnetically ordered at low temperatures. This could be verified with the platinum compound,<sup>[8]</sup> but for the time being not with Pd1038. Nevertheless there is every reason to expect very similar properties for Pd1038, however, the stronger tendency of palladium to substitute iron in the active layers is quite evident and may be difficult to circumvent.

### 2.3.3 Experimental Section

The compounds  $(\text{Ca}_{1-y}\text{RE}_y\text{Fe}_{1-x}\text{Pd}_x\text{As})_{10}\text{Pd}_z\text{As}_8$  were synthesized via solid state reactions. Stoichiometric mixtures of the pure elements (> 99.9 %) with a reduced amount of palladium according to  $z = 2.8$  were heated at 1000 °C under purified argon and annealed twice at 900 °C. The polycrystalline samples were characterized by X-ray powder diffraction measured on a Huber Imaging Plate Guinier diffractometer with primary monochromator and cobalt or copper radiation, respectively, using an oscillating sample holder. Rietveld refinements based on the Pseudo-Voigt profile were carried out using the TOPAS program package<sup>[18]</sup> including corrections for the Guinier imaging plate as well as sample absorption correction. Crystallite microstructure effects were described by the integral breadth crystallite size approach and the FWHM-based strain calculation. Strong texture effects caused by stacking disorder within the 1038 structure were included using spherical harmonics functions. Cell parameters and occupancies at the Ca/La, Fe/Pd, and Pd/ $\square$  sites were refined while the atomic positions were fixed.

Sample compositions were confirmed by X-ray spectroscopy (EDS) on a Jeol JSM-6500F scanning electron microscope with an Oxford Instruments EDS detector. Ac-susceptibility data of the polycrystalline samples were measured on a self-made ac-susceptometer at 1333 Hz and 3 Oe. Dc-susceptibilities were measured in *zero-field-cooled* and *field-cooled* modes using a Quantum Design MPMS-XL5 SQUID magnetometer at 15 Oe.

Electronic structure calculations were performed using the Vienna ab initio simulation package (VASP),<sup>[19,20]</sup> which is based on density functional theory (DFT) and plane wave basis sets. Projector-augmented waves (PAW)<sup>[21]</sup> were used and contributions of correlation and exchange were treated in the generalized-gradient approximation (GGA) as described by *Perdew, Burke, and Ernzerhof*.<sup>[22]</sup>

### 2.3.4 Conclusion

Solid solutions of the triclinic palladium iron arsenides  $(\text{Ca}_{1-y}\text{RE}_y\text{Fe}_{1-x}\text{Pd}_x\text{As})_{10}\text{Pd}_z\text{As}_8$  were synthesized through solid state reactions. The polycrystalline samples were characterized by X-ray powder diffraction. Substitution levels (Ca/RE, Fe/Pd, and Pd/□) obtained from Rietveld refinements coincide well with the nominal values according to EDS and the linear courses of the lattice parameters as expected from the ionic radii. The  $\text{RE}^{3+}$  ions prefer the one out of five crystallographic positions which is eightfold coordinated by arsenic. This site preference stabilizes the structure by about 40 kJ/mol according to DFT calculations and leads to improved sample quality. The additional electrons due to  $\text{Ca}^{2+}/\text{RE}^{3+}$  substitution are transferred to the FeAs layers, where they obviously diminish the otherwise strong Fe/Pd substitution present in RE-free samples. Since this over-doping by palladium in the FeAs layers suppresses superconductivity in pure Pd1038, the RE doped phases with low Fe/Pd mixing show superconductivity with onset critical temperatures up to 20 K.

### 2.3.5 References

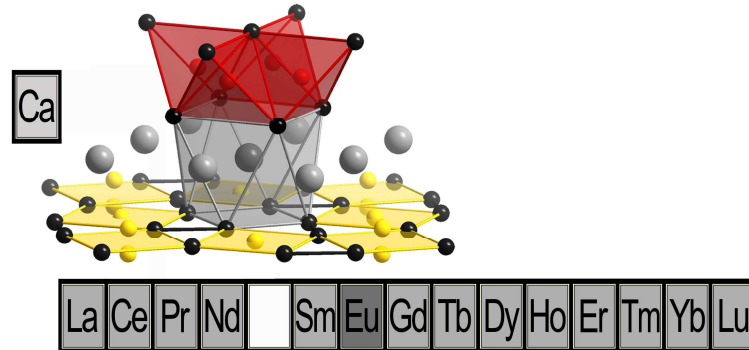
- [1] D. C. Johnston, *Adv. Phys.* **2010**, 59, 803.
- [2] G. R. Stewart, *Rev. Mod. Phys.* **2011**, 83, 1589.
- [3] D. Johrendt, *J. Mater. Chem.* **2011**, 21, 13726.
- [4] C. Löhnert, T. Stürzer, M. Tegel, R. Frankovsky, G. Friederichs, D. Johrendt, *Angew. Chem. Int. Ed.* **2011**, 50, 9195.

- [5] N. Ni, J. M. Allred, B. C. Chan, R. J. Cava, *Proc. Natl. Acad. Sci. U. S. A.* **2011**, *108*, E1019.
- [6] S. Kakiya, K. Kudo, Y. Nishikubo, K. Oku, E. Nishibori, H. Sawa, T. Yamamoto, T. Nozaka, M. Nohara, *J. Phys. Soc. Jpn.* **2011**, *80*, 093704.
- [7] T. Stürzer, G. Derondeau, D. Johrendt, *Phys. Rev. B* **2012**, *86*, 060516(R).
- [8] T. Stürzer, G. M. Friederichs, H. Luetkens, A. Amato, H.-H. Klauss, D. Johrendt, *J. Phys.: Condens. Matter* **2013**, *25*, 122203.
- [9] C. de la Cruz, Q. Huang, J. W. Lynn, J. Y. Li, W. Ratcliff, J. L. Zarestky, H. A. Mook, G. F. Chen, J. L. Luo, N. L. Wang, P. C. Dai, *Nature* **2008**, *453*, 899.
- [10] M. Rotter, M. Tegel, I. Schellenberg, W. Hermes, R. Pöttgen, D. Johrendt, *Phys. Rev. B* **2008**, *78*, 020503(R).
- [11] R. Pöttgen, D. Johrendt, *Intermetallics: Synthesis, Structure, Function*, DeGruyter, **2014**.
- [12] C. Hieke, J. Lippmann, T. Stürzer, G. Friederichs, F. Nitsche, F. Winter, R. Pöttgen, D. Johrendt, *Philos. Mag.* **2013**, *93*, 3680.
- [13] K. Cho, M. A. Tanatar, H. Kim, W. E. Straszheim, N. Ni, R. J. Cava, R. Prozorov, *Phys. Rev. B* **2012**, *85*, 020504.
- [14] T. Stürzer, G. Derondeau, D. Johrendt, *Solid State Commun.* **2015**, *201*, 36.
- [15] N. Ni, W. E. Straszheim, D. J. Williams, M. A. Tanatar, R. Prozorov, E. D. Bauer, F. Ronning, J. D. Thompson, R. J. Cava, *Phys. Rev. B* **2013**, *87*.
- [16] N. Ni, A. Thaler, A. Kracher, J. Q. Yan, S. L. Bud'ko, P. C. Canfield, *Phys. Rev. B* **2009**, *80*, 024511.
- [17] M. A. Tanatar, N. Ni, A. Thaler, S. L. Bud'ko, P. C. Canfield, R. Prozorov, *Phys. Rev. B* **2011**, *84*, 014519.
- [18] A. Coelho, TOPAS-Academic, Version 4.1, Coelho Software, Brisbane, **2007**.
- [19] G. Kresse, J. Furthmüller, *Comput. Mat. Sci.* **1996**, *6*, 15.
- [20] G. Kresse, J. Hafner, *Phys. Rev. B* **1994**, *49*, 14251.

[21] P. E. Blöchl, *Phys. Rev. B* **1994**, 50, 17953.

[22] J. P. Perdew, K. Burke, M. Ernzerhof, *Phys. Rev. Lett.* **1996**, 77, 3865.

## 2.4 $(\text{Ca}_{1-y}\text{RE}_y\text{FeAs})_{10}\text{Pd}_3\text{As}_8$ series with $\text{RE} = \text{La} - \text{Nd}, \text{Sm} - \text{Lu}$ and $y = 0.05, 0.10$



### 2.4.1 Introduction

Since 2011 the discovery of  $(\text{CaFe}_{1-x}\text{M}_x\text{FeAs})_{10}\text{M}_z\text{As}_8$  ( $M = \text{Pd}, \text{Pt}, \text{Ir}$ )<sup>[1-4]</sup> established a new class in the family of iron arsenides featuring an alternate stacking of calcium, iron arsenide, and so far unprecedented planar noble-metal arsenide layers. This exceptional structure chemistry together with the unusual low symmetry was initially matter of discussions about the origin of superconductivity in these compounds.<sup>[1,2,5]</sup> Nevertheless, further investigations revealed non-superconducting  $(\text{CaFeAs})_{10}\text{Pt}_3\text{As}_8$  (Pt1038) as a typical parent compound<sup>[6]</sup> with the characteristic phase transitions at low temperatures. In Chapter 2.2 the indication of an analogous parent state in  $(\text{CaFeAs})_{10}\text{Pd}_3\text{As}_8$  (Pd1038) is strongly suggested. Both electronic structures are comparable to less complex iron arsenides due to iron states dominant at the *Fermi* level, while the noble-metal layers hardly contribute.<sup>[2,3]</sup> Therefore starting from the platinum compound, the reliable concepts of direct and electronic doping were successfully applied to induce superconductivity. Based on these results comparable properties were also expected for the homologous compound Pd1038, but detailed experiments revealed distinct divergences.<sup>[3]</sup>

In contrast to  $(\text{CaFe}_{1-x}\text{M}_x\text{FeAs})_{10}\text{Pt}_3\text{As}_8$  with  $M = \text{Co}, \text{Ni}, \text{Pd}, \text{Pt}$ <sup>[7-9]</sup> no superconductivity could be induced in the homologous palladium compound  $(\text{CaFe}_{1-x}\text{Pd}_x\text{FeAs})_{10}\text{Pd}_3\text{As}_8$  so far. However, the crystal structure comprises two further possibilities to integrate substituents either in the second negatively charged or the cationic calcium layers.<sup>[9]</sup> Since additional electrons result in charge doping of the metallic iron layer responsible for superconductivity, electron doping is conceivable both by occupying the additional metal position in the  $\text{Pd}_z\text{As}_8$  layer yielding  $z = 4$  or by rare earth substitution at the calcium positions. So far no evidence

of high-temperature superconductivity was found in Pd1048 (Chapter 4) as was conversely measured for Pt1048 polymorphs.<sup>[1,2,5]</sup>

On the contrary the established scenario of electron doping<sup>[10-12]</sup> induced superconductivity in  $(\text{Ca}_{1-y}\text{RE}_y\text{FeAs})_{10}\text{Pd}_3\text{As}_8$ .<sup>[3,13]</sup> Concomitant, the intrinsic tendency of palladium to mix on the iron positions can be suppressed widely by rare earth induced structural stabilization and synthetic strategies. For platinum phases not only the emergence of superconductivity by lanthanum substitution,<sup>[9,14]</sup> but also the whole series of lanthanides was analyzed with a maximum  $T_c = 35$  K and moreover yielding an universal phase diagram of electron doping.<sup>[15]</sup> After first experiments on lanthanum doped Pd1038,<sup>[3]</sup> series of  $(\text{Ca}_{1-y}\text{RE}_y\text{FeAs})_{10}\text{Pd}_3\text{As}_8$  with  $\text{RE} = \text{La}, \text{Ce}, \text{Pr}$  and  $y = 0.025 - 0.20$  were studied so far, also revealing a site preference for the eightfold coordinated calcium position.<sup>[13]</sup> Figure 1 illustrates the crystal structure of rare earth doped Pd1038 with the relevant calcium arsenide motif emphasized. Among the five crystallographic calcium positions four are in sevenfold coordination, while the one next to the palladium vacancy is *anti*-prismatically eightfold coordinated by arsenic.

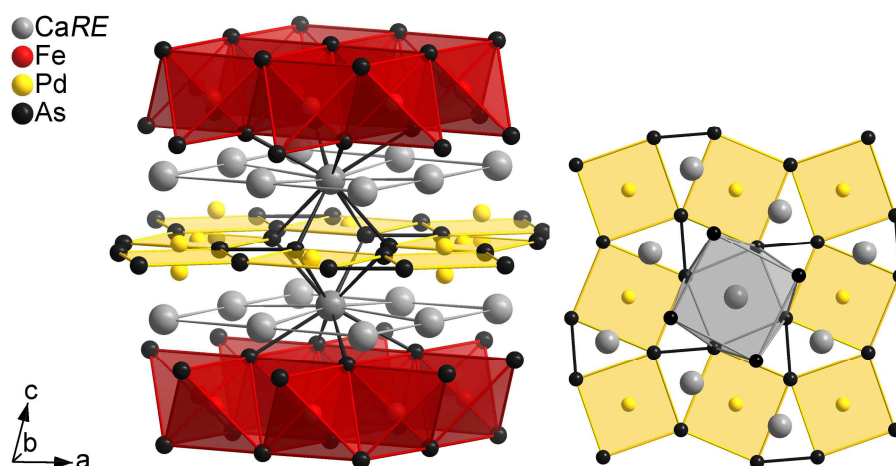


**Figure 1:** Crystal structure of  $(\text{Ca}_{1-y}\text{RE}_y\text{FeAs})_{10}\text{Pd}_3\text{As}_8$  with emphasized eightfold coordination of calcium (left) and top view of calcium palladium arsenide layer with *anti*-prismatic coordination of deflected metal position (right).

Here the complete lanthanide series with  $\text{RE} = \text{La} - \text{Lu}$  was investigated for two substituent concentrations  $y = 0.05$  and  $0.10$  with the focus on structural and superconducting features. The samples were characterized by X-ray powder diffraction and X-ray spectroscopy and their magnetic properties were investigated, also compared to the related platinum compounds.

## 2.4.2 Results and Discussion

### 2.4.2.1 X-ray Powder Diffraction

All samples were characterized by X-ray powder diffraction and Rietveld refinements. Polycrystalline samples of  $(\text{Ca}_{1-y}\text{RE}_y\text{FeAs})_{10}\text{Pd}_3\text{As}_8$  were obtained with small amounts of binary FeAs. For later lanthanides also minor concentrations of REAs as well as  $(\text{CaFeAs})_{10}\text{Pd}_4\text{As}_8$  and  $\text{CaFe}_2\text{As}_2$  were found. Figure 2 shows representative powder diffractograms with Rietveld fits of the series with  $y = 0.05$  and  $0.10$ .

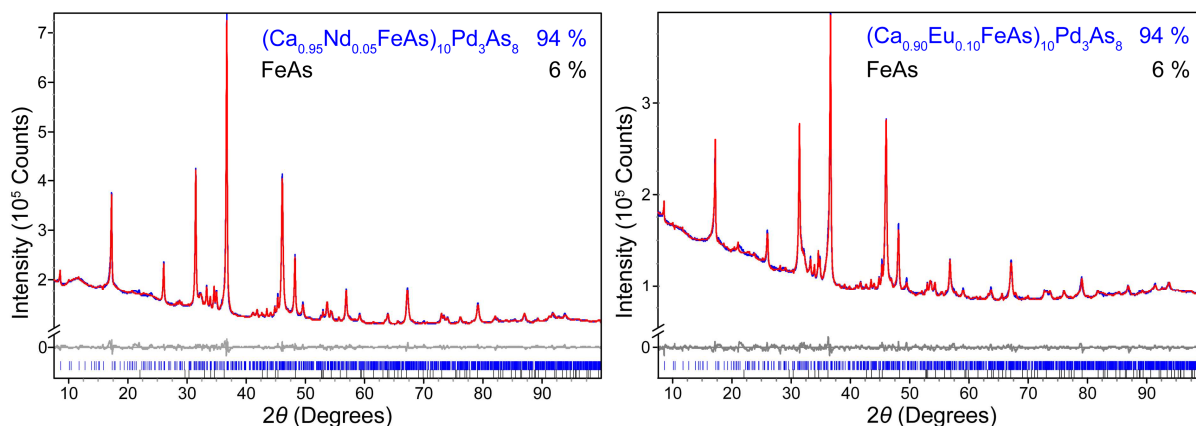


**Figure 2:** X-ray powder data (blue) with Rietveld fit (red) of the nominal compositions  $(\text{Ca}_{0.95}\text{Nd}_{0.05}\text{FeAs})_{10}\text{Pd}_3\text{As}_8$  (left) and  $(\text{Ca}_{0.90}\text{Eu}_{0.10}\text{FeAs})_{10}\text{Pd}_3\text{As}_8$  (right).

Sample compositions are in line with the doping ratios obtained from refined powder diffractograms and EDX measurements showing good agreement with the nominal composition of  $y = 0.05$  and  $0.10$ , respectively, for the earlier lanthanides. Smaller doping levels were obtained for the later lanthanides  $\text{RE} = \text{Gd} - \text{Lu}$  (Figure 3). This reduced substitution preference in  $(\text{Ca}_{1-y}\text{RE}_y\text{FeAs})_{10}\text{Pd}_3\text{As}_8$  is in line with the decreasing ionic radii due to the lanthanide contraction. Compared to the analogue platinum phases<sup>[15]</sup> the average solubility limit is decreased, which may be ascribed to the bigger unit cell volume of Pd1038 against Pt1038 and therewith complicated incorporation of smaller rare earth substituents.

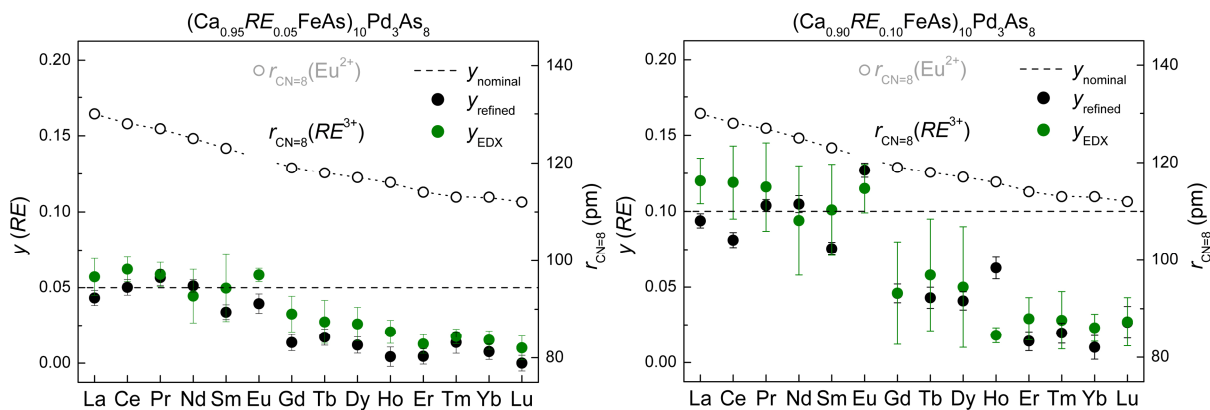


**Figure 3:** Experimental substitution level in  $(\text{Ca}_{1-y}\text{RE}_y\text{FeAs})_{10}\text{Pd}_3\text{As}_8$  from refined powder data (black points) and EDX analyses (green points). The nominal value of the series with  $y = 0.05$  (left) and  $y = 0.10$  (right) is emphasized as black dashed line. The trend of ionic radii of present substituents is added in circles.

Paralleled by the ionic radii is the course of lattice parameters  $a$ ,  $b$ , and  $c$  with varying dopants. Within the series  $y = 0.05$  the in-plane axes  $a$  and  $b$  hardly change in the range of constant substitution level with  $\text{RE} = \text{La} - \text{Sm}$ , while in stacking direction the  $c$  axis decreases with reduced rare earth radius. The effect is more distinct with the doubled doping level of  $y = 0.10$ , where  $c$  shows a significant decrease of 0.6 % from lanthanum to samarium and also  $a$  and  $b$  are reduced (Figure 4). No discernible change is observed for the angles  $\alpha$ ,  $\beta$ , and  $\gamma$  of the triclinic unit cell.

Despite the comparable substituent concentration europium reveals considerable increased lattice parameters. Unlike the remaining lanthanides the usage of europium yields divalent  $\text{Eu}^{2+}$ . Therefore the unit cell volume associated with the lattice parameters is increased compared to the rest of the series. Even in the 5 % doping variant the presence of  $\text{Eu}^{2+}$  already reflects the enlarged ionic radius in eightfold coordination of  $r = 139$  pm instead of 121 pm for  $\text{Eu}^{3+}$ .<sup>[16]</sup>

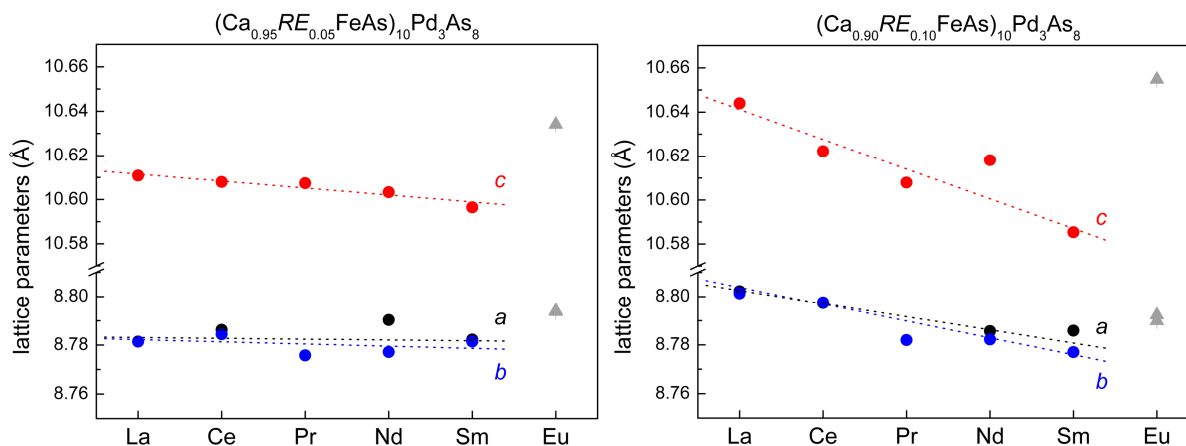


**Figure 4:** Lattice parameters obtained from refined powder data of  $(\text{Ca}_{1-y}\text{RE}_y\text{FeAs})_{10}\text{Pd}_3\text{As}_8$  with  $\text{RE} = \text{La} - \text{Eu}$ ,  $y = 0.05$  (left) and  $y = 0.10$  (right). Values of europium doped samples are colored in gray.

## 2.4.2.2 Magnetic Properties

Besides the known series with lanthanum, cerium, and praseodymium substitution<sup>[13]</sup> in  $(\text{Ca}_{0.95}\text{RE}_{0.05}\text{FeAs})_{10}\text{Pd}_3\text{As}_8$  bulk superconductivity was measured for  $\text{RE} = \text{Nd}, \text{Sm}$ . The critical temperatures of  $T_c = 17.2 \text{ K}$  and  $15.4 \text{ K}$ , respectively, for the onset of superconductivity and the main transition below  $7.5 \text{ K}$  follow the trend of the early lanthanides. With europium playing an exceptional role and promethium not investigated, the remaining trivalent dopants  $\text{RE} = \text{Gd} - \text{Lu}$  show only an onset of superconductivity with  $T_c = 4.7 - 6.7 \text{ K}$  most likely due to inhomogeneous  $\text{Ca}/\text{RE}$  distributions and the small doping level in the vicinity of the minimum necessary for superconductivity. Especially the samples containing the stronger magnetic rare earths as substituents revealed distinct paramagnetic behavior with the maximum progress for dysprosium, followed by holmium and erbium. This trend is in line with listed effective magnetic moments for  $4f$  ions with maximal values for  $\text{Dy}^{3+}$  and  $\text{Ho}^{3+}$ , previous to  $\text{Tb}^{3+}$  and  $\text{Er}^{3+}$ .<sup>[17]</sup> Due to this superposition of weak diamagnetism and strong paramagnetic behavior negative susceptibilities are reached only to some extent. In general superconducting volume fractions did not exceed 5 % at  $3.5 \text{ K}$ . Therefore the temperatures portending the onset of superconductivity with  $\text{RE} = \text{Gd} - \text{Lu}$  are merely indicated in Figure 6 and the compounds should be regarded as non-superconducting. Whereas the onsets of superconductivity slightly decrease for the early lanthanides  $\text{La} - \text{Sm}$  with the maximum  $T_c = 19 \text{ K}$  for lanthanum, a broadly independent relation of the critical temperatures from the present rare earth element was observed for  $\text{RE} = \text{Gd} - \text{Lu}$  with respect to the varying substitution concentrations obtained from EDX analyses.

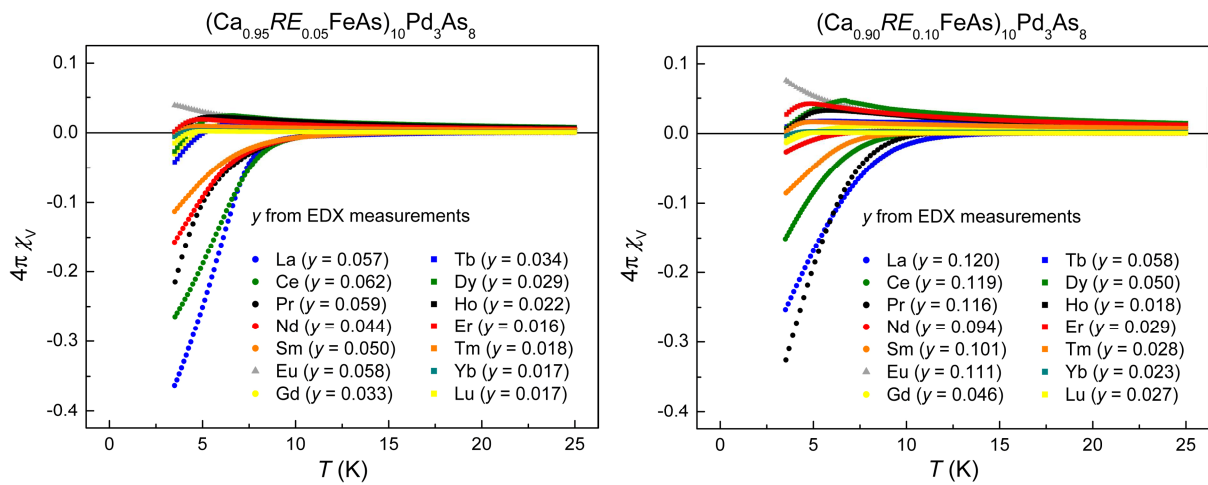


**Figure 5:** Ac-susceptibility data of  $(\text{Ca}_{1-y}\text{RE}_y\text{FeAs})_{10}\text{Pd}_3\text{As}_8$  at 3 Oe and 1333 Hz with  $\text{RE} = \text{La} - \text{Lu}$  for nominal values  $y = 0.05$  (left) and  $y = 0.10$  (right), each with doping amounts from EDX analyses. Measurements of europium doped samples are plotted in gray.

Similar results were obtained for  $(\text{Ca}_{0.90}\text{RE}_{0.10}\text{FeAs})_{10}\text{Pd}_3\text{As}_8$ . Next to lanthanum, cerium, and praseodymium superconductivity was evident in the samples containing neodymium and samarium with onset temperatures of  $T_c = 11.1$  K and 11.3 K. For compounds with  $\text{RE} = \text{Gd} - \text{Lu}$  the maximal diamagnetic amount was about 1 % and the samples showed paramagnetic behavior with dysprosium on top. Furthermore an onset of superconductivity was again present in all samples at temperatures of  $T_c = 4.7 - 7.6$  K indicated in Figure 6.

The lessons learned from  $(\text{Ca}_{1-y}\text{RE}_y\text{FeAs})_{10}\text{Pd}_3\text{As}_8$  with  $\text{RE} = \text{La}, \text{Ce}, \text{Pr}^{[13]}$  can be extended to the whole series of lanthanides. Maximal critical temperatures were obtained for lanthanum doped Pd1038. In contrast to other charge doped iron arsenide superconductors with a typically optimal doping level of about 15 %<sup>[9,18,19]</sup> here the optimal rare earth concentration is below 10 %. Compared to platinum compounds the samples containing  $\text{RE} = \text{Gd} - \text{Lu}$  cannot be characterized as superconductors. The onsets of superconductivity are mostly independent from the containing rare earth element for higher lanthanides. The effective doping levels  $y$  obtained from EDX analyses are listed in Figure 5. Since the values are almost constant and stay below the nominal substitution for  $\text{RE} = \text{Gd} - \text{Lu}$ , they can be taken as solubility limits for rare earth doping in Pd1038.

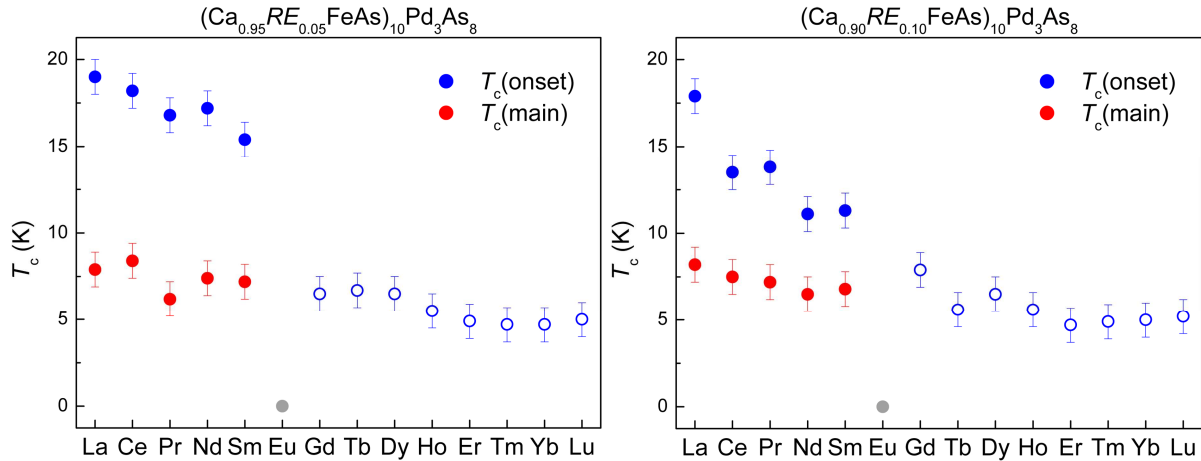


**Figure 6:** Critical temperatures from susceptibility measurements for  $y = 0.05$  (left) and  $y = 0.10$  (right).

Among the series of rare earth doped  $(\text{Ca}_{1-y}\text{RE}_y\text{FeAs})_{10}\text{Pd}_3\text{As}_8$  europium takes a special position, perceivable by the absence of superconductivity and enlarged lattice parameters. With no electron doping present by  $\text{Ca}^{2+}/\text{Eu}^{2+}$  substitution the lack of superconductivity is plausible. In line with this, magnetic measurements revealed paramagnetic behavior in  $(\text{Ca}_{1-y}\text{Eu}_y\text{FeAs})_{10}\text{Pd}_3\text{As}_8$ . Figure 7 shows the molar susceptibility of two europium doped compounds measured at different external fields. The value of susceptibility is slightly reduced at higher fields. The corresponding inverse susceptibilities approach ideal behavior

with increasing fields by suppressing impurity phase contributions. *Curie-Weiss* fits performed from 1.8 – 300 K of both samples with doping concentrations obtained from EDX ( $y_{\text{EDX}} = 0.058, 0.111$ ) at an external magnetic field of 20 kOe yielded effective magnetic moments of  $7.73 \mu_{\text{B}}$  and  $7.93 \mu_{\text{B}}$  per europium, respectively, being in excellent agreement with the reported value for  $\text{Eu}^{2+}$  of  $\mu_{\text{eff}} = 7.94 \mu_{\text{B}}$ . In contrast to other europium containing iron arsenides the statistical distribution of  $\text{Eu}^{2+}$  in  $(\text{Ca}_{1-y}\text{Eu}_y\text{FeAs})_{10}\text{Pd}_3\text{As}_8$  prevents magnetic ordering like in parent<sup>[20]</sup> or substituted<sup>[21]</sup>  $\text{EuFe}_2\text{As}_2$  at  $T_{\text{N}} = 20$  K.

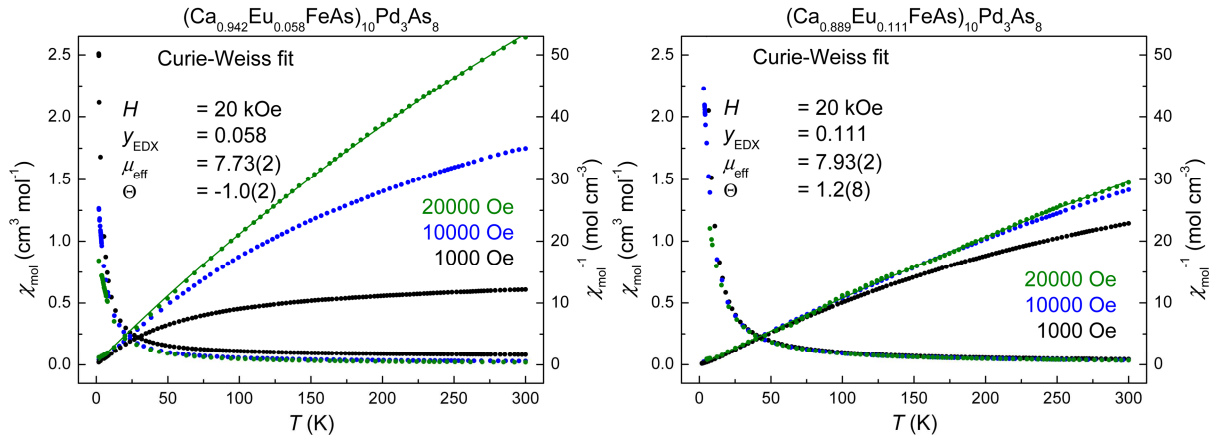


**Figure 7:** Magnetic susceptibilities and inverse data of  $(\text{Ca}_{0.942}\text{Eu}_{0.058}\text{FeAs})_{10}\text{Pd}_3\text{As}_8$  (left) and  $(\text{Ca}_{0.889}\text{Eu}_{0.111}\text{FeAs})_{10}\text{Pd}_3\text{As}_8$  (right) at different external fields. *Curie-Weiss* fits were performed with the doping level  $y$  obtained from EDX analyses for  $H = 20$  kOe.

The magnetization calculated for the respective amount of europium per formula unit at 1.8 K and 300 K are shown in Figure 8. Since no hystereses are observed in all curves the absence of ferromagnetic contamination of both samples is confirmed. Field-induced saturation is achieved at 50 kOe at  $8.1 \mu_{\text{B}}$  and  $10.1 \mu_{\text{B}}$ , respectively. Next to preparative effects caused by the polycrystalline samples, also the influence of the present iron can be considered as possible interpretation of the increased values.

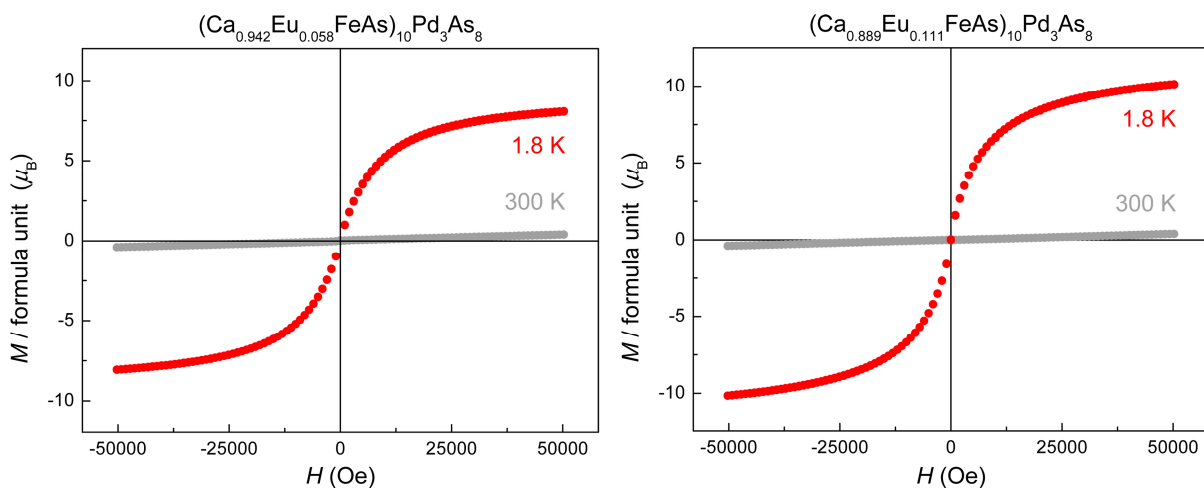


**Figure 8:** Magnetization of  $(\text{Ca}_{0.942}\text{Eu}_{0.058}\text{FeAs})_{10}\text{Pd}_3\text{As}_8$  (left) and  $(\text{Ca}_{0.889}\text{Eu}_{0.111}\text{FeAs})_{10}\text{Pd}_3\text{As}_8$  (right) at 1.8 K and 300 K with varying magnetic fields.

### 2.4.3 Experimental Section

Polycrystalline samples  $(\text{Ca}_{1-y}\text{RE}_y\text{FeAs})_{10}\text{Pd}_3\text{As}_8$  with  $\text{RE} = \text{La} - \text{Lu}$ ,  $y = 0.05, 0.10$  were synthesized via solid state reactions. Stoichiometric mixtures of the pure elements (> 99.5 %) were filled in alumina crucibles sealed under purified argon and heated for 10 h each at 600 °C followed by 1000 °C. The products were grounded in the crucible, sealed under argon and annealed at 900 °C for 25 or 30 h, respectively. Afterwards the samples were well homogenized, pelletized, and annealed at 900 °C for 25, 30 or 50 h, respectively. The obtained polycrystalline products were grounded and characterized by X-ray powder diffraction at room temperature using a Huber Imaging Plate Guinier diffractometer with primary monochromator and copper radiation. The corresponding Rietveld refinements were performed using the TOPAS program package<sup>[22]</sup> based on single crystal data of  $(\text{CaFe}_{1-x}\text{Pd}_x\text{As})_{10}\text{Pd}_3\text{As}_8$ . Sample compositions were confirmed by X-ray spectroscopy (EDX) on a Jeol JSM-6500F scanning electron microscope with an Oxford Instruments EDX detector or a Carl Zeiss EVO-MA 10 equipped with a Bruker Nano EDX detector, respectively. Ac-susceptibility data was measured on an ac-susceptometer at 1333 Hz and 3 Oe, dc-susceptibility and magnetization using a Quantum Design MPMS-XL5 SQUID magnetometer with variable magnetic fields.

### 2.4.4 Conclusion

The complete series of charge doped  $(\text{Ca}_{1-y}\text{RE}_y\text{FeAs})_{10}\text{Pd}_3\text{As}_8$  with  $\text{RE} = \text{La} - \text{Lu}$  was synthesized with two substitution levels  $y = 0.05$  and  $0.10$ . The compounds were obtained as high quality polycrystalline samples via solid state reactions. Rare earth concentrations were veri-

fied by refined X-ray powder data and EDX spectroscopy in good agreement with the nominal values for  $RE = \text{La} - \text{Eu}$ . The reduced levels for higher lanthanides were assigned as solubility limits due to the unfavorable incorporation of small rare earth ions as dopants in Pd1038. Unit cell axes shorten with decreasing rare earth radii at comparable occupation. The samples showed bulk superconductivity induced by electron doping with trivalent  $RE = \text{La}$ , Ce, Pr, Nd, and Sm, while  $RE = \text{Gd} - \text{Lu}$  revealed mainly paramagnetic behavior caused by weak superconductivity superimposed by significant  $f$  electron magnetism. Within the determined range the respective substitution levels for later lanthanides can be seen as the minimum concentration for the induction of superconductivity. Maximum critical temperatures were measured for lanthanum substituted samples. Compared to other charge doped iron arsenide superconductors rare earth substituted Pd1038 features atypical optimal doping levels below 10 %. The concept of superconductivity by electron doping in this system was furthermore substantiated by reverse reasoning since the presence of  $\text{Eu}^{2+}$  caused an absence of superconductivity in europium doped samples. Molar susceptibility and magnetization studies showed paramagnetic progress with no magnetic order and hystereses. The effective magnetic moments derived from *Curie-Weiss* fits are in excellent agreement with  $\text{Eu}^{2+}$ . The enlarged lattice parameters of  $(\text{Ca}_{1-y}\text{Eu}_y\text{FeAs})_{10}\text{Pd}_3\text{As}_8$  were attributed to the bigger ionic radius of the divalent ion. Even with a site preference for  $RE^{3+}$  the substitution of calcium by smaller rare earth ions is complicated in Pd1038, since the structure is enlarged in contrast to the related platinum compounds. Comparing both rare earth substituted 1038-type series divergent magnetic properties in terms of doping levels and the presence of superconductivity occur in  $(\text{Ca}_{1-y}\text{RE}_y\text{FeAs})_{10}\text{Pd}_3\text{As}_8$ .

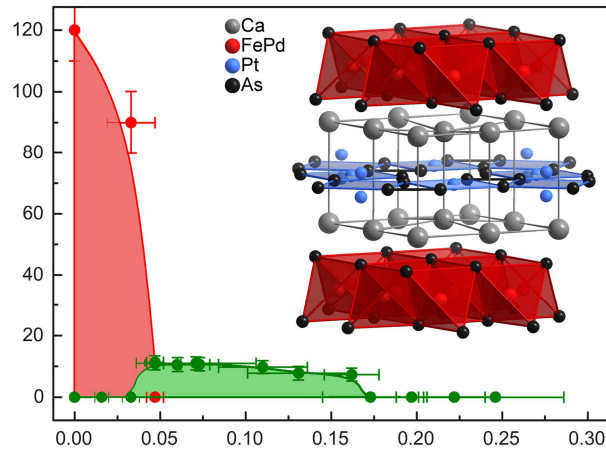
#### 2.4.5 References

- [1] N. Ni, J. M. Allred, B. C. Chan, R. J. Cava, *Proc. Natl. Acad. Sci.* **2011**, *108*, E1019.
- [2] C. Löhnert, T. Stürzer, M. Tegel, R. Frankovsky, G. Friederichs, D. Johrendt, *Angew. Chem. Int. Ed.* **2011**, *50*, 9195.
- [3] C. Hieke, J. Lippmann, T. Stürzer, G. M. Friederichs, F. Nitsche, F. Winter, R. Pöttgen, D. Johrendt, *Philos. Mag.* **2013**, *93*, 3680.
- [4] K. Kudo, D. Mitsuoka, M. Takasuga, Y. Sugiyama, K. Sugawara, N. Katayama, H. Sawa, H. S. Kubo, K. Takamori, M. Ichioka, T. Fujii, T. Mizokawa, M. Nohara, *Sci. Rep.* **2013**, *3*, 3101.

- [5] S. Kakiya, K. Kudo, Y. Nishikubo, K. Oku, E. Nishibori, H. Sawa, T. Yamamoto, T. Nozaka, M. Nohara, *J. Phys. Soc. Jpn.* **2011**, *80*, 093704.
- [6] T. Stürzer, G. M. Friederichs, H. Luetkens, A. Amato, H.-H. Klauss, F. Winter, R. Pöttgen, D. Johrendt, *J. Phys.: Condens. Matter* **2013**, *25*, 122203.
- [7] T. Stürzer, F. Kessler, D. Johrendt, *Philos. Mag.* **2014**, *94*, 3632.
- [8] C. Stürzer, D. Johrendt, **2015**, *in preparation*. (see Chapter 3)
- [9] T. Stürzer, G. Derondeau, D. Johrendt, *Phys. Rev. B* **2012**, *86*, 060516(R).
- [10] D. C. Johnston, *Adv. Phys.* **2010**, *59*, 803.
- [11] D. Johrendt, *J. Mater. Chem.* **2011**, *21*, 13726.
- [12] G. R. Stewart, *Rev. Mod. Phys.* **2011**, *83*, 1589.
- [13] C. Stürzer, A. Schulz, D. Johrendt, *Z. Anorg. Allg. Chem.* **2014**, *640*, 3143.
- [14] N. Ni, W. E. Straszheim, D. J. Williams, M. A. Tanatar, R. Prozorov, E. D. Bauer, F. Ronning, J. D. Thompson, R. J. Cava, *Phys. Rev. B* **2013**, *87*, 060507.
- [15] T. Stürzer, G. Derondeau, D. Johrendt, *Solid State Commun.* **2015**, *201*, 36.
- [16] A. F. Hollemann, E. Wiberg, N. Wiberg, *Lehrbuch der Anorganischen Chemie*, Walter de Gruyter, Berlin, **2007**.
- [17] H. Lueken, *Magnetochemie*, B. G. Teubner, Stuttgart Leipzig, **1999**.
- [18] Y. Qi, Z. Gao, L. Wang, D. Wang, X. Zhang, C. Yao, C. Wang, C. Wang, Y. Ma, *Supercond. Sci. Technol.* **2012**, *25*, 045007.
- [19] G. F. Chen, Z. Li, D. Wu, G. Li, W. Z. Hu, J. Dong, P. Zheng, J. L. Luo, N. L. Wang, *Phys. Rev. Lett.* **2008**, *100*, 247002.
- [20] H. S. Jeevan, Z. Hossain, D. Kasinathan, H. Rosner, C. Geibel, P. Gegenwart, *Phys. Rev. B* **2008**, *78*, 052502.
- [21] M. Zhang, J. J. Ying, Y. J. Yan, A. F. Wang, X. F. Wang, Z. J. Xiang, G. J. Ye, P. Cheng, X. G. Luo, J. Hu, X. H. Chen, *Phys. Rev. B* **2012**, *85*, 092503.
- [22] A. Coelho, TOPAS-Academic, Version 4.1, Coelho Software, Brisbane, **2007**.

### 3 Combination of Palladium and Platinum 1038 Phases in $(\text{CaFe}_{1-x}\text{Pd}_x\text{As})_{10}\text{Pt}_3\text{As}_8$

Christine Stürzer, Dirk Johrendt



*This chapter is in preparation to be published in a scientific journal.*

#### Abstract

The discovery of high- $T_c$  superconductivity in  $(\text{CaFeAs})_{10}\text{Pt}_z\text{As}_8$  added a new branch to the family of iron arsenide superconductors. Subsequently we also found the analogue palladium compound, both available as directly doped compounds with the respective noble-metal. Although the platinum phases show superconductivity, there was astonishingly none induced in Pd1038 phases without charge doping so far. Initial results suggested heavy palladium over-doping being responsible originating from omnipresent Fe/Pd mixing. In this paper we present the combination of palladium substitution into the platinum parent compound featuring surprisingly superconductivity in a wide doping range up to 16 %. Therefore significant palladium substitution seems not to be in charge for the not yet solved mystery of missing superconductivity in directly doped Pd1038. High quality samples of  $(\text{CaFe}_{1-x}\text{Pd}_x\text{As})_{10}\text{Pt}_3\text{As}_8$  were synthesized and characterized by X-ray powder diffraction as well as X-ray spectroscopy for structural and compositional data. Magnetic properties were investigated by susceptibility, *zero-field-cooled/ field-cooled*, and resistivity measurements. Along with temperature-depending X-ray diffraction our results allow for a first phase diagram in the system  $(\text{CaFe}_{1-x}\text{Pd}_x\text{As})_{10}\text{Pt}_3\text{As}_8$ .

### 3.1 Introduction

The discovery of superconductivity in fluorine doped  $\text{LaFeAsO}$  ( $T_c = 26 \text{ K}$ )<sup>[1]</sup> in 2008 established the second era of high-temperature superconductivity research. With  $(\text{CaFeAs})_{10}\text{Pt}_3\text{As}_8$ <sup>[2]</sup> (Pt1038) lately the group of parent compounds among this family of iron arsenide superconductors was complemented by another interesting member. Like almost all parent compounds undoped Pt1038 shows a structural and magnetic phase transition upon cooling to lower temperatures as well as antiferromagnetic ordering. In line with for example the known iron arsenide parents  $\text{BaFe}_2\text{As}_2$ <sup>[3]</sup> and  $\text{LaOFeAs}$ ,<sup>[4]</sup> superconductivity emerges only by the application of well established scenarios like direct or charge doping. Build up from not only the characteristic iron arsenide tetrahedra but a second metal arsenide layer, each separated by calcium, this new class stands out from the growing group of iron-based superconductors.<sup>[5-7]</sup> Although pure  $(\text{CaFeAs})_{10}\text{Pt}_3\text{As}_8$  does not show any superconducting properties, transition-metal doping on the iron sites gives rise to critical temperatures up to  $T_c = 15.3 \text{ K}$  for  $M = \text{Co}$ ,  $T_c = 13.4 \text{ K}$  for  $M = \text{Ni}$ ,<sup>[8]</sup> and  $T_c = 15 \text{ K}$  for notably platinum doped  $(\text{CaFe}_{1-x}\text{Pt}_x\text{As})_{10}\text{Pt}_3\text{As}_8$ .<sup>[9]</sup> Highest critical temperatures of  $T_c = 35 \text{ K}$  arise in electron doped compounds either by additional platinum in  $(\text{CaFeAs})_{10}\text{Pt}_4\text{As}_8$  (1048),<sup>[9]</sup> or rare earth doping on the calcium sites.<sup>[10]</sup> Beyond the platinum phases we also succeeded in synthesizing the structurally analogous palladium based compound  $(\text{CaFeAs})_{10}\text{Pd}_3\text{As}_8$  (Pd1038).<sup>[11]</sup> Remarkably, these samples show no superconductivity by palladium substitution on the iron positions so far. Though, on the other hand in rare earth substituted Pd1038 compounds charge doping can induced superconductivity with critical temperatures up to  $T_c = 20 \text{ K}$ .<sup>[12]</sup> Based on this knowledge it seems reasonable to combine these two closely related compounds in  $(\text{CaFe}_{1-x}\text{Pd}_x\text{As})_{10}\text{Pt}_3\text{As}_8$ , to investigate the underlying cause of the lacking superconductivity in directly palladium doped Pd1038.

In this paper we present a series of palladium substituted platinum iron arsenides. The compounds obtained via solid state synthesis show superconducting properties despite of palladium concentration up to 16 % on the iron sites, although related compounds like  $\text{Ba}(\text{Fe}_{1-x}\text{Pd}_x)_2\text{As}_2$  show superconductivity only below 8 % of the dopant with a maximum  $T_c$  of 19 K for  $x = 0.053$ .<sup>[13]</sup> The doping level  $x$  was checked by X-ray spectroscopy and refined X-ray powder data, also providing the alteration of lattice parameters with varying palladium content. Magnetic properties were characterized by ac-susceptibility and *zero-field-cooled/field-cooled* measurements as well as resistivity data. Temperature-dependending X-ray powder

diffraction gives rise to a phase diagram featuring both a parent state-like and superconducting range.

## 3.2 Results and Discussion

Polycrystalline samples of  $(\text{CaFe}_{1-x}\text{Pd}_x\text{As})_{10}\text{Pt}_3\text{As}_8$  with  $x = 0.0125 - 0.25$  and a step size of  $\Delta = 0.0125$  and  $0.025$ , respectively, were obtained via solid state reactions. The compounds crystallize in the 1038-type structure (space group  $P\bar{1}$ ), shown in Figure 1. The two negatively charged metal pnictide layers with iron tetrahedrally and platinum planar fourfold coordinated by arsenic are separated by calcium ions. The shifted stacking of the different layers, each showing tetragonal symmetry, leads to the triclinic structure.

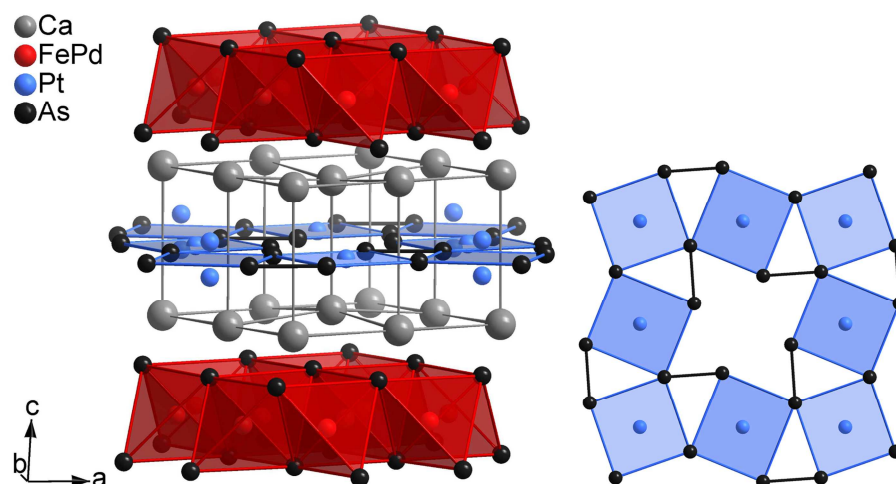


**Figure 1:** Crystal structure of  $(\text{CaFe}_{1-x}\text{Pd}_x\text{As})_{10}\text{Pt}_3\text{As}_8$  (left) with  $\text{Pt}_3\text{As}_8$  layer (right).

### 3.2.1 X-ray Powder Diffraction

The samples were characterized by X-ray powder diffraction. Rietveld refinements revealed either phase pure compounds, or partly included small percentages of the binary impurities  $\text{FeAs}$  and  $\text{PtAs}_2$  as well as an amount of 1048 in higher substituted samples. Figure 2 shows one diffractogram with Rietveld fit of a palladium doped  $(\text{CaFe}_{1-x}\text{Pd}_x\text{As})_{10}\text{Pt}_3\text{As}_8$  sample. The pronounced stacking disorder always present in this system is clearly visible by anisotropic reflex broadening. The magnitude of this intrinsic feature makes a satisfying revelation of structural details from single crystal data very difficult.

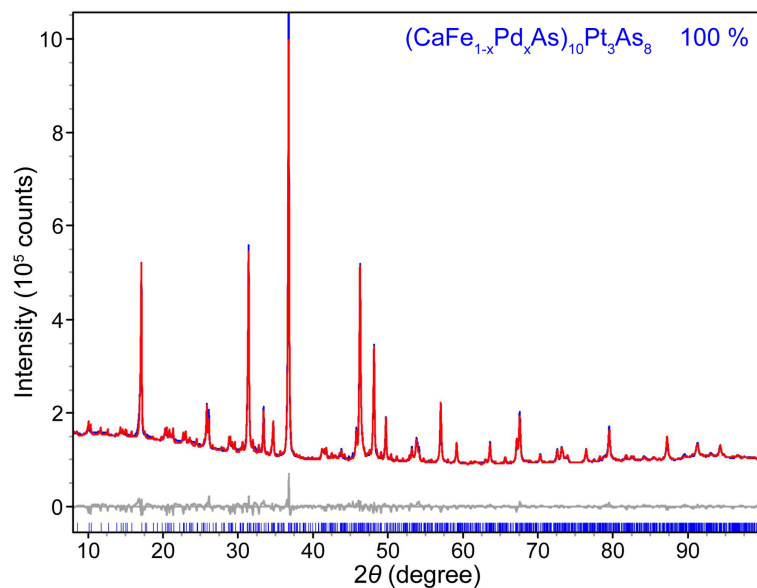


**Figure 2:** X-ray powder data (blue) with Rietveld fit (red) of palladium doped Pt1038 sample.

Lattice parameters of the whole substitution series were obtained from refined powder data. Figure 3 displays the trends with varying palladium concentration for the nominal values  $x = 0.0125 - 0.25$ . The unit cell undergoes a compression along the stacking direction with the  $c$  axis decreasing linearly accompanied with a steady enlargement of the axes parameters  $a$  and  $b$  while the angles remain constant. This behavior is in line with the idea of doping  $d^8$  palladium ions on tetrahedrally coordinated iron positions having in mind the almost identical ionic radii of iron and palladium. In total the unit cell volume increases approximately linear with increasing palladium concentration in the studied range.

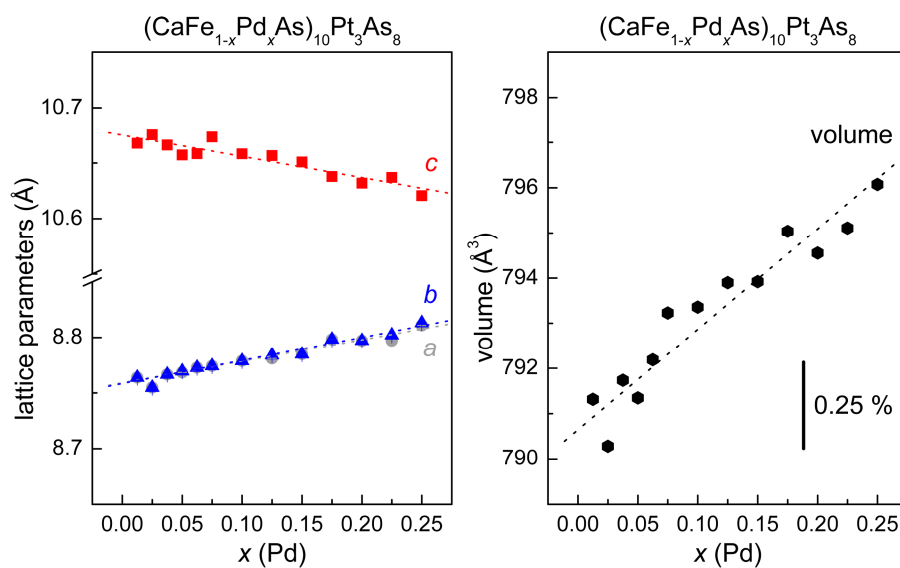


**Figure 3:** Refined lattice parameters (left) and unit cell volume (right) of  $(\text{CaFe}_{1-x}\text{Pd}_x\text{As})_{10}\text{Pt}_3\text{As}_8$  with  $x = 0.0125 - 0.25$ . Dotted lines are guides to the eye.

Additional to the structural parameters also the substitution level  $x$  in  $(\text{CaFe}_{1-x}\text{Pd}_x\text{As})_{10}\text{Pt}_3\text{As}_8$  was obtained by Rietveld refinements. The results imply the linear increase expected from the nominal values, however, especially at low doping concentration the analysis with X-ray diffraction is not entirely reliable. Therefore supplementary X-ray spectroscopy (EDX) measurements were carried out for all samples yielding very good agreement with the nominal values, thus confirming the successful synthesis of  $(\text{CaFe}_{1-x}\text{Pd}_x\text{As})_{10}\text{Pt}_3\text{As}_8$  (Figure 4).

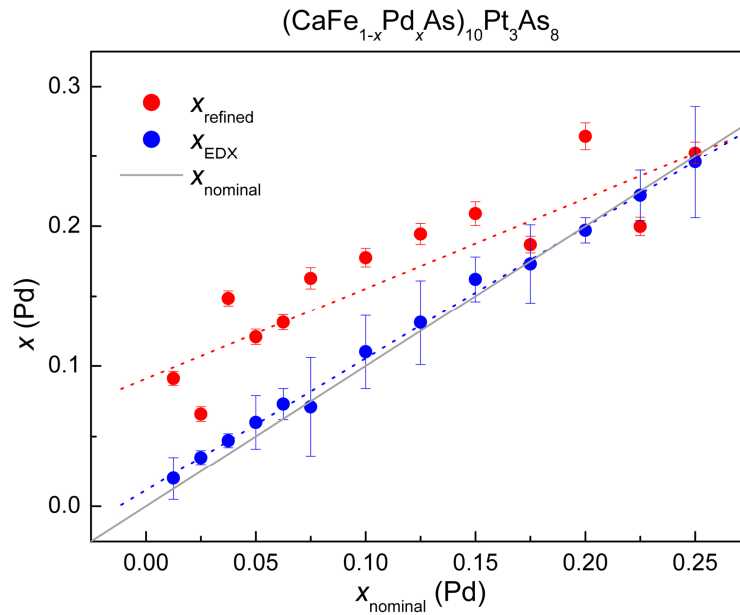


**Figure 4:** Substitution level obtained from Rietveld refinements (red) and EDX analyses (blue) of  $(\text{CaFe}_{1-x}\text{Pd}_x\text{As})_{10}\text{Pt}_3\text{As}_8$  series for nominal values of  $x = 0.0125 - 0.25$ . Dotted lines are guides to the eye.

### 3.2.2 Magnetic Properties

Ac-susceptibility measurements revealed superconducting properties in compounds with palladium concentration of 4.7 – 16.2 % obtained from EDX analyses. The shielding fractions of about 60 % for lower doping levels decrease to about 20 % for the higher palladium concentrations  $x = 0.131$  and  $0.162$ . In samples with  $x = 0.173$  and  $x = 0.197$  only traces of superconducting volume fractions remain, probably due to inhomogeneous substituent distribution. No superconductivity was obtained for very low palladium concentrations of  $x = 0.018, 0.035$ . Figure 5 (left) shows ac-susceptibility data of all superconducting samples at 3 Oe.

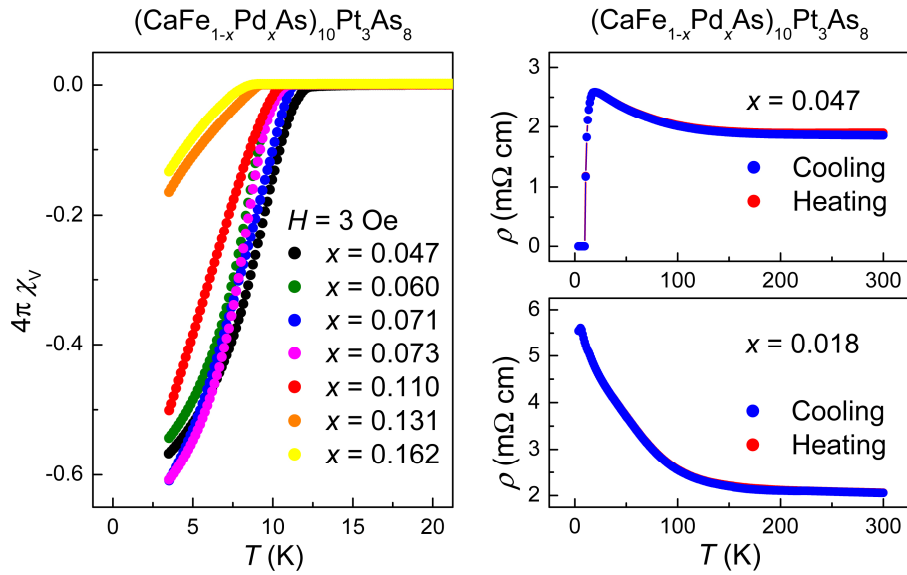


**Figure 5:** Ac-susceptibility data of superconducting  $(\text{CaFe}_{1-x}\text{Pd}_x\text{As})_{10}\text{Pt}_3\text{As}_8$  samples measured at 1333 Hz and 3 Oe with substitution levels obtained from EDX analysis (left), dc-resistivity measurements of a superconducting and non-superconducting sample each (right).

Dc-resistivity data of a superconducting sample shows the onset of superconductivity at 17.5 K and zero resistivity below 10.5 K, which is in good agreement with ac-susceptibility and *zero-field-cooled/ field-cooled* data. Moreover resistivity measurement of a non-superconducting compound ( $x = 0.018$ ) revealed under-doped  $(\text{CaFe}_{1-x}\text{Pd}_x\text{As})_{10}\text{Pt}_3\text{As}_8$  being similar to parent  $(\text{CaFeAs})_{10}\text{Pt}_3\text{As}_8$ . The semiconductor-like development at low temperatures is in contradiction to other iron arsenides. The absolute values are a bit reduced compared to the ones of pure Pt1038.<sup>[2]</sup>

$(\text{CaFe}_{1-x}\text{Pd}_x\text{As})_{10}\text{Pt}_3\text{As}_8$  yield a maximum critical temperature of  $T_c = 11.5$  K with an onset of 16.5 K for  $x = 0.047$ . SQUID measurement of highest- $T_c$  sample shows a main transition temperature of 11.5 K as displayed in the *zero-field-cooled/ field-cooled* graph in the inset of Figure 6 confirming the previously obtained data. In addition the analogue measurement of the under-doped non-superconducting compound with  $x = 0.035$  is shown for comparison. Hence the critical temperatures stay below the values of other transition-metal doped Pt1038 compounds with  $M = \text{Co}, \text{Ni}, \text{Pt}$  and maximal  $T_c$  of 15 K and 13 K, respectively. Therefore superconductivity inducible by palladium doping proves  $(\text{CaFeAs})_{10}\text{Pt}_3\text{As}_8$  again as a typical parent system for very different doping scenarios just like the well investigated  $\text{BaFe}_2\text{As}_2$ .<sup>[3,14]</sup> At the same time with no superconductivity at all induced in palladium substituted Pd1038 so far, this system reaffirms to be outstanding from the growing family of these new complex iron arsenides. Our results reveal palladium substitution in 1038 compounds up to about 16 % not to be an exclusion criterion for superconducting properties.

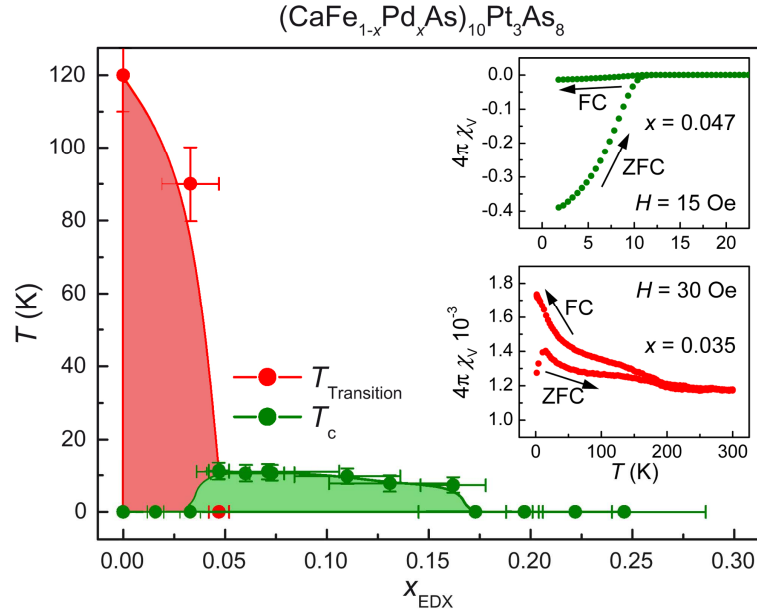


**Figure 6:** Phase diagram of  $(\text{CaFe}_{1-x}\text{Pd}_x\text{As})_{10}\text{Pt}_3\text{As}_8$ , data of undoped  $(\text{CaFeAs})_{10}\text{Pt}_3\text{As}_8$ <sup>[2]</sup> was added for completeness. Insets: ZFC/ FC measurements of compound with highest  $T_c$  of 11.5 K (green) and a non-superconducting sample (red).

The series  $(\text{CaFe}_{1-x}\text{Pd}_x\text{As})_{10}\text{Pt}_3\text{As}_8$  with  $x = 0 - 0.246$  reveals the typical  $T_c(x)$  dependency shown in the phase diagram of Figure 6 with a dome-like behavior for the superconducting doping range from  $x_{\text{SC}} = 0.047 - 0.162$ . Similar results were also reported for cobalt with  $x_{\text{SC}} = 0.047 - 0.136$  and nickel with  $x_{\text{SC}} = 0.022 - 0.092$  substitution,<sup>[8]</sup> while platinum doping faces a solubility limit at about 7 % in favor of the formation of 1048 phases.<sup>[9]</sup>

The undoped parent compound  $(\text{CaFeAs})_{10}\text{Pt}_3\text{As}_8$  undergoes a structured phase transition at 120 K<sup>[2]</sup> by losing the local fourfold symmetry within the layers. Thereby the lattice parameters  $a$  and  $b$  distort the square basal plane of the unit cell yielding  $a \neq b$ . An analogous transition was observed in minor substituted, non-superconducting  $(\text{CaFe}_{1-x}\text{Pd}_x\text{As})_{10}\text{Pt}_3\text{As}_8$  with  $x = 0.035$  at 90 K, while the minimal doped superconducting compound ( $x = 0.047$ ) shows no distortion (Figure 7). Therefore this structural phase transition is suppressed by palladium doping. Furthermore dc-susceptibility data for  $x = 0.035$  at 100 Oe features anomalies at about 100 K and 200 K, respectively, also indicating intrinsic transitions within non-superconducting  $(\text{CaFe}_{1-x}\text{Pd}_x\text{As})_{10}\text{Pt}_3\text{As}_8$ . These results give rise to a preliminary phase diagram with the values of parent Pt1038<sup>[2]</sup> added for completeness. Comparing to other palladium substituted iron arsenides with a coexistence of superconductivity and antiferromagnetic state like  $\text{Ba}(\text{Fe}_{1-x}\text{Pd}_x)_2\text{As}_2$ <sup>[13,15]</sup> and  $\text{Sr}(\text{Fe}_{1-x}\text{Pd}_x)_2\text{As}_2$ ,<sup>[16]</sup> it is not yet clear whether such a coexistence is also a property of  $(\text{CaFe}_{1-x}\text{Pd}_x\text{As})_{10}\text{Pt}_3\text{As}_8$ . Analogous considerations concerning the phase diagram of 1038 series  $(\text{Ca}_{1-y}\text{La}_y\text{FeAs})_{10}\text{Pt}_3\text{As}_8$ <sup>[17]</sup> are as well not fully clarified so far.

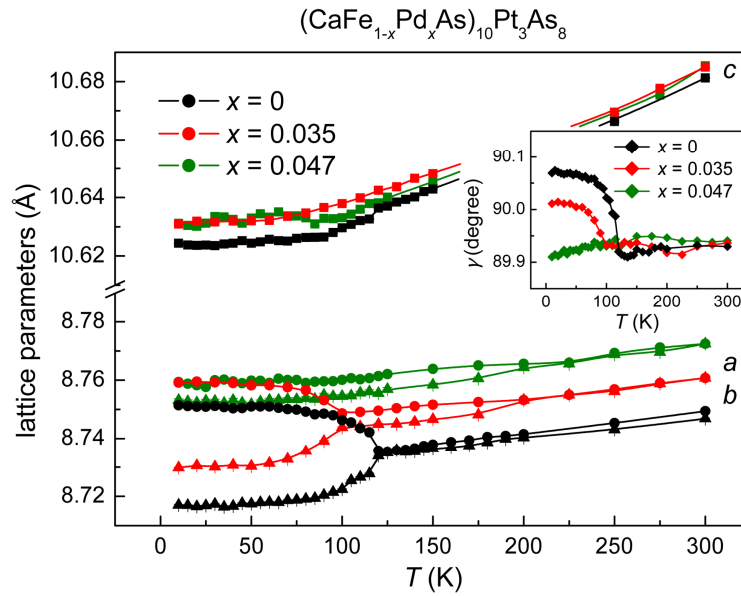


**Figure 7:** Refined lattice parameters  $a$  (circles),  $b$  (triangles), and  $c$  (squares) of  $(\text{CaFe}_{1-x}\text{Pd}_x\text{As})_{10}\text{Pt}_3\text{As}_8$  with  $x = 0.035, 0.047$  from temperature-depending XRD measurements, data of undoped  $(\text{CaFeAs})_{10}\text{Pt}_3\text{As}_8$ <sup>[2]</sup> was added for completeness. Inset:  $\gamma$ -angle.

### 3.3 Experimental Section

All samples of  $(\text{CaFe}_{1-x}\text{Pd}_x\text{As})_{10}\text{Pt}_3\text{As}_8$  were synthesized via solid state reaction with varying palladium concentrations of  $x = 0.0125 - 0.25$  and step sizes of  $\Delta = 0.0125$  and  $0.025$ , respectively. Stoichiometric mixtures of the pure elements ( $> 99.9\%$ ) with a reduced platinum content according to  $z = 2.9$  were heated at  $600\text{ }^\circ\text{C}$  followed by  $1000\text{ }^\circ\text{C}$  under purified argon and annealed twice at  $1000\text{ }^\circ\text{C}$ . The obtained polycrystalline samples were characterized by X-ray powder diffraction at room temperature using a Huber Imaging Plate Guinier diffractometer with primary monochromator and copper radiation. Temperature-dependent powder data were measured on a Huber Imaging Plate Guinier diffractometer with primary monochromator and cobalt radiation equipped with a close-cycle Helium cryostat. Rietveld refinements of all powder data were carried out using the TOPAS program package.<sup>[18]</sup> Sample compositions were confirmed by X-ray spectroscopy (EDX) on a Jeol JSM-6500F scanning electron microscope with an Oxford Instruments EDX detector or a Carl Zeiss EVO-MA 10 equipped with a Bruker Nano EDX detector, respectively. Ac-susceptibility data was measured on an ac-susceptometer at  $1333\text{ Hz}$  and  $3\text{ Oe}$ , dc-susceptibility in *zero-field-cooled* and *field-cooled* modes using a Quantum Design MPMS-XL5 SQUID magnetometer. Dc-resistivities were measured on cold pressed pellets which were annealed at  $1000\text{ }^\circ\text{C}$  for 25 h.

### 3.4 Conclusion

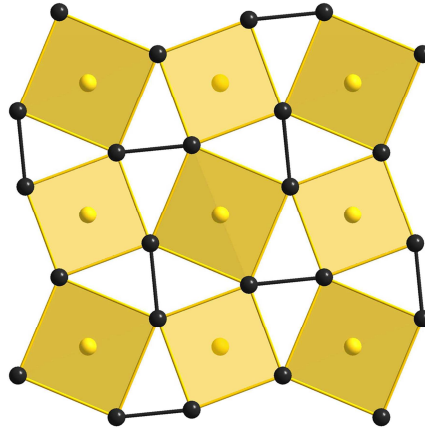
$(\text{CaFe}_{1-x}\text{Pd}_x\text{As})_{10}\text{Pt}_3\text{As}_8$  qualifies as an ideal system to investigate the magnetic effects of noble-metal substitution in 1038 phases, since  $(\text{CaFe}_{1-x}\text{Pt}_x\text{As})_{10}\text{Pt}_3\text{As}_8$  was proven to be a typical iron arsenide superconductor, while  $(\text{CaFe}_{1-x}\text{Pd}_x\text{As})_{10}\text{Pd}_3\text{As}_8$  is not. We successfully prepared the series of palladium doped Pt1038 with  $x = 0.0125 - 0.25$  yielding high quality samples. Remarkably, the simultaneous presence of palladium and platinum yields a distinctly separated occupation. While palladium substitutes the tetrahedrally coordinated positions within the iron arsenide layer, platinum prefers the planar coordinated sites within the  $M_3\text{As}_8$  layer. The nominal palladium substitution was perfectly confirmed by EDX analyses. The investigation by X-ray powder diffraction gives rise to the logical behavior of lattice parameters by varying the palladium concentration with the unit cell volume in total increasing with the doping level. We were able to detect superconductivity with palladium concentrations of  $x = 0.047 - 0.162$  featuring a maximal critical temperature of 11.5 K similar to other transition metal doped Pt1038. Therefore significant palladium doping seems not to be in charge for the absence of superconductivity in directly doped Pd1038. Additionally temperature-dependent powder diffraction offers a phase diagram with a range of parent-like state and superconducting dome. Electric resistivity as well as SQUID measurements confirmed the results.  $(\text{CaFe}_{1-x}\text{Pd}_x\text{As})_{10}\text{Pt}_3\text{As}_8$  was proven to be a typical directly doped iron arsenide with the substituent suppressing the phase transition of the undoped parent compound and thereby inducing superconductivity. Subsequent investigations on the related palladium 1038 system regarding a parent state and systematic palladium doping remain suspenseful.

### 3.5 References

- [1] Y. Kamihara, T. Watanabe, M. Hirano, H. Hosono, *J. Am. Chem. Soc.* **2008**, *130*, 3296.
- [2] T. Stürzer, G. M. Friederichs, H. Luetkens, A. Amato, H.-H. Klauss, F. Winter, R. Pöttgen, D. Johrendt, *J. Phys.: Condens. Matter* **2013**, *25*, 122203.
- [3] M. Rotter, M. Tegel, I. Schellenberg, W. Hermes, R. Pöttgen, D. Johrendt, *Phys. Rev. B* **2008**, *78*, 020503(R).
- [4] C. de la Cruz, Q. Huang, J. W. Lynn, J. Y. Li, W. Ratcliff, J. L. Zarestky, H. A. Mook, G. F. Chen, J. L. Luo, N. L. Wang, P. C. Dai, *Nature* **2008**, *453*, 899.

- [5] C. Löhnert, T. Stürzer, M. Tegel, R. Frankovsky, G. Friederichs, D. Johrendt, *Angew. Chem. Int. Ed.* **2011**, *50*, 9195.
- [6] N. Ni, J. M. Allred, B. C. Chan, R. J. Cava, *Proc. Natl. Acad. Sci. U. S. A.* **2011**, *108*, E1019.
- [7] S. Kakiya, K. Kudo, Y. Nishikubo, K. Oku, E. Nishibori, H. Sawa, T. Yamamoto, T. Nozaka, M. Nohara, *J. Phys. Soc. Jpn.* **2011**, *80*, 093704.
- [8] T. Stürzer, F. Kessler, D. Johrendt, *Philos. Mag.* **2014**, *94*, 3632.
- [9] T. Stürzer, G. Derondeau, D. Johrendt, *Phys. Rev. B* **2012**, *86*, 060516(R).
- [10] T. Stürzer, G. Derondeau, D. Johrendt, *Solid State Commun.* **2015**, *201*, 36.
- [11] C. Hieke, J. Lippmann, T. Stürzer, G. M. Friederichs, F. Nitsche, F. Winter, R. Pöttgen, D. Johrendt, *Philos. Mag.* **2013**, *93*, 3680.
- [12] C. Stürzer, A. Schulz, D. Johrendt, *Z. Anorg. Allg. Chem.* **2014**, *640*, 3147.
- [13] N. Ni, A. Thaler, A. Kracher, J. Q. Yan, S. L. Bud'ko, P. C. Canfield, *Phys. Rev. B* **2009**, *80*, 024511.
- [14] D. Johrendt, *J. Mater. Chem.* **2011**, *21*, 13726.
- [15] M. A. Tanatar, N. Ni, A. Thaler, S. L. Bud'ko, P. C. Canfield, R. Prozorov, *Phys. Rev. B* **2011**, *84*, 014519.
- [16] F. Han, X. Zhu, P. Cheng, G. Mu, Y. Jia, L. Fang, Y. Wang, H. Luo, B. Zeng, B. Shen, L. Shan, C. Ren, H.-H. Wen, *Phys. Rev. B* **2009**, *80*, 024506.
- [17] N. Ni, W. E. Straszheim, D. J. Williams, M. A. Tanatar, R. Prozorov, E. D. Bauer, F. Ronning, J. D. Thompson, R. J. Cava, *Phys. Rev. B* **2013**, *87*, 060507.
- [18] A. Coelho, TOPAS-Academic, Version 4.1, Coelho Software, Brisbane, **2007**.

## 4 Structure and Properties of $(\text{CaFe}_{1-x}\text{Pd}_x\text{As})_{10}\text{Pd}_4\text{As}_8$



### 4.1 Introduction

$(\text{CaFeAs})_{10}\text{Pt}_3\text{As}_8$  (Pt1038) was proven to be the parent compound of the 2011 discovered new sweeping class of iron arsenide superconductors by showing a structural and magnetic phase transition at 120 K<sup>[1]</sup> similar to other prominent iron arsenide parents.<sup>[2,3]</sup> Possessing a second negatively charged layer, this compound is both unique in the large family of iron arsenides and offers a versatile potential of doping scenarios to induce superconductivity. Besides directly doped phases of  $(\text{CaFe}_{1-x}\text{M}_x\text{As})_{10}\text{Pt}_3\text{As}_8$  with  $M = \text{Co}, \text{Ni}, \text{Pd}, \text{Pt}$ <sup>[4-6]</sup> and a maximum critical temperature of  $T_c = 15$  K, also the analogue palladium compound  $(\text{CaFeAs})_{10}\text{Pd}_3\text{As}_8$  (Pd1038)<sup>[7]</sup> was successfully obtained, surprisingly revealing no superconductivity by the same doping treatment so far. However, electron doping within the calcium layer by numerous rare earth elements revealed superconductivity up to  $T_c = 10$  K<sup>[8]</sup> in Pd1038 and  $T_c = 35$  K<sup>[9]</sup> in Pt1038, respectively. Due to the platinum/ palladium arsenide layer, which features one nobel-metal vacancy, these compounds facilitate the possibility for a second electron doping scenario. This can be realized filling the vacancy in the planar metal arsenide layer by a fourth nobel-metal yielding  $M_4\text{As}_8$ . So far only platinum phases  $(\text{CaFeAs})_{10}\text{Pt}_4\text{As}_8$  (Pt1048) have been successfully prepared and characterized. The compound features the same building blocks, however, the modified platinum arsenide slabs give rise to a different stacking of the layers. Depending on the stacking options  $(\text{CaFe}_{1-x}\text{Pt}_x\text{As})_{10}\text{Pt}_4\text{As}_8$  develops polymorphism with three limiting structure types identified so far yielding tetragonal  $\alpha$ -type ( $P4/n$ ) with perpendicular stacking to the  $ab$  plane, triclinic  $\beta$ -type ( $P\bar{1}$ ) with a steadily shifted stacking in one direction, and monoclinic  $\gamma$ -type ( $P2_1/n$ ) featuring a regularly *zigzag* stacked superstructure. Electronic structure calculations revealed

almost exclusively iron states at the *Fermi* energy for platinum and palladium 1038 as well as idealized Pt1048,<sup>[7,10]</sup> which shows a pseudo-gap of platinum states at  $E_F$  similar to  $(\text{CaFeAs})_{10}\text{Pt}_3\text{As}_8$ . Therefore in both cases of electron doping either by additional platinum in the 1048 compounds or rare earth doping of the calcium layer the additional charge is transferred to the superconducting iron arsenide layer.<sup>[9]</sup> Consequently similar critical temperatures as in rare earth substituted Pt1038 have been measured in  $(\text{CaFe}_{1-x}\text{Pt}_x\text{As})_{10}\text{Pt}_4\text{As}_8$  with a maximum of  $T_c = 38 \text{ K}$ .<sup>[11]</sup>

While intensive research on Pt1048 phases with exceptional structural complexity and remarkable electronic and magnetic properties is still in progress, there have been nonetheless no references on conceivable analogue palladium compounds so far. Now with an even more distinct stacking disorder present in the palladium system the existence of homologous Pd1048 phases was proven and two polymorphs are introduced in the following chapter. Tetragonal  $\alpha$ - $(\text{CaFe}_{1-x}\text{Pd}_x\text{As})_{10}\text{Pd}_4\text{As}_8$  was identified by single crystal structure determination, while triclinic  $\beta$ - $(\text{CaFe}_{1-x}\text{Pd}_x\text{As})_{10}\text{Pd}_4\text{As}_8$  could be deduced via powder diffraction data refinement from the platinum compound. Moreover first studies on electronic and magnetic properties of polycrystalline Pd1048 are presented.

## 4.2 Results and Discussion

### 4.2.1 Crystal Structure

The crystal structure of  $\alpha$ - $(\text{CaFe}_{1-x}\text{Pd}_x\text{As})_{10}\text{Pd}_4\text{As}_8$  (spacegroup  $P4/n$ ) was obtained by single crystal structure determination. Figure 1 illustrates the stacking of both metal arsenide layers each separated by calcium as well as the top view of the  $\text{Pd}_4\text{As}_8$  layer. All three present layers show tetragonal layer symmetry, while the array of neighboring palladium arsenide layers determines the final crystal system. Of the five possible stacking arrangements per unit<sup>[12]</sup> only the one steadily perpendicular to the  $ab$  plane gives rise to this tetragonal phase ( $\alpha$ -type). Triclinic ( $\beta$ -type, space group  $P\bar{1}$ ) and monoclinic ( $\gamma$ -type, space group  $P2_1/n$ ) structures are known as further limiting cases in the related platinum system.

In the first metal arsenide layer iron is tetrahedrally coordinated by arsenic featuring edge-sharing tetrahedra layers. In the second anionic layer palladium is planar fourfold coordinated by arsenic building up a pattern of corner-sharing squares stabilized by  $(\text{As}-\text{As})^{4-}$  dimers. Of the two palladium positions one is deflected from the almost planar array to either site of the

layer. Furthermore this situation gives rise to varying square sizes with a smaller one for the deflected position which is also compatible for vacancies. In contrast to both metal arsenide layers which are each stacked congruent, the neighboring squarish calcium layers are shifted by  $(0.3, 0.1, 0)$  featuring an offset  $|\vec{d}| = \sqrt{0.1}a$  in the tetragonal crystal system. This detail is one of the properties differentiating 1048 phases from closely related 1038 compounds.

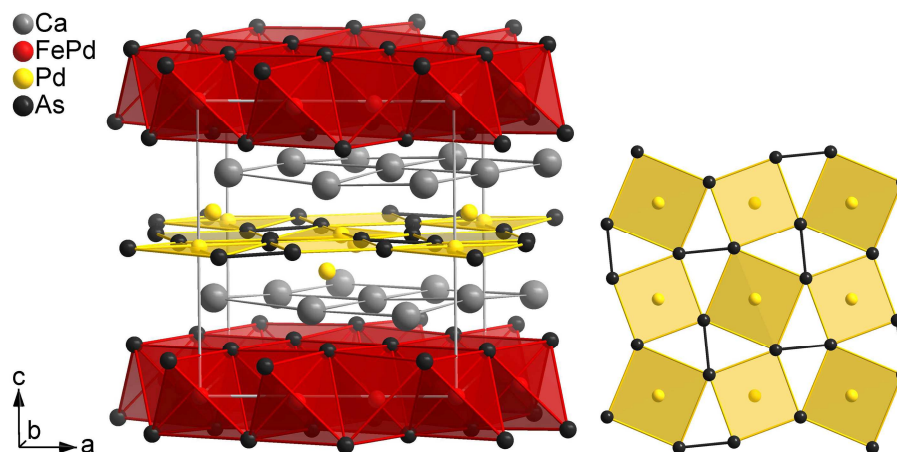


**Figure 1:** Crystal structure of  $\alpha\text{-(CaFe}_{1-x}\text{Pd}_x\text{As)}_{10}\text{Pd}_4\text{As}_8$  (left) with  $\text{Pd}_4\text{As}_8$  layer (right).

$\alpha\text{-(CaFe}_{1-x}\text{Pd}_x\text{As)}_{10}\text{Pd}_4\text{As}_8$  is built up of the same structure type as the homologous platinum phase and with respect to the noble-metal species and occupancies with comparable lattice parameters. The refinement revealed an average palladium mixing on the tetrahedrally coordinated iron position of  $x = 0.24$  and a distinct deficiency of the deflected palladium position yielding a total composition of  $(\text{CaFe}_{0.757}\text{Pd}_{0.243}\text{As})_{10}\text{Pd}_{2.83}\text{As}_8$ . In spite of the low palladium content, the  $\text{Pd}_z\text{As}_8$  layer with all conceivable metal sites occupied and the arrangement of the sandwiching calcium layers above and below the palladium arsenide layer requiring the present stacking classify the compound as a member of the 1048 system, even though the composition indicates the 1038 type. An excerpt of the single crystal data is listed in Table 1 next to selected interatomic distances and angles. The values of the tetrahedral layer are in the typical range of other substituted iron arsenide compounds. The bond lengths within the  $\text{Pd}_4\text{As}_8$  layer are slightly enlarged compared to the platinum compound due to the bigger ionic radius of the square coordinated metal with  $r(\text{Pd}^{2+}) = 0.78 \text{ \AA}$  and  $r(\text{Pt}^{2+}) = 0.74 \text{ \AA}$ ,<sup>[13]</sup> respectively.

**Table 1:** Single crystal data of  $\alpha\text{-(CaFe}_{0.757}\text{Pd}_{0.243}\text{As)}_{10}\text{Pd}_{2.83}\text{As}_8$  ( $Z = 1$ ).

|                      |  |
|----------------------|--|
| Empirical formula    | $\text{Ca}_{10}\text{Fe}_{7.57}\text{Pd}_{5.26}\text{As}_{18}$ |
| Molar mass           | $2731.8 \text{ g mol}^{-1}$                                    |
| Space group (number) | $P4/n$ (85)  |

|   |   |
|---|---|
| Unit cell dimensions<br>(single crystal)          | $a = 8.8533(12) \text{ \AA}$ , $b = a$ , $c = 10.229(3) \text{ \AA}$<br>$\alpha = \beta = \gamma = 90^\circ$ , $V = 801.76(30) \text{ \AA}^3$ |
| Calculated density                                | $5.6555 \text{ g cm}^{-3}$  |
| Absorption coefficient                            | $26.216 \text{ mm}^{-1}$  |
| $\Theta$ range                                    | $3.04 - 34.88^\circ$  |
| Range in $hkl$                                    | $\pm 13, \pm 13, \pm 15$  |
| Total number reflections                          | 13949   |
| Independent reflections / $R_{\text{int}}$        | 1216 / 0.2174   |
| Reflections with $I \geq 3\sigma(I)$ / $R_\sigma$ | 325 / 0.1936  |
| Data / parameters                                 | 1216 / 27   |
| Goodness-of-fit on $F$                            | 2.43 / 4.19   |
| $R1$ / $wR2$ for $I \geq 3\sigma(I)$              | 0.1076 / 0.0958   |
| $R1$ / $wR2$ for all data                         | 0.2956 / 0.1108   |
| Largest diff. peak / hole                         | $+24.66 / -23.82 \text{ e \AA}^{-3}$  |

## Interatomic distances and angles

|  |  |
|--|--|
| $d_{(\text{Fe-Pd-As})}$ , $\sphericalangle_{(\text{As-Fe-Pd-As})}$                           | $2.4070(97) - 2.5383(122) \text{ \AA}$ , $106.29(19) - 111.25(10)^\circ$   |
| $d_{(\text{Pd1-As})}$ , $\sphericalangle_{(\text{As-Pd1-As})}$                               | $2.5197(60) \text{ \AA}$ , $90.031(168)^\circ$                             |
| $d_{(\text{Pd2-As})}$ , $\sphericalangle_{(\text{As-Pd2-As})}$ , $d_{(\text{Pd2-As-Plane})}$ | $2.4549(75) \text{ \AA}$ , $83.181(180)^\circ$ , $0.7876(164) \text{ \AA}$ |
| $d_{(\text{As-As})}$   | $2.5261(88) \text{ \AA}$   |

Structure refinement turned out difficult due to the presence of considerable diffuse intensities along  $c^*$  caused by stacking disorder. Since all stacking variations conserve an ordered CaFeAs substructure the majority of the residual electronic density is located within the disordered palladium arsenide layer. The distinctly high residual values might also be reflected in the low palladium occupation of the  $\text{Pd}_7\text{As}_8$  layer obtained from the structure refinement. Furthermore partial merohedral twinning caused by broken layer symmetry of the  $\text{CaFe}_2\text{As}_2$  subsystem was revealed and refined with a rotation about (120) by  $180^\circ$  as one of the possible twinning elements. In Figure 2 the selected area diffraction pattern  $hk0$  shows the sharp reflections within the  $a^*b^*$  plane. A schematic reconstruction of all visible reflections of the same section in the range of  $-6 \leq h, k \leq 6$  illustrates the two twin domains and corresponding reciprocal lattice axes by different coloring as well as a twinning element. Furthermore the  $h0l$  lattice section shows the severe diffuse scattering for reflections complying with  $2h + k \neq 5n$ , which is most likely the main reason for the only moderate residual values. Nevertheless the solution and refinement of  $\alpha\text{-(CaFe}_{0.757}\text{Pd}_{0.243}\text{As})_{10}\text{Pd}_{2.83}\text{As}_8$  from single crystal data was

clearly feasible and so adding the first member of Pd1048 to this young branch of iron arsenide compounds.

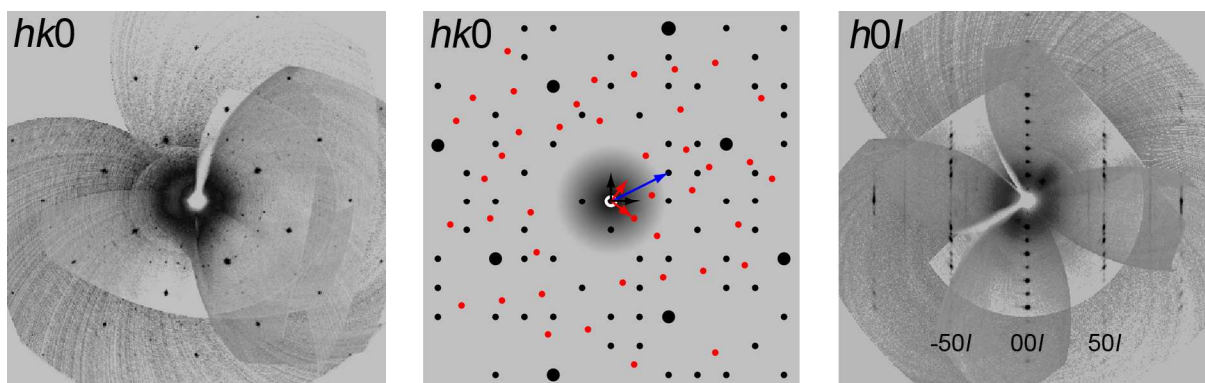


**Figure 2:** Selected area diffraction pattern  $hk0$  (left), schematic illustration of  $-6 \leq h, k \leq 6$  section with both twin domains emphasized by different coloring in black and red and indicated twinning element in blue (middle), and  $h0l$  section (right).

#### 4.2.2 X-Ray Powder Diffraction

Polycrystalline  $(\text{CaFeAs})_{10}\text{Pd}_4\text{As}_8$  was obtained via a four-step solid state reaction. The sample was characterized by X-ray powder diffraction. The corresponding Rietveld refinement (Figure 3) revealed Pd1048 as the main product with small amounts of  $\text{CaFe}_{1-x}\text{Pd}_x\text{As}_2$ <sup>[14]</sup> and  $\text{CaFe}_2\text{As}_2$  as impurity phases.

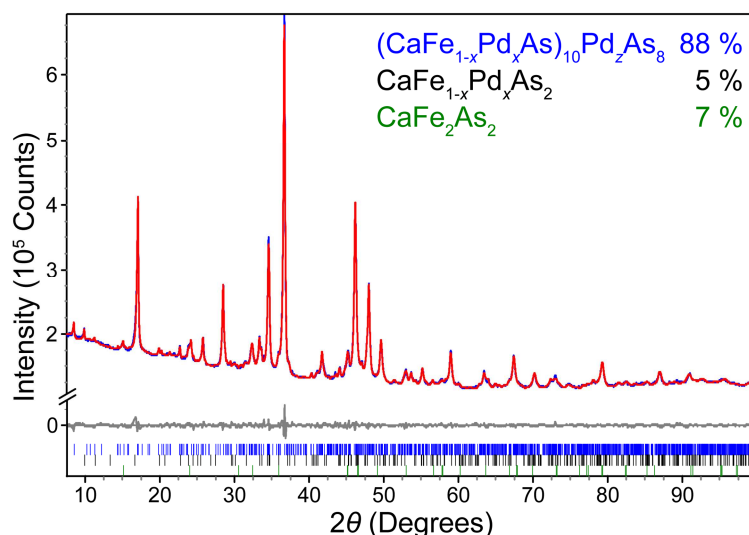


**Figure 3:** X-ray powder data (blue) with Rietveld fit (red) of  $(\text{CaFe}_{1-x}\text{Pd}_x\text{As})_{10}\text{Pd}_2\text{As}_8$ .

A refinement based on the single crystal data of  $\alpha$ - $(\text{CaFe}_{1-x}\text{Pd}_x\text{As})_{10}\text{Pd}_4\text{As}_8$  did not fit the experimental powder diffractogram. However, a more appropriate refinement based on single crystal data of  $\beta$ - $(\text{CaFe}_{1-x}\text{Pt}_x\text{As})_{10}\text{Pt}_4\text{As}_8$  (space group  $P\bar{1}$ ) was perfectly satisfying. Lattice parameters and free atomic positions as well as palladium mixing on the iron positions and

palladium occupancy within the  $\text{Pd}_z\text{As}_8$  layer were independently refined. Due to distinct stacking disorder problems always present in this system an unequivocal confirmation of  $\beta$ -Pd1048 via single crystal structure determination was not possible. In Table 2 the obtained structural details from powder data are listed in comparison to the corresponding platinum compound.

**Table 2:** Comparison of structural details of palladium and platinum  $\beta$ -1048 phases.

| Compound             | $\beta$ -Pt1048 <sup>[10]</sup>   | $\beta$ -Pd1048   |
|----------------------|---|---|
| Data source          | Single crystal diffraction  | Powder diffraction  |
| Empirical formula    | $(\text{CaFe}_{0.869(5)}\text{Pt}_{0.131(5)}\text{As})_{10}\text{Pt}_4\text{As}_8$  | $(\text{CaFe}_{0.963(5)}\text{Pd}_{0.037(5)}\text{As})_{10}\text{Pd}_{2.92(2)}\text{As}_8$  |
| Space group (number) | $P\bar{1}$ (2)  | $P\bar{1}$ (2)  |
| Unit cell dimensions | $a = 8.7382(4) \text{ \AA}$<br>$b = 8.7387(3) \text{ \AA}$<br>$c = 11.2245(5) \text{ \AA}$<br>$\alpha = 81.049(3)^\circ$<br>$\beta = 71.915(3)^\circ$<br>$\gamma = 89.980(3)^\circ$ | $a = 8.7761(1) \text{ \AA}$<br>$b = 8.7831(4) \text{ \AA}$<br>$c = 11.0659(3) \text{ \AA}$<br>$\alpha = 80.842(2)^\circ$<br>$\beta = 71.485(1)^\circ$<br>$\gamma = 90.000(1)^\circ$ |
| Unit cell volume     | $V = 803.79(6) \text{ \AA}^3$   | $V = 797.35(4) \text{ \AA}^3$   |

The refined composition revealed palladium mixed on the iron sites with  $x = 0.037(5)$ . Due to that very low substituent concentration the absolute value is not entirely reliable by X-ray diffraction methods. Therefore the result was confirmed by X-ray spectroscopy (EDX) yielding a final composition of  $(\text{Ca}_{1.11(3)}\text{Fe}_{0.95(5)}\text{Pd}_{0.05(5)}\text{As}_{0.91(4)})_{10}\text{Pd}_{2.9(3)}\text{As}_{7.3(4)}$  in very good agreement with the values from Rietveld refinement. The reduced palladium occupancy in the  $\text{Pd}_4\text{As}_8$  layer known from single crystal structure determination of both  $\alpha$ - $(\text{CaFe}_{1-x}\text{Pd}_x\text{As})_{10}\text{Pd}_4\text{As}_8$  and two platinum modifications was also a feature of polycrystalline  $\beta$ -Pd1048 visible in powder diffraction and EDX analyses.

With respect to the different noble-metal, varying occupancies within both metal pnictide layers, and the always present intrinsic structural complications causing methodic problems, the obtained Pd1048 compound seems to be isotypic to the underlying platinum  $\beta$ -phase. All freely refined structural parameters are comparable to the platinum compound, while e.g. the unit cell volume diverges by less than 1 %. Therefore the present stacking disorder realizes polymorphism also as a feature of Pd1048, since so far tetragonal  $\alpha$ - and triclinic  $\beta$ -limiting cases were identified.

### 4.2.3 Electronic Structure

The density of states (DOS) was calculated for idealized  $\alpha$ - $(\text{CaFeAs})_{10}\text{Pd}_4\text{As}_8$  including full structure relaxation (Figure 4). The result revealed iron states dominant at the *Fermi* level ( $E_F$ ) and a pseudo-gap for palladium 4*d* states. Therefore additional electrons introduced via the  $\text{Pd}_z\text{As}_8$  layer should be transferred to the iron arsenide layer. The requirements necessary to induce superconductivity in Pd1048 seem to be constituted by the electronic situation. Although the electronic structure appears similar to the analogue platinum 1048 compound,<sup>[10]</sup> the 3*d* Fe pDOS at  $E_F$  is distinctly reduced compared to the platinum phase. Possibly charge doping of  $(\text{CaFeAs})_{10}\text{Pd}_z\text{As}_8$  by a fully occupied palladium arsenide layer lifts the *Fermi* level too high for superconductivity, which can be induced in otherwise electron doped  $(\text{Ca}_{1-y}\text{RE}_y\text{FeAs})_{10}\text{Pd}_3\text{As}_8$ .<sup>[7,8]</sup> Moreover the pseudo-gap of the palladium states is considerable less significant compared to Pt1048. The present distinct contribution of the palladium states at  $E_F$  might additionally be responsible for the absence of superconductivity in Pd1048.

The calculated and merged *Fermi* surface topology is depicted in the right hand side of Figure 4. Around the zone corners cylinders along  $c^*$  reveal the two-dimensionality of the electronic structure. This feature is similar to other iron arsenides like the closely related  $(\text{CaFeAs})_{10}\text{Pd}_3\text{As}_8$  or  $\text{CaFe}_2\text{As}_2$ .<sup>[7]</sup> A different rather three-dimensional topology was observed in the center of the *Brillouin* zone, that is not common in the family of iron arsenide superconductors. This reduction of the two-dimensional character might be another reason for the divergent features of the palladium compounds compared to the platinum homologs.

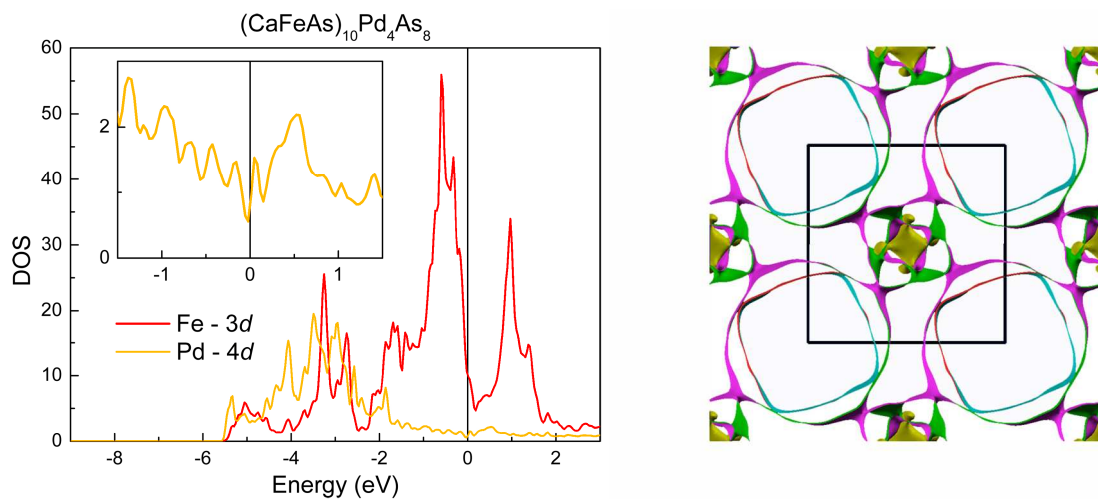


**Figure 4:** Density of states of idealized  $(\text{CaFeAs})_{10}\text{Pd}_4\text{As}_8$  (left) and merged *Fermi* surface (right).

#### 4.2.4 Magnetic Properties

Dc-resistivity of a cold pressed and annealed pellet (Figure 5, left) showed metallic behavior for polycrystalline  $\beta$ - $(\text{CaFe}_{1-x}\text{Pd}_x\text{As})_{10}\text{Pd}_z\text{As}_8$  until a sharp drop at  $T_c = 7.5$  K most likely indicating an onset of superconductivity, however, zero resistivity was not achieved. The temperature-dependent electric resistivity features a weak anomaly starting from ca. 120 K. Visible by an inflection point the metallic curve shape changes without rising. A similar, but more distinct shape was observed for polycrystalline  $(\text{CaFe}_{1-x}\text{Pd}_x\text{As})_{10}\text{Pd}_3\text{As}_8$  (Chapter 2.2). Until the onset of superconductivity metallic resistivity was also reported for platinum 1048 single crystals<sup>[15]</sup> and  $\alpha$ -Pt1048.<sup>[11]</sup> Absolute values of electric resistivity are about one magnitude lower as of the in this chapter investigated palladium compound. In contrast the related parent  $(\text{CaFeAs})_{10}\text{Pt}_3\text{As}_8$ ,<sup>[1]</sup> under-doped palladium substituted Pt1038,<sup>[5]</sup> and  $\beta$ -Pt1048 crystals revealed semiconductor-like behavior.

Molar susceptibility measurements showed weak paramagnetic behavior. No significant anomaly was observed in the range of 1.8 – 300 K. Despite the sharp drop visible in the electrical resistivity, no superconductivity was observed in magnetic susceptibilities of the same sample performed at different external fields (Figure 5, right). Therefore it is not fully clarified, whether superconductivity is actually a property of  $(\text{CaFe}_{1-x}\text{Pd}_x\text{As})_{10}\text{Pd}_4\text{As}_8$ . So far no superconductivity was observed in either of the identified side phases at ambient pressure.<sup>[14,16-18]</sup> However, the classification of Pd1048 as non-superconducting is suggested by the obtained results. Measurement in *zero-field-cooled* and *field-cooled* mode at 30 Oe featured paramagnetic behavior and only a minor splitting of the two branches at very low temperatures. Moreover magnetization at 1.8 K and 300 K did not reveal any hysteresis and therefore no ferromagnetic impurities. Saturation was not achieved in a range of -50 – 50 kOe.

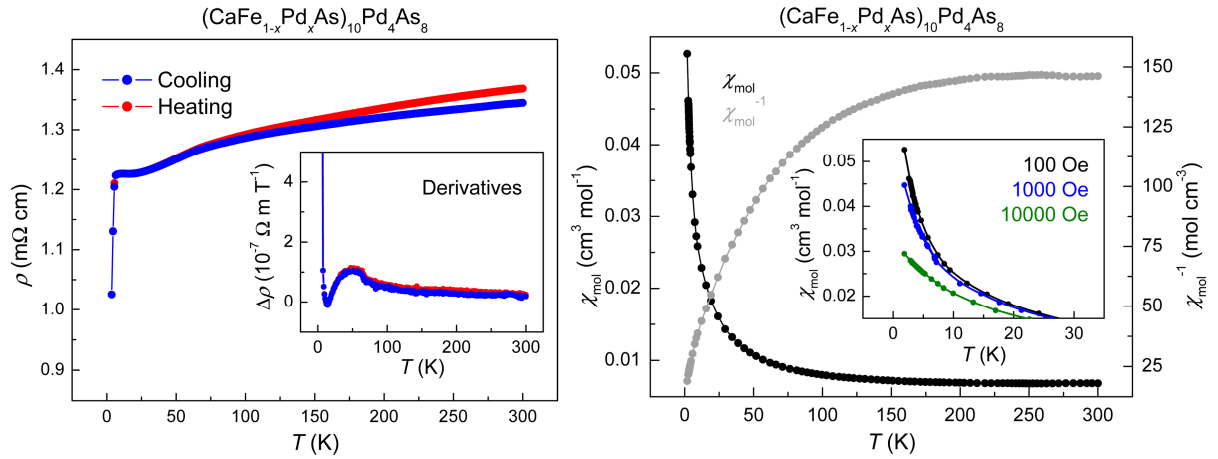


**Figure 5:** Electric resistivity data of  $(\text{CaFe}_{1-x}\text{Pd}_x\text{As})_{10}\text{Pd}_4\text{As}_8$  (left). Inset: Derivatives of cooling and heating curves. Molar magnetic susceptibility and inverse data of  $(\text{CaFe}_{1-x}\text{Pd}_x\text{As})_{10}\text{Pd}_4\text{As}_8$  at 100 Oe (right). Inset: Dc-susceptibility at different external fields at low temperatures.

### 4.3 Experimental Section

A  $(\text{CaFeAs})_{10}\text{Pd}_4\text{As}_8$  single crystal for structure determination was selected from FeAs flux charge. The stoichiometric mixture of the pure elements (> 99.9 %) and an excess of iron arsenide (1 : 2) were mixed in a glassy carbon crucible and sealed under purified argon. The sample was heated to 1050 °C for 100 h before cooling to room temperature with a rate of 5 K/h. The data was obtained from a Bruker D8 Quest diffractometer using Mo- $K\alpha$  radiation and absorption correction based on equivalent reflection was performed by SADABS.<sup>[19]</sup> The structure was solved and refined using the JANA2006 program package.<sup>[20]</sup>

A polycrystalline sample was synthesized by solid state reaction. The stoichiometric mixture of the pure elements (> 99.9 %) was heated for 10 h each at 600 °C followed by 1000 °C in an alumina crucible sealed under purified argon. The product was grounded and annealed twice at 1000 °C for 25 h, while in the second step the pelletized sample was cooled with a moderate rate of 5 K/h, afterwards homogenized, pelletized again, and annealed at 800 °C for 50 h. The obtained powder sample was characterized by X-ray powder diffraction at room temperature using a Huber Imaging Plate Guinier diffractometer with primary monochromator and copper radiation. Rietveld refinement was performed using the TOPAS program package<sup>[21]</sup> based on single crystal data of  $\beta$ - $(\text{CaFe}_{1-x}\text{Pt}_x\text{As})_{10}\text{Pt}_4\text{As}_8$ . Sample composition was confirmed by X-ray spectroscopy (EDX) on a Carl Zeiss EVO-MA 10 equipped with a Bruker Nano EDX detector. Density of states and *Fermi* surface of idealized  $(\text{CaFeAs})_{10}\text{Pd}_4\text{As}_8$  were calculated using the WIEN2k package.<sup>[22]</sup> Dc-resistivity was measured using a standard four-probe method on a cold pressed pellet which was annealed at

800 °C for 50 h. Dc-susceptibilities, magnetization, and *zero-field-cooled* and *field-cooled* data were measured using a Quantum Design MPMS-XL5 SQUID magnetometer at varying external fields in the range of -50 – 50 kOe.

#### 4.4 Conclusion

The synthesis and characterization of  $(\text{CaFe}_{1-x}\text{Pd}_x\text{As})_{10}\text{Pd}_z\text{As}_8$  with 1048-type structures added a new member to this still young family of iron arsenide compounds. With  $(\text{CaFe}_{0.757}\text{Pd}_{0.243}\text{As})_{10}\text{Pd}_{2.83}\text{As}_8$  ( $\alpha$ -type, space group  $P4/n$ ) and  $(\text{CaFe}_{0.963}\text{Pd}_{0.037}\text{As})_{10}\text{Pd}_{2.92}\text{As}_8$  ( $\beta$ -type, space group  $P\bar{1}$ ) two polymorphs of Pd1048 were identified. The tetragonal structure was solved and refined by single crystal structure determination. The structure turned out to be isotypic to the homologous  $\alpha$ -Pt1048 compound. Due to intrinsic crystallographic challenges like distinct stacking disorder and partly merohedral twinning structure determination by single crystal methods revealed moderate results. The triclinic  $\beta$ -phase was obtained from X-ray powder refinement based on the data of the analogue platinum structure. High quality powder sample of  $\beta$ -1048 facilitated the structure refinement by Rietveld methods and characterization of electronic and magnetic properties.  $(\text{CaFe}_{1-x}\text{Pd}_x\text{As})_{10}\text{Pd}_4\text{As}_8$  features metallic behavior with a weak anomaly starting from about 120 K until a sharp drop at low temperatures. Susceptibility measurements revealed no superconducting properties, but paramagnetic behavior. Therefore in contrast to the related platinum phases no bulk superconductivity emerges in Pd1048 so far. Investigations of the electronic structure revealed a two-dimensional *Fermi* surface similar to known iron arsenide superconductors, but superimposed with three-dimensional features. Although the *Fermi* level is still dominated by iron states in this compound, their density is distinctly reduced compared to the related platinum compounds. Additionally the clarity of a pseudo-gap within the palladium states is significantly reduced. Like  $(\text{CaFe}_{1-x}\text{Pd}_x\text{As})_{10}\text{Pd}_3\text{As}_8$  the electron doped compound Pd1048 does not show the expected properties known from the well investigated platinum analogs, despite the low palladium substitution on the iron positions determined by refined powder data and EDX spectroscopy. These minor differences in the electronic situation were suggested to play a key role for the occurrence of superconductivity in 1038/ 1048-type compounds. Subsequent investigations are necessary to further reveal the remarkable properties of  $(\text{CaFe}_{1-x}\text{Pd}_x\text{As})_{10}\text{Pd}_z\text{As}_8$  phases.

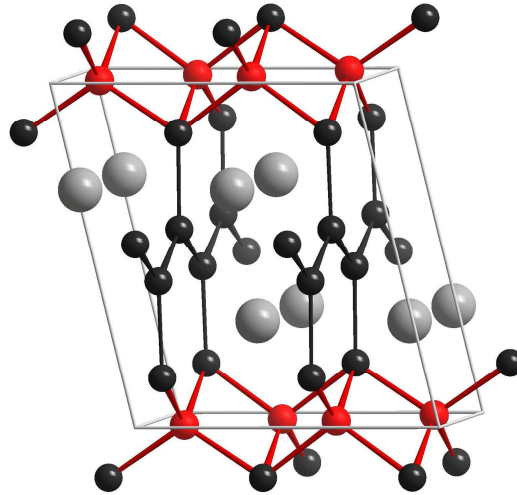
## 4.5 References

- [1] T. Stürzer, G. M. Friederichs, H. Luetkens, A. Amato, H.-H. Klauss, F. Winter, R. Pöttgen, D. Johrendt, *J. Phys.: Condens. Matter* **2013**, *25*, 122203.
- [2] M. Rotter, M. Tegel, I. Schellenberg, W. Hermes, R. Pöttgen, D. Johrendt, *Phys. Rev. B* **2008**, *78*, 020503(R).
- [3] J. Dong, H. J. Zhang, G. Xu, Z. Li, G. Li, W. Z. Hu, D. Wu, G. F. Chen, X. Dai, J. L. Luo, Z. Fang, N. L. Wang, *Europhys Lett.* **2008**, *83*, 27006.
- [4] T. Stürzer, F. Kessler, D. Johrendt, *Philos. Mag.* **2014**, *94*, 3632.
- [5] C. Stürzer, D. Johrendt, **2015**, *in preparation*. (see Chapter 3)
- [6] T. Stürzer, G. Derondeau, D. Johrendt, *Phys. Rev. B* **2012**, *86*, 060516(R).
- [7] C. Hieke, J. Lippmann, T. Stürzer, G. M. Friederichs, F. Nitsche, F. Winter, R. Pöttgen, D. Johrendt, *Philos. Mag.* **2013**, *93*, 3680.
- [8] C. Stürzer, A. Schulz, D. Johrendt, *Z. Anorg. Allg. Chem.* **2014**, *640*, 3143.
- [9] T. Stürzer, G. Derondeau, D. Johrendt, *Solid State Commun.* **2015**, *201*, 36.
- [10] C. Löhnert, T. Stürzer, M. Tegel, R. Frankovsky, G. Friederichs, D. Johrendt, *Angew. Chem. Int. Ed.* **2011**, *50*, 9195.
- [11] S. Kakiya, K. Kudo, Y. Nishikubo, K. Oku, E. Nishibori, H. Sawa, T. Yamamoto, T. Nozaka, M. Nohara, *J. Phys. Soc. Jpn.* **2011**, *80*, 093704.
- [12] T. Stürzer, *Dissertation*, LMU München, **2015**.
- [13] A. F. Hollemann, E. Wiberg, N. Wiberg, *Lehrbuch der Anorganischen Chemie*, Walter de Gruyter, Berlin, **2007**.
- [14] C. Stürzer, T. Stürzer, D. Johrendt, **2015**, *in preparation*. (see Chapter 5)
- [15] Q.-P. Ding, Y. Tsuchiya, S. Mohan, T. Taen, Y. Nakajima, T. Tamegai, *Phys. Rev. B* **2012**, *85*, 104512.
- [16] G. Wu, H. Chen, T. Wu, Y. L. Xie, Y. J. Yan, R. H. Liu, X. F. Wang, J. J. Ying, X. H. Chen, *J. Phys.: Condens. Matter* **2008**, *20*, 422201.

- [17] N. Ni, S. Nandi, A. Kreyssig, A. I. Goldman, E. D. Mun, S. L. Bud'ko, P. C. Canfield, *Phys. Rev. B* **2008**, 78, 014523.
- [18] F. Ronning, T. Klimczuk, E. D. Bauer, H. Volz, J. D. Thompson, *J. Phys.: Condens. Matter* **2008**, 20, 322201.
- [19] SADABS, Bruker AXS, Madison, **2012**.
- [20] V. Petricek, M. Dusek, L. Palatinus, JANA2006, Institute of Physics, Praha, **2013**.
- [21] A. Coelho, TOPAS-Academic, Version 4.1, Coelho Software, Brisbane, **2007**.
- [22] P. Blaha, K. Schwarz, G. K. H. Madsen, D. Kvasnicka, J. Luitz, WIEN2k – An Augmented Plane Wave + Local Orbitals Program for Calculating Crystal Properties, Technische Universität, Vienna, **2001**.

## 5 New Structure with substituted Iron Arsenides Layers $\text{CaFe}_{1-x}\text{Pd}_x\text{As}_2$

Christine Stürzer, Tobias Stürzer, Dirk Johrendt



*This chapter is in preparation to be published in a scientific journal.*

### Abstract

With novel  $\text{CaFe}_{1-x}\text{Pd}_x\text{As}_2$  the family of iron arsenides is enriched by a new structure type. Build up from an alternate stacking of the typical metal pnictide layers and arsenic *zigzag* chains separated by calcium, this so far unknown 112-type crystal structure can be derived from known structure types. Although, this compound seems to build up an unique one, it shows relations to  $\text{LaMnSi}_2$ -,  $\text{CeNiSi}_2$ -, and  $\text{NdRuSi}_2$ -type structures. Moreover structural resemblance to the lately published 112-type calcium iron arsenides with rare earth substitution is conspicuous.  $\text{CaFe}_{1-x}\text{Pd}_x\text{As}_2$  was identified by single crystal structure determination and X-ray powder data yielding typical values for metal arsenide tetrahedra layers. Electronic and magnetic properties were analyzed characterizing the new compound as a promising candidate for a further class of iron arsenide superconductors.

### 5.1 Introduction

Recently the field of iron-based superconductors was enlarged by a new class of calcium iron arsenides with substituted calcium layers  $\text{Ca}_{1-x}\text{RE}_x\text{FeAs}_2$ .<sup>[1,2]</sup> Although the new compounds were reported with monoclinic crystal structure they can be derived from already known

structures build up from tetrahedra layers and coplanar non-metallic interlayers separated by cations. These interlayers feature for example square nets in  $\text{HfCuSi}_2$ -type ( $P4/nmm$ ),<sup>[3]</sup> zigzag chains in  $\text{SrZnSb}_2$ -type ( $Pnma$ ),<sup>[4]</sup> and *cis-trans* chains in  $\text{CeAgAs}_2$ -type ( $Pbcm$ )<sup>[5]</sup> structures. Moreover rare earth doped  $\text{Ca}_{1-x}\text{RE}_x\text{FeAs}_2$ , referred to as 112 type, with typical iron arsenide tetrahedra and thereto coplanar orientated arsenic zigzag layers seem to fit into the since 2008 well established family of layered metal pnictide superconductors. In non-superconducting parent compounds like  $\text{LaFeAsO}$ <sup>[6]</sup> or  $\text{BaFe}_2\text{As}_2$ <sup>[7]</sup> the right choice and doping level of different substituents leads to the induction of superconductivity. In the newest 112-type representative a hypothetical parent compound was not published so far. By now substituted  $\text{Ca}_{1-x}\text{RE}_x\text{FeAs}_2$  shows superconductivity up to 40 K<sup>[8]</sup> with  $RE = \text{La}$ .

Here we present the so far unknown compound  $\text{CaFe}_{0.56}\text{Pd}_{0.44}\text{As}_2$  with a new crystal structure and the analog composition of 1 : 1 : 2.  $\text{CaFe}_{1-x}\text{Pd}_x\text{As}_2$  is also build up from tetrahedra layers and arsenic zigzag chains separated by calcium, however, unlike  $\text{Ca}_{1-x}\text{RE}_x\text{FeAs}_2$  the layers containing the zigzag sites are orientated perpendicular to the metal arsenide layers allowing for additional As–As bonding to the iron arsenide layers. Next to single crystal structure determination and X-ray powder refinement of polycrystalline samples we characterize the new compound by magnetic measurements and electronic structure calculations.

## 5.2 Results and Discussion

### 5.2.1 Crystal Structure

A single crystal was selected to determine the structure of the unknown compound and measured on a Stoe IPDS I (Mo- $K\alpha$  radiation, graphite monochromator). The structure was solved and refined using the JANA2006 program package.<sup>[9]</sup>  $\text{CaFe}_{0.56}\text{Pd}_{0.44}\text{As}_2$  crystallizes in the monoclinic crystal system (spacegroup  $P2_1/m$ ) with four formula units per elementary cell and is build up from an alternated stacking of different layers along the  $c^*$  axis (Figure 1).

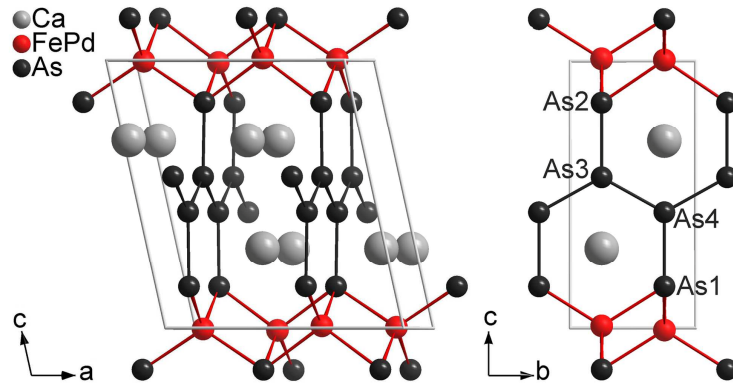


**Figure 1:** Crystal structure of  $\text{CaFe}_{0.56}\text{Pd}_{0.44}\text{As}_{1.95}$  with view along the  $b$  axis (left) and  $a$  axis (right).

Tetrahedra layers with iron and palladium mixed on the central positions take turns with arsenic *zigzag* chains along  $b$  spanning a plane arranged perpendicular to  $ab$ . With 2.45 – 2.50 Å Fe/Pd–As bond lengths are in the typical range known by other metal arsenide compounds with slightly elongated values compared to clean iron arsenide tetrahedra layers caused by the palladium substitution. The same criteria apply for As–Fe/Pd–As angles showing values, which most likely indicate metal-centered coordination polyhedra. Comparable compounds with pnictide-centered tetrahedra feature distinctly flatter layers. The distances within the *zigzag* layers amount 2.37 Å and from the positions within the *zigzag* chains to the arsenic of the tetrahedra layers 2.47 and 2.48 Å, respectively. On the assumption of  $\text{Ca}(\text{Fe,Pd})\text{As}_2$  being a valence compound with divalent alkaline earth ions we can discuss two possible limit cases. Electronically undoped and separated  $(M^{2+}\text{As}^{3-})_{4/4}$  layers and infinite  $^{\infty}_1[\text{As}^-]$  *zigzag* stands connected by strong single bonds within the layer reveal no bonding between the different arsenic positions. Otherwise *zigzag* positions of threefold bonded  $\text{As}^0$  atoms yield  $(M\text{As})_{4/5}^{2-}$  tetrahedra layers and therefore interlayer bonding. By viewing along the  $a$  axis a motif of planar hexagons with As–As–As angles of almost 120° is formed. A close look to the variable occupancies reveals an average palladium mixing on the iron sites of 44 % as well as minor vacancies within the arsenic *zigzag* layer yielding an exact formula of  $\text{Ca}(\text{Fe}_{0.56}\text{Pd}_{0.44})\text{As}_{1.95}$ . An excerpt of the crystal data is listed in Table 1.

**Table 1:** Single crystal data of  $\text{CaFe}_{0.56}\text{Pd}_{0.44}\text{As}_{1.95}$  ( $Z = 4$ ).

|   |  |
|---|--|
| Empirical formula                                   | $\text{CaFe}_{0.56}\text{Pd}_{0.44}\text{As}_{1.95}$   |
| Molar mass  | $263.9 \text{ g mol}^{-1}$   |
| Space group (number)                                | $P2_1/m$ (11)  |
| Unit cell dimensions<br>(single crystal)            | $a = 8.063(3) \text{ \AA}$<br>$b = 4.137(1) \text{ \AA}$<br>$c = 9.078(3) \text{ \AA}$<br>$\beta = 102.8(1)^\circ$<br>$V = 295.3(2) \text{ \AA}^3$ |
| Calculated density                                  | $5.9353 \text{ g cm}^{-3}$   |
| Transmission ratio (min / max)                      | 0.2980 / 0.5132  |
| Absorption coefficient                              | $28.672 \text{ mm}^{-1}$   |
| $\Theta$ range                                      | $2.59 - 30.3^\circ$  |
| Range in $hkl$                                      | $\pm 10, \pm 5, \pm 12$  |
| Total number reflections                            | 3483   |
| Independent reflections / $R_{\text{int}}$          | 988 / 0.047  |
| Reflections with $I \geq 3\sigma(I)$ / $R_\sigma$   | 390 / 0.050  |
| Data / parameters                                   | 988 / 53   |
| Goodness-of-fit on $F^2$                            | 1.04 / 1.56  |
| $R1$ / $wR2$ for $I \geq 3\sigma(I)$                | 0.026 / 0.053  |
| $R1$ / $wR2$ for all data                           | 0.059 / 0.089  |
| Largest diff. peak / hole                           | $+1.22 / -1.73 \text{ e \AA}^{-3}$   |
| <b>Interatomic distances and angles</b>             |  |
| $d_{(\text{Fe/Pd}-\text{As}1/2)}$                   | $2.4455(15) - 2.4977(15) \text{ \AA}$  |
| $\angle_{(\text{As}1/2-\text{Fe/Pd}-\text{As}1/2)}$ | $107.22(9) - 115.52(9)^\circ$  |
| $d_{(\text{As}3-\text{As}4)}$                       | $2.3662(14) \text{ \AA}$   |
| $d_{(\text{As}1/2-\text{As}3/4)}$                   | $2.4747(26), 2.4844(26) \text{ \AA}$   |
| $\angle_{(\text{As}-\text{As}-\text{As})}$          | $119.05(9) - 121.89(10)^\circ$   |

The new compound can be assigned to a long known class of structures. Many compounds  $\text{AMX}_2$ <sup>[10]</sup> with a ratio of 1 : 1 : 2 build up layered structures with an alternate stacking of tetrahedra layers and non-metal *zigzag* chains arranged perpendicular to the tetrahedra each separated by electropositive cations. In the literature several compounds with orthorhombic crystal system (spacegroup *Cmcm*) can be assigned either to the  $\text{LaMnSi}_2$ -type structure<sup>[11]</sup> showing “regular” metal-centered tetrahedra layers or to the  $\text{CeNiSi}_2$ -type structure<sup>[12]</sup> forming “inverted” layers with non-metal-centered tetrahedra layers. Additionally also a monoclinic

structure type ( $\text{NdRuSi}_2$  type<sup>[13]</sup>, spacegroup  $P2_1/m$ ) with inverted tetrahedra layers is known. A comparative summary together with our new structure is shown in Figure 2.

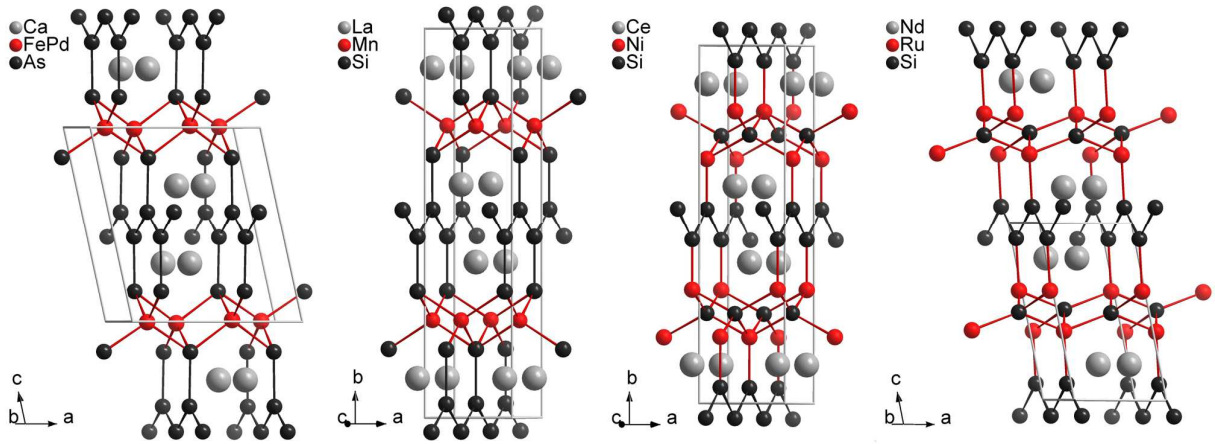


**Figure 2:** Comparison of our new crystal structure  $\text{CaFe}_{1-x}\text{Pd}_x\text{As}_2$  ( $P2_1/m$ ) with  $\text{LaMnSi}_2$ -type ( $Cmcm$ ),  $\text{CeNiSi}_2$ -type ( $Cmcm$ ), and  $\text{NdRuSi}_2$ -type ( $P2_1/m$ ) structures (from left to right).

The closest relation to our new iron palladium arsenide shows the  $\text{LaMnSi}_2$ -type structure. The lower symmetry of our new structure compared to this aristotype can be explained by a two-step descent from orthorhombic  $Cmcm$  to monoclinic  $C112_1/m$  via a *translationsgleiche* relation  $(\frac{1}{2}(a-b), \frac{1}{2}(a+b), c)$  yielding the monoclinic angle  $\beta = 102.8^\circ$ . To enable a splitting of the iron positions with different palladium concentrations the unit cell can be enlarged *klas-sengleich*  $(2a, b, c)$  to obtain the doubled  $a$  axis. Retention of orthorhombic symmetry by a one-step *translationsgleiche* decent from  $Cmcm$  to  $Cm2m$  or  $Amm2$ , respectively, and loss of the inversion center would lead to a different, unfavorable distribution of iron and palladium on the decisive positions.

According to Pearson's Crystal Data in comparison to  $\text{Ca}(\text{Fe},\text{Pd})\text{As}_2$  the iron-containing compounds  $RE\text{FeSi}_2$  ( $RE = \text{Nd}, \text{Sm}, \text{Gd}, \text{Tb}$ )<sup>[14]</sup> are known with monoclinic  $\text{NdRuSi}_2$ -type structure, while no palladium representatives are reported. In the huge family of  $AMX_2$  ( $A = \text{A}, \text{AE}, \text{RE}; M = \text{Mn}, \text{Fe}, \text{Co}, \text{Ni}, \text{Cu}, \text{Ru}, \text{Rh}, \text{Pd}, \text{Ag}, \text{Re}, \text{Ir}, \text{Pt}, \text{Au}; X = \text{Si}, \text{Ge}, \text{Sn}, \text{As}, \text{Sb}, \text{Cl}, \text{Br}$ )<sup>[10]</sup> compounds with spacegroup  $Cmcm$  only the iron compounds  $RE\text{FeSi}_2$  with  $RE = \text{La}, \text{Ce}, \text{Pr}$ ,<sup>[11]</sup>  $\text{Nd}$ ,<sup>[15]</sup> and  $\text{Tb}$ <sup>[16]</sup> as well as  $RE = \text{Dy}$  and  $\text{Ho}$ <sup>[17]</sup> with iron vacancies show metal positions in tetrahedral coordination aside a few manganese<sup>[11]</sup> compounds. All palladium compounds feature inverted layers. The only reported calcium compound is  $\text{CaNiGe}_2$ .<sup>[18]</sup> In combination with arsenic  $\text{BaPdAs}_2$  and  $\text{BaPtAs}_2$ <sup>[19]</sup> are known. Moreover  $\text{LaMnSi}_2$ -type phases containing four elements with a homogenous metal substitution of 25 % on the non-metal atoms were reported.<sup>[20-24]</sup>

It should also be mentioned that recently a new family of substituted calcium iron arsenide compounds<sup>[1,2,8,25]</sup> with the same ratio of 1 : 1 : 2 was published. In these compounds (space-group  $P2_1/m$  or  $P2_1$ ) also tetrahedra layers take turns with arsenic *zigzag* layers each separated by calcium, however, here the plane containing the *zigzag* chains is orientated coplanar to the tetrahedra layers. Without bonding between the tetrahedra and *zigzag* layers the *c* axis is enlarged compared to our structure. The undoped compound “ $\text{CaFeAs}_2$ ” was not reported so far, however, various rare earth substituted samples also show superconducting properties.

### 5.2.2 X-Ray Powder Diffraction

We were able to obtain high quality polycrystalline samples of the new compound via solid state reactions. A mixture of pure elements (> 99.9 %) was heated up to 850 °C in alumina crucibles under purified argon and annealed twice at 750 °C. For characterization the samples were measured on a Huber Imagine Plate Guinier diffractometer and refined by the Rietveld method with the TOPAS program package.<sup>[26]</sup> Based on the crystal parameters from the single crystal structure determination we refined the parameters of  $\text{Ca}(\text{Fe}_{0.56}\text{Pd}_{0.44})\text{As}_{2-z}$  with  $a = 8.060(1)$ ,  $b = 4.124(1)$ ,  $c = 9.096(1)$ , and  $\beta = 102.8(1)$  as well as the atomic positions and occupancies with  $R_{\text{wp}} = 1.37$ . Figure 3 shows the measured X-ray powder data with Rietveld fit of the new compound. Minor amounts of binary FeAs were obtained as impurity phase.

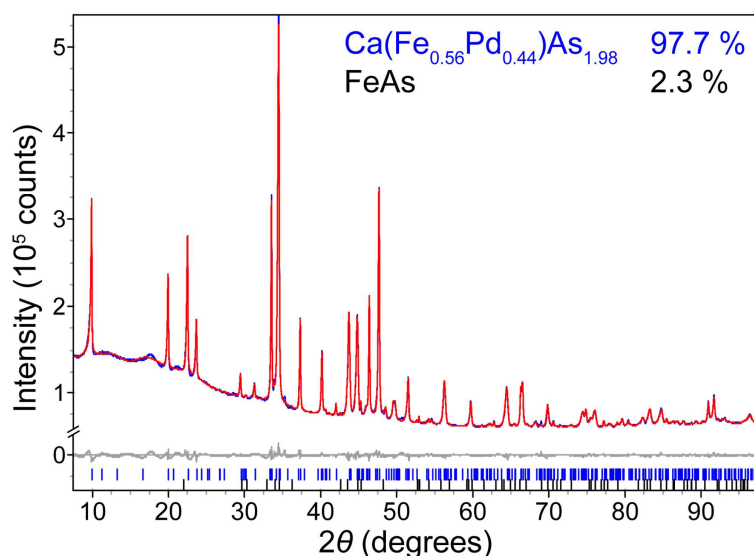


**Figure 3:** X-ray powder data (blue) with Rietveld fit (red) of polycrystalline  $\text{Ca}(\text{Fe}_{0.56}\text{Pd}_{0.44})\text{As}_{1.98}$ .

All parameters keep close to the results from the single crystal structure refinement in addition to the identical substitution level of iron and palladium. Admitting free occupancies on the *zigzag* sites also minor vacancies of the arsenic position can be derived from the powder

data. Polycrystalline samples of the two stoichiometric parent compounds  $\text{CaFeAs}_2$  and  $\text{CaPdAs}_2$  could not be obtained so far.

### 5.2.3 Magnetic Properties

Dc-susceptibility data of  $\text{CaFe}_{0.56}\text{Pd}_{0.44}\text{As}_2$  from 1.8 K to 300 K was measured on a SQUID magnetometer (Quantum Design MPMS-XL5) at different external fields. The polycrystalline sample reveals paramagnetic behavior with  $\chi_{\text{mol}}(300 \text{ K}) = 1.00 \cdot 10^{-3} \text{ cm}^3 \text{ mol}^{-1}$  at 100 Oe, which is a few orders of magnitude too high for *Pauli* paramagnetism (Figure 4, left). Below about 60 K a steady increase of susceptibility conceivably indicates magnetic ordering also visible by a slight anomaly at about 16 K in the inverse curve. The measurements at higher external fields of 1000 Oe and 10000 Oe show slightly lower values of molar susceptibility as displayed on the right hand side of Figure 4. The *zero-field-cooled/ field-cooled* measurement confirms the presence of a magnetic ordering within the sample by the splitting of both branches at ca. 16 K.

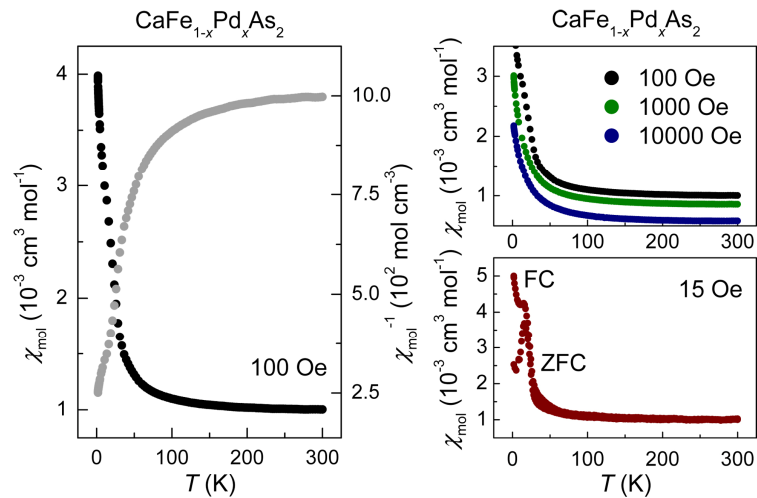


**Figure 4:** Molar magnetic susceptibility and inverse data of polycrystalline  $\text{Ca}(\text{Fe}_{0.56}\text{Pd}_{0.44})\text{As}_2$  (left). Comparison of measurements with increasing external field and *zero-field-cooled/ field-cooled* measurement at 15 Oe (right).

Because of the high substitution rate of iron and palladium we did not expect superconducting properties in this sample. However, molar susceptibility is in the order of other over-doped<sup>[27]</sup> or undoped<sup>[28]</sup> non-superconducting iron-based pnictides. With this new structure a further class of iron pnictide superconductors based on  $\text{Ca}(\text{Fe}_{1-x}\text{Pd}_x)\text{As}_2$  is easily conceivable for example induced by different doping levels and components.

#### 5.2.4 Electronic Structure

Electronic structures of four idealized variants of  $\text{Ca}(\text{Fe}_{1-x}\text{Pd}_x)\text{As}_2$  with our newly discovered crystal structure featuring vertical *zigzag* chains perpendicular to the basal plane were calculated using the WIEN2k package.<sup>[29]</sup> Figure 5 shows the total density of states (DOS) for  $\text{CaFeAs}_2$  (a),  $\text{CaFe}_{0.5}\text{Pd}_{0.5}\text{As}_2$  (b), and  $\text{CaPdAs}_2$  (c) as well as projections of the partial density of states. The DOS calculated for the other possible mixed compound with the exchanged occupancies of the two transition metal positions in  $\text{CaPd}_{0.5}\text{Fe}_{0.5}\text{As}_2$  appears similar to  $\text{CaFe}_{0.5}\text{Pd}_{0.5}\text{As}_2$ . As expected only the crucial pDOS of the respective transition metal changes, while the calcium and arsenic states remain apparently identical. At the *Fermi* energy ( $E_F$ ) only the iron and palladium states, respectively, are dominant. In the pure iron compound the total value at  $E_F$  shows a relatively high DOS. However, addition of palladium yielding stepwise reduced states leads to a decrease of the entire DOS at  $E_F$  in the mixed samples and even more (44 %) in the pure palladium compound. Therefore we suppose the reduction of iron pDOS at  $E_F$  by high palladium mixing to prevent the induction of superconductivity in  $\text{Ca}(\text{Fe}_{0.56}\text{Pd}_{0.44})\text{As}_2$ .

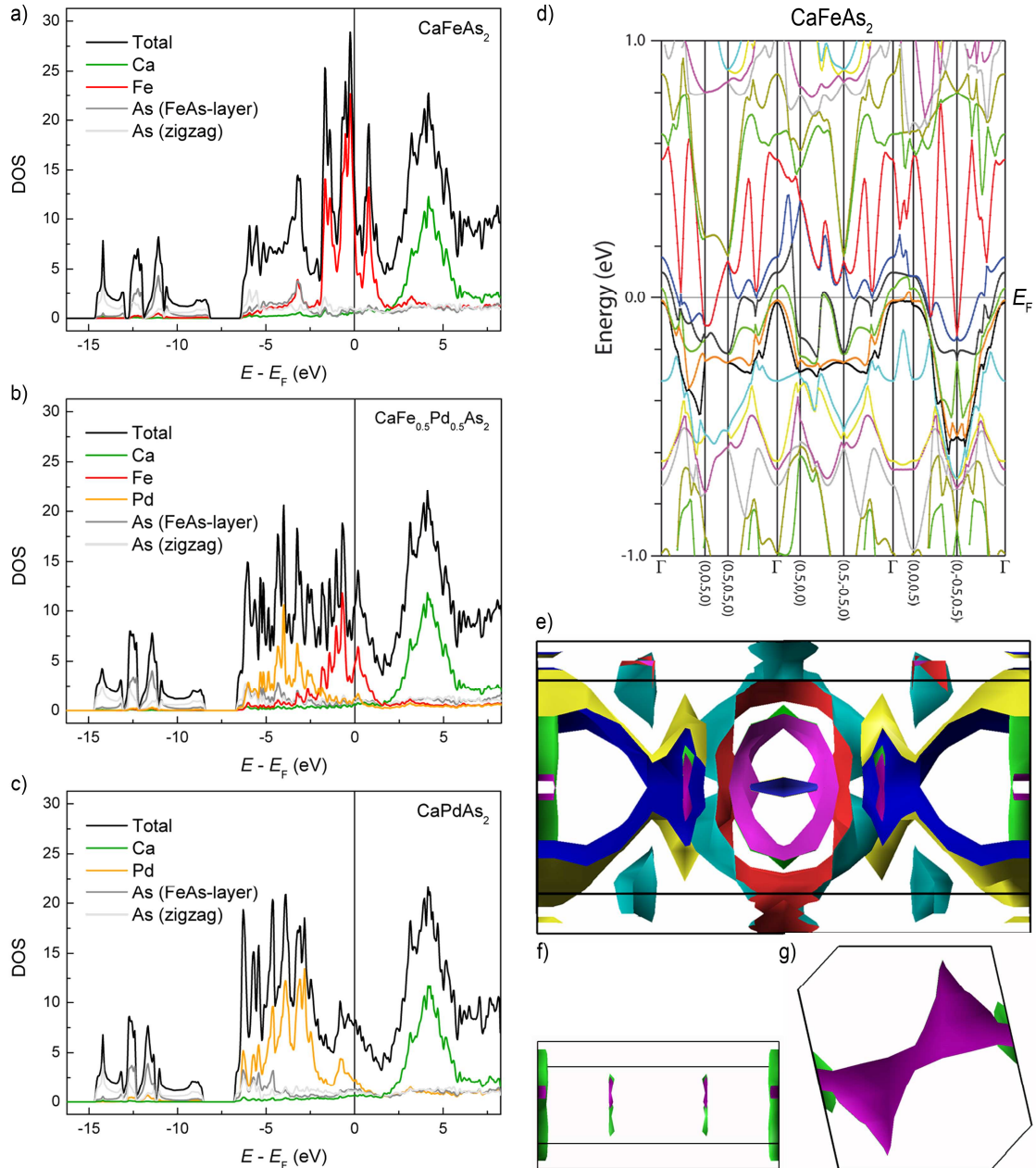


**Figure 5:** Electronic density of states of idealized compounds  $\text{CaFeAs}_2$  (a),  $\text{CaFe}_{0.5}\text{Pd}_{0.5}\text{As}_2$  (b), and  $\text{CaPdAs}_2$  (c); Band structure from DFT calculations for  $\text{CaFeAs}_2$  (d); Merged *Fermi* surface sheets of  $\text{CaFeAs}_2$  (e) and not-cylindrical sheet (f) and (g).

On the right hand side of Figure 5 the calculated band structure (d) of  $\text{CaFeAs}_2$  is illustrated. Hole-like *Fermi* sheets at  $\Gamma$  and electron-like at  $(\frac{1}{2} 0 0)$  and  $(0 \frac{1}{2} 0)$  indicate nesting, which is discussed as a decisive factor for superconductivity in iron arsenide compounds.<sup>[30,31]</sup> Some kind of two-dimensionality is evident in the merged *Fermi* surface of  $\text{CaFeAs}_2$  (e) featuring mainly cylinder-like sheets. However, one deviation is present by a non-cylindrical *Fermi* sheet (f) coplanar to the  $a^*c^*$  plane (g).

### 5.3 Conclusion

The new iron palladium arsenide  $\text{CaFe}_{1-x}\text{Pd}_x\text{As}_2$  was identified. The compound was synthesized by solid state methods and characterized by single crystal structure determination. The new monoclinic crystal structure is build up from metal-centered tetrahedra layers and arsenic *zigzag* chains both separated by calcium ions. Next to short As–As bonds within the infinite arsenic stands (2.37 Å) elongated bonds to the tetrahedra layers (2.47 and 2.48 Å) are present. Crystal structure refinement as well as X-ray powder diffraction data of a high quality powder sample revealed distinct palladium mixing on the tetrahedral coordinated positions as well as minor arsenic deficiencies within the *zigzag* layers. The new structure being virtually an ordered variant of the well-known  $\text{LaMnSi}_2$ -type structure was derived from this orthorhombic aristotype and compared to other related structure types. Magnetic measurements showed paramagnetic behavior with an anomaly at 16 K. From electronic structure calculation of several idealized compounds a stepwise reduction of transition-metal states at the *Fermi* level with increasing palladium substitution was revealed. The low iron pDOS was assumed as impediment for the induction of superconductivity, however, we expect other results for reduced doping levels or different substituents. The *Fermi* surface features two-dimensional character from cylindrical sheets with one deviation present. These initializing studies characterize  $\text{CaFe}_{1-x}\text{Pd}_x\text{As}_2$  as a new member of the family of iron arsenides featuring a new crystal structure related and isocompositional to recently published high- $T_c$  superconductor  $\text{Ca}_{1-x}\text{RE}_x\text{FeAs}_2$ .

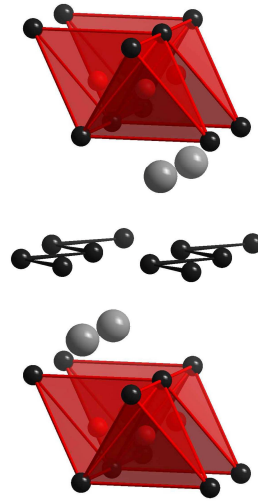
### 5.4 References

- [1] N. Katayama, K. Kudo, S. Onari, T. Mizukami, K. Sugawara, Y. Kitahama, K. Iba, K. Fujimura, N. Nishimoto, M. Nohara, H. Sawa, *J. Phys. Soc. Jpn.* **2013**, 82, 123702.
- [2] H. Yakita, H. Ogino, T. Okada, A. Yamamoto, K. Kishio, T. Tohei, Y. Ikuhara, Y. Gotoh, H. Fujihisa, K. Kataoka, H. Eisaki, J. Shimoyama, *J. Am. Chem. Soc.* **2014**, 136, 846.
- [3] H. Sprenger, *J. Less-Common Met.* **1974**, 34, 39.
- [4] E. Brechtel, G. Cordier, H. Schäfer, *Z. Naturforsch. B* **1979**, 34, 251.
- [5] R. O. Demchyna, J. P. F. Jemetio, Y. M. Prots, T. Doert, L. G. Akselrud, W. Schnelle, Y. B. Kuz'ma, Y. Grin, *Z. Anorg. Allg. Chem.* **2004**, 630, 635.

- [6] J. Dong, H. J. Zhang, G. Xu, Z. Li, G. Li, W. Z. Hu, D. Wu, G. F. Chen, X. Dai, J. L. Luo, Z. Fang, N. L. Wang, *Europhys. Lett.* **2008**, *83*, 27006.
- [7] M. Rotter, M. Tegel, I. Schellenberg, W. Hermes, R. Pöttgen, D. Johrendt, *Phys. Rev. B* **2008**, *78*, 020503(R).
- [8] K. Kudo, T. Mizukami, Y. Kitahama, D. Mitsuoka, K. Iba, K. Fujimura, N. Nishimoto, Y. Hiraoka, M. Nohara, *J. Phys. Soc. Jpn.* **2014**, *83*, 025001.
- [9] V. Petricek, M. Dusek, L. Palatinus, JANA2006, Institute of Physics, Praha, **2009**.
- [10] P. Villars, K. Cenzual, *Pearson's Crystal Data – Crystal Structure Database for Inorganic Compounds*, ASM International, Materials Park, Ohio, **2009/10**.
- [11] G. Venturini, B. Malaman, M. Meot Mayer, D. Fruchart, G. Le Caer, D. Malterre, B. Roques, *Rev. Chim, Miner.* **1986**, *23*, 162.
- [12] O. I. Bodak, E. I. Gladyshevskii, *Inorg. Mater.* **1969**, *5*, 1754.
- [13] K. Cenzual, R. E. Gladyshevskii, E. Parthé, *Acta Crystallogr. C* **1992**, *48*, 225.
- [14] I. Ijjaali, G. Venturini, B. Malaman, *J. Alloys Compd.* **1999**, *282*, 153.
- [15] B. Malaman, G. Venturini, G. Le Cear, L. Pontonnier, D. Fruchart, K. Tomala, J. P. Sanchez, *Phys. Rev. B: Condens. Matter* **1990**, *41*, 4700.
- [16] V. I. Yarovets, Y. K. Gorelenko, *Visn. L'viv. Derzh., Univ. (Ser. Khim.)* **1981**, 23-20.
- [17] L. Paccard, D. Paccard, J. Allemand, *J. Less-Common Met.* **1990**, *161*, 295.
- [18] V. Hlukhyy, S. Eck, T. F. Fässler, *Inorg. Chem.* **2006**, *45*, 7408.
- [19] D. Johrendt, C. Lux, A. Mewis, *Z. Naturforsch. B* **1996**, *51*, 1213.
- [20] G. Venturini, M. N. Norlidah, B. Malaman, *J. Alloys Compd.* **1996**, *236*, 117.
- [21] M. N. Norlidah, G. Venturini, B. Malaman, E. Ressouche, *J. Alloys Compd.* **1997**, *257*, 30.
- [22] M. N. Norlidah, G. Venturini, B. Malaman, E. Ressouche, *J. Alloys Compd.* **1997**, *259*, 11.
- [23] M. N. Norlidah, G. Venturini, B. Malaman, *J. Alloys Compd.* **1998**, *267*, 182.

- [24] M. N. Norlidah, G. Venturini, B. Malaman, *J. Alloys Compd.* **1998**, 268, 193.
- [25] A. Sala, H. Yakita, H. Ogino, T. Okada, A. Yamamoto, K. Kishio, S. Ishida, A. Iyo, H. Eisaki, M. Fujioka, Y. Takano, M. Putti, J. Shimoyama, *Appl. Phys. Express* **2014**, 7, 073102.
- [26] A. Coelho, TOPAS-Academic, Version 4.1, Coelho Software, Brisbane, **2007**.
- [27] M. Tegel, *Dissertation*, LMU Munich, **2011**.
- [28] M. R. Cimberle, F. Canepa, M. Ferretti, A. Martinelli, A. Palenzona, A. S. Siri, C. Tarantini, M. Tropeano, C. Ferdeghini, *J. Magn. Magn. Mater.* **2009**, 321, 3024.
- [29] P. Blaha, K. Schwarz, G. K. H. Madsen, D. Kvasnicka, J. Luitz, WIEN2k – An Augmented Plane Wave + Local Orbitals Program for Calculating Crystal Properties, Technische Universität, Vienna, **2001**.
- [30] I. I. Mazin, *Nature* **2010**, 464, 183.
- [31] D. Johrendt, *J. Mater. Chem.* **2011**, 21, 13726.

## 6 Properties of $\text{Ca}_{1-x}\text{Pr}_x\text{FeAs}_2$ with $x = 0.15 - 0.25$



### 6.1 Introduction

In 2014 a new type of layered iron arsenide superconductors was discovered. *Yakita* et al. reported the novel phase  $\text{Ca}_{1-x}\text{Pr}_x\text{FeAs}_2$  with an onset of superconductivity at  $T_c = 24$  K.<sup>[1]</sup> The crystal structure is build up from an alternated stacking of iron arsenide tetrahedra layers and isolated arsenic *zigzag* chains arranged coplanar to the basal plane. Both negatively charged layers are separated by calcium ions with partial praseodymium substitution. Since the lattice parameters  $a$  and  $b$  differ slightly and  $\beta$  is disparate from  $90^\circ$  the stacking yields a monoclinic structure with spacegroup  $P2_1/m$ . As a related orthorhombic variant of this structure several  $AMPn_2$  compounds with  $A = RE$ ,  $AE$ ,  $M = \text{Mn}$ ,  $\text{Zn}$ ,  $\text{Ag}$ , and  $Pn = \text{As}$ ,  $\text{Sb}$  ( $\text{SrZnSb}_2$  type, spacegroup  $Pnma$ ) are known.<sup>[2-4]</sup> Next to the praseodymium doped phase also the lanthanum compound was reported as a novel 112-type iron-based superconductor.<sup>[5]</sup> Subsequently, *Sala* et al. reported the synthesis and properties with  $RE = \text{La} - \text{Gd}$ ,<sup>[6]</sup> while *Kudo* et al. succeeded in the enhancement of the critical temperature by simultaneous pnictide substitution up to  $T_c = 43$  K<sup>[7]</sup> and eventually  $T_c = 47$  K.<sup>[8]</sup> However, the undoped hypothetical parent compound  $\text{CaFeAs}_2$  was not reported so far. Electronic structure calculations of  $\text{Ca}_{0.75}\text{Pr}_{0.25}\text{FeAs}_2$  revealed iron states dominant at the *Fermi* level ( $E_F$ ). Compared to calculations of the assumed parent compound *Fermi* surface nesting is suppressed by praseodymium doping featuring promising conditions for a superconducting state.<sup>[9]</sup>

So far structure and properties of  $\text{Ca}_{1-x}\text{Pr}_x\text{FeAs}_2$  single crystals were reported.<sup>[1,8]</sup> The structure was solved and refined with rather moderate residual values of  $R = 0.116$ .<sup>[1]</sup> Furthermore a low quality powder sample with a nominal composition of

$\text{Ca}_{0.9}\text{Pr}_{0.1}\text{Fe}_{1.3}\text{As}_{1.8}\text{O}_{0.2}$  showed superconductivity with  $T_c = 20$  K. Despite the small external field of  $H = 1$  Oe the sample did not reach full shielding with  $4\pi M / H < -0.4$ . Moreover the preparation of oxygen-free  $\text{Ca}_{0.9}\text{Pr}_{0.1}\text{FeAs}_2$  yielded only a minimal splitting of the *zero-field-cooled* and *field-cooled* curve. Both samples contained significant amounts of impurity phases. Therefore the unambiguous assignment of superconducting properties to the discussed phase  $\text{Ca}_{1-x}\text{Pr}_x\text{FeAs}_2$  is equivocal, precisely because only in the oxygen-containing phase superconductivity is evident. Due to the mixture of components for example the presence of  $\text{PrFeAsO}_{1-y}$  (1111 type) within the sample is conceivable. Moreover  $\text{FeAs}$ ,  $\text{CaFe}_2\text{As}_2$ ,  $\text{FeAs}_2$ , and  $\text{PrAs}$  were already noticed as impurities, however, not all present reflections are covered by these compounds. Depending on the level of oxygen deficiency or fluorine substitution, respectively, as well as performed synthesis strategy a wide range of magnetic properties can be achieved in hole doped Pr1111 compounds.  $\text{PrFeAsO}_{1-y}\text{F}_y$  features a dome-like phase diagram with maximum  $T_c = 47$  K at ambient pressure,<sup>[10]</sup> whereas in  $\text{PrFeAsO}_{1-y}$  the value of  $y$  results in different critical temperature up to  $T_c = 52$  K.<sup>[11,12]</sup>

To clarify the ambiguities raised on  $\text{Ca}_{1-x}\text{Pr}_x\text{FeAs}_2$  further experiments based on high quality powder samples with  $x = 0.15 - 0.25$  and a step width of  $\Delta = 0.025$  were accomplished.  $\text{Ca}_{1-x}\text{Pr}_x\text{FeAs}_2$  was synthesized under oxygen and moisture absence. The polycrystalline compounds were characterized by X-ray powder diffraction with Rietveld refinements and magnetic measurements to investigate potential superconducting properties.

## 6.2 Results and Discussion

Due to performed synthesis optimization all samples were obtained as polycrystalline powder material from solid state reactions. In Figure 1 the refined crystal structure of  $\text{Ca}_{0.77}\text{Pr}_{0.23}\text{FeAs}_2$  from X-ray powder diffraction is illustrated.

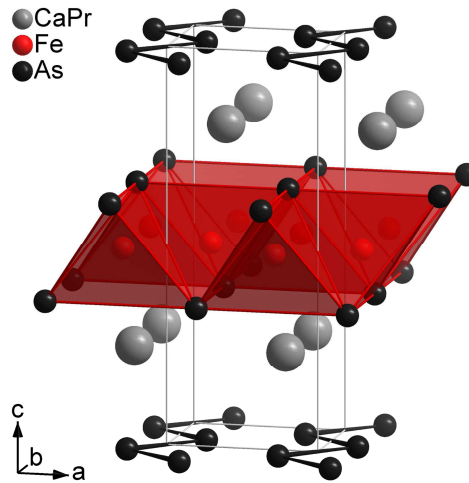


**Figure 1:** Refined crystal structure of  $\text{Ca}_{1-x}\text{Pr}_x\text{FeAs}_2$  from X-ray powder data. Obtained lattice parameters yielded  $a = 3.936(1)$ ,  $b = 3.872(1)$ ,  $c = 10.31(1)$ , and  $\beta = 91.14(1)$  with  $x = 0.228(2)$  and  $R_{\text{wp}} = 1.70$ .

### 6.2.1 X-Ray Powder Diffraction

The polycrystalline samples were characterized by X-ray powder diffraction including Rietveld refinements. Based on published single crystal data of  $\text{Ca}_{1-x}\text{Pr}_x\text{FeAs}_2$  (space group  $P2_1/m$ ) all free lattice parameters as well as atomic positions and calcium/ praseodymium occupancies were independently refined. The results revealed  $\text{Ca}_{1-x}\text{Pr}_x\text{FeAs}_2$  as main component with 80 – 88 wt%. The binary arsenides FeAs and PrAs as well as  $\text{CaFe}_2\text{As}_2$  were present as impurity phases in varying proportions. Figure 2 shows the refined diffractograms for nominal  $x = 0.15, 0.175, 0.20, 0.225,$  and  $0.25$ .

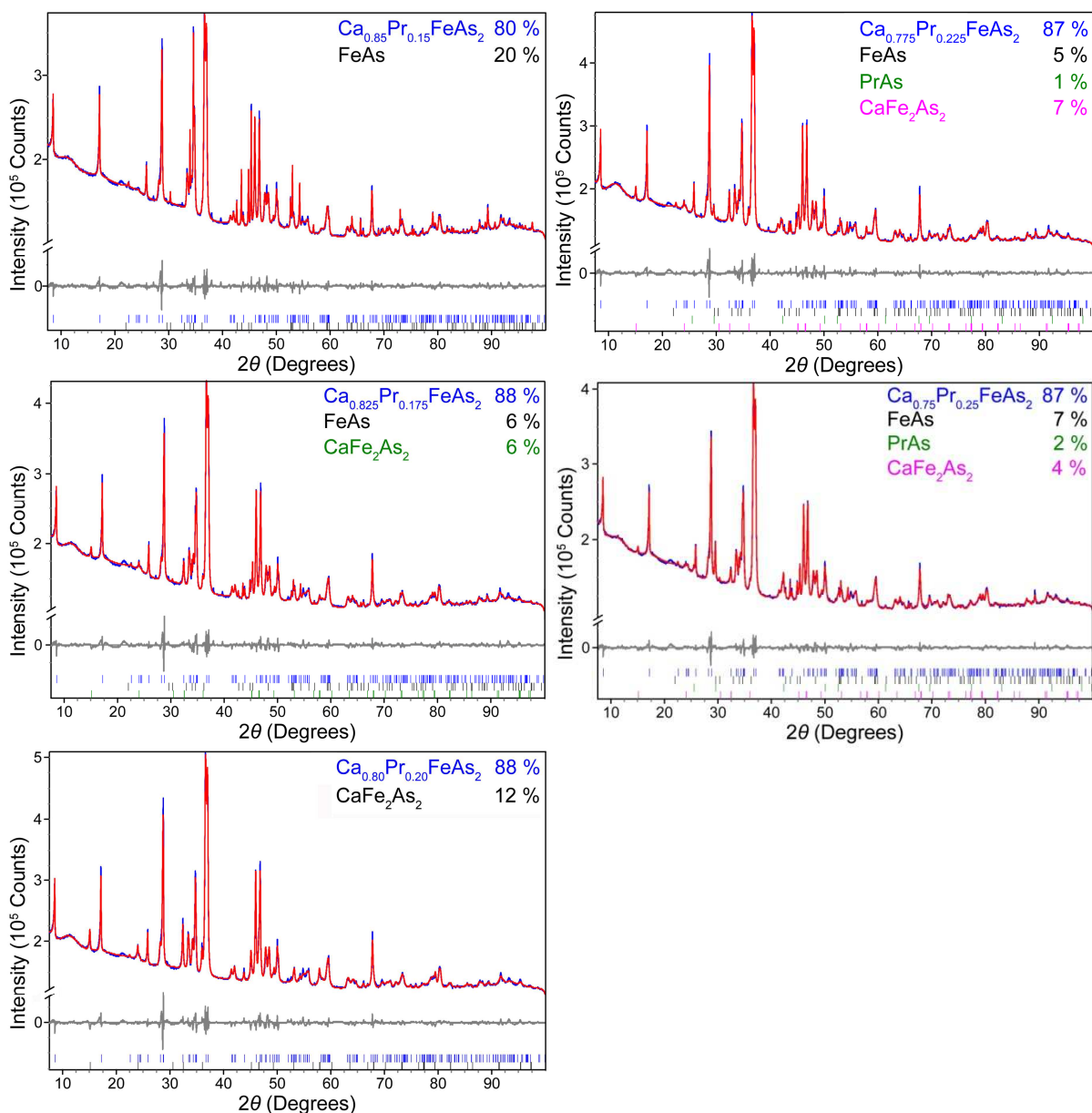


**Figure 2:** X-ray powder data (blue) with Rietveld fits (red) of  $\text{Ca}_{1-x}\text{Pr}_x\text{FeAs}_2$  for  $x = 0.15, 0.175, 0.20$  (left),  $0.225$ , and  $0.25$  (right).

In  $\text{Ca}_{1-x}\text{Pr}_x\text{FeAs}_2$  the substituted metal position is eightfold *anti*-prismatically coordinated by arsenic. The ionic radii of  $\text{Pr}^{3+}$  ( $r_{\text{CN}=8} = 1.27 \text{ \AA}$ ) and  $\text{Ca}^{2+}$  ( $r_{\text{CN}=8} = 1.26 \text{ \AA}$ )<sup>[13]</sup> differ only slightly. Considering additionally the increased electronic attraction of trivalent praseodymium the lattice parameters should hardly change with varying substituent concentration in the investigated series. The results of powder data refinements confirm these assumption featuring almost constant values for  $x = 0.15 - 0.25$ . Refined unit cell axes as well as the monoclinic  $\beta$  angle and the unit cell volume of  $\text{Ca}_{1-x}\text{Pr}_x\text{FeAs}_2$  are depicted in Figure 3. Minor variations can be ascribed to the actual substituent concentrations obtained from refined powder data and EDX measurements (Figure 4).

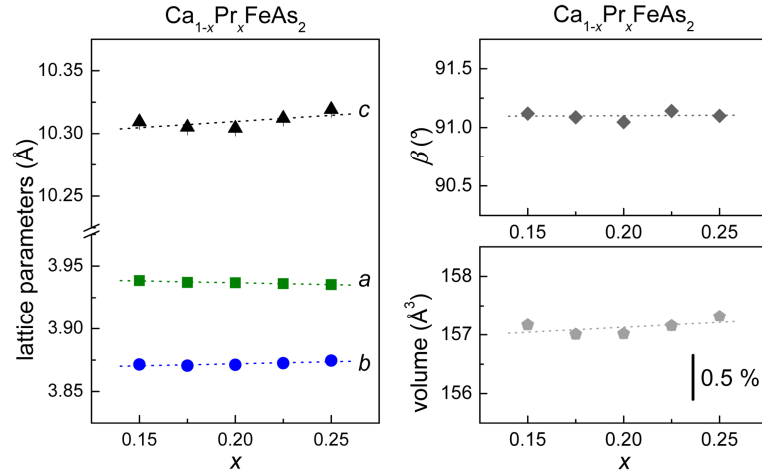


**Figure 3:** Unit cell axes (left),  $\beta$  angle, and volume (right) of  $\text{Ca}_{1-x}\text{Pr}_x\text{FeAs}_2$  with  $x = 0.15 - 0.25$ . Dotted lines are guides to the eye.

Furthermore also the occupation of calcium positions by praseodymium was obtained from refined powder data, illustrated in Figure 4 together with the corresponding phase amount of  $\text{Ca}_{1-x}\text{Pr}_x\text{FeAs}_2$ . The results show the trend of increasing praseodymium content  $x$  and fit very well to the nominal values, especially for higher substitution levels. Additionally performed X-ray spectroscopy measurements (EDX) obtained also good agreement of the doping level with the nominal values. Both methods show a favored higher praseodymium concentration for lower nominal values  $x = 0.15$  and  $0.175$ . This is in line with a distinct decline of sample quality as well as phase amount of  $\text{Ca}_{1-x}\text{Pr}_x\text{FeAs}_2$  for smaller substitution levels  $x \leq 0.15$ . Similar results were reported for other praseodymium doped samples with nominal values of  $x = 0.10$ , but experimental concentration of 15 – 27 %.<sup>[1,8]</sup> With no apparent structural change taking place by the substitution of calcium by praseodymium the intrinsic stabilization probably originates from the electronic contribution. Not yet reported hypothetical  $\text{CaFeAs}_2$  can be described as a valence compound with isolated arsenic *zigzag* chains  $^{\infty}_1[\text{As}^-]$ . Nevertheless the experimental results indicate an optimal doping level by trivalent praseodymium of  $x > 0.15$ . Probably the electronic situation prevents a stable state of the potential stoichiometric parent compound under regular conditions, while electronic doping with trivalent substituents stabilizes the so accessible compounds within a favored doping range. The so far experimental inaccessibility of undoped  $\text{CaFeAs}_2$  supports this assumption.

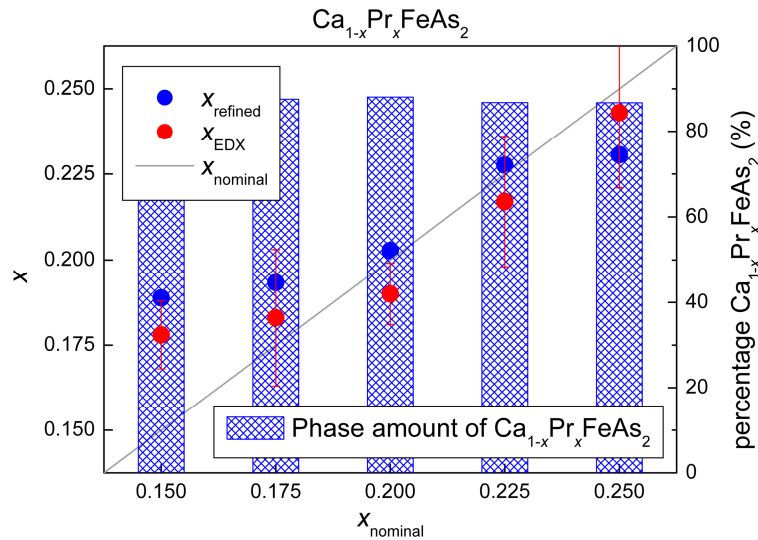


**Figure 4:** Praseodymium content  $x$  obtained from Rietveld refinements (blue circles) and EDX analyses (red circles). Phase amount of  $\text{Ca}_{1-x}\text{Pr}_x\text{FeAs}_2$  in the polycrystalline samples (blue columns).

### 6.2.2 Magnetic Properties

$\text{Ca}_{1-x}\text{Pr}_x\text{FeAs}_2$  was characterized by ac-susceptibility investigations measured at a small external field of 3 Oe. All samples with nominal doping levels of  $x = 0.15 - 0.25$  showed paramagnetic behavior with a continuous increase of molar susceptibilities with decreasing temperature. Inverse molar susceptibility featured *Curie Weiss* behavior. No superconductivity was induced in the polycrystalline samples of  $\text{Ca}_{1-x}\text{Pr}_x\text{FeAs}_2$  in the investigated range (Figure 5).

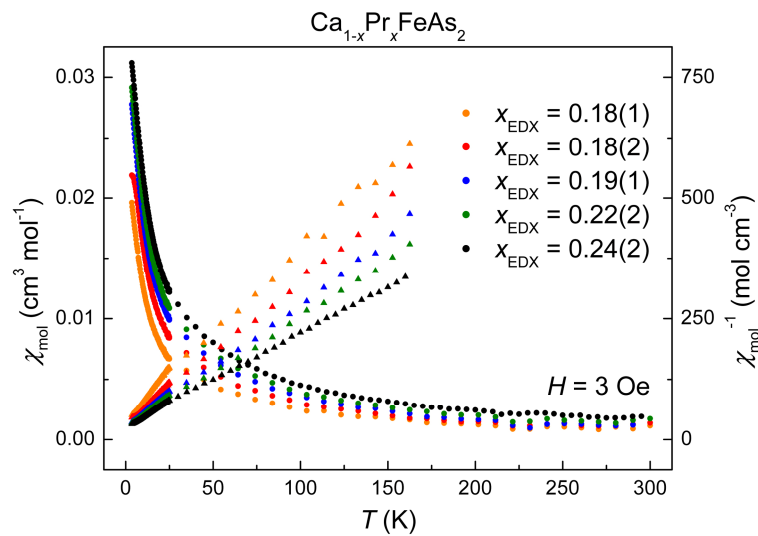


**Figure 5:** Molar ac-susceptibility (circles) and inverse susceptibility (triangles) of  $\text{Ca}_{1-x}\text{Pr}_x\text{FeAs}_2$  at 1333 Hz and 3 Oe with doping level  $x$  from EDX analyses.

Exemplarily the molar susceptibility of  $\text{Ca}_{0.81}\text{Pr}_{0.19}\text{FeAs}_2$  was additionally measured on a SQUID magnetometer at an external magnetic field of 10 kOe (Figure 6). A *Curie Weiss* fit of the inverse data in the range of 1.8 – 300 K obtained an effective magnetic moment of  $\mu_{\text{eff}} = 3.57(1)$ . The exact substitution level was taken from EDX analysis. With the magnetic moment of trivalent praseodymium  $\mu_{\text{eff}}(\text{Pr}^{3+}) = 3.4 - 3.6$  listed in the literature,<sup>[14]</sup> the obtained result can clearly be ascribed to the rare earth dopant. Again no superconductivity was observed.

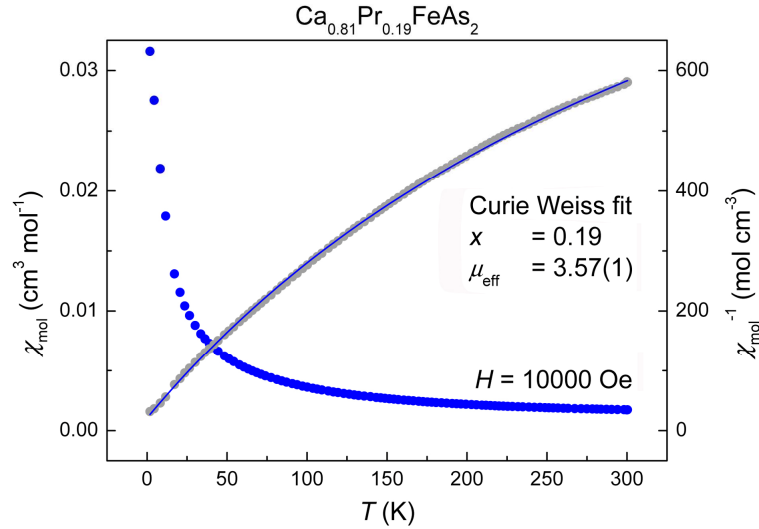


**Figure 6:** Molar (blue circles) and inverse (gray circles) susceptibility of  $\text{Ca}_{0.81}\text{Pr}_{0.19}\text{FeAs}_2$  with *Curie Weiss* fit (blue curve) measured at 10 kOe.

Previously  $\text{Ca}_{1-x}\text{Pr}_x\text{FeAs}_2$  was described as superconductor with initially  $T_c = 20$  K without further doping. Despite the nominal value was given by 10 %, EDX analysis yielded  $x = 0.17$  and  $x = 0.20$ , respectively, while single crystal data obtained 27 %.<sup>[1,8]</sup> This range is covered by the here analyzed samples, however, the experimental results differ. Magnetization measurements of  $\text{Ca}_{0.9}\text{Pr}_{0.1}\text{Fe}_{1.3}\text{As}_{1.8}\text{O}_{0.2}$  with conscious oxygen content showed superconducting properties, while only a minimal splitting of the *zero-field-cooled* and *field-cooled* curve was observed for the sample with a nominal composition of  $\text{Ca}_{0.9}\text{Pr}_{0.1}\text{FeAs}_2$ .<sup>[1]</sup> Therefore the classification of  $\text{Ca}_{1-x}\text{Pr}_x\text{FeAs}_2$  as superconductor was not confirmed by the current experiments. Due to the reported low sample quality featuring several impurity phases the alleged superconducting properties can definitely not be assigned doubtlessly to  $\text{Ca}_{1-x}\text{Pr}_x\text{FeAs}_2$ . More likely the presence of oxygen contributes to the induction of superconductivity in a different phase, while the here synthesized samples in absolute absence of air and moisture remain paramagnetic.

### 6.3 Experimental Section

All samples of  $\text{Ca}_{1-x}\text{Pr}_x\text{FeAs}_2$  were synthesized by solid state reactions with a varying praseodymium concentration of  $x = 0.15 - 0.25$  and a step width of  $\Delta = 0.025$ . Stoichiometric mixtures of the pure elements ( $> 99.9\%$ ) were heated to  $600\text{ }^\circ\text{C}$  followed by  $950\text{ }^\circ\text{C}$  under purified argon and annealed two to three times at  $850\text{ }^\circ\text{C}$  and  $900\text{ }^\circ\text{C}$ , respectively. The obtained polycrystalline samples were characterized by X-ray powder diffraction at room temperature using a Huber Imaging Plate Guinier diffractometer with primary monochromator and copper radiation. Rietveld refinements of all powder data based on published single crystal data<sup>[1]</sup> were carried out using the TOPAS program package.<sup>[15]</sup> All free lattice parameters and atomic positions as well as the calcium/ praseodymium mixing were independently refined. Sample compositions were confirmed by X-ray spectroscopy (EDX) on a Carl Zeiss EVO MA-10 scanning electron microscope with Bruker Nano EDX detector. AC-susceptibility data were measured on an ac-susceptometer at  $1333\text{ Hz}$  and  $3\text{ Oe}$ , dc-susceptibility using a Quantum Design MPMS-XL5 SQUID magnetometer at  $10\text{ kOe}$ .

### 6.4 Conclusion

Polycrystalline samples of  $\text{Ca}_{1-x}\text{Pr}_x\text{FeAs}_2$  with  $x = 0.15 - 0.25$  were synthesized by solid state reactions using *Schlenk* technique in the absence of air and moisture. The samples were characterized by X-ray powder data refinement. Obtained structural parameters revealed no change of the lattice parameters in line with the ionic radii of the substituents. Praseodymium contents were confirmed by refined powder diffractograms and EDX analyses in good overall agreement with the nominal values. The experimental doping concentrations fit very well for higher nominal values  $x \geq 0.20$ . With decreasing praseodymium concentration sample quality is reduced and substituent amount increased. A favored electronic situation by charge doping is visible for the distinct stabilization of  $\text{Ca}_{1-x}\text{Pr}_x\text{FeAs}_2$  with  $x > 0.15$ . Since structural factors were not found as decisive, electronic reasons were assumed responsible for the still inaccessibility of the undoped parent compound  $\text{CaFeAs}_2$ . Despite reports on superconductivity in  $\text{Ca}_{1-x}\text{Pr}_x\text{FeAs}_2$  and promising electronic structure calculations the samples showed no superconducting properties at all. Paramagnetic behavior was observed by susceptibility measurements. A *Curie Weiss* fit performed on the magnetic data revealed an effective magnetic moment, which is in excellent agreement with reported values for praseodymium. If both experimental results can actually be attributed to the same series of compounds, the peculiar divergence of magnetic properties is so far inexplicable and requires additional

investigations. Otherwise reported superconductivity cannot be ascribed as intrinsic property to the discussed compounds  $\text{Ca}_{1-x}\text{Pr}_x\text{FeAs}_2$ .

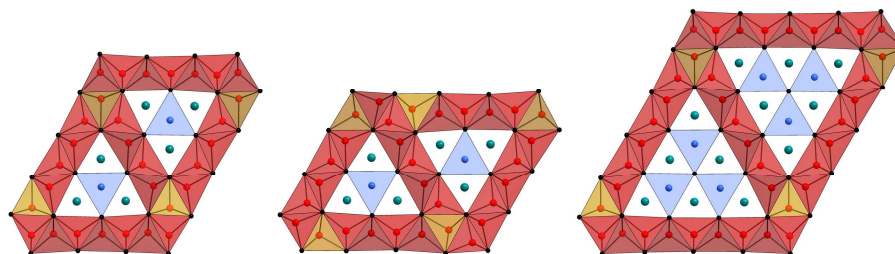
## 6.5 References

- [1] H. Yakita, H. Ogino, T. Okada, A. Yamamoto, K. Kishio, T. Tohei, Y. Ikuhara, Y. Gotoh, H. Fujihisa, K. Kataoka, H. Eisaki, J. Shimoyama, *J. Am. Chem. Soc.* **2014**, *136*, 846.
- [2] E. Brechtel, G. Cordier, H. Schäfer, *Z. Naturforsch. B* **1979**, *34*, 251.
- [3] E. Brechtel, G. Cordier, H. Schäfer, *J. Less-Common Met.* **1981**, *79*, 131.
- [4] M. Eschen, W. Jeitschko, *Z. Naturforsch. B* **2003**, *58*, 399.
- [5] N. Katayama, K. Kudo, S. Onari, T. Mizukami, K. Sugawara, Y. Kitahama, K. Iba, K. Fujimura, N. Nishimoto, M. Nohara, H. Sawa, *J. Phys. Soc. Jpn.* **2013**, *82*, 123702.
- [6] A. Sala, H. Yakita, H. Ogino, T. Okada, A. Yamamoto, K. Kishio, S. Ishida, A. Iyo, H. Eisaki, M. Fujioka, Y. Takano, M. Putti, J. Shimoyama, *Appl. Phys. Express* **2014**, *7*, 073102.
- [7] K. Kudo, T. Mizukami, Y. Kitahama, D. Mitsuoka, K. Iba, K. Fujimura, N. Nishimoto, Y. Hiraoka, M. Nohara, *J. Phys. Soc. Jpn.* **2014**, *83*, 025001.
- [8] K. Kudo, Y. Kitahama, K. Fujimura, T. Mizukami, H. Ota, M. Nohara, *J. Phys. Soc. Jpn.* **2014**, *83*, 093705.
- [9] Y.-N. Huang, X.-L. Yu, D.-Y. Liu, L.-J. Zou, *J. Appl. Phys.* **2015**, *117*, 17E113.
- [10] C. R. Rotundu, D. T. Keane, B. Freelon, S. D. Wilson, A. Kim, P. N. Valdivia, E. Bourret-Courchesne, R. J. Birgeneau, *Phys. Rev. B* **2009**, *80*, 144517.
- [11] T. Fukuda, A. Q. R. Baron, H. Nakamura, S. Shamoto, M. Ishikado, M. Machida, H. Uchiyama, A. Iyo, H. Kito, J. Mizuki, M. Arai, H. Eisaki, *Phys. Rev. B* **2011**, *84*, 064504.
- [12] J. Zhao, Q. Huang, C. de la Cruz, J. W. Lynn, M. D. Lumsden, Z. A. Ren, J. Yang, X. Shen, X. Dong, Z. Zhao, P. Dai, *Phys. Rev. B* **2008**, *78*, 132504.

- [13] A. F. Hollemann, E. Wiberg, N. Wiberg, *Lehrbuch der Anorganischen Chemie*, Walter de Gruyter, Berlin, **2007**.
- [14] H. Lueken, *Magnetochemie*, Teubner, Stuttgart Leipzig, **1999**.
- [15] A. Coelho, TOPAS-Academic, Version 4.1, Coelho Software, Brisbane, **2007**.

## 7 Framework Structures of interconnected Layers in Calcium Iron Arsenides

T. Stürzer, C. Hieke, C. Löhnert, F. Nitsche, J. Stahl, C. Maak, R. Pobel, D. Johrendt



published in: *Inorg. Chem.* **2014**, *53*, 6235 – 6240.

Copyright 2014, American Physical Society.

### Abstract

The new calcium iron arsenide compounds  $\text{Ca}_{n(n+1)/2}(\text{Fe}_{1-x}\text{M}_x)_{(2+3n)}\text{M}'_{n(n-1)/2}\text{As}_{(n+1)(n+2)/2}$  ( $n = 1 - 3$ ;  $M = \text{Nb, Pd, Pt}$ ;  $M' = \square, \text{Pd, Pt}$ ) were synthesized and their crystal structures determined by single crystal X-ray diffraction. The series demonstrates the structural flexibility of iron arsenide materials, which otherwise prefer layered structures, as is known from the family of iron-based superconductors. In the new compounds, iron arsenide tetrahedral layers are bridged by iron-centered pyramids, giving rise to so far unknown frameworks of interconnected FeAs layers. Channels within the structures are occupied with calcium and palladium or platinum, respectively. Common basic building blocks are identified that lead to a better understanding of the building principles of these structures and their relation to  $\text{CaFe}_4\text{As}_3$ .

### 7.1 Introduction

Layered iron arsenides have earned sweeping prominence in the solid state chemistry and physics communities during the last years because of the emergence of high-temperature superconductivity up to 55 K.<sup>[1-4]</sup> Therewith, the family of layered iron arsenides was found to be a new class of high  $T_c$  superconductors beyond the copper oxides discovered in the 1980s.<sup>[5]</sup> Intensive research has meanwhile identified a growing family of layered compounds each containing two-dimensional FeAs layers.<sup>[6]</sup> A magnetic instability in the iron layers intertwined with the superconducting properties has been uncovered,<sup>[7]</sup> which can be

manipulated by chemical doping, pressure, or complete replacement of the separating layers by other two-dimensional structure fragments.<sup>[6,8]</sup> The presence of layered structures in both high  $T_c$  superconductor families has raised the question about the general necessity of low dimensionality, but no final consent has been found on this topic so far. Besides, other structures, featuring fragments of FeAs tetrahedral layers, are also expected to reveal very interesting properties, although it is not clear whether superconductivity could arise in such systems. In 2009, the compound  $\text{CaFe}_4\text{As}_3$  with a structure consisting of interconnected  $\text{FeAs}_{4/4}$  tetrahedral bands forming channels occupied with calcium was identified.<sup>[9]</sup> At the band joints, iron is pyramidally coordinated by five arsenic ions connecting two bands. Magnetic measurements identified iron(II) in the  $\text{FeAs}_{4/4}$  tetrahedra but also remarkably iron(I) in the  $\text{FeAs}_{5/5}$  pyramids.<sup>[10]</sup> Also, hints to a spin density wave were reported similar to the layered compounds, but despite diverse substitution attempts, no superconducting properties were achieved.<sup>[11]</sup> In this paper, we report five new structure types in the iron arsenide family with the general composition  $\text{Ca}_{n(n+1)/2}(\text{Fe}_{1-x}\text{M}_x)_{(2+3n)}\text{M}'_{n(n-1)/2}\text{As}_{(n+1)(n+2)/2}$  ( $M = \text{Nb, Pd, Pt}$ ;  $M' = \square, \text{Pd, Pt}$ ) with  $n = 1 - 3$ , featuring three-dimensional frameworks of interconnected layers. A structural breakdown of these compounds to basic building blocks is given, yielding a systematic understanding of the relationship of these structures to each other and their close relationship to  $\text{CaFe}_4\text{As}_3$  as well as to layered iron pnictides. Finally, the connection to a long-known class of intermetallic compounds with a metal-to-pnictide ratio of 2 : 1 is illustrated.

## 7.2 Experimental Details

Polycrystalline samples of the compounds  $\text{Ca}_{n(n+1)/2}(\text{Fe}_{1-x}\text{M}_x)_{(2+3n)}\text{M}'_{n(n-1)/2}\text{As}_{(n+1)(n+2)/2}$  with  $n = 2$  and 3 and  $(\text{Ca,Na})_3(\text{Fe,Nb})_8\text{As}_6$  were synthesized by solid state methods under ambient pressure. Stoichiometric mixtures of pure elements (> 99.5 %) were heated at 900 – 1000 °C in alumina crucibles or niobium tubes, respectively, and sealed in silica tubes under purified argon. The samples were thoroughly homogenized and annealed twice at 900 – 1000 °C. The  $\alpha$ -polymorphs of the compounds with  $n = 1$  and 2 were synthesized from a mixture of binary starting materials and pure elements (> 99.5 %) by high-pressure synthesis in boron nitride crucibles at 6 GPa and 1000 °C, using a modified *Walker*-type multianvil apparatus.<sup>[12,13]</sup> Bulk  $\alpha$ - $\text{Ca}_3\text{Fe}_8\text{PtAs}_6$  was obtained by both high-pressure and high-temperature synthesis, whereas  $\text{CaFe}_5\text{As}_3$  was accessible only by high-pressure synthesis.  $\beta$ - $\text{Ca}_3\text{Fe}_8\text{PtAs}_6$  was only obtainable as a side phase. In the Ca–Fe–Pd–As system, solid state synthesis always yielded a

mixture of the  $\beta$ - and  $\gamma$ -modifications. An  $\alpha$ -type compound has not been identified so far. All samples were characterized by powder X-ray diffraction using a Huber G670 diffractometer with Cu-K $\alpha_1$  or Co-K $\alpha_1$  radiation. Singles crystals were selected from the polycrystalline samples, and X-ray intensity data were measured on a Stoe IPDS-I or a Bruker D8 Quest diffractometer. Energy dispersive X-ray spectroscopy was used to check the compositions. The structure refinements were performed against  $F^2$  using the JANA2006 program package.<sup>[14]</sup> Rietveld refinements of the powder diffraction data were performed with the TOPAS package<sup>[15]</sup> by using the structural data obtained by the single crystal experiments. A typical pattern with a Rietveld fit is exemplarily shown in Figure 1. Up to 10 % of impurity phases were detected in the bulk samples, mostly binary arsenides.

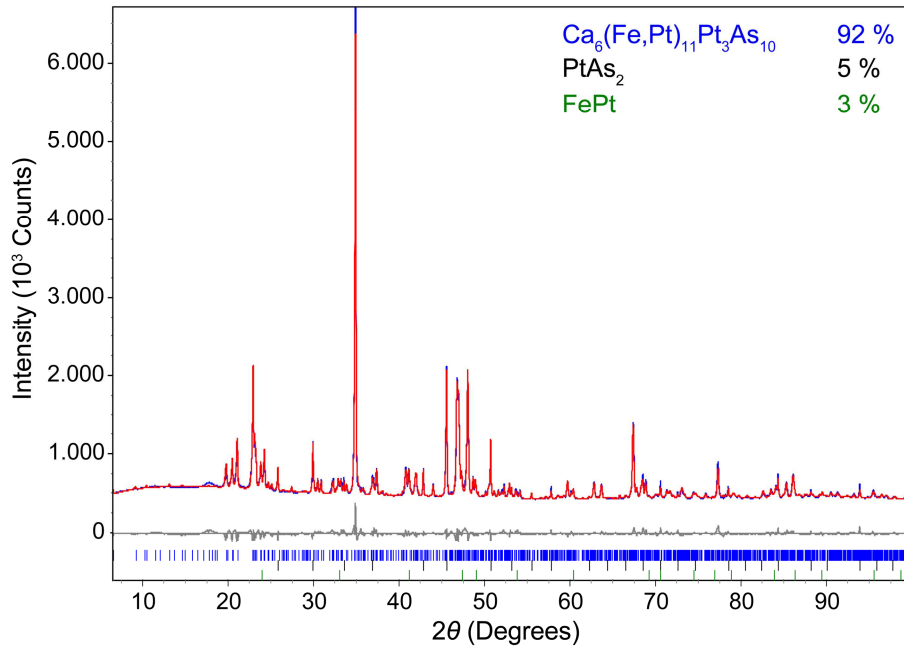


**Figure 1:** Powder X-ray diffraction pattern (blue) and Rietveld fit (red) of  $\text{Ca}_6(\text{Fe,Pt})_{11}\text{Pt}_3\text{As}_{10}$ .

**Table 1:** Crystal data and refinement parameters.

| compound      | $\text{CaFe}_5\text{As}_3$        | $\text{Ca}_3\text{Fe}_8\text{As}_6$   | $\text{Ca}_3\text{Fe}_8\text{PtAs}_6$                      | $\text{Ca}_3\text{Fe}_8\text{PdAs}_6$                    |
|---------------|-----------------------------------|---|--|--|
| structure     | $\alpha\text{-CaFe}_5\text{As}_3$ | $\alpha\text{-Ca}_3\text{Fe}_8\text{As}_6$                                    | $\alpha\text{-Ca}_3\text{Fe}_8\text{PtAs}_6$               | $\beta\text{-Ca}_3\text{Fe}_8\text{PdAs}_6$              |
| composition   | $\text{CaFe}_5\text{As}_3$        | $\text{Ca}_{2.56}\text{Na}_{0.44}\text{Fe}_{7.49}\text{Nb}_{0.51}\text{As}_6$ | $\text{Ca}_3\text{Fe}_{7.705}\text{Pt}_{1.295}\text{As}_6$ | $\text{Ca}_3\text{Fe}_{7.04}\text{Pd}_{1.96}\text{As}_6$ |
| space group   | $P2_1/m$                          | $P2_1/m$  | $P2_1/m$   | $Pnma$   |
| Z             | 2                                 | 2   | 2  | 4  |
| $a$ (Å)       | 7.2734(6)                         | 11.3307(9)  | 11.3169(5)   | 26.363(4)  |
| $b$ (Å)       | 3.8149(3)                         | 3.8078(3)   | 3.8809(2)  | 3.8699(5)  |
| $c$ (Å)       | 9.7577(8)                         | 13.6298(11)   | 13.7008(6)   | 11.330(1)  |
| $\beta$ (deg) | 100.704(2)                        | 106.154(3)  | 105.957(2)   | 90   |

|                        |  |  |   |   |
|------------------------|--|--|---|---|
| Vol ( $\text{\AA}^3$ ) | 266.04(4)  | 564.84(8)  | 578.55(5)   | 1155.9(2)   |
| $R_1(\text{obs/all})$  | 0.033/0.037  | 0.081/0.134  | 0.024/0.031   | 0.038/0.068   |
| $wR_2(\text{obs/all})$ | 0.085/0.094  | 0.178/0.197  | 0.066/0.072   | 0.082/0.085   |
| compound               | $\text{Ca}_3\text{Fe}_8\text{PtAs}_6$                    | $\text{Ca}_3\text{Fe}_8\text{PdAs}_6$                    | $\text{Ca}_6\text{Fe}_{11}\text{Pd}_3\text{As}_{10}$        | $\text{Ca}_6\text{Fe}_{11}\text{Pt}_3\text{As}_{10}$        |
| structure              | $\beta\text{-Ca}_3\text{Fe}_8\text{PtAs}_6$              | $\gamma\text{-Ca}_3\text{Fe}_8\text{PdAs}_6$             | $\alpha\text{-Ca}_6\text{Fe}_{11}\text{Pd}_3\text{As}_{10}$ | $\alpha\text{-Ca}_6\text{Fe}_{11}\text{Pt}_3\text{As}_{10}$ |
| composition            | $\text{Ca}_3\text{Fe}_{6.72}\text{Pt}_{2.28}\text{As}_6$ | $\text{Ca}_3\text{Fe}_{4.74}\text{Pd}_{4.26}\text{As}_6$ | $\text{Ca}_6\text{Fe}_{7.88}\text{Pd}_{6.12}\text{As}_{10}$ | $\text{Ca}_6\text{Fe}_{7.62}\text{Pt}_{6.38}\text{As}_{10}$ |
| space group            | $Pnma$   | $Pnma$   | $P2_1/m$  | $P2_1/m$  |
| $Z$                    | 4  | 4  | 2   | 2   |
| $a$ ( $\text{\AA}$ )   | 26.435(3)  | 19.856(3)  | 15.564(3)   | 15.499(1)   |
| $b$ ( $\text{\AA}$ )   | 3.9177(10)   | 3.9461(5)  | 3.9679(6)   | 3.9807(2)   |
| $c$ ( $\text{\AA}$ )   | 11.345(2)  | 15.343(2)  | 17.880(3)   | 17.814(1)   |
| $\beta$ (deg)          | 90   | 90   | 108.748(5)  | 109.169(1)  |
| Vol ( $\text{\AA}^3$ ) | 1174.9(4)  | 1202.2(3)  | 1045.7(3)   | 1038.1(1)   |
| $R_1(\text{obs/all})$  | 0.051/0.137  | 0.023/0.066  | 0.064/0.125   | 0.036/0.058   |
| $wR_2(\text{obs/all})$ | 0.103/0.113  | 0.044/0.049  | 0.142/0.153   | 0.076/0.081   |

### 7.3 Results and Discussion

During the course of exploration in the field of iron arsenides, five so far unknown crystal structures were identified by single crystal X-ray structure determination (Table 1). The compounds obey the general composition of  $\text{Ca}_{n(n+1)/2}(\text{Fe}_{1-x}\text{M}_x)_{(2+3n)}\text{M}'_{n(n-1)/2}\text{As}_{(n+1)(n+2)/2}$  ( $M = \text{Nb}, \text{Pd}, \text{Pt}$ ;  $M' = \square, \text{Pd}, \text{Pt}$ ) with  $n = 1 - 3$ . They crystallize in monoclinic or orthorhombic crystal systems and feature three-dimensional frameworks of interconnected layers forming parallel channels. Figure 2 depicts the triangular shape of the channels for  $n = 1 - 3$ . With  $n > 1$ , additional sites occur within the channels, which can be occupied by  $M'$ .

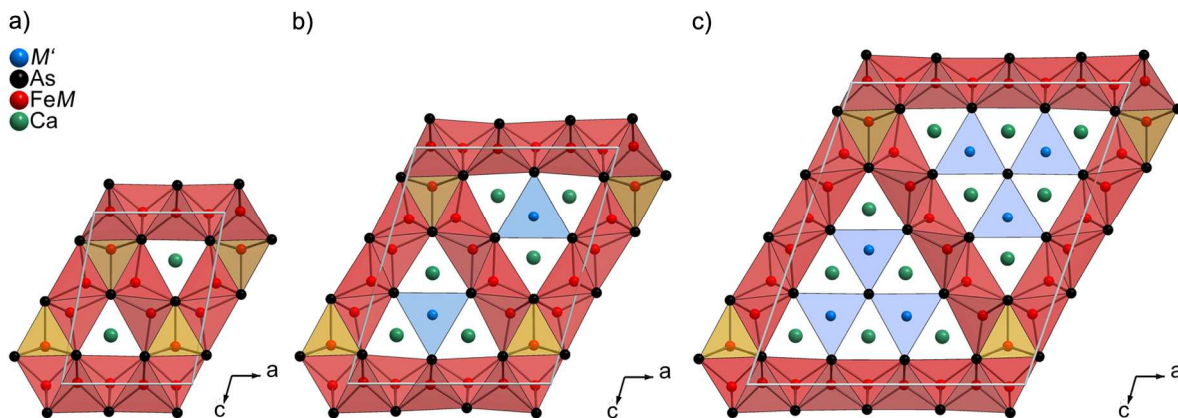


**Figure 2:** Crystal structures of the monoclinic compounds  $\text{Ca}_{n(n+1)/2}(\text{Fe}_{1-x}\text{M}_x)_{(2+3n)}\text{M}'_{n(n-1)/2}\text{As}_{(n+1)(n+2)/2}$  ( $M = \text{Pd}, \text{Pt}$ ;  $M' = \square, \text{Pd}, \text{Pt}$ ) with  $n = 1 - 3$  showing the channel shapes for varying  $n$ .

The new structures crystallize in the space groups  $P2_1/m$  or  $Pnma$ , respectively, where they all share a short  $b$  axis of about 3.9 Å with atomic sites exclusively on mirror planes at  $y = 1/4$  and  $3/4$ . A three-dimensional framework is formed by covalently bonded and interconnected iron arsenide layers, assembling equilateral triangular channels. Illustrations of the basic building units as well as the designation of labels of distances and angles for a later discussion are depicted in Figure 3. Similar to a scaffold, the framework can be divided into coplanar two-dimensional frames of  ${}^\infty_2[\text{Fe}_{2(n+1)}(\text{As}_{4/4})_{2(n-1)}(\text{As}_{4/7})_4]$ , diagonal braces  ${}^\infty_1[\text{Fe}_{2n}(\text{As}_{4/4})_{2(n-1)}(\text{As}_{3/7})_2(\text{As}_{1/7})_2]$ , and joints  ${}^\infty_1[\text{Fe}(\text{As}_{2/7})_2\text{As}_{1/7}]$ , generally keeping in mind their infinite arrangement along the short  $b$  axis. This metaphoric description of the building blocks will be conveniently used for further structure discussion. The channels within the structures are populated with calcium and, depending on the compound composition, as well with arsenic and palladium or platinum in trigonal-planar coordination.

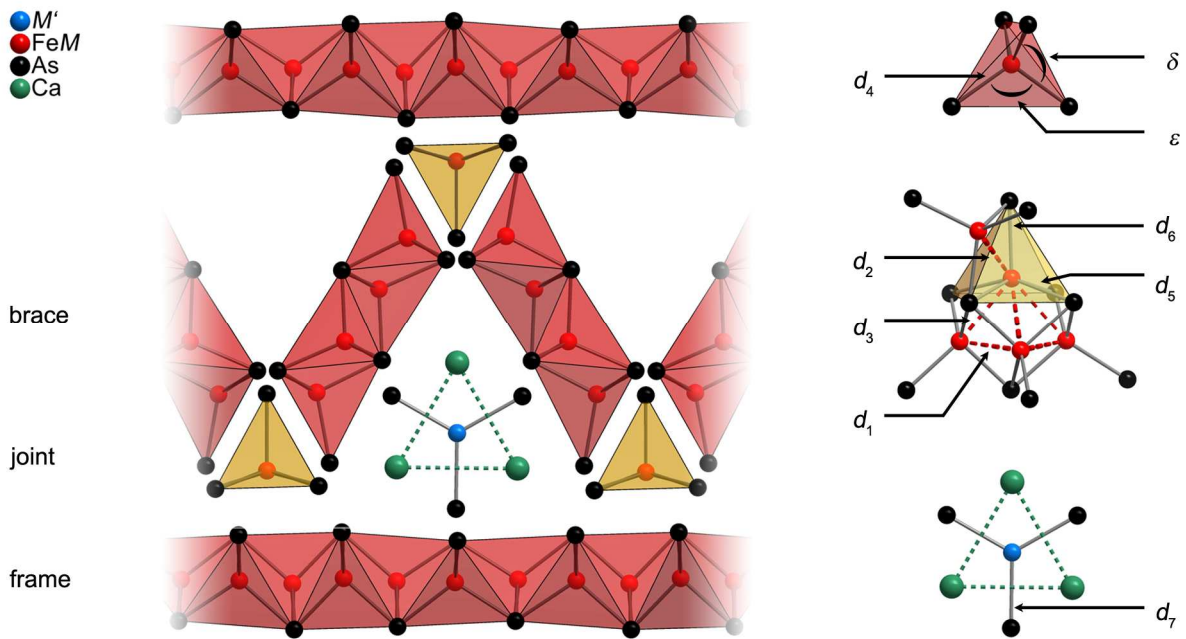


**Figure 3:** Basic building blocks of the compounds  $\text{Ca}_{n(n+1)/2}(\text{Fe}_{1-x}\text{M}_x)_{(2+3n)}\text{M}'_{n(n-1)/2}\text{As}_{(n+1)(n+2)/2}$  (left) and coordination polyhedra and labels for distances and angles (right).

The frames are formed by edge-sharing  $\text{FeAs}_{4/4}$  tetrahedral layers corresponding to the *anti*-PbO type. The atomic distances ( $d_4$ ) and angles ( $\delta$  and  $\epsilon$ ) are comparable to the values found in the structures of the layered iron arsenides, including in-plane Fe–Fe metal bonding ( $d_1$ ).<sup>[6]</sup> Corresponding features were found for the braces with the mere difference of their restricted extent in the second dimension. A distinctly different situation was found for the joints. There, iron is surrounded by five arsenic atoms in pyramidal coordination. The base plane is formed by a rectangular arrangement of arsenic. Within these pyramids, the Fe–As bond

lengths ( $d_5$  and  $d_6$ ) are significantly enlarged compared to the tetrahedral layers ( $d_4$ ). The same situation was found regarding Fe–Fe distances ( $d_2$  and  $d_3$ ). Thus, the interaction of the braces to the frames is decreased, leading to a certain degree of two-dimensionality conserved in this structures, which can be also seen from the presence of continuous frames, being reminiscent of the layered iron arsenide structures. Nevertheless, the rectangular base plane of the joint pyramids leads to a local distortion within the frames. Therefore, each structure features one very small  $\varepsilon$  angle caused by a frame iron capping the short edge of the pyramid base. Table 2 gives a comparison summary of selected distances and angles for the compounds investigated.

**Table 2:** Selected interatomic distances (Å) and bond angles (deg).

| structure                | $\alpha$ -CaFe <sub>5</sub> As <sub>3</sub> | $\alpha$ -Ca <sub>3</sub> Fe <sub>8</sub> □As <sub>6</sub>                                  | $\alpha$ -Ca <sub>3</sub> Fe <sub>8</sub> PtAs <sub>6</sub>           | $\beta$ -Ca <sub>3</sub> Fe <sub>8</sub> PdAs <sub>6</sub>            |
|--------------------------|---|---|---|---|
| composition              | CaFe <sub>5</sub> As <sub>3</sub>           | Ca <sub>2.56</sub> Na <sub>0.44</sub> Fe <sub>7.49</sub> Nb <sub>0.51</sub> As <sub>6</sub> | Ca <sub>3</sub> Fe <sub>7.71</sub> Pt <sub>1.29</sub> As <sub>6</sub> | Ca <sub>3</sub> Fe <sub>7.04</sub> Pd <sub>1.96</sub> As <sub>6</sub> |
| $d_1$ (Fe–Fe)            | 2.5973(9)-<br>2.7634(13)                    | 2.6440(4)-<br>2.8029(4)   | 2.6023(15)-<br>2.8731(11)   | 2.6069(5)-<br>2.8500(23)  |
| $d_2$ (Fe–Fe)            | 2.9824(9)-<br>3.0241(10)                    | 2.9397(3)-<br>2.9582(4)   | 2.9425(12)-<br>2.9762(17)   | 2.9481(19)-<br>2.9902(19)   |
| $d_3$ (Fe–Fe)            | 2.6982(12)-<br>2.7697(14)                   | 2.7800(4)-<br>2.8916(3)   | 2.7275(22)-<br>2.9591(14)   | 2.7159(21)-<br>2.9367(21)   |
| $d_4$ (Fe–As)            | 2.3830(10)-<br>2.4712(11)                   | 2.3983(4)-<br>2.4623(3)   | 2.3861(9)-<br>2.4767(10)  | 2.3855(19)-<br>2.4998(16)   |
| $d_5$ (Fe–As)            | 2.6158(9)-<br>2.6235(9)                     | 2.6753(3)-<br>2.6803(3)   | 2.6565(12)-<br>2.6718(14)   | 2.6577(6)-<br>2.6836(7)   |
| $d_6$ (Fe–As)            | 2.5062(9)                                   | 2.6202(4)   | 2.5703(16)  | 2.5772(23)  |
| $\varepsilon$ (As–Fe–As) | 92.468(30)-<br>106.950(34)                  | 96.431(15)-<br>108.352(13)  | 92.219(62)-<br>111.216(55)  | 93.918(19)-<br>111.154(94)  |
| $\delta$ (As–Fe–As)      | 109.424(33)-<br>116.309(34)                 | 109.153(4)-<br>115.268(4)   | 106.464(3)-<br>115.670(3)   | 107.552(5)-<br>114.892(4)   |
| $d_7$ (M–As)             | -   | -   | 2.4785(12)-<br>2.4929(10)   | 2.4459(22)-<br>2.4592(19)   |

| structure     | $\beta$ -Ca <sub>3</sub> Fe <sub>8</sub> PtAs <sub>6</sub>            | $\gamma$ -Ca <sub>3</sub> Fe <sub>8</sub> PdAs <sub>6</sub>           | $\alpha$ -Ca <sub>6</sub> Fe <sub>11</sub> Pd <sub>3</sub> As <sub>10</sub> | $\alpha$ -Ca <sub>6</sub> Fe <sub>11</sub> Pt <sub>3</sub> As <sub>10</sub> |
|---------------|---|---|---|---|
| composition   | Ca <sub>3</sub> Fe <sub>6.72</sub> Pt <sub>2.28</sub> As <sub>6</sub> | Ca <sub>3</sub> Fe <sub>4.74</sub> Pd <sub>4.26</sub> As <sub>6</sub> | Ca <sub>6</sub> Fe <sub>7.88</sub> Pd <sub>6.12</sub> As <sub>10</sub>      | Ca <sub>6</sub> Fe <sub>7.62</sub> Pt <sub>6.38</sub> As <sub>10</sub>      |
| $d_1$ (Fe–Fe) | 2.6232(20)-<br>2.8859(13)   | 2.6827(14)-<br>2.8766(14)   | 2.7041(3)-<br>2.8830(3)   | 2.6409(14)-<br>2.8881(5)  |
| $d_2$ (Fe–Fe) | 2.9651(18)-<br>2.9979(20)   | 2.9881(12)-<br>3.0224(13)   | 3.0232(3)-<br>3.0299(3)   | 2.9714(10)-<br>3.0033(14)   |
| $d_3$ (Fe–Fe) | 2.6958(29)-<br>2.9675(21)   | 2.7802(19)-<br>2.9594(14)   | 2.7879(4)-<br>2.7975(4)   | 2.7214(17)-<br>3.0074(14)   |
| $d_4$ (Fe–As) | 2.3732(21)-<br>2.5513(12)   | 2.3485(18)-<br>2.5626(11)   | 2.3618(3)-<br>2.5828(3)   | 2.3952(12)-<br>2.5775(9)  |
| $d_5$ (Fe–As) | 2.6748(18)-<br>2.7123(18)   | 2.7610(13)-<br>2.7427(12)   | 2.7520(3)-<br>2.7647(3)   | 2.7135(12)-<br>2.7443(15)   |
| $d_6$ (Fe–As) | 2.5579(27)  | 2.5700(18)  | 2.5905(4)   | 2.5531(17)  |

|                                |                            |                           |                            |                            |
|--------------------------------|----------------------------|---------------------------|----------------------------|----------------------------|
| $\varepsilon(\text{As-Fe-As})$ | 93.631(85)-<br>111.786(64) | 99.098(6)-<br>110.940(53) | 98.506(10)-<br>112.772(10) | 94.900(64)-<br>112.246(49) |
| $\delta(\text{As-Fe-As})$      | 105.123(3)-<br>114.849(8)  | 107.791(4)-<br>113.733(3) | 107.580(9)-<br>113.265(10) | 107.567(2)-<br>113.820(2)  |
| $d_7(M\text{-As})$             | 2.4496(15)-<br>2.4594(15)  | 2.4481(13)-<br>2.4614(16) | 2.4424(3)-<br>2.4683(4)    | 2.4305(13)-<br>2.4478(9)   |

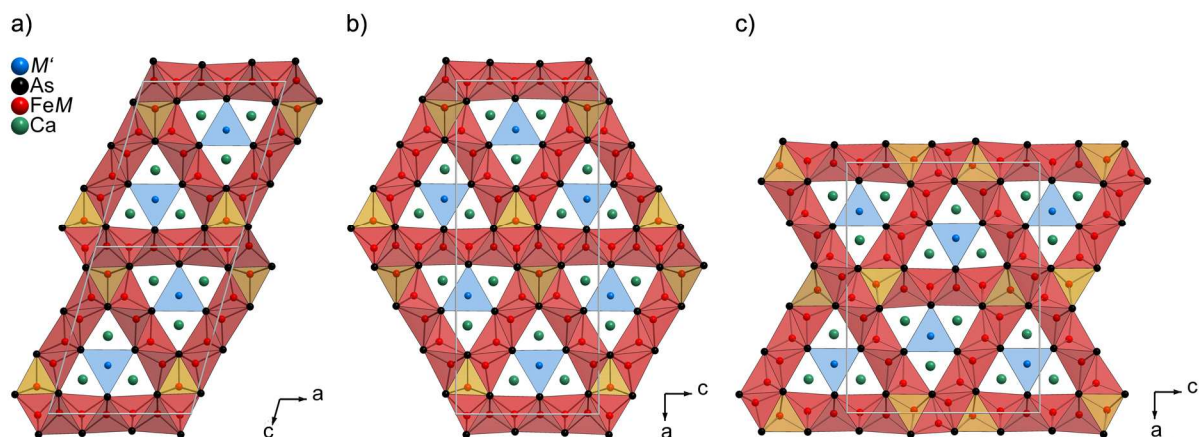


**Figure 4:** Different polymorphs of  $\text{Ca}_{n(n+1)/2}(\text{Fe}_{1-x}\text{M}_x)_{(2+3n)}\text{M}'_{n(n-1)/2}\text{As}_{(n+1)(n+2)/2}$  with  $n = 2$ ; (a)  $\alpha\text{-Ca}_3\text{Fe}_8\text{M}'\text{As}_6$ ; (b)  $\beta\text{-Ca}_3\text{Fe}_8\text{M}'\text{As}_6$ ; (c)  $\gamma\text{-Ca}_3\text{Fe}_8\text{M}'\text{As}_6$ .

The compounds  $\text{Ca}_{n(n+1)/2}(\text{Fe}_{1-x}\text{M}_x)_{(2+3n)}\text{M}'_{n(n-1)/2}\text{As}_{(n+1)(n+2)/2}$  comprise channels of varying size defined by the iron arsenide framework. Thus, depending on its size, each channel is populated with  $n(n + 1)/2$  calcium atoms, each trigonal-prismatically coordinated by arsenic. These  $\text{CaAs}_6$  prisms share faces, giving rise to strands within the channels. Additionally, compounds with  $n \geq 2$  feature the possibility to host further metal atoms  $M'$  in each center of three edge connected strands, while this particular site is trigonal-planar coordinated by arsenic. Compounds with a vacancy, palladium, or platinum at this site were found for  $n = 2$ , and palladium or platinum for a structure with  $n = 3$  could be identified so far. Similar planar coordination of palladium and platinum by arsenic was found in  $\text{CaPtAs}$  and in other compounds.<sup>[16,17]</sup> For compounds exceeding  $n = 2$ , the channel size within the iron arsenide framework cannot coordinate all calcium atoms anymore. Therefore, additional arsenic is incorporated for  $n > 2$ , saturating the coordination of calcium. Generally, the iron arsenide frames and braces allow for partial palladium and platinum substitution of the iron sites, whereas hardly any mixing was traceable at the joints. However, adding niobium and sodium to the reaction gives rise to significant Fe/Nb mixing exclusively at the joints and Na/Ca mixing within the channels. Similar results were reported for chromium doped  $\text{CaFe}_4\text{As}_3$ .<sup>[10]</sup>

The availability of fundamental structural building blocks as frames, braces, and joints allows for a multitude of different structures, facilitating both different arrangements

of the channels and different channel sizes with a general composition of  $\text{Ca}_{n(n+1)/2}(\text{Fe}_{1-x}\text{M}_x)_{(2+3n)}\text{M}'_{n(n-1)/2}\text{As}_{(n+1)(n+2)/2}$  and  $n = 1, 2, 3, \dots$ . So far we could identify homologous structures for  $n = 1 - 3$  as well as three different polymorphs for  $n = 2$ . Figure 2 illustrates the structures with constant channel arrangement and  $n = 1 - 3$ , while Figure 4 shows the different polymorphs found with constant  $n = 2$ . The  $\gamma$ -polymorph takes a special position within the presented structure discussion. The frames are intermitted every second channel, therewith losing their infinite extent in one direction. Considering the case  $n = 0$ , the general formula of this compound yields  $\text{Fe}_2\text{As}$ . The resulting structure for this type should lack any channels. Indeed, the structure of  $\text{Fe}_2\text{As}$  ( $\text{Cu}_2\text{Sb}$  type) reveals layers of edge-connected  $\text{FeAs}_4$  tetrahedra as well as edge-connected  $\text{FeAs}_5$  pyramids. Thus, even this long-known binary can be reduced to the basic building units that we described, however, in this special case, braces and channels are absent. Going the other way to the infinite limit  $n = \infty$ , a hypothetical structure would consist of a mere one “channel” with no iron arsenide frames, braces, and joints presented anymore.  $\text{CaPtAs}$  might be considered in this context,<sup>[18]</sup> locally featuring trigonal-planar coordinated platinum sites as well as edge-connected parallel strands of  $\text{CaAs}_6$ . Another more distorted representative would be  $\text{CaPdAs}$ .<sup>[19]</sup>

The view of fundamental building blocks described so far even allows for an easy understanding of the close relationship of our new structures to  $\text{CaFe}_4\text{As}_3$  reported in 2009.<sup>[9]</sup> In this context, the structure of  $\text{CaFe}_4\text{As}_3$  can be interpreted as a defect polymorph of the compound with  $n = 1$  with an ordered vacancy of one iron site. A closer view actually reveals  $\text{CaFe}_4\text{As}_3$  as the defect  $\gamma$ -polytype with  $n = 1$ . With the frames being discontinuous, the  $\gamma$ -type structures can be understood as two connected sawtooth layers, with each formed by one frame fragment, one brace, and two joints. Figure 5 compares both structures with the defect polyhedra of  $\text{CaFe}_4\text{As}_3$  highlighted and contains a schematic illustration of the sawtooth-like motif of the  $\gamma$ -type.

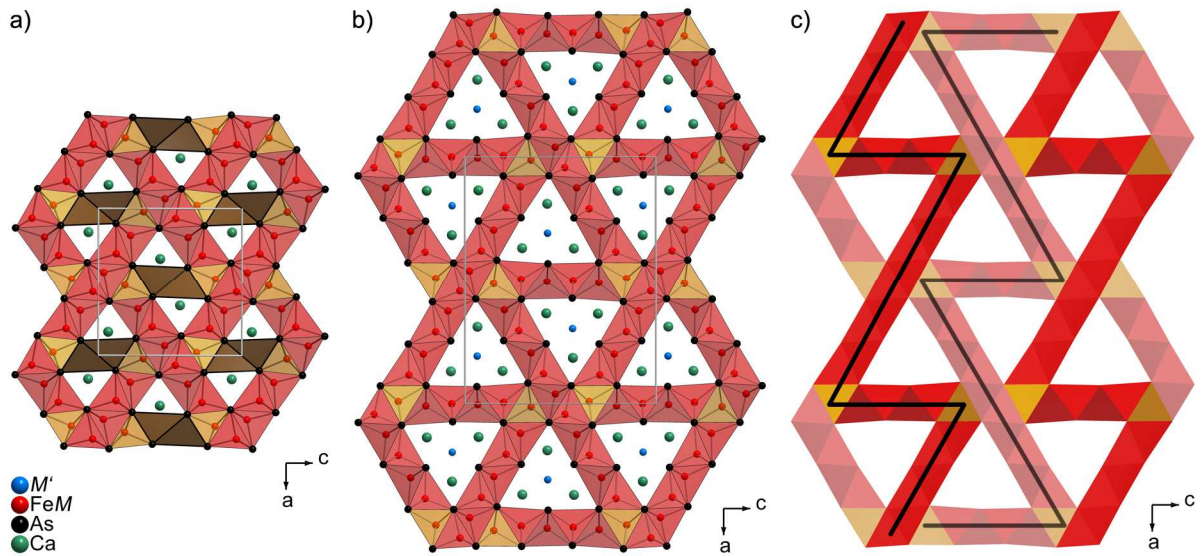


**Figure 5:** Comparing the structures of  $\text{CaFe}_4\text{As}_3$  (left) in terms of a defect variant to  $\gamma\text{-Ca}_3\text{Fe}_8M'\text{As}_6$  (middle). Defect sites are highlighted in brown. Sawtooth motif in the  $\gamma$ -type structures (right).

Although the existence of frameworks built by tetrahedra frames, braces, and pyramidal joints is quite new in the iron arsenide family, it is not exclusively restricted to this class of compounds. Most recently, *Khatun et al.* reported the structures of  $\text{Rb}_4M_7Pn_7$  and  $\text{Rb}_7M_{12}\text{Sb}_{12}$  with  $M = \text{Mn, Zn, and Cd}$  featuring coplanar *zigzag* layers of edge-connected  $MPn_4$  tetrahedra including  $MPn_5$  pyramids at every kink.<sup>[20]</sup> In terms of the building block concept that we applied on our structures, these structures may be rationalized as frameworks lacking frames and thus forming *zigzag* layers of braces and joints.

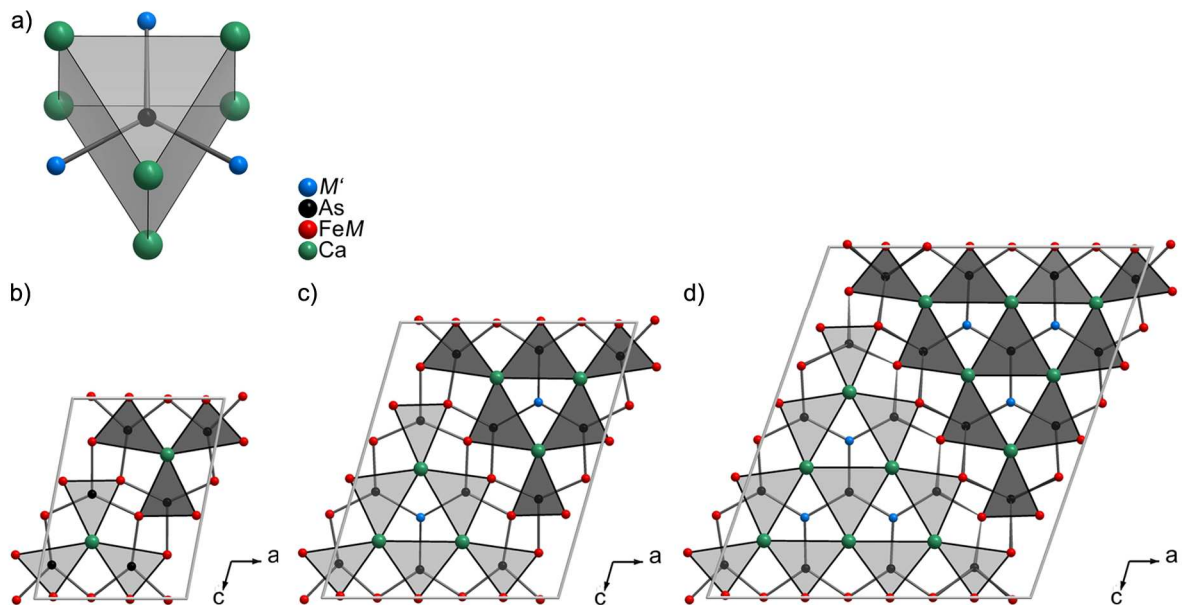


**Figure 6:** Crystal structures of  $\text{Ca}_{n(n+1)/2}(\text{Fe}_{1-x}M_x)_{(2+3n)}M'_{n(n-1)/2}\text{As}_{(n+1)(n+2)/2}$  with  $n = 1, 2, 3$ , emphasizing the tri-capped trigonal-prismatic  $\text{AsM}_9$  coordination.

A different approach of framework transition metal pnictides and related silicides was given earlier by *Jeitschko* and coworkers<sup>[21,22]</sup> and other authors,<sup>[23,24]</sup> reporting, for instance, rare earth cobalt phosphides featuring structure types very similar to those of our iron arsenides  $\text{Ca}_{n(n+1)/2}(\text{Fe}_{1-x}\text{M}_x)_{(2+3n)}\text{M}'_{n(n-1)/2}\text{As}_{(n+1)(n+2)/2}$ . They describe these structures in terms of a frequently reappearing relation of metal to pnictide in nature of 2 : 1, including also metal-rich binaries like  $\text{Co}_2\text{P}$ . The common building unit is a tricapped trigonal-prismatic coordination of the pnictide by metal atoms, whereas the different arrangements of these  $PnM_9$  units yield the large plethora of crystal structures known in this class. The structures of the monoclinic compounds  $\text{Ca}_{n(n+1)/2}(\text{Fe}_{1-x}\text{M}_x)_{(2+3n)}\text{M}'_{n(n-1)/2}\text{As}_{(n+1)(n+2)/2}$  with  $n = 1 - 3$  are exemplarily illustrated in Figure 6, emphasizing the tricapped prismatic coordination of the arsenic. In the structures presented in this paper, each arsenic atom is in the center of an  $\text{AsM}_9$  unit, with  $M$  being all metal atoms present. Within the channels, these units are edge-connected but separated from neighboring channels by  $\text{FeAs}$  tetrahedra layers. Very similar structures were reported for the compounds  $\text{HoCo}_3\text{P}_2$ ,  $\text{ScCo}_5\text{P}_3$ , and  $\text{Sc}_5\text{Co}_{19}\text{P}_{12}$ ,<sup>[21]</sup> but with different arrangements of the triangular channels and partial incorporation of different channel sizes as well as other building blocks in the same structure.

The iron arsenide framework structures reported in this paper are supposed to feature interesting magnetic and electronic properties. For  $\text{CaFe}_4\text{As}_3$  iron(II) was evidenced for tetrahedral coordination and iron(I) in the pyramidal environment.<sup>[9]</sup> We have conducted preliminary density functional theory calculations and found exclusively magnetic ground states for all compounds. Calculated magnetic moments range from  $\sim 0.3$  to  $2.0 \mu_B$  at the iron atoms of the frames and braces and up to  $\sim 2.5 \mu_B$  at the joints. However, detailed magnetic measurements and neutron diffraction experiments are necessary to prove this. For the time being, it seems reasonable to assume a similar situation of two different iron species for our compounds. Because the compounds  $\text{Ca}_{n(n+1)/2}(\text{Fe}_{1-x}\text{M}_x)_{(2+3n)}\text{M}'_{n(n-1)/2}\text{As}_{(n+1)(n+2)/2}$  allow for different distances and arrangements of the iron sites, they present an excellent model system to study the geometry-dependent interplay of a variety of different magnetic centers. Still, no superconductivity was observed yet in any of the compounds described, despite the presence of two-dimensional iron arsenide tetrahedral layers. Nevertheless, these new phases clarify that layered iron arsenide structures are not just restricted to two-dimensional stacking structures but facilitate the formation of complex three-dimensional frameworks.

## 7.4 Conclusion

In conclusion, we reported the eight new calcium iron arsenide compounds  $\text{Ca}_{n(n+1)/2}(\text{Fe}_{1-x}\text{M}_x)_{(2+3n)}\text{M}'_{n(n-1)/2}\text{As}_{(n+1)(n+2)/2}$  with  $n = 1, 2, 3$ ,  $M = \text{Nb, Pd, Pt}$ , and  $M' = \square, \text{Pd, Pt}$ . The structures reveal three-dimensional frameworks of cross-linked iron arsenide layers with trigonal channels along a short  $b$  axis of 3.9 Å. Thereby the size and arrangement of the channels give rise to the different structures. This relationship was also rationalized by the identification of common structural building blocks and their resemblance to  $\text{CaFe}_4\text{As}_3$ . The compounds feature coordination of arsenic typical for compounds with a metal-to-pnictide ratio of 2 : 1. The identification of these new structures elucidates the structural flexibility of iron arsenide layers toward rearrangements. Unlike  $\text{CaFe}_4\text{As}_3$ ,  $\text{Ca}_{n(n+1)/2}(\text{Fe}_{1-x}\text{M}_x)_{(2+3n)}\text{M}'_{n(n-1)/2}\text{As}_{(n+1)(n+2)/2}$  still feature continuous coplanar  $\text{FeAs}_{4/4}$  layers and therewith a certain degree of two-dimensionality. Although no superconductivity has been observed in these compounds so far, interesting magnetic and electronic properties are expected.

## 7.5 References

- [1] Y. Kamihara, T. Watanabe, M. Hirano, H. Hosono, *J. Am. Chem. Soc.* **2008**, *130*, 3296.
- [2] H. Takahashi, K. Igawa, K. Arii, Y. Kamihara, M. Hirano, H. Hosono, *Nature* **2008**, *453*, 376.
- [3] Z.-A. Ren, W. Lu, J. Yang, W. Yi, X.-L. Shen, Z.-C. Li, G.-C. Che, X.-L. Dong, L.-L. Sun, F. Zhou, Z.-X. Zhao, *Chin. Phys. Lett.* **2008**, *25*, 2215.
- [4] D. Johrendt, *J. Mater. Chem.* **2011**, *21*, 13726.
- [5] D. Johrendt, R. Pöttgen, *Angew. Chem. Int. Ed.* **2008**, *47*, 4782.
- [6] D. C. Johnston, *Adv. Phys.* **2010**, *59*, 803.
- [7] P. Dai, J. Hu, E. Dagotto, *Nat. Phys.* **2012**, *8*, 709.
- [8] G. R. Stewart, *Rev. Mod. Phys.* **2011**, *83*, 1589.

- [9] I. Todorov, D. Y. Chung, C. D. Malliakas, Q. A. Li, T. Bakas, A. Douvalis, G. Trimarchi, K. Gray, J. F. Mitchell, A. J. Freeman, M. G. Kanatzidis, *J. Am. Chem. Soc.* **2009**, *131*, 5405.
- [10] I. Todorov, D. Y. Chung, H. Claus, K. E. Gray, Q. A. Li, J. Schleuter, T. Bakas, A. P. Douvalis, M. Gutmann, M. G. Kanatzidis, *Chem. Mater.* **2010**, *22*, 4996.
- [11] Y. Nambu, L. L. Zhao, E. Morosan, K. Kim, G. Kotliar, P. Zajdel, M. A. Green, W. Ratcliff, J. A. Rodriguez-Rivera, C. Broholm, *Phys. Rev. Lett.* **2011**, *106*, 037201.
- [12] D. Walker, M. A. Carpenter, C. M. Hitch, *Am. Mineral.* **1990**, *75*, 1020.
- [13] H. Huppertz, *Z. Kristallogr.* **2004**, *219*, 330.
- [14] V. Petricek, M. Dusek, L. Palatinus, JANA2006, Institute of Physics, Praha, **2006**.
- [15] A. Coelho, TOPAS-Academic, Version 4.1, Coelho Software, Brisbane, **2007**.
- [16] C. Hieke, J. Lippmann, T. Stürzer, G. Friederichs, F. Nitsche, F. Winter, R. Pöttgen, D. Johrendt, *Philos. Mag.* **2013**, *93*, 3680.
- [17] C. Löhnert, T. Stürzer, M. Tegel, R. Frankovsky, G. Friederichs, D. Johrendt, *Angew. Chem. Int. Ed.* **2011**, *50*, 9195.
- [18] G. Wenski, A. Mewis, *Z. Anorg. Allg. Chem.* **1986**, *543*, 49.
- [19] D. Johrendt, A. Mewis, *Z. Anorg. Allg. Chem.* **1992**, *618*, 30.
- [20] M. Khatun, S. S. Stoyko, A. Mar, *Inorg. Chem.* **2013**, *52*, 3148.
- [21] W. Jeitschko, E. J. Reinbold, *Z. Naturforsch.* **1985**, *40b*, 900.
- [22] Y. M. Prots, W. Jeitschko, *Inorg. Chem.* **1998**, *37*, 5431.
- [23] C. Le Sénéchal, V. Babizhetskyy, S. Députier, J. Y. Pivan, R. Guérin, *J. Solid State Chem.* **1999**, *144*, 277.
- [24] Y. Kuz'ma, S. Chykhrij, *Phosphides*, In *Handbook on the Physics and Chemistry of Rare Earths*; K. A. Gschneidner, L. Eyring, Eds.; Elsevier Science, Amsterdam, **1996**, *23*, 285.

## 8 Summary

### Superconductivity and Crystal Structure of the Palladium Iron Arsenides $(\text{CaFe}_{1-x}\text{Pd}_x\text{As})_{10}\text{Pd}_3\text{As}_8$

The new compound  $(\text{CaFe}_{1-x}\text{Pd}_x\text{As})_{10}\text{Pd}_3\text{As}_8$  (Pd1038) was obtained via solid state synthesis and identified to be isotypic to the recently reported platinum analogue. Single crystal structure determination turned out challenging due to diffuse scattering and partial merohedral twinning. As a member of the iron arsenide family Pd1038 is build up from an alternate stacking of edge-sharing  $\text{FeAs}_{4/4}$  tetrahedra and planar  $\text{Pd}_3\text{As}_8$  layers, each separated by calcium. The second negatively charged layer forms corner-sharing  $\text{PdAs}_{4/2}$  squares stabilized by  $\text{As}_2$  dimers. Next to a systematic palladium vacancy additionally minor deficiencies of palladium are evident. Moreover significant iron/ palladium mixing on the tetrahedral coordinated positions is omnipresent. Despite every layer preserves fourfold rotational symmetry the skew stacking yields a triclinic structure. Lanthanum doping on the calcium positions improves the sample quality by increasing the lattice energy. Electrical resistivity and magnetic susceptibility measurements revealed superconductivity in electron doped  $(\text{Ca}_{1-y}\text{La}_y\text{Fe}_{1-x}\text{Pd}_x\text{As})_{10}\text{Pd}_3\text{As}_8$  with zero resistivity below 10 K. Since the shielding fraction was not fully developed at 3.5 K an inhomogeneous distribution of the three types of substituted positions was assumed. Especially for lower palladium doping on the iron sites higher critical temperatures and superconducting volume fractions were predicted. In  $^{57}\text{Fe}$ -Mössbauer spectra the superposition of the five crystallographic iron positions is visible. With an absent hyperfine field contribution no magnetic ordering is present in  $(\text{Ca}_{1-y}\text{La}_y\text{Fe}_{1-x}\text{Pd}_x\text{As})_{10}\text{Pd}_3\text{As}_8$ . The absolute values of the isomer shift compare well to other iron arsenides. Electronic structure calculations of  $(\text{CaFeAs})_{10}\text{Pd}_3\text{As}_8$  revealed iron states dominant at the *Fermi* level with only a small contribution of the palladium pDOS. Similar to other iron arsenide superconductors cylinder-like sheets along  $c^*$  show the widely two-dimensionality of the electronic structure including weak perturbations. Therefore in terms of electronic structure partial *Fermi* surface nesting qualifies Pd1038 as new iron arsenide superconductor.

### $(\text{CaFe}_{1-x}\text{Pd}_x\text{As})_{10}\text{Pd}_3\text{As}_8$ with Parent-like Properties

Stoichiometric iron arsenides feature a parent state with structural phase transition via a distortion from tetragonal to orthorhombic symmetry. The majority of these parent compounds

are not superconducting, but pass a magnetic ordering in the vicinity of the structural transition. Such a parent state was also assumed for  $(\text{CaFeAs})_{10}\text{Pd}_3\text{As}_8$ , however, experimental evidence is missing due to high intrinsic palladium substitution on the iron sites. Finally successful synthesis optimization yielded high quality  $(\text{CaFe}_{1-x}\text{Pd}_x\text{As})_{10}\text{Pd}_z\text{As}_8$  powder samples. The palladium content was determined by refined of X-ray powder data with  $x = 0.04(1)$  and  $z = 2.9(1)$  as well as from EDX analyses yielding a total iron/ palladium amount of  $\text{Fe}_{9.8(3)}\text{Pd}_{2.8(2)}$ . Due to this low substitution level investigations in the scope of a hypothetical parent state in Pd1038 were possible. The lattice parameters of the square basal plane distort below 90 K to  $a > b$  by a small but significant splitting. A more distinct effect was assumed to be prevented by minor palladium substitution. In triclinic  $(\text{CaFe}_{1-x}\text{Pd}_x\text{As})_{10}\text{Pd}_3\text{As}_8$  the iron arsenide layer showing fourfold rotation symmetry undergoes a structural distortion according to  $p4mm \rightarrow p2mm$  in terms of layer symmetry. Indications of an associated magnetic phase transition were evident from magnetic and electric measurements. Superconductivity discernable in the electrical measurement with zero resistivity at 3.5 K was not confirmed by susceptibility analyses. Therefore this effect was not attributed as a property of Pd1038, but is rather assigned to the presence of impurity phases or varying substitution dispersion. The results substantiated the previously discussed parent-like state in  $(\text{CaFe}_{1-x}\text{Pd}_x\text{As})_{10}\text{Pd}_3\text{As}_8$  analogue to Pt1038 and other iron arsenide compounds.

### Site Preference of Rare Earth Doping in Palladium Iron Arsenide Superconductors

The solid solutions  $(\text{Ca}_{1-y}\text{RE}_y\text{Fe}_{1-x}\text{Pd}_x\text{As})_{10}\text{Pd}_z\text{As}_8$  with  $\text{RE} = \text{La}, \text{Ce}, \text{Pr}$  and  $y = 0.025 - 0.20$  were synthesized and characterized yielding linear courses of the lattice parameters with increasing rare earth substitution according to the ionic radii. The doping level obtained from refined powder data as well as X-ray spectroscopy confirmed the nominal values excellently. Refined compositions of the three variable positions approved the high sample quality with palladium mixing on the iron sites well below 5 %. Of the five crystallographic calcium positions four feature sevenfold, one eightfold coordination by arsenic. This *anti-prismatic* eightfold coordinated site is favored by rare earth dopants resulting in a significant stabilization of 40 kJ/mol as found by electronic structure calculations. Since this doping scenario prevents palladium over-doping strongly present in  $(\text{CaFe}_{1-x}\text{Pd}_x\text{As})_{10}\text{Pd}_3\text{As}_8$ , superconductivity is induced by rare earth substitution. With iron states dominating the *Fermi* level additional charge carriers from electron doping according to  $\text{Ca}^{2+}/\text{RE}^{3+}$  are transferred to the iron arsenide layer. The onset of critical temperatures rises up to  $T_c = 20$  K in lanthanum doped

Pd1038, while main transitions stay below 10 K. Maximum values in all three series were obtained for  $y = 0.05 - 0.075$  in contrast to other electron doped iron arsenide superconductors. The optimal combination of electron doping, structural stabilization, and diminished iron/ palladium mixing in rare earth doped  $(\text{Ca}_{1-y}\text{RE}_y\text{Fe}_{1-x}\text{Pd}_x\text{As})_{10}\text{Pd}_3\text{As}_8$  enables the induction of superconductivity in 1038-type palladium iron arsenides.

**$(\text{Ca}_{1-y}\text{RE}_y\text{FeAs})_{10}\text{Pd}_3\text{As}_8$  series with  $RE = \text{La} - \text{Nd}, \text{Sm} - \text{Lu}$  and  $y = 0.05, 0.10$**

The complete lanthanide series of  $(\text{Ca}_{1-y}\text{RE}_y\text{FeAs})_{10}\text{Pd}_3\text{As}_8$  ( $RE = \text{La} - \text{Lu}$ ) was studied with the two doping ratios  $y = 0.05$  and  $0.10$ . Refined X-ray powder data and EDX analyses revealed good agreements of the substitution levels for the early lanthanides, while  $RE = \text{Gd} - \text{Lu}$  feature a reduced dopant tolerance. These values were assigned as solubility limits, which were decreased compared to the analogue platinum series. Due to the lanthanide contraction this result can be understood by the bigger unit cell volume of the palladium structures unsuitable for the integration of small rare earth ions. The lattice axes decrease for  $RE = \text{La} - \text{Sm}$  with constant substitution level and varying dopants in line with the ionic radii. Next to La, Ce, and Pr doped samples bulk superconductivity was induced for  $RE = \text{Nd}, \text{Sm}$  in both series with slightly reduced onset temperatures following the trend of the early lanthanides. Therefore maximum values were obtained by lanthanum doping. In  $(\text{Ca}_{1-y}\text{RE}_y\text{FeAs})_{10}\text{Pd}_3\text{As}_8$  with  $RE = \text{Gd} - \text{Lu}$  only an onset of superconductivity was evident classifying the compounds as non-superconducting. This effect was on the one hand ascribed to inhomogeneous Ca/RE distributions and minimum doping levels. On the other hand magnetic susceptibility measurements revealed a superposition of the weak diamagnetism with paramagnetic behavior of the magnetic rare earths. A qualitative trend of the respective paramagnetic effect with listed effective magnetic moments was discernable. The comparison of both series yielded an optimal doping level of  $y < 10\%$  atypical for iron arsenide superconductors. As an exception the presence of divalent europium showed considerable increased lattice parameters for  $(\text{Ca}_{1-y}\text{Eu}_y\text{FeAs})_{10}\text{Pd}_3\text{As}_8$  and paramagnetism. The obtained effective magnetic moments are in excellent agreement with the reported value of  $\text{Eu}^{2+}$ . Therefore the experiments on europium give a reverse reasoning of the concept of superconductivity by electron doping in Pd1038. Compared to the related platinum compounds  $(\text{Ca}_{1-y}\text{RE}_y\text{FeAs})_{10}\text{Pd}_3\text{As}_8$  is counter the expectations in the scope of the magnetic properties as well as the doping range.

**Combination of Palladium and Platinum 1038 Phases in  $(\text{CaFe}_{1-x}\text{Pd}_x\text{As})_{10}\text{Pt}_3\text{As}_8$** 

$(\text{CaFe}_{1-x}\text{Pd}_x\text{As})_{10}\text{Pd}_3\text{As}_8$  being isotypic to the 2011 discovered Pt1038 superconductors, however, revealed surprisingly no superconducting properties. Since omnipresent palladium mixing on the iron position was assumed responsible for this result,  $(\text{CaFe}_{1-x}\text{Pd}_x\text{As})_{10}\text{Pt}_3\text{As}_8$  qualified as the perfect system to investigate noble-metal substitution in the 1038 family in the scope of superconductivity. High quality samples were obtained synthesizing the series with  $x = 0.0125 - 0.25$ . EDX analyses perfectly confirmed the nominal doping levels, which were also verified by refined X-ray powder data. Moreover the compression of the unit cell along the stacking direction with increasing palladium content was obtained comprehensible by the stepwise substitution of  $d^8$  palladium ions on tetrahedrally coordinated iron positions. In magnetic susceptibility measurements superconductivity was found for  $x_{\text{EDX}} = 0.047 - 0.162$ . Samples with higher substitution levels showed only traces of superconducting properties probably due to inhomogeneous substituent distribution. Dc-susceptibility and electrical resistivity measurements confirmed the maximal critical temperature of  $T_c = 11.5$  K for  $x = 0.047$ . Compounds comprising lower palladium compounds were not superconducting, but show semiconductor-like behavior similar to the parent compound. Moreover an analogous structural phase transition was evident at 90 K with  $x = 0.035$ , while no distortion was observed for  $x = 0.047$ . These results gave rise to a phase diagram with parent state range and superconducting dome. The series  $(\text{CaFe}_{1-x}\text{Pd}_x\text{As})_{10}\text{Pt}_3\text{As}_8$  proved palladium substitution up to 16 % not to be an exclusion criterion for superconductivity in 1038 compounds, but rather as an effective doping scenario similar to cobalt or nickel substitution. Meanwhile the uniqueness of  $(\text{CaFe}_{1-x}\text{Pd}_x\text{As})_{10}\text{Pd}_3\text{As}_8$  was once more substantiated.

**Structure and Properties of  $(\text{CaFe}_{1-x}\text{Pd}_x\text{As})_{10}\text{Pd}_4\text{As}_8$** 

In the scope of this thesis the corresponding palladium compound to intensively researched  $(\text{CaFe}_{1-x}\text{Pt}_x\text{As})_{10}\text{Pt}_4\text{As}_8$  ( $T_c = 35$  K) was discovered.  $\alpha$ - $(\text{CaFe}_{1-x}\text{Pd}_x\text{As})_{10}\text{Pd}_4\text{As}_8$  (spacegroup  $P4/n$ ) was identified by single crystal structure determination to be isotypic to the homologous tetragonal platinum phase. The refinement revealed typical structural parameters, while compared to Pt1048 the lattice parameters are enlarged with respect to the bigger ionic radius of palladium. All metal positions within the  $\text{Pd}_z\text{As}_8$  layer are occupied, however, the deflected site gives rise to varying square sizes and is compatible for vacancies yielding a total composition of  $(\text{CaFe}_{0.757}\text{Pd}_{0.243}\text{As})_{10}\text{Pd}_{2.83}\text{As}_8$ . Despite partial merohedral twinning and distinct

stacking disorder challenging structure determination succeeded, but yielded moderate residual values. In addition to that refinement of high quality powder data gave every indication for the existence of  $\beta$ -(CaFe<sub>1-x</sub>Pd<sub>x</sub>As)<sub>10</sub>Pd<sub>4</sub>As<sub>8</sub> (spacegroup  $P\bar{1}$ ). All structural parameters, atomic positions, and changeable palladium occupancies in both layers were independently refined and compared to the isotypic platinum compound. The refined composition was confirmed by EDX analyses yielding minor palladium substitution on the iron site and deficiencies within the palladium arsenide layer. Therefore the present stacking disorder in Pd1048 enables polymorphism with the two limiting cases of tetragonal  $\alpha$ -type and triclinic  $\beta$ -type identified. Electronic structure calculations of  $\alpha$ -(CaFeAs)<sub>10</sub>Pd<sub>4</sub>As<sub>8</sub> revealed iron states dominant at the *Fermi* level and a pseudo-gap for palladium states. Although the density of states appears analogue to the corresponding Pt1048 compound, iron pDOS is distinctly reduced at  $E_F$  and the gap within the palladium pDOS hardly significant. The *Fermi* surface shows the typical topology known from other iron arsenide superconductors, but also comprises unusual three-dimensional features. Investigations on the electric resistivity of Pd1048 showed metallic properties. Measurements of the magnetic susceptibility revealed paramagnetism with no trace of superconductivity, which was therefore not attributed as a property to Pd1048 in contrast to the platinum homologs. With (CaFeAs)<sub>10</sub>Pd<sub>4</sub>As<sub>8</sub> two new members were added to the still growing family of 1038/ 1048 compounds featuring unexpected and remarkable properties.

### **New Structure with substituted Iron Arsenide Layers CaFe<sub>1-x</sub>Pd<sub>x</sub>As<sub>2</sub>**

CaFe<sub>1-x</sub>Pd<sub>x</sub>As<sub>2</sub> was discovered as a potential new class in the family of iron arsenide superconductors. Single crystal structure determination revealed CaFe<sub>0.56</sub>Pd<sub>0.44</sub>As<sub>1.95</sub> with a so far unknown monoclinic crystal structure of two alternately stacked arsenic-containing layers separated by calcium. One comprises metal-centered tetrahedra layers with high iron/ palladium mixing and typical structural parameters. The second features parallel arsenic *zigzag* chains with short bond lengths of 2.37 Å. The perpendicular orientation of the infinite chains to the tetrahedra slices allows for bonding between both layers. In terms of the electronic situation two limiting cases with isolated *zigzag* chains or triple-bonded arsenic were discussed. The new structure was described in relation to the known LaMnSi<sub>2</sub>, CeNiSi<sub>2</sub>, and NdRuSi<sub>2</sub> structure types and derived from the orthorhombic aristotype. Magnetic measurements revealed paramagnetism with indication of magnetic ordering at low temperature. The high substitution amount was hold responsible for the absence of superconductivity, which might

be expected for lower doping levels or different substituents. This presumption was substantiated by electronic structure calculations of several idealized compounds with  $x = 0, 0.5, 1$ . Too low iron pDOS at  $E_F$  was considered as a possible reason for the absence of superconductivity in the investigated sample. Cylinder-like sheets at the *Fermi* surface broken only by one perturbation characterize hypothetical  $\text{CaFeAs}_2$  similar to other iron arsenide compounds. Therefore initially discovered  $\text{CaFe}_{1-x}\text{Pd}_x\text{As}_2$  can be assigned to the group of iron arsenides featuring a new auspicious crystal structure.

### **Properties of $\text{Ca}_{1-x}\text{Pr}_x\text{FeAs}_2$ with $x = 0.15 - 0.25$**

Novel  $\text{Ca}_{1-x}\text{Pr}_x\text{FeAs}_2$  was discovered 2014 featuring iron arsenide tetrahedra layers alternately stacked with coplanar arsenic *zigzag* chains separated by calcium ions. However, so far undoped  $\text{CaFeAs}_2$  was not obtained, praseodymium substituted samples were characterized as superconducting with  $T_c = 20$  K. This result based on an oxygen-containing low quality powder sample with the nominal composition  $\text{Ca}_{0.9}\text{Pr}_{0.1}\text{Fe}_{1.3}\text{As}_{1.8}\text{O}_{0.2}$ . Since the assignment of superconducting properties to  $\text{Ca}_{1-x}\text{Pr}_x\text{FeAs}_2$  is equivocal high quality powder samples with  $x = 0.15 - 0.25$  were synthesized under oxygen and moisture absence. Constant values of the lattice parameters with varying doping level were in line with ionic radii and oxidation states of the mixed substituents. Praseodymium concentrations obtained from Rietveld refinements as well as EDX measurements were in very good agreement to the nominal doping amounts. The experiments revealed an increased level favored for reduced substitutions  $x = 0.15, 0.175$  accompanied with a decrease of the sample quality. With no decisive change of the structural parameters electronic effects were assumed as probable reason why the undoped parent compound is still inaccessible. Ac- and dc-susceptibility measurements revealed paramagnetic behavior instead of superconductivity. The effective magnetic moment derived from *Curie Weiss* fit was perfectly ascribed to praseodymium. Although the investigated samples cover the doping range of the reported phases the results concerning superconducting properties differ. The presence of oxygen is supposed to contribute to the emergence of superconductivity in impurity phases, while the samples synthesized in the absence of air and moisture remain paramagnetic. Therefore the presence of superconductivity in  $\text{Ca}_{1-x}\text{Pr}_x\text{FeAs}_2$  was not confirmed, but remains questionable.

**Framework Structures of interconnected Layers in Calcium Iron Arsenides**

Eight new calcium iron arsenide compounds with the common formula  $\text{Ca}_{n(n+1)/2}(\text{Fe}_{1-x}\text{M}_x)_{(2+3n)}\text{M}'_{n(n-1)/2}\text{As}_{(n+1)(n+2)/2}$  ( $n = 1 - 3$ ;  $M = \text{Nb, Pd, Pt}$ ;  $M' = \square, \text{Pd, Pt}$ ) were discovered featuring five so far unknown crystal structures. Crystallizing with monoclinic or orthorhombic symmetry all compounds share a short  $b$  axis of 3.9 Å. These structures form frameworks of interconnected iron arsenide layers sparing parallel channels. As common building blocks frames of iron arsenide tetrahedra preserving a two-dimensional character are bridged by tetrahedra braces and joints with iron in fivefold pyramidal coordination. The triangular channels are occupied by calcium, palladium or platinum as well as arsenic depending on the structure type. Varying channel sizes give rise to homologous structures with  $n = 1 - 3$ , while different framework settings reveal polymorphism for  $n = 2$ . As one limiting case the long-known binary  $\text{Fe}_2\text{As}$  ( $n = 0$ ) can be described within this concept featuring only iron arsenide tetrahedra and pyramids. Moreover  $\text{CaPtAs}$  and distorted  $\text{CaPdAs}$  were discussed in the scope of an infinite extension of the channels ( $n = \infty$ ). The systematic description comprises also reported  $\text{CaFe}_4\text{As}_3$  as defect  $\gamma$ -polytype with  $n = 1$ . With an overall metal to pnictide ratio of 2 : 1 the new compounds belong to a huge family of metal-rich pnictides featuring tricapped trigonal-prismatic coordination of each arsenic atom in the center of an  $\text{AsM}_9$  unit. However, yet no superconductivity was observed within these compounds, the special features of different iron positions presents the prospect of interesting electronic and magnetic properties. The novel structures  $\text{Ca}_{n(n+1)/2}(\text{Fe}_{1-x}\text{M}_x)_{(2+3n)}\text{M}'_{n(n-1)/2}\text{As}_{(n+1)(n+2)/2}$  illustrate the structural flexibility of iron arsenide compounds, which typically prefer layered structures.



## 9 Conclusion

The system of calcium iron palladium arsenides was studied in the scope of its structural chemistry as well as electronic, magnetic, and superconducting behavior. The impressive diversity of crystal structures, properties, and their interrelation allows for several conclusions. Initially investigated  $(\text{CaFe}_{1-x}\text{Pd}_x\text{As})_{10}\text{Pd}_3\text{As}_8$  comprises all structural and electronic requirements of a typical iron arsenide superconductor, however, the complex structural chemistry features severe stacking disorder and significant iron/ palladium mixing. Every evidence of a parent state in Pd1038 is present, while superconductivity is induced via electron doping by rare earth substitution with a detectable site preference. No superconductivity was found in  $(\text{CaFe}_{1-x}\text{Pd}_x\text{As})_{10}\text{Pd}_3\text{As}_8$ , whereas  $(\text{CaFe}_{1-x}\text{Pd}_x\text{As})_{10}\text{Pt}_3\text{As}_8$  revealed a characteristic phase diagram with wide superconducting doping range. Polymorphic  $(\text{CaFe}_{1-x}\text{Pd}_x\text{As})_{10}\text{Pd}_4\text{As}_8$  was discovered and characterized isotopic to the corresponding platinum phases. The principles of charge doping within the 1038 system are violated by the absence of superconductivity in Pd1048 possibly caused by atypical features within the electronic structure. The impact of minor differences in the *Fermi* surface topologies appears pertinent discussing the unexpected and exceptional properties of  $(\text{CaFe}_{1-x}\text{Pd}_x\text{As})_{10}\text{Pd}_z\text{As}_8$ . Therefore next to preferable undoped iron arsenide layers, the prevention of interlayer contributions at the *Fermi* level is required to characterize typical iron arsenide superconductors. Deviations of the two-dimensional *Fermi* surface topology and reduced iron states at  $E_F$  provide additional interference. In this context  $\text{CaFe}_{1-x}\text{Pd}_x\text{As}_2$  was firstly identified with novel crystal structure, which can be derived from a known aristotype. Electronic structure calculations confirm reduced iron states at the *Fermi* level due to high iron/ palladium mixing, which possibly prevents the emergence of superconductivity so far. Conversely reported superconducting properties in  $\text{Ca}_{1-x}\text{Pr}_x\text{FeAs}_2$ , being another 112-type family with closely related structural chemistry, were not confirmed in validating studies. Besides several new compounds with the common formula  $\text{Ca}_{n(n+1)/2}(\text{Fe}_{1-x}\text{M}_x)_{(2+3n)}\text{M}'_{n(n-1)/2}\text{As}_{(n+1)(n+2)/2}$  ( $n = 1 - 3$ ;  $M = \text{Nb, Pd, Pt}$ ;  $M' = \square, \text{Pd, Pt}$ ) were discovered. Build up from the same structural features the unprecedented frameworks of interconnected metal arsenide layers enriched the complexity of iron pnictide compounds. All investigated structures feature the same motif of iron arsenide tetrahedra layers embedded in various crystal structures and therewith associated unique physical properties. These investigations evince the structural repertoire of iron arsenides not limited to highly symmetric layered structures with insulating interlayers, but rather testify a sophisticated diversity based on the complexity of the structural chemistry with no end in sight.

## 10 Appendix

In the following chapter crystallographic data of compounds investigated within this thesis as well as CSD numbers of presented structures are listed.

### 10.1 Crystallographic Data of $(\text{CaFeAs})_{10}\text{Pd}_3\text{As}_8$

**Table 1:** Crystallographic data of  $(\text{CaFe}_{0.842}\text{Pd}_{0.158}\text{As})_{10}\text{Pd}_{2.80}\text{As}_8$ .

| Empirical formula  | $\text{Ca}_{10}\text{Fe}_{8.42}\text{Pd}_{4.38}\text{As}_{18}$ |            |           |           |           |                       |
|--|--|------------|-----------|-----------|-----------|-----------------------|
| Crystal system, space group, number                            | Triclinic, $P1$ , 2  |            |           |           |           |                       |
| $a, b, c$ (Å)  | 8.800(1), 8.800(1), 10.603(2)                                  |            |           |           |           |                       |
| $\alpha, \beta, \gamma$ (degree)                               | 85.271(2), 75.561(2), 90.003(6)                                |            |           |           |           |                       |
| Cell volume (Å <sup>3</sup> )                                  | 792.2(1)   |            |           |           |           |                       |
| Calculated density (g cm <sup>-3</sup> ), $Z$                  | 5.627, 1   |            |           |           |           |                       |
| Radiation type, $\lambda$ (Å)                                  | Mo-K $\alpha$ , 0.71073  |            |           |           |           |                       |
| $2\theta$ range (degree)                                       | 1.99 – 30.31   |            |           |           |           |                       |
| Reflections (total, independent, $I > 3\sigma(I)$ )            | 121430, 27887, 7090  |            |           |           |           |                       |
| $R_{\text{int}}, R_{\sigma}$                                   | 0.1369, 0.1239   |            |           |           |           |                       |
| GooF (all) / Goof ( $I \geq 3\sigma(I)$ )                      | 4.29 / 4.29  |            |           |           |           |                       |
| Refined parameters, refinement                                 | 147, $F$   |            |           |           |           |                       |
| $R1 / wR2$ ( $I \geq 3\sigma(I)$ )                             | 0.0883 / 0.986   |            |           |           |           |                       |
| $R1 / wR2$ (all)   | 0.0883 / 0.986   |            |           |           |           |                       |
| Largest residual peak / hole (e <sup>-</sup> Å <sup>-3</sup> ) | +8.82 / -3.43  |            |           |           |           |                       |
| <i>Site</i>  | <i>Wyckoff</i>   | <i>SOF</i> | <i>x</i>  | <i>y</i>  | <i>z</i>  | <i>U<sub>eq</sub></i> |
| Ca1  | 2i   | 1          | 0.5312(5) | 0.1825(5) | 0.2318(3) | 0.0082(12)            |
| Ca2  | 2i   | 1          | 0.1356(4) | 0.3773(5) | 0.2329(3) | 0.0069(12)            |
| Ca3  | 2i   | 1          | 0.3311(5) | 0.7713(5) | 0.2315(3) | 0.0097(13)            |
| Ca4  | 2i   | 1          | 0.7250(5) | 0.5763(5) | 0.2343(3) | 0.0073(12)            |
| Ca5  | 2i   | 1          | 0.9394(4) | 0.9800(5) | 0.2044(3) | 0.0110(13)            |
| Fe1  | 2i   | 0.784(9)   | 0.4485(2) | 0.6522(2) | 0.4994(4) | 0.0073(7)             |
| Pd11   | 2i   | 0.216(9)   | 0.4485(2) | 0.6522(2) | 0.4994(4) | 0.0073(7)             |
| Fe2  | 2i   | 0.842(8)   | 0.2488(3) | 0.2486(3) | 0.4996(4) | 0.0073(7)             |
| Pd22   | 2i   | 0.158(8)   | 0.2488(3) | 0.2486(3) | 0.4996(4) | 0.0073(7)             |

## Appendix

---

|      |    |          |           |           |           |           |
|------|----|----------|-----------|-----------|-----------|-----------|
| Fe3  | 2i | 0.825(8) | 0.1490(2) | 0.5495(2) | 0.5017(4) | 0.0073(7) |
| Pd33 | 2i | 0.175(8) | 0.1490(2) | 0.5495(2) | 0.5017(4) | 0.0073(7) |
| Fe4  | 2i | 0.871(8) | 0.3500(2) | 0.9496(3) | 0.4994(4) | 0.0073(7) |
| Pd44 | 2i | 0.129(8) | 0.3500(2) | 0.9496(3) | 0.4994(4) | 0.0073(7) |
| Fe5  | 2i | 0.886(8) | 0.0482(3) | 0.8517(3) | 0.4994(4) | 0.0073(7) |
| Pd55 | 2i | 0.114(8) | 0.0482(3) | 0.8517(3) | 0.4994(4) | 0.0073(7) |
| As1  | 2i | 1        | 0.5877(2) | 0.8686(2) | 0.3623(2) | 0.0060(7) |
| As2  | 2i | 1        | 0.7895(2) | 0.2629(2) | 0.3622(2) | 0.0061(7) |
| As3  | 2i | 1        | 0.9864(2) | 0.6682(2) | 0.3622(2) | 0.0055(6) |
| As4  | 2i | 1        | 0.1857(2) | 0.0643(2) | 0.3618(2) | 0.0057(6) |
| As5  | 2i | 1        | 0.3847(2) | 0.4648(2) | 0.3651(2) | 0.0054(6) |
| Pd1  | 1c | 1        | 0         | 0.5       | 0         | 0.0066(3) |
| Pd2  | 1d | 1        | 0.5       | 0         | 0         | 0.0066(3) |
| Pd3  | 2i | 0.398(3) | 0.4864(4) | 0.4954(3) | 0.0455(3) | 0.0058(8) |
| As6  | 2i | 1        | 0.7660(2) | 0.0967(2) | 0.0002(2) | 0.0084(2) |
| As7  | 2i | 1        | 0.9000(2) | 0.7666(2) | 0.0002(2) | 0.0084(2) |
| As8  | 2i | 1        | 0.6182(2) | 0.7436(2) | 0.0002(2) | 0.0084(2) |
| As9  | 2i | 1        | 0.2551(2) | 0.6175(2) | 0.0001(2) | 0.0084(2) |

---

The crystal showed strong intense maxima of the tetragonal  $\text{CaFe}_2\text{As}_2$  substructure next to weak reflection of the  $\sqrt{5} \times \sqrt{5}$  superstructure. For  $2h + k \neq 5n$  significant diffuse scattering was evident. With present partial merohedral twinning all reflections were ascribed using four twin domains resulting from rotations of  $180^\circ$  around (310), (130), and (001).

## 10.2 Crystallographic Data of $\alpha$ -(CaFeAs)<sub>10</sub>Pd<sub>4</sub>As<sub>8</sub>

**Table 2:** Crystallographic data of  $\alpha$ -(CaFe<sub>0.757</sub>Pd<sub>0.243</sub>As)<sub>10</sub>Pd<sub>2.83</sub>As<sub>8</sub>.

| Empirical formula  | Ca <sub>10</sub> Fe <sub>7.57</sub> Pd <sub>5.26</sub> As <sub>18</sub> |            |            |            |            |                 |
|--|---|------------|------------|------------|------------|-----------------|
| Crystal system, space group, number                            | Tetragonal, <i>P4/n</i> , 85  |            |            |            |            |                 |
| <i>a</i> , <i>b</i> , <i>c</i> (Å)                             | 8.8533(12), 8.8533(12), 10.229(3)                                       |            |            |            |            |                 |
| $\alpha$ , $\beta$ , $\gamma$ (degree)                         | 90, 90, 90  |            |            |            |            |                 |
| Cell volume (Å <sup>3</sup> )                                  | 801.76(32)  |            |            |            |            |                 |
| Calculated density (g cm <sup>-3</sup> ), <i>Z</i>             | 5.6555, 1   |            |            |            |            |                 |
| Radiation type, $\lambda$ (Å)                                  | Mo-K $\alpha$ , 0.71073   |            |            |            |            |                 |
| $2\theta$ range (degree)                                       | 3.04 – 34.88  |            |            |            |            |                 |
| Reflections (total, independent, $I > 3\sigma(I)$ )            | 13949, 1216, 325  |            |            |            |            |                 |
| $R_{\text{int}}$ , $R_{\sigma}$                                | 0.2174, 0.1936  |            |            |            |            |                 |
| GooF (all) / Goof ( $I \geq 3\sigma(I)$ )                      | 2.43 / 4.19   |            |            |            |            |                 |
| Refined parameters, refinement                                 | 27, <i>F</i>  |            |            |            |            |                 |
| $R1$ / $wR2$ ( $I \geq 3\sigma(I)$ )                           | 0.1076 / 0.0958   |            |            |            |            |                 |
| $R1$ / $wR2$ (all)   | 0.2956 / 0.1108   |            |            |            |            |                 |
| Largest residual peak / hole (e <sup>-</sup> Å <sup>-3</sup> ) | +24.66 / -23.82   |            |            |            |            |                 |
| <i>Site</i>  | <i>Wyckoff</i>  | <i>SOF</i> | <i>x</i>   | <i>y</i>   | <i>z</i>   | $U_{\text{eq}}$ |
| Ca1  | 2 <i>c</i>  |            | 0          | 0.5        | 0.2909(26) | 0.0132(12)      |
| Ca2  | 8 <i>g</i>  |            | 0.7958(20) | 0.0945(21) | 0.2618(5)  | 0.0132(12)      |
| Fe1  | 2 <i>a</i>  | 0.746(57)  | 0          | 0          | 0          | 0.0094(7)       |
| Pd11   | 2 <i>a</i>  | 0.254(57)  | 0          | 0          | 0          | 0.0094(7)       |
| Fe2  | 8 <i>g</i>  | 0.759(19)  | 0.0988(10) | 0.7004(8)  | 0          | 0.0094(7)       |
| Pd22   | 8 <i>g</i>  | 0.241(19)  | 0.0988(10) | 0.7004(8)  | 0          | 0.0094(7)       |
| As1  | 2 <i>c</i>  |            | 0.5        | 0          | 0.1555(16) | 0.0086(5)       |
| As2  | 8 <i>g</i>  |            | 0.1005(10) | 0.2002(10) | 0.1349(3)  | 0.0086(5)       |
| Pd1  | 2 <i>b</i>  |            | 0          | 0          | 0.5        | 0.0126(18)      |
| Pd2  | 2 <i>c</i>  | 0.413(16)  | 0.5        | 0          | 0.4230(16) | 0.0126(18)      |
| As3  | 8 <i>g</i>  |            | 0.2632(5)  | 0.1081(7)  | 0.5057(6)  | 0.0086(5)       |

The crystal featured typical intense maxima of the CaFe<sub>2</sub>As<sub>2</sub> substructure and significant weaker intensities for  $2h + k \neq 5n$ . The moderate refinement can be ascribed to the high residual electronic density mainly within the palladium arsenide layer resulting from strong diffuse scattering along *l* for superstructure reflections. Due to partial merohedral twinning the structure was described by two twin domains implementing a rotation of 180° around (120).

### 10.3 Crystallographic data of $\text{Ca}(\text{Fe}_{1-x}\text{Pd}_x)\text{As}_{2-z}$

**Table 3:** Crystallographic data of  $\text{CaFe}_{0.56}\text{Pd}_{0.44}\text{As}_{1.95}$ .

| Empirical formula  | $\text{CaFe}_{0.56}\text{Pd}_{0.44}\text{As}_{1.95}$ |            |           |          |           |                       |
|--|--|------------|-----------|----------|-----------|-----------------------|
| Crystal system, space group, number                            | Monoclinic, $P2_1/m$ , 11                            |            |           |          |           |                       |
| $a, b, c$ (Å)  | 8.063(3), 4.137(1), 9.078(3)                         |            |           |          |           |                       |
| $\alpha, \beta, \gamma$ (degree)                               | 90, 102.8(1), 90                                     |            |           |          |           |                       |
| Cell volume (Å <sup>3</sup> )                                  | 295.3(2)   |            |           |          |           |                       |
| Calculated density (g cm <sup>-3</sup> ), $Z$                  | 5.9353, 4  |            |           |          |           |                       |
| Radiation type, $\lambda$ (Å)                                  | Mo-K $\alpha$ , 0.71069                              |            |           |          |           |                       |
| $2\theta$ range (degree)                                       | 2.59 – 30.3  |            |           |          |           |                       |
| Reflections (total, independent, $I > 3\sigma(I)$ )            | 3483, 988, 390                                       |            |           |          |           |                       |
| $R_{\text{int}}, R_{\sigma}$                                   | 0.047, 0.050   |            |           |          |           |                       |
| Goof (all) / Goof ( $I \geq 3\sigma(I)$ )                      | 1.04 / 1.56  |            |           |          |           |                       |
| Refined parameters, refinement                                 | 53, $F^2$  |            |           |          |           |                       |
| $R1 / wR2$ ( $I \geq 3\sigma(I)$ )                             | 0.026 / 0.053  |            |           |          |           |                       |
| $R1 / wR2$ (all)   | 0.059 / 0.089  |            |           |          |           |                       |
| Largest residual peak / hole (e <sup>-</sup> Å <sup>-3</sup> ) | +1.22 / -1.73  |            |           |          |           |                       |
| <i>Site</i>  | <i>Wyckoff</i>                                       | <i>SOF</i> | <i>x</i>  | <i>y</i> | <i>z</i>  | <i>U<sub>eq</sub></i> |
| Ca1  | 2e   |            | 0.9496(5) | 0.25     | 0.2985(4) | 0.0123(14)            |
| Ca2  | 2e   |            | 0.4498(5) | 0.25     | 0.2992(4) | 0.0115(14)            |
| Fe1  | 2e   | 0.55(2)    | 0.1242(3) | 0.25     | 0.9966(2) | 0.0111(7)             |
| Pd1  | 2e   | 0.45(2)    | 0.1242(3) | 0.25     | 0.9966(2) | 0.0111(7)             |
| Fe2  | 2e   | 0.58(2)    | 0.6271(3) | 0.25     | 0.0081(2) | 0.0090(7)             |
| Pd2  | 2e   | 0.42(2)    | 0.6271(3) | 0.25     | 0.0081(2) | 0.0090(7)             |
| As1  | 2e   |            | 0.3406(3) | 0.25     | 0.8446(2) | 0.0152(7)             |
| As2  | 2e   |            | 0.8322(3) | 0.25     | 0.8453(2) | 0.0153(7)             |
| As3  | 2e   | 0.89(1)    | 0.7663(3) | 0.25     | 0.5647(2) | 0.0115(9)             |
| As4  | 2e   | 1.00(2)    | 0.2660(3) | 0.25     | 0.5651(2) | 0.0198(9)             |

## 10.4 Crystallographic Data of Framework Structures

### 10.4.1 $\beta$ -Ca<sub>3</sub>Fe<sub>8</sub>PdAs<sub>6</sub>

**Table 4:** Crystallographic data of  $\beta$ -Ca<sub>3</sub>(Fe<sub>0.880</sub>Pd<sub>0.120</sub>)<sub>8</sub>PdAs<sub>6</sub>.

| Empirical formula  | Ca <sub>3</sub> Fe <sub>7.04</sub> Pd <sub>1.96</sub> As <sub>6</sub> |            |             |          |             |                 |
|--|---|------------|-------------|----------|-------------|-----------------|
| Crystal system, space group, number                            | Orthorhombic, <i>Pnma</i> , 62  |            |             |          |             |                 |
| <i>a</i> , <i>b</i> , <i>c</i> (Å)                             | 26.363(4), 3.8699(5), 11.330(1)                                       |            |             |          |             |                 |
| $\alpha$ , $\beta$ , $\gamma$ (degree)                         | 90, 90, 90  |            |             |          |             |                 |
| Cell volume (Å <sup>3</sup> )                                  | 1155.9(2)   |            |             |          |             |                 |
| Calculated density (g cm <sup>-3</sup> ), <i>Z</i>             | 6.7302, 4   |            |             |          |             |                 |
| Radiation type, $\lambda$ (Å)                                  | Mo-K $\alpha$ , 0.71073   |            |             |          |             |                 |
| $2\theta$ range (degree)                                       | 2.93 – 30.34  |            |             |          |             |                 |
| Reflections (total, independent, $I > 3\sigma(I)$ )            | 13562, 1965, 1072   |            |             |          |             |                 |
| $R_{\text{int}}$ , $R_{\sigma}$                                | 0.061, 0.033  |            |             |          |             |                 |
| Goof (all) / Goof ( $I \geq 3\sigma(I)$ )                      | 1.69 / 2.28   |            |             |          |             |                 |
| Refined parameters, refinement                                 | 117, $F^2$  |            |             |          |             |                 |
| $R1$ / $wR2$ ( $I \geq 3\sigma(I)$ )                           | 0.038 / 0.082   |            |             |          |             |                 |
| $R1$ / $wR2$ (all)   | 0.068 / 0.085   |            |             |          |             |                 |
| Largest residual peak / hole (e <sup>-</sup> Å <sup>-3</sup> ) | +1.60 / -4.19   |            |             |          |             |                 |
| <i>Site</i>  | <i>Wyckoff</i>  | <i>SOF</i> | <i>x</i>    | <i>y</i> | <i>z</i>    | $U_{\text{eq}}$ |
| Ca1  | 4 <i>c</i>  |            | 0.26547(10) | 0.25     | 0.58270(3)  | 0.0122(6)       |
| Ca2  | 4 <i>c</i>  |            | 0.89722(13) | 0.25     | 0.74030(3)  | 0.0105(7)       |
| Ca3  | 4 <i>c</i>  |            | 0.10131(11) | 0.75     | 0.90660(3)  | 0.0110(7)       |
| Fe1  | 4 <i>c</i>  | 0.681(18)  | 0.14736(8)  | 0.25     | 0.70187(15) | 0.0137(6)       |
| Pd11   | 4 <i>c</i>  | 0.319(18)  | 0.14736(8)  | 0.25     | 0.70187(15) | 0.0137(6)       |
| Fe2  | 4 <i>c</i>  | 0.798(17)  | 0.15044(8)  | 0.25     | 0.46435(16) | 0.0151(6)       |
| Pd22   | 4 <i>c</i>  | 0.202(17)  | 0.15044(8)  | 0.25     | 0.46435(16) | 0.0151(6)       |
| Fe3  | 4 <i>c</i>  | 0.885(17)  | 0.28404(9)  | 0.25     | 0.28328(15) | 0.0124(7)       |
| Pd33   | 4 <i>c</i>  | 0.115(17)  | 0.28404(9)  | 0.25     | 0.28328(15) | 0.0124(7)       |
| Fe4  | 4 <i>c</i>  | 0.874(16)  | 0.21722(9)  | 0.75     | 0.38296(15) | 0.0128(7)       |
| Pd44   | 4 <i>c</i>  | 0.126(16)  | 0.21722(9)  | 0.75     | 0.38296(15) | 0.0128(7)       |
| Fe5  | 4 <i>c</i>  | 0.993(15)  | 0.00007(10) | 0.25     | 0.26420(3)  | 0.0105(8)       |
| Pd55   | 4 <i>c</i>  | 0.007(15)  | 0.00007(10) | 0.25     | 0.26420(3)  | 0.0105(8)       |
| Fe6  | 4 <i>c</i>  | 0.920(14)  | 0.99869(8)  | 0.75     | 0.09060(4)  | 0.0125(6)       |
| Pd66   | 4 <i>c</i>  | 0.080(14)  | 0.99869(8)  | 0.75     | 0.09060(4)  | 0.0125(6)       |

|      |    |           |            |      |             |           |
|------|----|-----------|------------|------|-------------|-----------|
| Fe7  | 4c | 0.939(14) | 0.00335(8) | 0.75 | 0.42330(4)  | 0.0130(6) |
| Pd77 | 4c | 0.061(14) | 0.00335(8) | 0.75 | 0.42330(4)  | 0.0130(6) |
| Fe8  | 4c | 0.948(14) | 0.08041(7) | 0.75 | 0.58240(2)  | 0.0160(6) |
| Pd88 | 4c | 0.052(14) | 0.08041(7) | 0.75 | 0.58240(2)  | 0.0160(6) |
| Pd1  | 4c |           | 0.14554(5) | 0.25 | 0.08356(16) | 0.0219(3) |
| As1  | 4c |           | 0.05226(5) | 0.25 | 0.08550(3)  | 0.0094(3) |
| As2  | 4c |           | 0.05625(7) | 0.25 | 0.73660(2)  | 0.0110(5) |
| As3  | 4c |           | 0.19229(6) | 0.25 | 0.27106(11) | 0.0110(4) |
| As4  | 4c |           | 0.93920(6) | 0.75 | 0.57180(2)  | 0.0107(4) |
| As5  | 4c |           | 0.19115(6) | 0.25 | 0.89557(11) | 0.0114(4) |
| As6  | 4c |           | 0.17817(5) | 0.75 | 0.58198(15) | 0.0125(3) |

### 10.4.2 $\gamma$ -Ca<sub>3</sub>Fe<sub>8</sub>PdAs<sub>6</sub>

**Table 5:** Crystallographic data of  $\gamma$ -Ca<sub>3</sub>(Fe<sub>0.593</sub>Pd<sub>0.407</sub>)<sub>8</sub>PdAs<sub>6</sub>.

| Empirical formula  | Ca <sub>3</sub> Fe <sub>4.74</sub> Pd <sub>4.26</sub> As <sub>6</sub> |            |             |          |             |                 |
|--|---|------------|-------------|----------|-------------|-----------------|
| Crystal system, space group, number                            | Orthorhombic, <i>Pnma</i> , 62  |            |             |          |             |                 |
| <i>a</i> , <i>b</i> , <i>c</i> (Å)                             | 19.856(3), 3.9461(5), 15.343(2)                                       |            |             |          |             |                 |
| $\alpha$ , $\beta$ , $\gamma$ (degree)                         | 90, 90, 90  |            |             |          |             |                 |
| Cell volume (Å <sup>3</sup> )                                  | 1202.2(3)   |            |             |          |             |                 |
| Calculated density (g cm <sup>-3</sup> ), <i>Z</i>             | 7.1124, 4   |            |             |          |             |                 |
| Radiation type, $\lambda$ (Å)                                  | Mo-K $\alpha$ , 0.71069   |            |             |          |             |                 |
| $2\theta$ range (degree)                                       | 2.44 – 30.26  |            |             |          |             |                 |
| Reflections (total, independent, $I > 3\sigma(I)$ )            | 12494, 2035, 993  |            |             |          |             |                 |
| $R_{\text{int}}$ , $R_{\sigma}$                                | 0.095, 0.067  |            |             |          |             |                 |
| Goof (all) / Goof ( $I \geq 3\sigma(I)$ )                      | 0.76 / 1.01   |            |             |          |             |                 |
| Refined parameters, refinement                                 | 117, $F^2$  |            |             |          |             |                 |
| $R1$ / $wR2$ ( $I \geq 3\sigma(I)$ )                           | 0.023 / 0.044   |            |             |          |             |                 |
| $R1$ / $wR2$ (all)   | 0.066 / 0.049   |            |             |          |             |                 |
| Largest residual peak / hole (e <sup>-</sup> Å <sup>-3</sup> ) | +1.29 / -1.53   |            |             |          |             |                 |
| <i>Site</i>  | <i>Wyckoff</i>  | <i>SOF</i> | <i>x</i>    | <i>y</i> | <i>z</i>    | $U_{\text{eq}}$ |
| Ca1  | 4c  |            | 0.63426(11) | 0.25     | 0.19848(15) | 0.0094(6)       |
| Ca2  | 4c  |            | 0.36720(10) | 0.75     | 0.07234(15) | 0.0097(5)       |
| Ca3  | 4c  |            | 0.81303(9)  | 0.25     | 0.06700(16) | 0.0085(5)       |
| Fe1  | 4c  | 0.143(11)  | 0.50712(5)  | 0.75     | 0.20389(6)  | 0.0102(3)       |
| Pd11   | 4c  | 0.857(11)  | 0.50712(5)  | 0.75     | 0.20389(6)  | 0.0102(3)       |
| Fe2  | 4c  | 0.245(11)  | 0.88208(5)  | 0.75     | 0.20804(6)  | 0.0095(3)       |
| Pd22   | 4c  | 0.755(11)  | 0.88208(5)  | 0.75     | 0.20804(6)  | 0.0095(3)       |

|      |    |           |            |      |            |           |
|------|----|-----------|------------|------|------------|-----------|
| Fe3  | 4c | 0.586(10) | 0.70285(6) | 0.75 | 0.78334(8) | 0.0077(4) |
| Pd33 | 4c | 0.414(10) | 0.70285(6) | 0.75 | 0.78334(8) | 0.0077(4) |
| Fe4  | 4c | 0.579(10) | 0.98888(7) | 0.25 | 0.15177(8) | 0.0122(4) |
| Pd44 | 4c | 0.421(10) | 0.98888(7) | 0.25 | 0.15177(8) | 0.0122(4) |
| Fe5  | 4c | 0.639(9)  | 0.50209(5) | 0.75 | 0.93184(9) | 0.0087(3) |
| Pd55 | 4c | 0.361(9)  | 0.50209(5) | 0.75 | 0.93184(9) | 0.0087(3) |
| Fe6  | 4c | 0.756(10) | 0.87728(6) | 0.75 | 0.91257(8) | 0.0079(4) |
| Pd66 | 4c | 0.244(10) | 0.87728(6) | 0.75 | 0.91257(8) | 0.0079(4) |
| Fe7  | 4c | 0.820(11) | 0.70738(7) | 0.75 | 0.34778(9) | 0.0083(4) |
| Pd77 | 4c | 0.180(11) | 0.70738(7) | 0.75 | 0.34778(9) | 0.0083(4) |
| Fe8  | 4c | 0.974(10) | 0.04145(7) | 0.75 | 0.02513(9) | 0.0082(5) |
| Pd88 | 4c | 0.026(10) | 0.04145(7) | 0.75 | 0.02513(9) | 0.0082(5) |
| Pd1  | 4c |           | 0.69442(4) | 0.75 | 0.06549(7) | 0.0100(2) |
| As1  | 4c |           | 0.57113(5) | 0.75 | 0.06374(9) | 0.0101(3) |
| As2  | 4c |           | 0.75610(5) | 0.75 | 0.92699(8) | 0.0105(3) |
| As3  | 4c |           | 0.75679(6) | 0.75 | 0.20413(8) | 0.0101(3) |
| As4  | 4c |           | 0.92594(5) | 0.75 | 0.05805(8) | 0.0091(3) |
| As5  | 4c |           | 0.58525(6) | 0.75 | 0.33111(7) | 0.0106(3) |
| As6  | 4c |           | 0.92477(7) | 0.25 | 0.29728(8) | 0.0130(3) |

### 10.4.3 $\alpha$ -Ca<sub>6</sub>Fe<sub>11</sub>Pd<sub>3</sub>As<sub>10</sub>

**Table 6:** Crystallographic data of  $\alpha$ -Ca<sub>6</sub>(Fe<sub>0.716</sub>Pd<sub>0.284</sub>)<sub>11</sub>Pd<sub>3</sub>As<sub>10</sub>.

|  |  |
|--|--|
| Empirical formula  | Ca <sub>6</sub> Fe <sub>7.88</sub> Pd <sub>6.12</sub> As <sub>10</sub> |
| Crystal system, space group, number                            | Monoclinic, $P2_1/m$ , 11  |
| $a, b, c$ (Å)  | 15.564(3), 3.9679(6), 17.880(3)  |
| $\alpha, \beta, \gamma$ (degree)                               | 90, 108.75(1), 90  |
| Cell volume (Å <sup>3</sup> )                                  | 1045.7(3)  |
| Calculated density (g cm <sup>-3</sup> ), $Z$                  | 6.6072, 2  |
| Radiation type, $\lambda$ (Å)                                  | Mo-K $\alpha$ , 0.71073  |
| $2\theta$ range (degree)                                       | 2.36 – 39.93   |
| Reflections (total, independent, $I > 3\sigma(I)$ )            | 25471, 3004, 1604  |
| $R_{\text{int}}, R_{\sigma}$                                   | 0.1378, 0.2029   |
| GooF (all) / Goof ( $I \geq 3\sigma(I)$ )                      | 2.09 / 2.70  |
| Refined parameters, refinement                                 | 132, $F^2$   |
| $R1 / wR2$ ( $I \geq 3\sigma(I)$ )                             | 0.064 / 0.142  |
| $R1 / wR2$ (all)   | 0.125 / 0.153  |
| Largest residual peak / hole (e <sup>-</sup> Å <sup>-3</sup> ) | +6.42 / -5.18  |

## Appendix

| <i>Site</i> | <i>Wyckoff</i> | <i>SOF</i> | <i>x</i>  | <i>y</i> | <i>z</i>  | <i>U<sub>eq</sub></i> |
|-------------|----------------|------------|-----------|----------|-----------|-----------------------|
| Ca1         | 2e             |            | 0.3856(5) | 0.75     | 0.1606(6) | 0.0096(8)             |
| Ca2         | 2e             |            | 0.0696(6) | 0.75     | 0.3668(5) | 0.0096(8)             |
| Ca3         | 2e             |            | 0.8587(5) | 0.75     | 0.1604(6) | 0.0096(8)             |
| Ca4         | 2e             |            | 0.3323(6) | 0.75     | 0.3697(5) | 0.0096(8)             |
| Ca5         | 2e             |            | 0.2802(6) | 0.75     | 0.5829(4) | 0.0096(8)             |
| Ca6         | 2e             |            | 0.1232(6) | 0.75     | 0.1604(4) | 0.0096(8)             |
| Fe1         | 2e             | 0.309(20)  | 0.2593(2) | 0.75     | 0.7689(2) | 0.0060(6)             |
| Pd11        | 2e             | 0.691(20)  | 0.2593(2) | 0.75     | 0.7689(2) | 0.0060(6)             |
| Fe2         | 2e             | 0.405(17)  | 0.4397(2) | 0.75     | 0.7661(2) | 0.0060(6)             |
| Pd22        | 2e             | 0.595(17)  | 0.4397(2) | 0.75     | 0.7661(2) | 0.0060(6)             |
| Fe3         | 2e             | 0.736(17)  | 0.9337(4) | 0.75     | 0.9987(3) | 0.0084(8)             |
| Pd33        | 2e             | 0.264(17)  | 0.9337(4) | 0.75     | 0.9987(3) | 0.0084(8)             |
| Fe4         | 2e             | 0.600(17)  | 0.5432(2) | 0.75     | 0.3439(3) | 0.0060(6)             |
| Pd44        | 2e             | 0.400(17)  | 0.5432(2) | 0.75     | 0.3439(3) | 0.0060(6)             |
| Fe5         | 2e             | 0.687(16)  | 0.8400(3) | 0.75     | 0.3418(3) | 0.0060(6)             |
| Pd55        | 2e             | 0.313(16)  | 0.8400(3) | 0.75     | 0.3418(3) | 0.0060(6)             |
| Fe6         | 2e             | 0.778(19)  | 0.1963(4) | 0.75     | 0.0003(4) | 0.0084(8)             |
| Pd66        | 2e             | 0.222(19)  | 0.1963(4) | 0.75     | 0.0003(4) | 0.0084(8)             |
| Fe7         | 2e             | 0.873(20)  | 0.0509(3) | 0.75     | 0.5528(4) | 0.0060(6)             |
| Pd77        | 2e             | 0.127(20)  | 0.0509(3) | 0.75     | 0.5528(4) | 0.0060(6)             |
| Fe8         | 2e             | 0.824(19)  | 0.4883(3) | 0.75     | 0.5523(4) | 0.0060(6)             |
| Pd88        | 2e             | 0.176(19)  | 0.4883(3) | 0.75     | 0.5523(4) | 0.0060(6)             |
| Fe9         | 2e             | 0.777(21)  | 0.6780(3) | 0.75     | 0.0005(4) | 0.0084(8)             |
| Pd99        | 2e             | 0.223(21)  | 0.6780(3) | 0.75     | 0.0005(4) | 0.0084(8)             |
| Fe10        | 2e             |            | 0.4428(4) | 0.75     | 0.0043(3) | 0.0084(8)             |
| Fe11        | 2e             | 0.931(14)  | 0.6090(3) | 0.75     | 0.1264(2) | 0.0060(6)             |
| Pd111       | 2e             | 0.069(14)  | 0.6090(3) | 0.75     | 0.1264(2) | 0.0060(6)             |
| Pd1         | 2e             |            | 0.9880(2) | 0.75     | 0.7736(2) | 0.0116(11)            |
| Pd2         | 2e             |            | 0.7147(2) | 0.75     | 0.7727(2) | 0.0108(11)            |
| Pd3         | 2e             |            | 0.7701(3) | 0.75     | 0.5544(2) | 0.0133(10)            |
| As1         | 2e             |            | 0.8239(3) | 0.75     | 0.7001(2) | 0.0095(13)            |
| As2         | 2e             |            | 0.7728(3) | 0.75     | 0.9179(3) | 0.0082(14)            |
| As3         | 2e             |            | 0.2918(3) | 0.75     | 0.9143(3) | 0.0071(8)             |
| As4         | 2e             |            | 0.0371(3) | 0.75     | 0.9181(2) | 0.0114(13)            |
| As5         | 2e             |            | 0.5217(3) | 0.75     | 0.9114(2) | 0.0071(8)             |
| As6         | 2e             |            | 0.0934(3) | 0.75     | 0.6976(3) | 0.0130(18)            |
| As7         | 2e             |            | 0.8849(3) | 0.75     | 0.4878(3) | 0.0107(14)            |

|      |    |           |      |           |            |
|------|----|-----------|------|-----------|------------|
| As8  | 2e | 0.6057(3) | 0.75 | 0.4877(3) | 0.0120(14) |
| As9  | 2e | 0.5531(3) | 0.75 | 0.6959(3) | 0.0113(17) |
| As10 | 2e | 0.6661(3) | 0.75 | 0.2794(2) | 0.0156(12) |

To describe all obtained reflection the structure was refined including two twin domains using a rotation of 180 ° around (001).

## 10.5 CSD Numbers

The crystallographic data (.cif files) of investigated compounds can be obtained by quoting the corresponding depository number from the Fachinformationszentrum Karlsruhe, 76344 Eggenstein-Leopoldshafen, Germany (fax: (+49) 7247 80 86 66, e-mail: crysdata@fiz-karlsruhe.de).

**Table 7:** CSD numbers of compounds investigated within this thesis.

| Compound  | Structure   | CSD entry  |
|---|---|------------|
| $\text{Ca}_{10}\text{Fe}_{8.42}\text{Pd}_{4.38}\text{As}_{18}$                | Pd1038  | CSD-426107 |
| $\text{CaFe}_{0.562}\text{Pd}_{0.438}\text{As}_{1.947}$                       | $\text{Ca}(\text{Fe}_{1-x}\text{Pd}_x)\text{As}_2$          | CSD-429054 |
| $\text{CaFe}_5\text{As}_3$  | $\alpha\text{-CaFe}_5\text{As}_3$                           | CSD-427443 |
| $\text{Ca}_{2.56}\text{Na}_{0.44}\text{Fe}_{7.49}\text{Nb}_{0.51}\text{As}_6$ | $\alpha\text{-Ca}_3\text{Fe}_8\text{As}_6$                  | CSD-427439 |
| $\text{Ca}_3\text{Fe}_{7.705}\text{Pt}_{1.295}\text{As}_6$                    | $\alpha\text{-Ca}_3\text{Fe}_8\text{PtAs}_6$                | CSD-427440 |
| $\text{Ca}_3\text{Fe}_{7.038}\text{Pd}_{1.962}\text{As}_6$                    | $\beta\text{-Ca}_3\text{Fe}_8\text{PdAs}_6$                 | CSD-427444 |
| $\text{Ca}_3\text{Fe}_{6.750}\text{Pt}_{2.250}\text{As}_6$                    | $\beta\text{-Ca}_3\text{Fe}_8\text{PtAs}_6$                 | CSD-427445 |
| $\text{Ca}_3\text{Fe}_{4.741}\text{Pd}_{4.259}\text{As}_6$                    | $\gamma\text{-Ca}_3\text{Fe}_8\text{PdAs}_6$                | CSD-427446 |
| $\text{Ca}_6\text{Fe}_{7.879}\text{Pd}_{6.121}\text{As}_{10}$                 | $\alpha\text{-Ca}_6\text{Fe}_{11}\text{Pd}_3\text{As}_{10}$ | CSD-427441 |
| $\text{Ca}_6\text{Fe}_{7.627}\text{Pt}_{6.373}\text{As}_{10}$                 | $\alpha\text{-Ca}_6\text{Fe}_{11}\text{Pt}_3\text{As}_{10}$ | CSD-427442 |

## 11 Abbreviations and Quantities

### 11.1 Abbreviations

|           |   |
|-----------|---|
| 1038      | $(\text{CaFe}_{1-x}\text{M}_x\text{As})_{10}\text{M}_3\text{As}_8$ ( $M = \text{Pd}, \text{Pt}$ ) |
| 1048      | $(\text{CaFe}_{1-x}\text{M}_x\text{As})_{10}\text{M}_4\text{As}_8$ ( $M = \text{Pd}, \text{Pt}$ ) |
| A         | alkaline metal  |
| ac        | alternating current   |
| AE        | alkaline earth metal  |
| AFM       | antiferromagnetic order   |
| a.u.      | arbitrary units   |
| BCS       | acronym of <i>Bardeen, Cooper and Schrieffer</i>  |
| CDW       | charge density wave   |
| CN        | coordination number   |
| COHP      | crystal orbital <i>Hamilton</i> population  |
| dc        | direct current  |
| DFT       | density functional theory   |
| DOS       | density of states   |
| EDS/ EDX  | energy dispersive X-ray spectroscopy  |
| <i>fc</i> | field cooling   |
| FS        | <i>Fermi</i> surface  |
| FWHM      | full width at half maximum  |
| IPDS      | imaging plate diffraction system  |
| <i>k</i>  | impulse vector  |
| LMU       | Ludwig-Maximilians-Universität  |
| <i>M</i>  | metal   |
| MPMS      | magnetic property measurement system  |

|         |  |
|---------|--|
| MRI     | magnetic resonance imaging   |
| NMR     | nuclear magnetic resonance   |
| Pd1038  | $(\text{CaFe}_{1-x}\text{Pd}_x\text{As})_{10}\text{Pd}_3\text{As}_8$ |
| Pd1048  | $(\text{CaFe}_{1-x}\text{Pd}_x\text{As})_{10}\text{Pd}_4\text{As}_8$ |
| pDOS    | partial density of states  |
| $Pn$    | pnictide   |
| Pt1038  | $(\text{CaFe}_{1-x}\text{Pt}_x\text{As})_{10}\text{Pt}_3\text{As}_8$ |
| Pt1048  | $(\text{CaFe}_{1-x}\text{Pt}_x\text{As})_{10}\text{Pt}_4\text{As}_8$ |
| $RE$    | rare earth metal   |
| RT      | room temperature   |
| SC      | superconductivity  |
| SDW     | spin density wave  |
| SG      | space group  |
| SOF     | site occupation factor   |
| SQUID   | superconducting quantum interference device                          |
| VASP    | Vienna ab-initio simulation package                                  |
| Wyckoff | <i>Wyckoff</i> position  |
| XRD     | X-ray diffraction  |
| $zfc$   | zero field cooling   |

## 11.2 Magnetic Quantities

|                  |  |
|------------------|--|
| $4\pi \chi_V$    | magnetic volume fraction                       |
| $B$              | magnetic flux density                          |
| $B_{\text{hyp}}$ | magnetic hyperfine field splitting (Mössbauer) |
| $C$              | <i>Curie</i> constant                          |
| $H$              | magnetic field                                 |
| $H_c$            | critical field                                 |

|                    |  |
|--------------------|--|
| $M$                | magnetization                                      |
| $T_N$              | <i>Néel</i> temperature                            |
| $\mu$              | magnetic moment in <i>Bohr</i> magnetons           |
| $\mu_B$            | <i>Bohr</i> magneton                               |
| $\mu_{\text{eff}}$ | effective magnetic moment in <i>Bohr</i> magnetons |
| $\chi$             | magnetic susceptibility                            |
| $\chi_V$           | volume susceptibility                              |

### 11.3 Crystallographic Quantities

|                 |   |
|-----------------|---|
| $\square$       | vacancy position                            |
| deg.            | degree                                      |
| $F$             | structure factor                            |
| GooF            | goodness of fit                             |
| $h, k, l$       | <i>Miller</i> indices                       |
| $I$             | intensity                                   |
| $R$             | residual factor                             |
| $U_{\text{eq}}$ | equivalent thermal displacement parameter   |
| $w$             | weighting factor                            |
| $wR$            | weighted residual factor                    |
| $Z$             | number for empirical formulas per unit cell |
| $\theta$        | diffraction angle                           |
| $\lambda$       | wave length                                 |

### 11.4 Other Quantities

|                 |                           |
|-----------------|---------------------------|
| $a, b, c$       | unit cell axes            |
| $a^*, b^*, c^*$ | reciprocal unit cell axes |
| at%             | atom percent              |

## Abbreviations and Quantities

---

|                         |  |
|-------------------------|--|
| $E$                     | energy   |
| $E_F$                   | <i>Fermi</i> energy  |
| eV                      | electron Volt  |
| J                       | Joule  |
| $J_c$                   | critical current density   |
| K                       | Kelvin   |
| mol                     | mole   |
| $p$                     | pressure   |
| $q$                     | nesting vector   |
| $T$                     | temperature  |
| $T_c$                   | critical temperature of a superconductor                         |
| $T_{\text{Transition}}$ | transition temperature   |
| $V_{ZZ}$                | main component of the magnetic field gradient tensor (Mössbauer) |
| wt%                     | weight percent   |
| $x, y, z$               | mixed or deficient occupancies                                   |
| $\alpha, \beta, \gamma$ | unit cell angles   |
| $\Gamma$                | experimental line width (Mössbauer)                              |
| $\Delta E_Q$            | electric quadrupole splitting parameter (Mössbauer)              |
| $\delta$                | isomer shift (Mössbauer)   |
| $\delta$                | structural order parameter                                       |
| $\delta$ angle          | tetrahedra angle (fourfold)                                      |
| $\varepsilon$ angle     | tetrahedra angle (twofold)                                       |
| $\rho$                  | density  |
| $\rho$                  | electrical resistivity   |
| $\sigma$                | standard deviation   |

## 12 Publications

A considerable part of the results within this thesis was published in scientific journals as described in the following list. Publications beyond this work, talks, and poster presentations at scientific conferences are summarized in the subsequent chapters.

### 12.1 Publications within this Thesis

#### Superconductivity and Crystal Structure of the Palladium Iron Arsenides $(\text{CaFe}_{1-x}\text{Pd}_x\text{As})_{10}\text{Pt}_3\text{As}_8$

C. Hieke, J. Lippmann, T. Stürzer, G. Friederichs, F. Nitsche, F. Winter, R. Pöttgen, D. Johrendt

*Philos. Mag.* **2013**, 93, 3680 – 3689.

For this publication synthesis of  $(\text{CaFe}_{1-x}\text{Pd}_x\text{As})_{10}\text{Pd}_3\text{As}_8$ , crystal selection, and preparation was done by Christine Stürzer (née Hieke). Single crystal data was measured by Tobias Stürzer. Structure determination and refinement was performed by Christine Stürzer in association with Fabian Nitsche and Tobias Stürzer. Polycrystalline samples of  $(\text{Ca}_{1-y}\text{La}_y\text{Fe}_{1-x}\text{Pd}_x\text{As})_{10}\text{Pd}_3\text{As}_8$  were synthesized by Christine Stürzer with assistance of Judith Lippmann. Powder X-ray diffraction and ac-susceptibility measurements, Rietveld refinement, data analysis, and picture editing were done by Christine Stürzer, electrical resistivity was measured by Christine Stürzer with assistance of Gina Friederichs.  $^{57}\text{Fe}$ -Mössbauer studies were performed and evaluated by Florian Winter and Rainer Pöttgen. DFT calculations were done by Dirk Johrendt. The manuscript was written by Dirk Johrendt in association with Christine Stürzer and Rainer Pöttgen. Tobias Stürzer contributed to discussion and manuscript revision.

#### Site Preference of Rare Earth Doping in Palladium Iron Arsenide Superconductors

C. Stürzer, A. Schulz, D. Johrendt

*Z. Anorg. Allg. Chem.* **2014**, 640, 3143 – 3147.

The syntheses of  $(\text{Ca}_{1-y}\text{RE}_y\text{Fe}_{1-x}\text{Pd}_x\text{As})_{10}\text{Pd}_z\text{As}_8$  with  $\text{RE} = \text{La}, \text{Ce}, \text{Pr}$  were done by Christine Stürzer and Anne Schulz. The implementation of analytical measurements, Rietveld

refinements, evaluation and interpretation were performed by Christine Stürzer. EDX measurements were done by Christian Minke, SQUID measurements by Gina Friederichs, and DFT calculation by Dirk Johrendt. Manuscript writing, picture editing, and literature screening were performed by Christine Stürzer. Tobias Stürzer and Dirk Johrendt assisted by discussion and manuscript revision.

### **Combination of Palladium and Platinum 1038 Phases in $(\text{CaFe}_{1-x}\text{Pd}_x\text{As})_{10}\text{Pt}_3\text{As}_8$**

Christine Stürzer, Dirk Johrendt

*This chapter is in preparation to be published in a scientific journal.*

For this publication the samples of  $(\text{CaFe}_{1-x}\text{Pd}_x\text{As})_{10}\text{Pt}_3\text{As}_8$  with  $x = 0.0125 - 0.25$  were synthesized by Christine Stürzer. X-ray diffraction, EDX, and magnetic data were measured by Christine Stürzer, who also performed Rietveld refinements, data evaluation, interpretation, and illustration. Running the measurements on electrical resistivity and dc-susceptibility were assisted by Gina Friederichs and Simon Peschke. Low temperature X-ray diffraction data was measured by Franziska Hummel. Literature research, setup, and writing the manuscript were done by Christine Stürzer. The manuscript was revised by Tobias Stürzer and Dirk Johrendt. Tobias Stürzer contributed to discussions.

### **New Structure with substituted Iron Arsenides Layers $\text{CaFe}_{1-x}\text{Pd}_x\text{As}_2$**

Christine Stürzer, Tobias Stürzer, Dirk Johrendt

*This chapter is in preparation to be published in a scientific journal.*

Synthesis, crystal selection, and preparation of the  $\text{CaFe}_{1-x}\text{Pd}_x\text{As}_2$  single crystal were done by Christine Stürzer. Single crystal X-ray data was measured by Tobias Stürzer. Structure elucidation and refinement were performed by Christine Stürzer. Synthesis optimization of polycrystalline  $\text{CaFe}_{1-x}\text{Pd}_x\text{As}_2$ , X-ray powder diffraction and refinement as well as EDX measurements were done by Christine Stürzer, SQUID measurements were run by Gina Friederichs. Tobias Stürzer performed electronic structure calculations. Data evaluation, picture editing, literature screening, and writing the manuscript were done by Christine Stürzer. Tobias Stürzer contributed to discussions. The manuscript was revised by Tobias Stürzer and Dirk Johrendt.

**Framework Structures of interconnected Layers in Calcium Iron Arsenides**

T. Stürzer, C. Hieke, C. Löhnert, F. Nitsche, J. Stahl, C. Maak, R. Pobel, D. Johrendt

*Inorg. Chem.* **2014**, *53*, 6235 – 6240.

Within this publication  $\text{CaFe}_5\text{As}_3$  was synthesized by Roman Pobel with the assistance of Christian Maak.  $\alpha\text{-Ca}_3(\text{Fe,Pt})_8\text{PtAs}_6$ ,  $\beta\text{-Ca}_3(\text{Fe,Pt})_8\text{PtAs}_6$ , and  $\alpha\text{-Ca}_6(\text{Fe,Pt})_{11}\text{Pt}_3\text{As}_{10}$  were prepared by Tobias Stürzer with assistance of Juliane Stahl, while Christine Stürzer (née Hieke) synthesized  $\beta\text{-Ca}_3(\text{Fe,Pd})_8\text{PdAs}_6$ ,  $\gamma\text{-Ca}_3(\text{Fe,Pd})_8\text{PdAs}_6$ , and  $\alpha\text{-Ca}_6(\text{Fe,Pd})_{11}\text{Pd}_3\text{As}_{10}$ . Catrin Löhnert prepared  $(\text{Ca,Na})_3(\text{Fe,Nb})_8\text{As}_6$ . Single crystal X-ray diffraction data was collected by Tobias Stürzer and Fabian Nitsche. The structures of  $\text{CaFe}_5\text{As}_3$ ,  $\alpha\text{-Ca}_3(\text{Fe,Pt})_8\text{PtAs}_6$ , and  $\alpha\text{-Ca}_6(\text{Fe,Pt})_{11}\text{Pt}_3\text{As}_{10}$  were elucidated by Tobias Stürzer,  $\beta\text{-Ca}_3(\text{Fe,Pt})_8\text{PtAs}_6$  by Dirk Johrendt,  $\beta\text{-Ca}_3(\text{Fe,Pd})_8\text{PdAs}_6$ ,  $\gamma\text{-Ca}_3(\text{Fe,Pd})_8\text{PdAs}_6$ , and  $\alpha\text{-Ca}_6(\text{Fe,Pd})_{11}\text{Pd}_3\text{As}_{10}$  by Christine Stürzer, and  $(\text{Ca,Na})_3(\text{Fe,Nb})_8\text{As}_6$  by Fabian Nitsche. DFT calculations, the analysis of structural relations, and development of a common classification of the new compounds were done by Tobias Stürzer, who also performed literature research and writing the manuscript. Picture editing was done by Tobias and Christine Stürzer. Christine Stürzer and Fabian Nitsche contributed to data analysis and discussion. The manuscript was revised by Christine Stürzer, Fabian Nitsche, and Dirk Johrendt.

**12.2 Publications beyond this Thesis****Different Response of the Crystal Structure to isoelectronic Doping in  $\text{BaFe}_2(\text{As}_{1-x}\text{P}_x)_2$  and  $(\text{Ba}_{1-x}\text{Sr}_x)\text{Fe}_2\text{As}_2$** 

M. Rotter, C. Hieke, D. Johrendt

*Phys. Rev. B* **2010**, *82*, 014513.**Transition Metal Pnictides**

D. Johrendt, C. Hieke, T. Stürzer

*Comprehensive Inorganic Chemistry II* (second edition), Elsevier **2013**, 111 – 135.

### 12.3 Conference Contributions

#### **Superconductivity and Crystal Structure of Palladium Iron Arsenides** (poster)

C. Hieke, T. Stürzer, G. Friederichs, F. Nitsche, D. Johrendt

SUPER-IRON 2nd Student Workshop, Tsukuba, Japan, **2014**.

#### **New Framework Structures with interconnected Iron Arsenide Layers** (poster)

T. Stürzer, C. Hieke, C. Löhnert, F. Nitsche, D. Johrendt

SUPER-IRON 2nd Student Workshop, Tsukuba, Japan, **2014**.

#### **Des Palladiums Zähmung** (talk)

C. Hieke, D. Johrendt

Hemdsärmelkolloquium, Köln, Germany, **2014**.

#### **Supraleitung in Palladium–substituiertem $(\text{CaFe}_{1-x}\text{Pd}_x\text{As})_{10}\text{Pt}_3\text{As}_8$** (talk)

C. Hieke, D. Johrendt

Erstes Obergurgl-Seminar Festkörperchemie, Obergurgl, Austria, **2014**.

#### **Kristallstruktur und Supraleitung der neuen Palladium-Eisenarsenide $(\text{CaFe}_{1-x}\text{Pd}_x\text{As})_{10}\text{Pd}_3\text{As}_8$** (talk)

C. Hieke, D. Johrendt

Hirschegg-Seminar on Solid State Chemistry, Hirschegg, Austria, **2013**.

#### **Neue polymorphe Verbindungen mit verknüpften Eisenarsenid-Schichten $\text{Ca}_3(\text{Fe}_{1-x}\text{Pd}_x)_8\text{PdAs}_6$** (talk)

C. Hieke, D. Johrendt

Hirschegg-Seminar on Solid State Chemistry, Hirschegg, Austria, **2012**.

## **13 Curriculum Vitae**